Biochemical Characterization of 14S Dynein Isolated from the Cilia of *Tetrahymena Thermophila*

Thesis submitted for the degree of Doctor of Philosophy at the University of Leicester

by

Hazel Ann Tharia BSc (York)

Department of Biochemistry

University of Leicester

June 1995

UMI Number: U085404

UMI®

Dissertation Publishing

ProQuest®

To
Mum and Dad

Biochemical Characterisation of 14S Dynein Isolated from the Cilia of *Tetrahymena thermophila.*

Hazel A. Tharia

Dynein is the ATPase responsible for cilia and flagella motility in eukaryotic organisms. At least two ATPases have been identified in *Tetrahymena thermophila* and are termed 22S and 14S on account of their differing sedimentation coefficients.

14S dynein was fractionated, using anion-exchange Fast Protein Liquid Chromatography, into four fractions (designated 1-4). Electron microscopy analysis revealed that the four fractions were structurally distinct. Fraction 1 comprised two globular heads interconnected via two stems; fraction 2 consisted of at least two clearly different globular structures; fraction 3 was a single globular head; and fraction 4 comprised three globular heads interconnected via three stems to a base. Further structural characterisation involved the use of hydrodynamic techniques in which the mass and sedimentation coefficient were determined for each fraction. In the presence of 40mM NaCl, fraction 1 had a mass of 654kDa and a sedimentation coefficient of 20.1S. Fraction 2 had a variable mass due to aggregation (616-966kDa), and a sedimentation coefficient of 16.6S, whereas fractions 3 and 4 had variable sedimentation coefficients but were of mass 701kDa and 527kDa respectively. These parameters were then utilised, in conjunction with electron microscopy data, in the construction of low-resolution bead models to represent the fractions.

The four fractions had a unique polypeptide composition as shown by SDS polyacrylamide gel electrophoresis. At least four unique heavy chains were identified immunologically; two associated with fraction 1, one associated with fraction 2, and one associated with fractions 3 and 4.

Fractions 1 and 2 were readily distinguished from fractions 3 and 4 using the technique of vanadate-dependent photolysis. The requirement for ATP in the photolysis reaction indicated differences in the structure of the heavy chain. The fractions were also distinguished with respect to the number and location of V2 sites, and the specific ATPase activity. These latter studies also showed that, for all four fractions, an increase in ionic strength resulted in a decrease in ATPase activity. This was coincident with an observed change in the structure and/or conformation of the fractions as determined by hydrodynamic analysis under equivalent conditions.

Acknowledgements

Abbreviations

APS	ammonium persulphate
ATP	adenosine 5' triphosphate
bis-acrylamide	N,N'-methylene bisacrylamide
DEAE	diethylaminoethyl
DMF	N,N- dimethylformamide
DTT	DL-dithiothreitol
EDTA	ethylenediamine tetra-acetic acid
EGTA	ethylenebis (oxyethylenenitrilo)-tetra-acetic acid
FPLC	fast protein liquid chromatography
GTP	guanosine 5' triphosphate
Hepes	N-2-hydroxyethylpiperazine-N'-2-ethanesulfonic acid
HC	heavy chain
HPLC	high performance liquid chromatography
kDa	kiloDaltons
Mes	2-(N-morpholino) ethanesulfonic acid
NAD^+	nicotinamide-adenine dinucleotide, oxidised
NADH	nicotinamide-adenine dinucleotide, reduced
PBS	phosphate buffered saline
PEG	polyethylene glycol
PEP	phosphoenol pyruvate
Pipes	piperazine-N,N'-bis-[2-ethanesulfonic acid]
PMSF	phenylmethanesulfonyl fluoride
rpm	revolutions per minute
SDS-PAGE	sodium dodecyl sulphate polyacrylamide gel electrophoresis
TEMED	N,N,N',N'-tetramethylethylenediamine
Tris	tris (hydroxymethyl) aminomethane
UV	ultra violet

Contents

Chapter 1

Introduction

<u>Section A</u>

Motor Proteins

Motor proteins are specialised enzymes which enable a wide variety of mechanical tasks to be accomplished in eukaryotic organisms. Tasks such as the contraction of muscle, beating of cilia or flagella, translocation of vesicular organelles, and movement of chromosomes during cell division, are all achieved through the action of specific motors. By definition, motor proteins utilise the energy from nucleotide hydrolysis to generate a controlled translocational movement along a cytoskeletal polymer (Vale & Goldstein, 1990). The polymer with which the motor interacts is either of actin or tubulin and consequently motors are termed actin-based or microtubule-based respectively.

Molecular motors can be categorised into three families of proteins: myosins, dyneins and kinesins (figure 1.1). Myosins are actin-based motors, whereas both dyneins and kinesins translocate along microtubules. The three motor protein families share a common overall structure. In each case, the force generating unit of the protein is identified as a globular head domain which is typically attached to a tail or stem structure. The head domain has conserved sites for nucleotide and polymer (actin filaments or microtubules) binding, whereas the tail is a highly variable region presumed to confer functional and possible regulatory properties on the intact molecule (Spudich & Warrick, 1991). The microtubule-based motors can be categorised further. Dyneins are often termed 'minus' end-directed motors whereas kinesins are generally 'plus' end-directed. This terminology reflects the specific direction in which the two classes of motor protein actively translocate along microtubules and arises due to the intrinsic polarity of the microtubule structure (section 1.5.1).

Despite basic similarities, the three motor families differ significantly with respect to size, composition, specific function, and location. In this section, each family of motors will be considered in turn with the exclusion of axonemal dynein which will be discussed in section B.
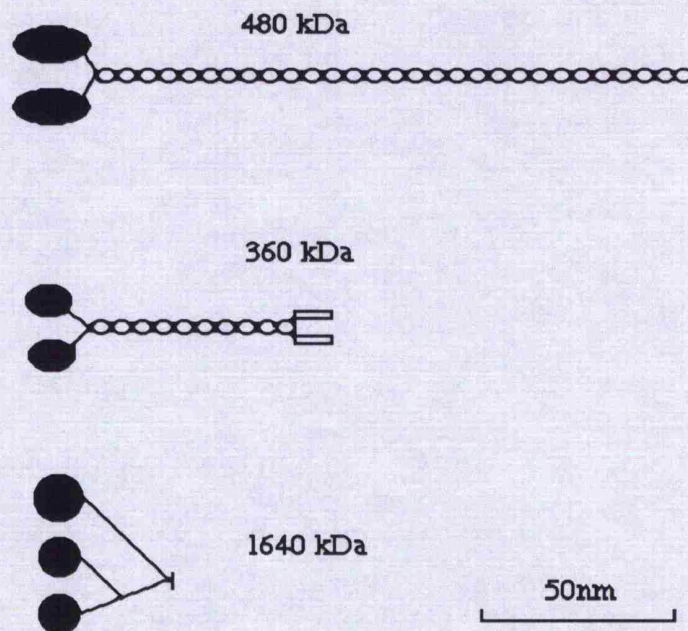
Figure 1.1. Diagrammatic representation of myosin II (top) from striated muscle (redrawn from Amos & Amos, 1991), 'conventional' kinesin (middle) from porcine brain (redrawn from Amos & Amos, 1991), and 22S dynein (below) from *Tetrahymena* axonemes (Johnson & Wall, 1983; Goodenough & Heuser, 1984). The globular heads in each case indicate the sites of ATPase activity.

1.1. Myosins

Myosins represent a superfamily of actin-based motor proteins. These can be subdivided into two major classes; myosins I and II, so called since they represent single-headed and double-headed molecules respectively (figure 1.2).

By far the most extensively studied actin-based motor is myosin II isolated from striated muscle. The general structure is well established and can be simply described as two pear-shaped head domains which are interconnected via a long flexible tail (figure 1.2). The heads (known as subfragment 1) represent the motor unit of the protein and each possesses ATPase activity and an ATP-sensitive actin-binding site. In contrast, the tail is derived from the flexible extensions of the two head domains which entwine to form a coiled-coil. Each two-headed myosin molecule is comprised of two identical high molecular mass polypeptides or **heavy chains** (220kDa), and two pairs (termed regulatory and essential) of

light chains (20kDa). The amino terminus of each heavy chain folds to form the globular head domain whereas the carboxy-terminus adopts the α-helical coiled-coil conformation of the tail. In addition, each of the heads is associated with one of each pair of light chains. The function of myosin II in striated muscle has been well documented (for *eg* see Warrick & Spudich, 1987; Bagshaw, 1993). In this context, myosin molecules assemble to form 'thick' bipolar filaments which exhibit ATPase activity and are activated by actin or 'thin' filaments. The interaction of thick and thin filaments is known as the crossbridge cycle reaction and is the basis of muscle contraction. In contrast, myosin II isolated from nonmuscle cells does not exhibit such an ordered structure and only forms active filaments after phosphorylation of the regulatory light chains. This mechanism of myosin assembly ensures the controlled formation of filaments both spatially and temporally within the cell. The filaments then function to generate tension or cause movements of actin filaments. Functional roles include contractile events of the cell such as the formation of the contractile ring during cell division and cytoplasmic streaming.
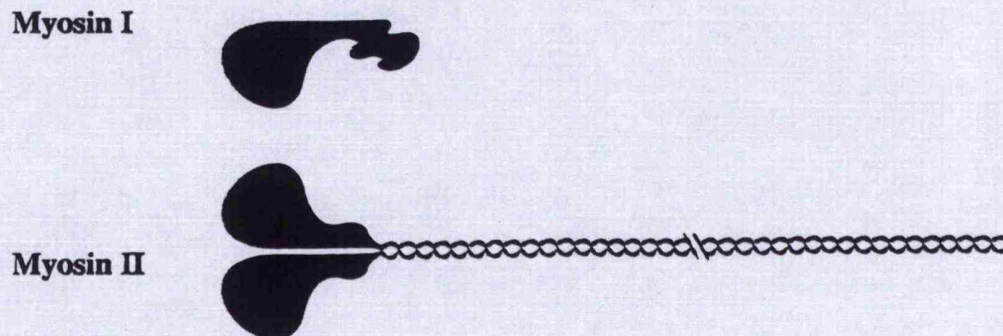
Myosin I

Myosin II

Figure 1.2. Diagrammatic representation of myosin I and II (from Hammer, 1991).

Myosins belonging to class I have also been isolated from non-muscle cells (for reviews see Hammer, 1991; Pollard *et al.*, 1991). These are single-headed or monomeric molecules which consist of a single heavy chain (figure 1.2). The tail region is highly variable in both structure and amino acid composition, and is generally short or globular.

In addition, the tail comprises a characteristic secondary actin-binding site. This unique site is ATP-insensitive and thought to be functionally significant since a single myosin I molecule can bind two actin filaments simultaneously. In this way, myosin Is are presumed to move actin filaments relative to one another, as well as to bind and translocate membranes and organelles. Myosin Is have been isolated from a variety of sources which include vertebrate, invertebrate, fungal, and protozoan.

1.2. Kinesins

Kinesin was discovered following the development of an assay for organelle or microtubule motility (Allen *et al.*, 1982; Brady *et al.*, 1982). This *in vitro* motility assay showed that 'soluble factors' within the axoplasm of squid giant axons could induce ATP-dependent motility of organelles along tracks of microtubules (Vale *et al.*, 1985a, b). Kinesin was then identified (Vale *et al.*, 1985c) when the non-hydrolysable ATP analogue adenylyl imidodiphosphate (AMP-PNP) was shown to specifically inhibit kinesin-dependent vesicle motility (Lasek & Brady, 1985). This property, in particular, distinguished kinesin from myosins or dyneins and, in conjunction with motility assays, provided a means for the identification of kinesin. Indeed, kinesin was subsequently purified from microtubules isolated from a range of tissue types using taxol and AMP-PNP. Taxol enabled microtubules to be purified in the absence of GTP (which inhibits kinesin-microtubule binding), whereas AMP-PNP immobilised kinesin on the microtubule surface (for reviews see Brady, 1995; Bloom & Endow, 1994).

Kinesin was initially considered to have a specialised function in anterograde fast axonal transport where vesicles and organelles are translocated along microtubules from the nerve cell body to the synapse (Vale *et al.*, 1985c; Hirokawa *et al.*, 1991). The identification of kinesin from a non-axonal form (sea urchin eggs), however, revealed an association with the mitotic spindle (Scholey *et al.*, 1985). As a result, kinesin was proposed to have some function in the events of cell division presumed to be related to the translocation of chromosomes. The subsequent localisation of kinesin to vesicles and tubules within a range of tissues and cell types then implicated this motor in a variety of plus end-directed transport processes (Hollenbeck, 1989; Wright *et al.*, 1991; Marks *et al.*, 1994). In each

case, kinesin was identified by characteristic properties which included microtubule-activated ATPase activity, and the plus end-directed translocation of vesicles and microtubules *in vitro*.

The kinesin molecule consists of two head domains and a rod-shaped tail (Amos, 1987; Hirokawa *et al.*, 1989). Each head represents the force-generating unit of the motor which was shown to be sufficient for ATP-sensitive microtubule-binding and translocation (Yang *et al.*, 1990). In contrast, the tail region comprises an α-helical coiled-coil stem and a fan-shaped tail which was thought to interact with chromosomes or vesicular organelles awaiting translocation (Vale & Goldstein, 1990). Each kinesin molecule possesses two identical heavy chains (110-140kDa) and two light chains of approximately 60-80kDa (Vale *et al.*, 1985c; Scholey *et al.*, 1985). The amino-terminus of each heavy chain represents the force-generating head domain, whereas the carboxy-terminal region corresponds to the tail (Yang *et al.*, 1989; Gilbert & Johnson, 1993). In addition, the two light chains, which have been localised to the fan-shaped tail of the molecule (Hirokawa *et al.*, 1989), are thought to associate with the carboxy-terminal ends of the heavy chains.

This 'conventional' kinesin was originally thought to represent the sole member of a unique class of motor protein distinguishable from both myosins and dyneins (figure 1.1). Since its discovery, however, many 'kinesin-like' proteins have been identified (figure 1.3).

Kinesin-like proteins have been categorised with respect to structural, functional and/or locational similarities into five classes (Goodson *et al.*, 1994). Two of the classes (including conventional kinesin) represent motors showing significant amino acid sequence homology within both the head and tail regions of the molecule. A third class categorises molecules in which the force-generating motor unit or head domain is represented by the carboxy-terminus of the heavy chain sequence rather than the typically amino-terminal region. Class four segregates motors specifically associated with the mitotic spindle, whereas the fifth class represents monomer molecules which lack a coiled-coil tail. In general, kinesin and kinesin-like proteins share a high level of homology within the region of heavy chain corresponding to the motor domain. The limited similarity within the non-motor or tail region of the molecule, however, is considered indicative of functional specialisation. Indeed, the large number of kinesin-related proteins

currently emerging are thought to reflect the wide variety of microtubule force-generating events that occur within the cell (for reviews see Goldstein, 1991; Vale, 1992; Pereira & Goldstein, 1994).
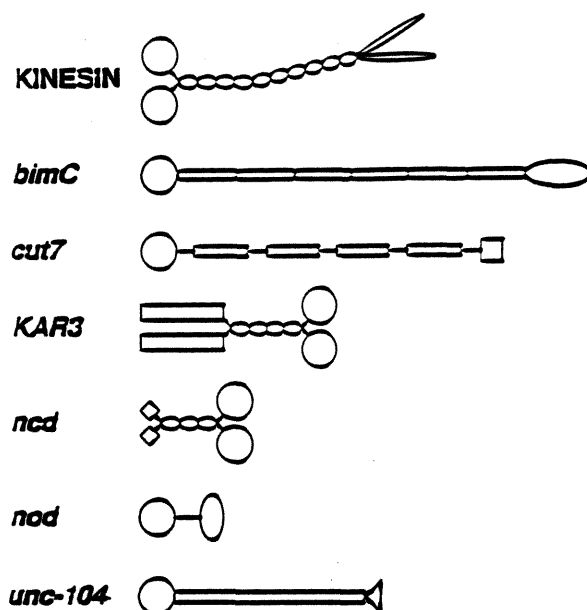
Figure 1.3. Schematic diagram of some members of the kinesin superfamily (from Goldstein, 1991). The force-generating motor domains are represented as circles whereas the various tail structures are indicated by a range of shapes.

1.3. Dyneins

Dynein was first identified as the ATPase responsible for cilia and flagella motility in eukaryotic organisms (Gibbons & Rowe, 1965). This **axonemal** dynein was so-called since it was shown to be an intergral part of the highly ordered stucture of cilia and flagella known as the axoneme (section 1.4). A second, more recently-isolated, form was identified in association with microtubules in the cytoplasm of a wide range of organisms and termed **cytoplasmic** dynein (section 1.3.2). Both were identified as dyneins on the basis of a number of common features (figure 1.4).

By definition, dyneins are large multisubunit complexes which exhibit a similar structure and polypeptide composition. They possess a number of large globular head domains

interconnected via an equivalent number of stems to a common base (Johnson & Wall, 1983; Goodenough & Heuser, 1984; Sale *et al.*, 1985; Vallee *et al.*, 1988; Marchese-Ragona *et al.*, 1988). Cytoplasmic dyneins generally possess two identical heads, whereas the heads associated with axonemal dynein are distinct and more variable in number. The polypeptide composition typically comprises one or more heavy chain components (350-540kDa), and a variable number of intermediate (57-140kDa) and light chains (6-22kDa). As well as their large size, dynein heavy chains are identified with respect to their ability to undergo cleavage at specific sites in the presence of nucleotide, inorganic vanadate, and UV light (Lee-Eiford *et al.*, 1986). Indeed, this phenomenon, known as vanadate-dependent photolysis, is often utilised as a diagnostic tool for the identification of dyneins (section 4.6.1). In terms of function, dyneins exhibit ATPase activity which can be activated by the presence of microtubules (section 4.2.1), and translocate microtubules *in vitro* from the minus to the plus end (Paschal *et al.*, 1987; Vale & Toyoshima, 1988; Paschal & Vallee, 1987).
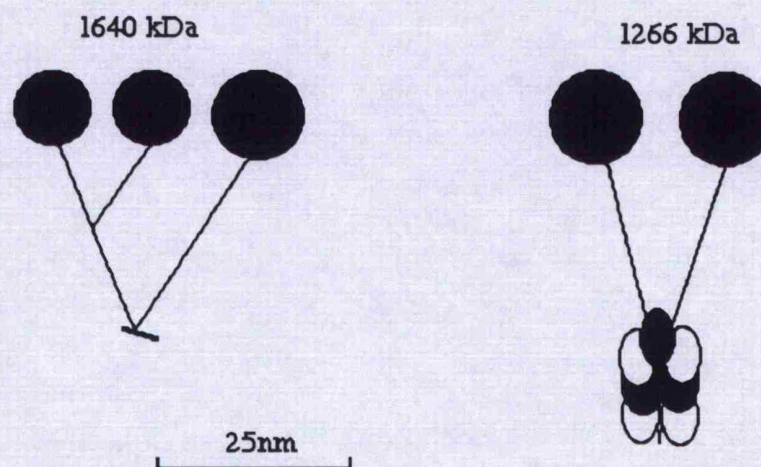
Figure 1.4. Schematic diagram of axonemal 22S dynein (left) isolated from the cilia of *Tetrahymena* (Johnson & Wall, 1983; Goodenough & Heuser, 1984), and cytoplasmic dynein (right) isolated from bovine brain (redrawn from Vallee, 1991). Mass estimates for axonemal (Wells *et al.*, 1990) and cytoplasmic (Vallee *et al.*, 1988) dynein are indicated.

1.3.1. Sequence analysis

Other dynein characteristics have been more recently identified as a direct result of amino acid sequence analysis of heavy chains from both cytoplasmic and axonemal dyneins. Amino acid sequences have been published for the β heavy chain of outer arm sea urchin dynein (Gibbons *et al.*, 1991; Ogawa, 1991), and the three heavy chains of *Chlamydomonas* outer arm (Mitchell & Brown, 1994; Wilkerson *et al.*, 1994). In comparison, several cytoplasmic heavy chain sequences have been determined including those from rat brain (Zhang *et al.*, 1993; Mikami *et al.*, 1993) and *Dictyostelium* (Koonce *et al.*, 1992).

These studies revealed that dynein heavy chains have a highly conserved polypeptide structure and are unique in that they possess multiple putative ATP-binding sites (figure 1.5). The most conserved region corresponds to the central third of the heavy chain in which four evenly spaced phosphate-binding pockets or **P-loops** have been identified (Gibbons *et al.*, 1991; Ogawa, 1991). These P-loops are thought to represent nucleotide-binding sites since the consensus sequence resembles that identified in several other nucleotide-metabolising enzymes (Walker *et al.*, 1982). One of the four P-loops (designated P1) shows absolute conservation throughout the dyneins and is thought to represent the ATP hydrolysis site that is fundamental to dynein-microtubule interaction (section 1.5.2). The role of the remaining P-loops, however, is uncertain and a possible function in ATP-binding has yet to be established. A potential microtubule-binding site has also been identified in the heavy chain sequences of both cytoplasmic and axonemal dyneins (figure 1.5).

Despite the presence of common characteristics, a comparison of the sequence data from cytoplasmic and axonemal dyneins has revealed some striking differences. Heavy chain sequences, for example, have been shown to be homologous within the carboxy-terminal region, but divergent within the amino-terminus (Mikami *et al.*, 1993; Wilkerson *et al.*, 1994; Mitchell & Brown, 1994; Koonce *et al.*, 1992). Similarly, a comparison of intermediate chain sequences derived for a 74kDa cytoplasmic (Paschal *et al.*, 1992) and a 78kDa axonemal subunit (King *et al.*, 1992), indicated no homology within the amino-terminus but significant homology within the carboxy-terminus. These and other

observations led to a proposal for the molecular organisation of the dynein molecule. An analysis of mass indicated that each heavy chain could be equated to a single globular head and some proportion of the stem (Witman *et al.*, 1983; Vallee *et al.*, 1988). The force-generating head of the molecule was thought to represent the highly conserved carboxy-terminal region of the heavy chain since this domain is fundamental to both axonemal and cytoplasmic dyneins (Koonce *et al.*, 1992; Mikami *et al.*, 1993; Zhang *et al.*, 1993; Wilkerson *et al.*, 1994; Mitchell & Brown, 1994). In contrast, the divergent amino-terminus was considered to represent the variable stem and confer the specialisation associated with the different forms of dynein. The stem portion of axonemal dynein, for example, is permanently attached to an A-subfiber within the structure of the axoneme (section 1.4), whereas cytoplasmic dynein must attach to (and actively translocate) a range of intracellular structures (section 1.3.2). Consequently, the variable amino-terminal region of the heavy chain is thought to reflect different anchorage sites of the dynein molecule *in situ*. It is uncertain, however, whether the heavy chain is involved directly or indirectly (through interactions with intermediate and light chains) with these specific sites of attachment.

Cytoplasmic dynein also differs from the axonemal form in that the former is thought to represent a 'primitive' dynein species since it is composed of two similar, or identical, heavy chains which are thought to be the products of a single gene (Mikami *et al.*, 1993). In contrast, axonemal dynein has two or three heavy chains (depending on the species) which are considered to be the products of separate genes (Endow & Titus, 1992). Similarly, a difference in substrate specificity for the two forms of dynein (Shpetner *et al.*, 1988) is thought to reflect variation within the heavy chain (Mikami *et al.*, 1993). The non-specificity exhibited by cytoplasmic dynein (in which ATP, CTP, TTP, and GTP can be hydrolysed) may indicate the presence of primitive partially-functional nucleotide-binding sites which are presumed to be inactive in the ATP-specific axonemal dynein.
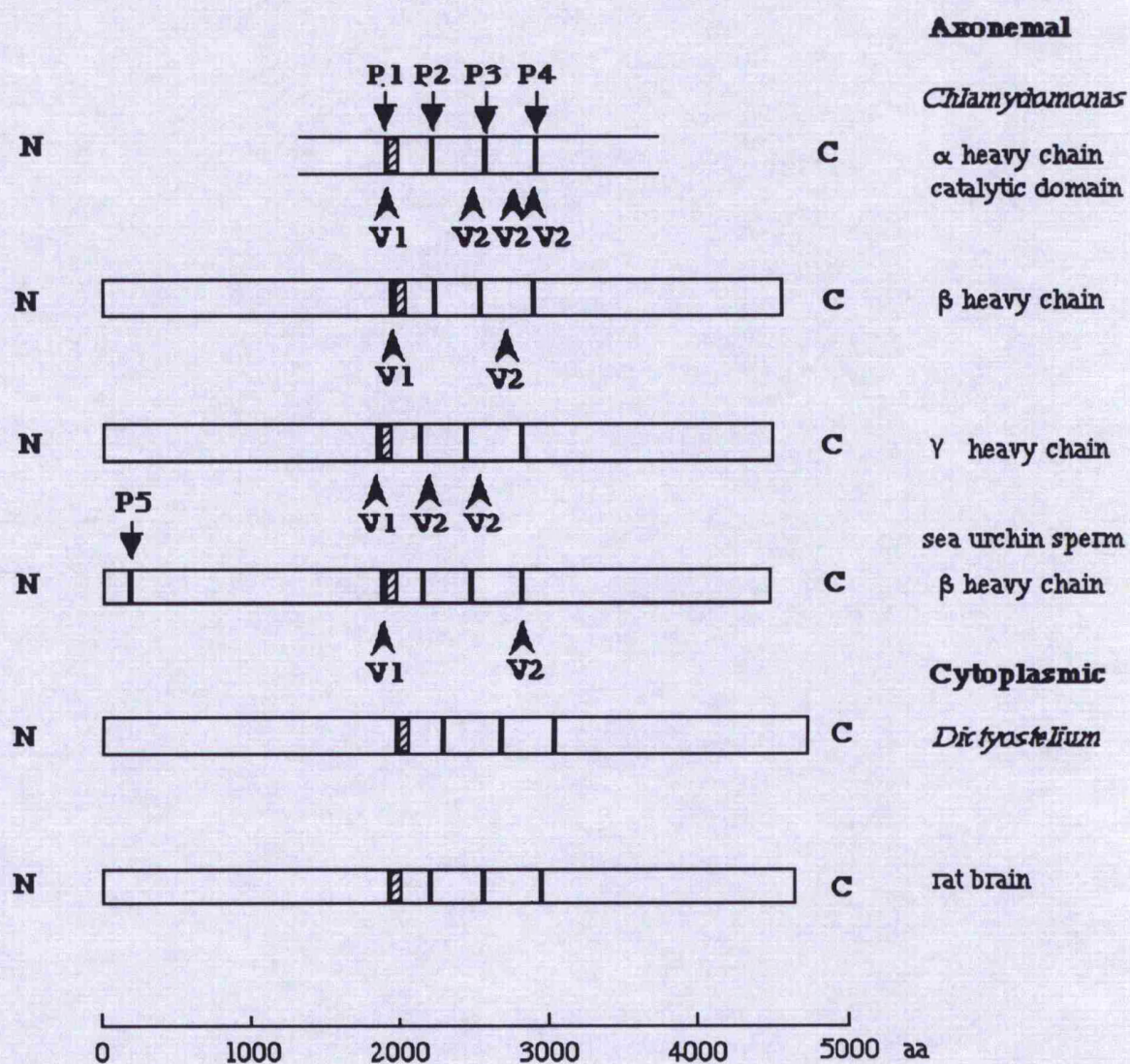
Figure 1.5. Schematic diagram of the heavy chain amino acid sequences from axonemal (sea urchin sperm (Gibbons *et al.*, 1991); *Chlamydomonas* (Mitchell & Brown, 1994; Wilkerson *et al.*, 1994)) and cytoplasmic (rat brain (Mikami *et al.*, 1993); *Dictyostelium* (Koonce *et al.*, 1992)) dyneins. The proposed site of ATP hydrolysis (P1), putative ATP-binding sites (P2-P5), potential microtubule-binding sites (shaded area), and sites of vanadate-dependent cleavage (V1 and V2) {see section 4.4} are indicated.

1.3.2. Cytoplasmic dynein

Cytoplasmic dynein (initially called MAP 1C) was identified as a member of the dynein motor protein family following its isolation from mammalian brain microtubule preparations (Paschal & Vallee, 1987; Paschal *et al.*, 1987). This protein was shown to translocate microtubules (in an ATP-dependent manner) *in vitro* from the minus to the plus end (Paschal & Vallee, 1987), have a structure comparable to that of axonemal dynein (Vallee *et al.*, 1988), and exhibit microtubule-activated ATPase activity (Paschal *et al.*, 1987; Shpetner *et al.*, 1988). Cytoplasmic dynein was shown to be a double-headed molecule connected via two stems to a basal structure comprising several smaller globular domains (figure 1.4; Vallee *et al.*, 1988). The polypeptide composition comprises two identical heavy chains (~410kDa), three 74kDa intermediate polypeptides, and four light chains of mass 59, 57, 55, and 53kDa (Vallee *et al.*, 1988; Paschal *et al.*, 1987). It is thought that each heavy chain comprises the majority of each globular head domain, and that the intermediate and light chains are localised at the base of the stem (Vallee *et al.*, 1988; Schroer, 1994).

The function of cytoplasmic dynein was indicated by *in vitro* motility assays in which dynein was shown to actively translocate membrane vesicles toward the minus end of microtubules (Schnapp & Reese, 1989; Schroer *et al.*, 1989). This *in vitro* function was thought to reflect the role of the motor protein *in vivo*. Dynein has been shown, for example, to exhibit the directional properties expected of a retrograde translocator (*ie* from the periphery to the cell body) in fast axonal transport (Paschal & Vallee, 1987), and has been localised *in vivo* to axonal vesicles destined for minus-end directed translocation (Hirokawa *et al.*, 1990). Similarly, in non-neuronal cells, immunocytochemical studies localised cytoplasmic dynein to membrane-bound vesicles (such as lysosomes) expected to be translocated within the cell (Lin & Collins, 1992). In addition, a specialised role was implicated in spindle separation and possibly chromosome movements, by the localisation of dynein to the mitotic kinetochore of chromosomes in early metaphase (Pfarr *et al.*, 1990; Steuer *et al.*, 1990).

The regulation of dynein-driven motility has yet to be established, although at least two levels of control have been implicated. One mechanism is thought to involve the

conversion of dynein to an active form, since cytoplasmic dynein has been shown to localise to membranous organelles in both the proximal and distal region of neurones (Hirokawa et al., 1990). The activation of dynein for retrograde translocation is thought to involve phosphorylation. In axonal transport, for example, the extent of phosphate incorporated into dynein heavy, intermediate, and light chains was shown to be reduced in a fraction of anterograde material compared to the total levels in the cytoplasm (Dillman & Pfister, 1994). Similarly, in non-neuronal cells, phophorylation was implicated as a regulatory mechanism since the removal of calcium was shown to cause dynein, associated with lysosomes (in cultured fibroblasts), to redistribute into a cytoplasmic pool (Lin & Collins, 1993).

A second level of control has been indicated by in vitro studies in which cytoplasmic dynein-dependent motility has been shown to require at least one additional component known as the dynactin (dynein activator) or Glued complex (Gill et al., 1991; Holzbaur et al., 1991). The exact role of this complex is unknown although one proposal is that dynactin acts as a receptor and targets organelles for dynein-dependent translocation (Holzbaur et al., 1994). In contrast, a second proposed action is that the complex facilitates binding of cytoplasmic dynein to organelles by the formation of a transient link between the organelle and microtubule 'track'. This latter proposal was based on the observation that one component of the dynactin complex (150kDa) showed a region of homology with two repeats in a cytoplasmic linker protein (CLIP 170) involved in the binding of endocytic vesicles to microtubules (Pierre et al., 1992). This consensus sequence was thought to represent a potential microtubule-binding motif and, as a result, the 150kDa peptide was implicated as a potential mediator between the dynactin complex and microtubules (Holzbaur et al., 1994). In addition, a second component (45kDa) of the dynactin complex was identified as an actin-related protein which shared approximately 50% sequence homology with conventional actin (Paschal et al., 1993). This component may associate into short filaments and provide a possible link between actin- and microtubule-based motors (Langford, 1995).

Axonemal Dynein

1.4. The axoneme

Axonemal dynein is localised specifically to the highly conserved structural unit of eukaryotic cilia and flagella known as the axoneme (for reviews see Murray, 1994; Gibbons, 1981). This organelle is characterised by the presence of a '9 + 2' array of microtubules (figure 1.6). Nine peripheral doublet microtubules, comprising an A-subfibre and B-subfibre, surround two central singlet microtubules (section 1.5.1). The outer doublets are interconnected by a permanent elastic link involving the protein nexin, whereas the two central microtubules (referred to as the central pair) are interconnected by cross-bridges, which also project outwards towards the peripheral doublet microtubules, to form a roughly cylindrical structure. Radial spoke proteins emanate from the central pair to each A-subfibre of the outer doublet microtubules, and dynein is identifiable on the A-subfibre as two 'arm-like' projections (figure 1.6).
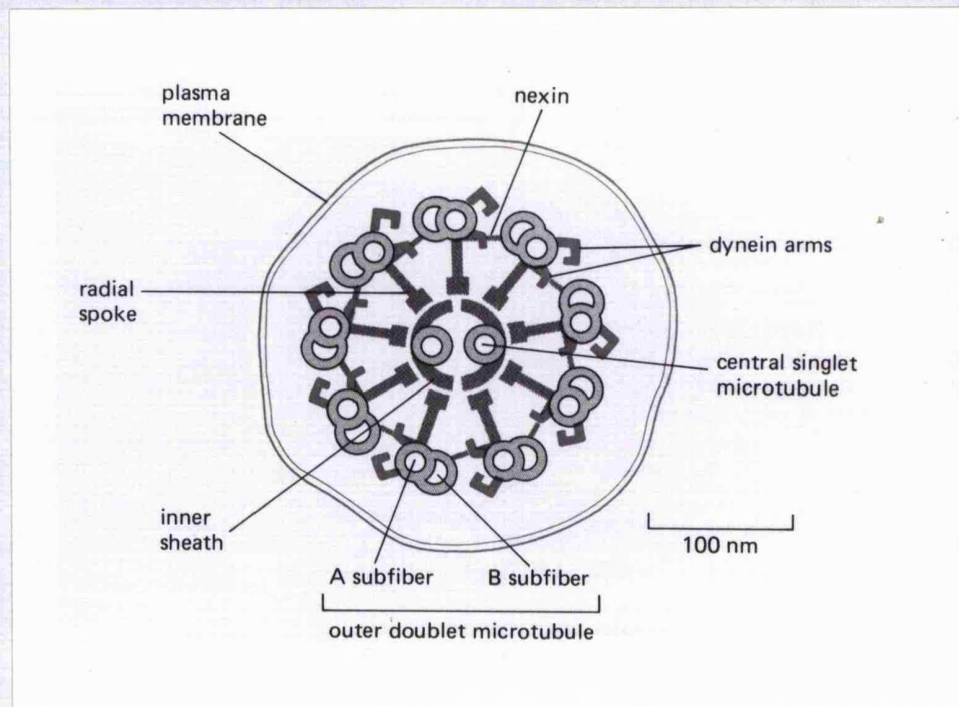
Figure 1.6. Schematic representation of the axoneme as shown in tranverse section (from Alberts *et al.*, 1983).

13

Two dynein arms are apparent within the axoneme and have been designated (with reference to their relative positions) as outer and inner arms (Gibbons, 1963; Gibbons & Rowe, 1965). The outer arm repeats with a regular 24nm periodicity along the entire length of the A-subfibre (Takahashi & Tonomura, 1978; Avolio et al., 1986). In contrast, the inner arm structure, though much less well-defined, is thought to adopt a periodicity identical to that of the radial spoke proteins (Goodenough & Heuser, 1985). Radial spoke proteins comprise at least 17 distinct polypeptides (Piperno et al., 1981) and form a connection between the central apparatus and each A-subfibre of the outer doublet pairs of microtubules (Goodenough & Heuser, 1985). Two (in *Chlamydomonas*) or three (in *Tetrahymena*) radial spokes are arranged periodically (figure 1.7) along the length of the axoneme in a 96nm-repeating helical unit.
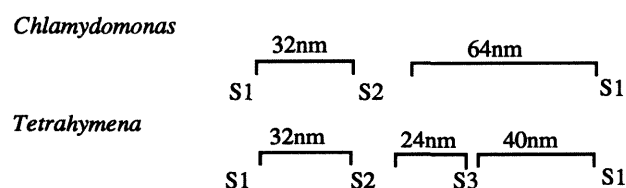
Figure 1.7. Schematic representation of the periodicity of radial spoke proteins (designated S1, S2 and S3) along the length of *Chlamydomonas* and *Tetrahymena* axonemes.

The central pair microtubules and associated cross-bridges (commonly referred to as the central apparatus) comprise at least 18 different polypeptides (Adams et al., 1981) including three kinesin-like proteins (Bernstein & Rosenbaum, 1994). The role of the complex is thought to involve regulation of cilia and flagella beating and is presumed to take effect through a close association with radial spoke proteins and dynein arms (section 1.6.1).

1.5. The interaction between dynein and microtubules

The outer arm is by far the most well characterised dynein and has a defined structure comprising two or three globular heads attached via an equivalent number of stems to a common basal structure (see figure 1.4). The basal (or structural) end of the molecule is permanently attached to the A-subfibre of the outer doublet microtubules via an ATP-insensitive site (figure 1.8). In contrast, the force-generating (or active) globular heads of the molecule interact in an ATP-sensitive manner with an adjacent B-subfibre (section 1.5.2).

1.5.1. Microtubule structure

The A- and B-subfibres of the outer doublet microtubule pairs (as with all microtubules) are polar structures composed almost entirely of α and β tubulin heterodimers. Heterodimers form microtubules by polymerisation in which the $\alpha-\beta$ subunits arrange end-to-end in longitudinal helical rows called protofilaments (figure 1.8). The central pair microtubules and A-subfibre comprise 13 protofilaments composed of tubulin heterodimers arranged in a so-called A-lattice (see Amos & Amos, 1991). In contrast, the B-subfibre has 10 protofilaments and exhibits a B-lattice assembly. The differential lattice arrangement reflects the association of $\alpha-\beta$ heterodimers which is either unlike (ie $\alpha-\beta.\alpha-\beta$) or like (ie $\alpha-\beta.\beta-\alpha$) in the A- and B-lattice respectively.

Microtubule polarity arises as a consequence of the asymmetric addition of tubulin dimers to the free ends of the microtubule structure during growth. The end which polymerises fastest is designated the 'plus' end, whereas the slower growing terminus is referred to as the 'minus' end. Microtubules present within the cytoplasm undergo polymerisation and depolymerisation as required for their various functions within the cell. In contrast, the microtubules of the axoneme are highly stable and thought to persist as a consequence of microtubule-associated proteins (MAPs) which are believed to induce stability (see Margolis & Job, 1994). These stable axonemal microtubules are uniformly arranged within the cilium or flagellum such that the plus end is located at the tip.

15
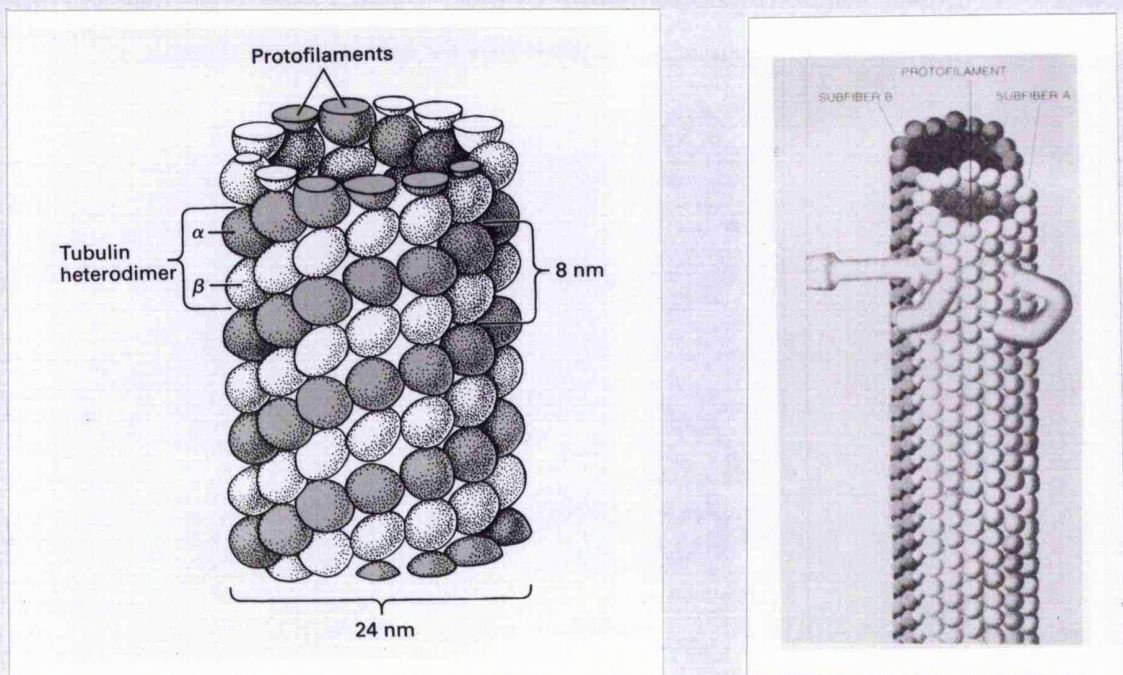
Figure 1.8. Microtubule structure to show (left) arrangement of α–β tubulin dimers in the A-subfibre (from Darnell *et al.*, 1986) and (right) attachment of the outer and inner dynein arms (from Satir, 1976).

1.5.2. Microtubule sliding

The dynein arms interact with the B-subfibre of outer doublet microtubules in an ATP-driven cyclical interaction (figure 1.9) which results in the relative sliding of microtubules. In the absence of ATP, the globular heads of the dynein arms form a rigor attachment with the B-subfibre of an adjacent doublet pair. On addition of MgATP, the heads rapidly detach (k_d) following the binding of ATP (k_1) to a single site location within each of the globular heads (Shimizu & Johnson, 1983a). The bound ATP is then hydrolysed in a less rapid reaction (k_2) to produce ADP and P_i (Johnson, 1983). These products are subsequently released from the dynein hydrolysis site in a slow (rate limiting) reaction which is activated by the presence of microtubules (Omoto & Johnson, 1986).

$$
\begin{array}{cccccc}
& k_1 & & & k_5 & \\
\text{D-MT} + \text{ATP} \longrightarrow & \text{D-MT-ATP} \longrightarrow & \text{D-MT-ADP-P}_i \longrightarrow & \text{D-MT} + \text{ADP} + \text{P}_i \\
| & \downarrow k_d & \uparrow k_4 & | \\
\text{D} + \text{ATP} \longrightarrow & \text{D-ATP} \xrightarrow{k_2} & \text{D-ADP-P}_i \xrightarrow{k_3} & \text{D} + \text{ADP} + \text{P}_i
\end{array}
$$
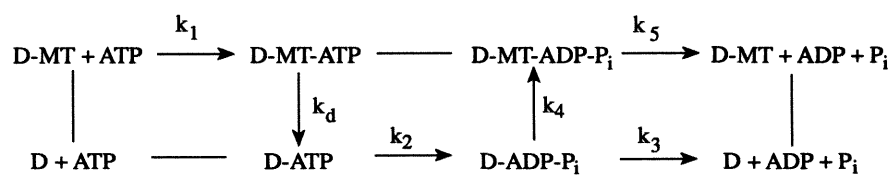
Figure 1.9. Diagrammatic representation of the cyclical ATP-dependent interaction between dynein (D) and microtubules (MT) (from Porter & Johnson, 1989).

The cycle of dynein arm attachment and detachment, to cause microtubule sliding, provides the basis for axonemal motility and evidence for its existence has been shown by a number of studies (for reviews see Gibbons, 1981; Johnson, 1985). The first evidence for a sliding microtubule model was demonstrated by the extrusion of microtubules from sea urchin sperm axonemes briefly pretreated with trypsin and then exposed to MgATP (Summers & Gibbons, 1971, 1973). Under these conditions, physical constraints such as nexin links and radial spoke heads were removed. Microtubules were then shown to telescope out of the axoneme structure as a result of ATP-dependent active sliding between the outer doublet microtubule pairs (figure 1.10). A similar study of *Tetrahymena* cilia then revealed the unidirectional nature of microtubule sliding in which dynein arms attached to the A-subfibre were shown to translocate the B-sufibre in a base to tipward direction (Sale & Satir, 1977). The active role of dynein in this process was confirmed by reconstitution experiments. The selective removal of outer arm dynein from the axonemes of sea urchin spermatozoa, for example, showed a reduced beat frequency (Gibbons & Gibbons, 1973), which could be partially restored by the recombination of outer arm extract with dynein-depleted axonemes (Gibbons & Gibbons, 1979; Yano & Miki-Noumura, 1981a). Similarly, outer arm extract restored wildtype motility in a slow swimming *Chlamydomonas* mutant lacking the entire outer arm (Sakakibara & Kamiya, 1989).

Other studies revealed more specific aspects of the dynein ATPase cyclical interaction (figure 1.9). Electron microscopy analysis revealed the presence of crossbridges formed by the dynein arms in the absence of MgATP (Gibbons & Gibbons, 1974). In addition, a

study involving purified *Tetrahymena* dynein and extracted doublet microtubules revealed that dynein, bound specifically to the B-subfibre, was released upon the addition of MgATP (Takahashi & Tonomura, 1978; Mitchell & Warner, 1980). Dynein ATPase activity was also shown to be activated either as a result of reconstitution into dynein-depleted axonemes (Gibbons & Fronk, 1979; Yokota *et al.*, 1987), or as a consequence of exposure to purified microtubules (Omoto & Johnson, 1986; Shimizu *et al.*, 1992). Furthermore, the interaction between dynein and microtubules was studied with the development of *in vitro* motility assays in which dynein adsorbed to a glass coverslip was shown to cause the ATP-dependent translocation of microtubules (Paschal *et al.*, 1987; Vale & Toyoshima, 1988, 1989; Sale & Fox, 1988). Taken together these experimental observations provided evidence for the ATP-driven dynein-microtubule cyclical interaction underlying cilia and flagella motility.

free doublets   doublets slide apart   doublets held in   doublet sliding
(cross-links removed   cilium by   leads to bend formation
by detergent)   cross-links
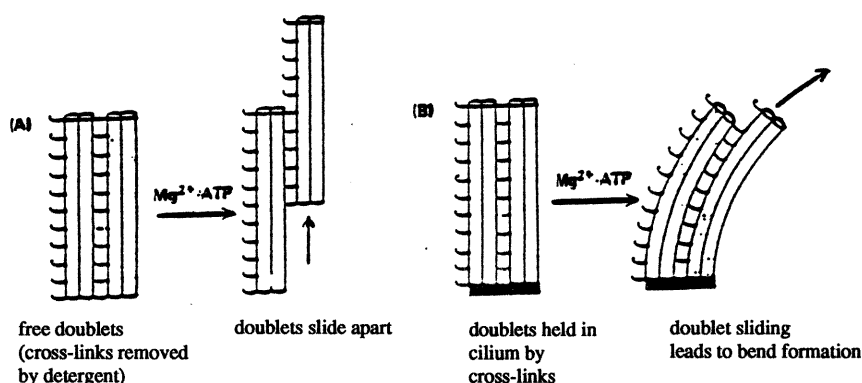
Figure 1.10. Diagrammatic representation of microtubule sliding within a partially proteolysed axoneme (from Alberts *et al.*, 1983).

18

1.6. Regulation of motility

The coordination of dynein and microtubules required to produce the characteristic bending of cilia and flagella is a complex process and precisely how microtubule sliding is converted into bending is currently unclear. The differential functions of the inner and outer arms, however, indicate at least two levels of control. The fundamental role of the inner arm is demonstrated by the complete paralysis of some inner arm-deficient *Chlamydomonas* mutants (Huang *et al.*, 1979; Kamiya *et al.*, 1991). In contrast, *Chlamydomonas* mutants deficient in the outer arm are generally motile but exhibit a reduced beat frequency (Mitchell & Rosenbaum, 1985; Kamiya & Okamota, 1985). The generation and frequency of flagella beating may therefore be differentially controlled within the axoneme.

1.6.1 Radial spokes and the dynein regulatory complex

A possible regulatory mechanism for motility could involve the dynein arms (particularly the inner arm), radial spoke proteins, and a recently discovered 'dynein regulatory complex'. The association of these axonemal components with a potential regulatory role was identified by the discovery of an unusual class of *Chlamydomonas* mutations known to suppress the paralysis of axonemes devoid of radial spoke proteins or central pair microtubules (Huang *et al.*, 1982). Several *suppressor* mutations, as they are known, restored the motility of previously paralysed spoke-less mutants without restoring the lost axonemal components. This resumed motility was thought to indicate a potential regulatory mechanism for flagellar beating and was investigated further.

The analysis of *Chlamydomonas* suppressor mutations revealed defects in the dynein arms (most notably the inner arm) involving subsets of six polypeptides of mass 108, 83, 65, 60, 40, and 29kDa (Piperno *et al.*, 1992). This complement of peptides was thought to represent a radial spoke specific control system (Huang *et al.*, 1982) or more recently termed 'dynein regulatory complex' (Piperno *et al.*, 1992). This complex of peptides was shown to represent a crescent-shaped structure located within the axoneme above the radial spoke protein designated S2 (Mastronarde *et al.*, 1992; Gardner *et al.*, 1994). Furthermore, the complex was thought to be physically linked to a specific inner arm species designated

I2 (Piperno *et al.*, 1992; Piperno *et al.*, 1994) {section 1.12.2}. Three low molecular mass polypeptides {actin (42kDa), p28 (28kDa) and centrin (19kDa)} were shown to associate with the inner arms (via an actin-p28-centrin complex) and provide a means of interaction between the inner arms, dynein regulatory complex, and the closely-associated radial spokes proteins (Piperno *et al.*, 1992). These components were then considered to represent a regulatory system through which the inner arms could be controlled.

Further study showed that microtubule sliding, induced by the inner dynein arm, could be activated by a radial spoke-dependent modification mechanism. This effect was discovered in an analysis of suppressor mutants using the sliding-disintegration assay previously described (figure 1.10). In this way, flagella bending and microtubule sliding were uncoupled and could be studied independently (Smith & Sale, 1992). Microtubule sliding velocities were then measured for two *Chlamydomonas* mutants; one lacking the outer dynein arm (*pf*28), and the other deficient in both outer arms and radial spokes (*pf*14*pf*28). The study revealed that flagella lacking both outer dynein arms and radial spoke proteins (*pf*14*pf*28), had significantly slower microtubule sliding velocities than a mutant solely deficient in the outer arm (*pf*28). This suggested that the radial spokes had, in some way, modified the inner arm to activate microtubule sliding. Furthermore, this activation was regarded as stable since the dynein-depleted axonemes of both mutants (*pf*28 and *pf*14*pf*28) exhibited equivalent sliding velocites after reconstitution with their respective dynein extracts. The inner dynein arms were therefore shown to be activated by the radial spokes (Smith & Sale, 1992). A similar interaction with the outer dynein arm was also indicated by the identification of suppressor mutations with defects in the β heavy chain of *Chlamydomonas* outer arms (Huang *et al.*, 1982; Porter *et al.*, 1994). Consequently, in *Chlamydomonas* at least, both the outer and inner dynein arm are thought to be regulated by a radial spoke-dependent modification mechanism.

1.6.2. Phosphorylation

Another level of regulation was indicated by the phosphorylation of polypeptide components associated with the outer dynein arm. These polypeptides include a 29kDa light chain from *Paramecium* (Barkalow *et al.*, 1994; Walczak & Nelson, 1993), four

components (78, 76, 47 and 23kDa) from *Tetrahymena* (Chilcote & Johnson, 1990), and multiple sites within the α heavy chain of *Chlamydomonas* outer dynein arm (Piperno & Luck, 1981; King & Witman, 1994).

The effect of either outer or inner arm phosphorylation is as yet undefined. A potential mechanism, however, is thought to involve calcium ions and cyclic AMP (cAMP), as second messengers, since both have been shown to affect motility in dynein (for review see Satir *et al.*, 1993). Despite differences in the overall response, at least one action of both cAMP and calcium ions is thought to involve the phosphorylation of proteins. Calcium ions are believed to operate through a calcium/calmodulin-dependent kinase. Evidence for this pathway comes from the identification of the calcium-binding protein calmodulin in the axonemes of *Tetrahymena* (Jamieson *et al.*, 1979), and the observation that calcium ions and calmodulin have a stimulatory effect on the axonemes of calmodulin-deficient cilia (Blum *et al.*, 1980). In contrast, support for a pathway involving cAMP-dependent protein kinases originates from the isolation of an axonemal *Tetrahymena* kinase (Chilcote & Johnson, 1990), and a 29kDa light chain (thought to be associated with the outer arm) in *Paramecium* which was shown to be exclusively phosphorylated by a cAMP-dependent protein kinase (Walczak & Nelson, 1993).

In summary, axonemal dynein is a large multisubunit motor protein responsible for the motility of eukaryotic cilia and flagella. The fundamental role is that of a minus-end directed translocator in which adjacent microtubules in the axoneme are translocated relative to one another in a proximal direction. The conversion of microtubule sliding into bending is a complex process which may involve a radial spoke-dependent modification mechanism and the phosphorylation of inner and outer arm components.

Section C

Studies on Dyneins Isolated from *Tetrahymena, Chlamydomonas*, and Sea
Urchin Sperm

The work presented in this thesis involves the study of axonemal dynein isolated
exclusively from the protozoan *Tetrahymena thermophila*. *Tetrahymena* represents one of
the three main species from which dynein has been extensively studied. These species,
and their main advantages and disadvantages, are outlined in table 1.1.

Species	Advantages	Disadvantages
Tetrahymena	Maximal dynein yield (multiciliate) Stability of dynein	No selective extraction of inner and outer dynein arms
Chlamydomonas	Axonemal mutants easily generated	Minimal dynein yield (bi-flagellate)
Sea urchin	Selective extraction of outer dynein arm	Low yield (single flagellum) and seasonal variation

Table 1.1. Main advantages and disadvantages associated with the three main species
utilised in the study of dynein.

Tetrahymena

Many of the early investigations on axonemal dynein utilised the multiciliated protozoan *Tetrahymena* from which two dynein ATPases were isolated and designated **14S** and **22S** (formally 30S) to reflect their differing sedimentation coefficients.

1.7. Structure and polypeptide composition

1.7.1. 22S dynein

The structure of 22S dynein (commonly called a "bouquet") comprises three globular heads attached via an equivalent number of stems to a common base (Johnson & Wall, 1983). Two of the heads measure 10nm in diameter, whereas the third head is slightly larger with a diameter of 12nm (figure 1.4). Other studies confirmed the structure (Toyoshima, 1987a) and identified additional features (Goodenough & Heuser, 1984). In particular, Goodenough & Heuser identified small globular subunits (referred to as 'feet') decorating the three stems of the bouquet structure, and less conspicuous 'stalk' projections emanating from the globular heads and measuring 13-16nm in length.

The polypeptide composition of the 22S molecule has been analysed by SDS-PAGE and shown to consist predominantly of three high molecular mass components (designated α, β, and γ) called **heavy chains** (Porter & Johnson, 1983). These heavy chains are immunologically distinct (Toyoshima, 1987b), and estimated masses have ranged from 360kDa (Warner *et al.*, 1977) to 560kDa (Mabuchi & Shimizu, 1974) as a consequence of the inadequacey of electrophoresis, and lack of appropriate standards, in the high molecular mass range. Improved mass estimates have been more recently determined using the technique of vanadate-dependent photolysis (section 4.6.3). The application of this technique has enabled the three heavy chains α, β, and γ, to be estimated as 417kDa, 420kDa, and 403kDa respectively (Marchese-Ragona *et al.*, 1989).

In addition to the heavy chains, 22S dynein consists of at least three intermediate chains of approximately 100, 85, and 70kDa (Porter & Johnson, 1983) and an, as yet, undetermined number of light chains. The precise molecular organisation of these polypeptides is currently unclear, although a comparison with other species suggests that the intermediate

and light chains form a tight complex localised at the base of the molecule (section 1.11.1). In addition, each globular head has been shown to equate to a significant proportion of the dynein heavy chain since the estimated mass of each heavy chain (predicted using vanadate-dependent photolysis), was shown to be comparable to the mass of a single head determined by scanning transmission electron microscopy (Marchese-Ragona et al., 1989; Johnson & Wall, 1983).

1.7.2. 14S dynein

By comparison, the structure of 14S dynein is much less well-defined and studies are restricted to those of Marchese-Ragona et al. (1988) in which a heterogeneous population of two types of molecule were discovered. One population was described as a single ellipsoidal globular head (9.5nm x 14.5nm), whilst the other comprised a globular head, of equivalent dimensions, but with an additional 24nm stem or tail region (figure 3.1). The work presented in this thesis, however, indicates that the composition of 14S dynein is more complex than originally proposed.

1.8. Localisation

1.8.1. 22S dynein

The widespread acceptance that 22S is an outer arm dynein has come from a number of studies. Electron microscopy of the *in situ* outer arm and isolated 22S species showed significant similarities (Goodenough & Heuser, 1984). Minor differences observed, such as the splayed arrangement of the three globular head domains in the 22S structure and the tight triangular configuration of the outer arm, were thought to reflect artefacts of the extraction procedure. An outer arm location was also indicated by the regular periodicity with which both the outer arm and isolated 22S dynein bound along the length of the A-subfibre within the axoneme. In longitudinal section the outer arms from *Tetrahymena thermophila* were shown to repeat with a regular 24nm-periodicity (Avolio et al., 1986). In comparison, studies on purified 22S dynein showed this molecule bound with an equivalent periodicity to outer arm-deficient axonemes (Hyams, 1985), purified bovine brain microtubules (Porter & Johnson, 1983a) and repolymerised axonemal microtubules

(Omoto & Johnson, 1986). In addition, immuno-electron microscopy investigations of axonemes showed that antibodies raised against 22S dynein bound specifically to the outer arm location (Crossley *et al.*, 1991). More recently, investigations involving a temperature-sensitive mutant of *Tetrahymena thermophila* revealed that mutant axonemes lacked 90% of the outer arms when cultivated at the restrictive temperature of 39°C (Attwell *et al.*, 1992). This outer arm deficiency was then correlated to a significant reduction in levels of 22S dynein within the axoneme (Ludmann *et al.*, 1993).

1.8.2. 14S dynein

The location of 14S dynein within the axoneme is much more controversial though the most likely location is thought to be that of the inner dynein arm. The possibility of alternative or additional locations, however, cannot be excluded. Dynein ATPases distinct from the arm-like appendages, for example, have been identified in the ciliary membranes of the axoneme (Dentler *et al.*, 1980; Dentler, 1988). In addition, 14S dynein has been implicated in the protein complex surrounding the two central singlet microtubules of the axoneme (section 1.4). Evidence for this location originates from an observation of the translocational properties of the isolated protein. In the presence of MgATP, 14S dynein, which had been adsorbed to a glass surface, was shown to cause the rotational translocation of purified microtubules (Vale & Toyoshima, 1988). This motion was thought to resemble the rotational element previously described in association with the central pair microtubules of *Chlamydomonas* (Hosokawa & Miki-Noumura, 1987), *Paramecium* (Omoto & Kung, 1980), and sea urchin sperm (Gibbons *et al.*, 1987b). Consequently, the central pair is considered a possible location for 14S dynein.

1.9. Function

1.9.1. 22S dynein

The functional role of 22S dynein in the cyclical ATP-sensitive reaction underlying cilia and flagella motility (section 1.5.2) has been indicated by a number of studies including the determination of the complete microtubule-dynein ATPase pathway (Johnson, 1983; Shimizu & Johnson, 1983a; Omoto & Johnson, 1986) {figure 1.9}. Preliminary studies

revealed that 22S dynein bound in an ATP-sensitive manner to microtubules (Takahashi & Tonomura, 1978; Mitchell & Warner, 1980; Porter & Johnson, 1983). This transient interaction was shown to occur via the 'broader' end of the molecule corresponding to the three globular heads (Porter & Johnson, 1983). Subsequent studies then showed that ATPase activity was localised to the three head domains of the molecule. Proteolytic analysis revealed that double-headed and single-headed molecules exhibited ATPase activity (Toyoshima, 1987b; Niino & Miki-Noumura, 1992), whereas kinetic studies indicated three ATP-sensitive sites per molecule (Shimizu & Johnson, 1983a).

Further evidence for the interaction between dynein and microtubules was indicated by the activation of ATPase activity in the presence of microtubules (Omoto & Johnson, 1986). In addition, the microtubule-dynein interaction was analysed by the use an *in vitro* motility assay in which the ATP-dependent translocational movements of microtubules, by dynein adsorbed to a glass surface, could be monitored. Preliminary studies showed that in the presence of MgATP, 22S dynein caused a short and discontinuous minus-end directed translocation of microtubules (Vale & Toyoshima, 1988). More recently, however, this erratic motion has been attributed to an artefact of the assay procedure and is now thought to reflect the random orientation of 22S molecules on the glass surface. Improved assays have shown that 22S dynein translocates microtubules *in vitro* at a faster rate (12μm/second as opposed to 8μm/second) and in a smooth and continuous manner (Mimori & Miki-Noumura, 1994).

1.9.2. 14S dynein

The uncertain location of 14S dynein has made it particularly difficult to suggest a functional role for this motor. Nevertheless, the 14S does exhibit characteristic properties of a motor protein presumed to partake in the force-generating processes underlying cilia and flagella motility. The 14S exhibits a microtubule-activated ATPase activity, can bind to purified microtubules in an ATP-sensitive manner (Shimizu *et al.*, 1992), and can translocate microtubules in the presence of MgATP (Vale & Toyoshima, 1988).

1.10. Regulation

Regulation of 22S dynein may involve phosphorylation since an axonemal cAMP-dependent protein kinase was shown to phosphorylate 22S dynein *in vitro* (Chilcote & Johnson, 1990). The targets of phosphorylation were identified as four intermediate and light chains of estimated mass 78, 76, 47, and 23kDa. The regulation of 14S dynein has been implicated by the copurification of the calcium-binding protein calmodulin (Jamieson *et al.*, 1979). Furthermore, a significant enhancement of ATPase activity was demonstrated following the exposure of calmodulin-depleted 14S dynein to a calcium/calmodulin mix thus implicating a calcium-dependent regulatory pathway (Blum *et al.*, 1980).

Chlamydomonas

Chlamydomonas is a unicellular green algae characterised by the presence of two flagella. This species has been particularly valuable in the investigation of dynein since the relative ease with which specific axonemal mutants can be isolated has enabled the **outer** and **inner** dynein arms to be unambiguously studied.

1.11. The outer arm

1.11.1. Structure and polypeptide composition

The outer dynein arm of *Chlamydomonas* has been identified by electron microscopy analysis of a mutant (*pf23*) specifically deficient in the inner dynein arm (Goodenough & Heuser, 1984). The dynein isolated from this mutant was shown to be similar in structure to the "bouquet" arrangement previously described for *Tetrahymena* 22S dynein (section 1.7.1). Three globular heads are interconnected via three stems to a common base. As with *Tetrahymena*, additional components include stem-associated decorative elements and stalk projections emanating from each globular head. Similarly, the isolated dynein molecule and the *in situ* arm are regarded as equivalent. One distinguishing feature of the isolated *Chlamydomonas* outer arm, however, is that the bouquet structure readily dissociates under conditions of high ionic strength to form a two-headed and a single-headed species. These structures are referred to as 18S and 12S respectively since they are considered to be equivalent to two dynein ATPases previously identified by the high-salt extraction of inner arm-deficient mutants (Huang *et al.*, 1979; Piperno & Luck, 1979a). The 18S possesses two globular head domains measuring 12.7nm in diameter and interconnected by a "Y-shaped" filamentous stem (Witman *et al.*, 1983), whereas the 12S species is described as a single globular head with a stem attachment (Goodenough *et al.*, 1987).

The high salt-induced dissociation of the isolated outer dynein arm facilitated the analysis of polypeptide composition. The single-headed 12S species was shown to consist of one heavy chain component, designated γ, and three light chains (Piperno & Luck, 1979a; King & Witman, 1988). In contrast, the 18S comprised two heavy chains, termed α and β, two

intermediate chains, and eight light chains (Piperno & Luck, 1979a; Pfister & Witman, 1984). This latter complement of polypeptides could be further investigated by the subfractionation of the 18S species. Two smaller components (derived from the low ionic strength-dissociation of 18S) were separated by density gradient centrifugation and the polypeptides associated with each subunit investigated (Pfister & Witman, 1984). One subunit, termed α, comprised the α heavy chain and a 16kDa light chain whereas, the β subunit possessed the β heavy chain and remaining intermediate (78kDa and 69kDa) and light chains (8-20kDa).

An analysis of heavy chain mass indicated that each globular head visualised by electron microscopy was too small to include an entire heavy chain. Consequently, a proportion of each heavy chain was thought to contribute to the 'non-head' regions of the dynein molecule (King & Witman, 1987, 1988; Witman *et al.*, 1983). Other polypeptide components were also localised. Antibodies recognising epitopes on a specific intermediate chain (IC-69) associated with 18S dynein were shown to localise to the base of the molecule (King & Witman, 1990). In addition, the tight association of this polypeptide with the 78kDa intermediate chain (IC-78) and four light chains, led to the proposal that the base of the molecule was the location of an intermediate-light chain complex (King & Witman, 1990; Mitchell & Rosenbaum, 1986; King *et al.*, 1991). Furthermore, IC-78 was shown to interact *in situ* with α-tubulin and therefore thought to provide a potential site for structural attachment (King *et al.*, 1991).

1.11.2. Function and regulation

The fundamental role of the outer dynein arm is that of a force-generator in the cyclical microtubule-dynein ATPase reaction underlying flagella motility. Detailed analysis of this function has been possible following the identification of *Chlamydomonas* mutants specifically deficient in outer arm components. The α and β heavy chains, for example, have been localised to two of the three force-generating head domains associated with the outer arm. The outer most appendage of the *in situ* three-headed molecule was shown to be absent in a mutant lacking the α heavy chain (Sakakibara *et al.*, 1991), whereas the β heavy chain was localised to the second of the three heads (Sakakibara *et al.*, 1993). In

terms of function, the outer arms were indicated as generators of force and speed since mutants completely deficient in this structure were slow swimming and had a reduced beat frequency (Kamiya & Okamoto, 1985; Mitchell & Rosenbaum, 1985). More specifically, the function of each head was determined by an analysis of mutants deficient in outer arm components. One mutant (designated $oda11$), shown to lack the α heavy chain and a 16kDa light chain, exhibited a reduced (119μm/sec) swimming speed (Sakakibara et al., 1991). In contrast, a mutant (designated oda4-s7) lacking the carboxy-terminus of the β heavy chain was shown to have a considerably more marked effect on motility since the swimming speed was reduced to 65μm/sec (Sakakibara et al., 1993). This polypeptide was therefore implicated as a major force-generating unit of the outer arm.

The α and β heavy chains of the outer dynein arm are thought to be regulated by at least two levels of control. Firstly, phosphorylation has been implicated by the observation that the α heavy chain has been shown to undergo phosphorylation in vivo (King & Witman, 1994). Secondly, a radial spoke-dependent regulatory mechanism may be involved since suppressor mutations have been identified within the β heavy chain of the outer dynein arm (Huang et al., 1982; Porter et al., 1994).

1.12. The inner arm

1.12.1. Structure

The inner dynein arm of Chlamydomonas is much more complex than that of the outer arm as indicated from the number of different inner arm mutants obtainable. Evidence for inner arm heterogeneity was first indicated when five heavy chain components possessing ATPase activity were identified for an outer arm-deficient mutant (Huang et al., 1979; Piperno & Luck, 1979a, 1981). The heavy chains were thought to originate from the inner arm since they were not only distinguishable from previously described outer arm dynein heavy chains, but were also specifically lacking in mutants displaying variable levels of inner arm deficiency (Huang et al., 1979; Piperno & Luck, 1981). These multiple inner arm heavy chains indicated the existence of more than one type of inner arm structure within the axoneme (Piperno, 1988) since dyneins with more than three heads (and more than three heavy chains) have not been identified. Furthermore, two morphologically

distinct inner arm structures were identified within the axoneme (Goodenough & Heuser, 1985). These structures represented three-headed (termed triad) and double-headed (termed dyad) molecules shown to repeat with a 96nmn periodicity (in accordance with the radial spoke proteins) along the length of the axoneme in a dyad-dyad-triad array (figure 1.11).
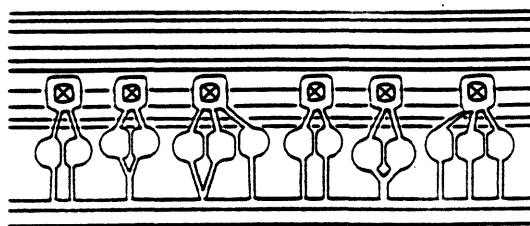
Figure 1.11. Schematic representation of the dyad-dyad-triad array of inner dynein arms situated along the A-subfibre of the outer doublet microtubules and extending (by stalk projections from the heads) to an adjacent B-subfibre (from Goodenough & Heuser, 1985). Radial spokes are represented as X's and project outwards from the page.

The relationship between the inner arm heavy chain composition and the two distinct inner arm structures visualised on the axoneme were investigated further. A detailed structural study involved a comparison of the *in situ* inner arm structure with that of the isolated dynein (Goodenough *et al.*, 1987). In this work, high-salt extracted dynein was fractionated into five peaks (using HPLC) and identified as inner or outer dynein arm components by comparison of the fractionation profile for both wild type and dynein arm mutant axonemes. Three peaks were then identified as inner arm components and shown to consist predominantly of one or two heavy chains. Electron microscopy analysis of these peaks revealed three structures; two distinct single-headed species (each with a single slender stem and a stalk projection), and a double-headed structure connected by two stems. Comparisons with the heavy chain composition showed that, as with outer arm dyneins, the number of heavy chains and globular-head domains were equivalent. The structures associated with the three isolated fractions were then compared to the dyad-

dyad-triad morphology of the *in situ* inner arm (Goodenough & Heuser, 1985).
Similarities between the structures suggested that the isolated double-headed species was
equivalent to the *in situ* triad (although a third head was not identified), whereas the single-
headed species were thought to constitute the dyad either as homo- or hetero-dimers
(Goodenough *et al.*, 1987).

<u>1.12.2. Polypeptide composition and inner arm organisation</u>

A model for the organisation of the inner arms was proposed following the studies of
Piperno *et al.* (1990) in which a sixth heavy chain was identified. In this study, specific
mutants were used to compare deficiencies in heavy chain composition with changes in
inner arm structure. Two mutants (*pf*30 and *pf*23) were shown to be specifically deficient
in subsets of the six inner arm heavy chains which were designated 1α, 1β, 2, 2', 3, and 3'.
The *pf*30 mutant was shown to be deficient in the two heavy chains 1α and 1β, whereas the
*pf*23 mutant lacked the four heavy chains 1α, 1β, 2 and 2'. These heavy chain deficiencies
were then investigated with respect to the dyad-dyad-triad inner arm structures associated
with the wildtype axoneme (figure 1.11). Electron microscopy analysis revealed a loss of
one or two of the three discrete structures described for the inner arm which was correlated
with deficiencies in pairs of heavy chains. The *pf*30 mutant for example, which was
known to lack heavy chains 1α and 1β, was deficient in a discrete inner arm structure
designated I1. In comparison, the *pf*23 mutant, which was deficient for the four heavy
chains 1α, 1β, 2 and 2', was characterised by an absence of two discrete units referred to as
I1 and I2 respectively. In addition, a third inner arm I3 was unaffected by either mutant
but was thought to represent the third inner arm structure identified in wildtype axonemes
and was believed to correspond to the two remaining heavy chains designated 3 and 3'
(Piperno *et al.*, 1990).

These results were thought to reflect the existence of three types of inner arm each
comprising two heavy chain components. The three species of inner arm were termed I1,
I2, and I3 and were shown to consist of the pairs of heavy chains denoted 1α, 1β; 2, 2'; and
3, 3' respectively. In addition to heavy chain composition, each inner arm structure was
shown to consist of a unique complement of intermediate and light chain components. I1

was shown to comprise at least one (140kDa), and possibly two (97kDa), intermediate chains (Piperno *et al.*, 1990; Smith & Sale, 1991). In contrast, the heavy chains associated with I2 and I3 were shown to cosediment with four components (133, 42, 28, and 19kDa) on density gradients as an 11S mixture (Piperno *et al.*, 1990). One light chain (42kDa) was previously identified as as a form of actin (Piperno & Luck, 1979b), whereas another (19kDa) was shown to be closely related to the calcium-binding protein centrin (Piperno *et al.*, 1990). The exact relationship of these components to either inner arms I2 and I3 has yet to established. Indeed, the existence of the I3 inner arm remains uncertain since mutants specifically deficient in these heavy chain components (3 and 3') have yet to be identified. Furthermore, I2 and I3 are structurally indistinguishable and sediment on density gradients as an 11S mixture (Smith & Sale, 1991).

This model of inner arm organisation was further refined by a more detailed analysis of mutant and wildtype axonemes (Piperno & Ramanis, 1991). As a result of this study, two significant modifications of the model were defined. Firstly, it was suggested that the inner arms I2 and I3 were composed of identical subunits. I2 was predicted to consist either of two heavy chains denoted 2, or of a pair of heavy chains denoted 2', but not of a combination. This interpretation was based upon studies of mutant axonemes in which deficiencies in identical pairs of heavy chains associated with I2 or I3 were correlated with a complete loss of the corresponding inner arm structure (Piperno & Ramanis, 1991). Secondly, this loss in structure was only identified when specific regions of the axoneme were analysed. As a result, inner arms I2 and I3 were proposed to be differentially distributed along the length of the axoneme. Mutants affecting motility and flagella length, for example, exhibited a specific deficiency in a subset of heavy chains corresponding to inner arms I2 and I3. In addition, the molecular composition of the proximal and distal regions of axonemes were shown to be specific (Piperno & Ramanis, 1991). The proximal region of the axoneme consisted predominantly of heavy chains 2 and 3', whereas the distal region comprised heavy chains 2' and 3 (figure 1.12).

	S1 S2
○ 1 α	
≋ 1 β	I1 ⊤ I2 ⊤ I3
● 2'	
○ 2	
⊙ 3	
⬢ 3'	

Proximal   Distal
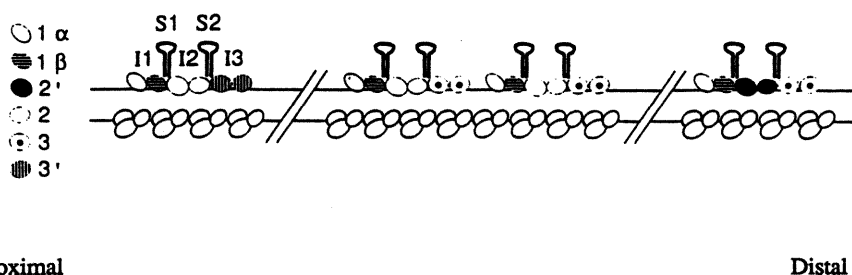
Figure 1.12. Schematic representation of the proposed inner arm organisation for the three species of inner arm (I1, I2, and I3) viewed in longitudinal section along the axoneme of *Chlamydomonas* (from Piperno & Ramanis, 1991). Inner arm heavy chains (HC's) are indicated by ellipses as shown. Inner arm I1 (comprised of HC's 1α and 1β) is located along the entire axoneme. HC 2 (associated with inner arm I2) is localised to the proximal and middle regions; HC 2' (associated with inner arm I2) is localised in the distal region; HC 3 is localised in the middle and distal regions; HC 3' is localised in the proximal region. The position of radial spoke proteins (S1 and S2) and the outer dynein arm (three overlapping ellipses) are indicated.

The increasing complexity of the arrangement of inner dynein arms was further revealed by two independent studies. One study showed the existence of two rows of inner arm and at least ten discrete globular structures in each 96nm repeating unit (section 1.4) using electron microscopy analysis (Muto *et al.*, 1991; Mastronarde *et al.*, 1992). In addition, a second study identified two additional heavy chains bringing the total number of distinct inner arm heavy chains to eight (Kagami & Kamiya, 1992). Both observations indicated that several more species of inner dynein arm exist.

1.12.3. Function and regulation

The function of multiple inner arm dyneins in *Chlamydomonas* has yet to be established. Preliminary investigations involving *in vitro* motility assays, however, have revealed that most are capable of microtubule translocation when adsorbed onto a glass surface. Six of seven inner arm subspecies (isolated by the HPLC fractionation of outer arm-deficient mutants) were identified as minus-end directed microtubule translocators (Kagami & Kamiya, 1992). In addition, five of these species demonstrated a rotation of microtubules

34

similar to that previously reported in *Tetrahymena* 14S dynein (Vale & Toyoshima, 1988). The isolated inner arm designated I1 was also shown to bind and cross-link microtubules in an ATP-dependent manner, whereas an 11S mixture of inner arms I2 and I3, revealed no microtubule-binding capabilities (Smith & Sale, 1991).

Regulation of the multiple inner arm species has been implicated by the close association of the dynein regulatory complex and some species of inner arm (Piperno *et al.*, 1992; Mastronarde *et al.*, 1992; Gardner *et al.*, 1994). Furthermore, the identification of inner arm suppressor mutations, which override the paralysis of radial-spoke deficient mutants, supports a role for some inner arm species in the radial spoke-dependent regulatory mechanism (Huang *et al.*, 1982; Smith & Sale, 1992). Finally, the close association of the calcium-binding protein centrin with inner arm species suggest that control of motility may involve a calcium-mediated regulatory pathway (Piperno *et al.*, 1990).

Sea Urchin Sperm

Another source of dynein has been the spermatozoa of some sea urchin species which include *Tripneustes, Colobocentrotus, Strongylocentrotus,* and *Psedocentrotus.* One major advantage of this dynein source is that the outer and inner arms can be unambiguously identified since the outer arm can be selectively removed from the axoneme following a high-salt extraction procedure (Gibbons & Gibbons, 1973).

1.13. The outer arm

1.13.1. Structure and polypeptide composition

The structure of the isolated outer arm (or 21S dynein) was first described as a double-headed molecule in which each head domain measured approximately 10nm in diameter (Yano & Miki-Noumura, 1981b). A more detailed structural analysis then showed that the two globular heads were interconnected by two irregularly-shaped stems (Sale *et al.,* 1985). One of the head domains was described as 'pear-shaped' with diameters of 18.5nm and 12.5nm, whilst the other head measured 14.5nm in diameter and was roughly spherical. In addition, decorative elements were described in association with the stem.

The isolated dynein structure was then proposed to be equivalent to the *in situ* outer dynein arm (Sale *et al.,* 1985). As well as significant structural similarity, 21S dynein (then called dynein 1) was shown to recombine with high-salt extracted axonemes to restore both structural and functional characteristics of the outer arm (Gibbons & Gibbons, 1979; Yano & Miki-Noumura, 1981a). In addition, this high-salt extraction was shown to correlate to the selective removal of the outer arms whilst the inner arms remained intact (Gibbons & Gibbons, 1973).

The polypeptide composition of the 21S outer dynein arm was shown to comprise two heavy chains (designated α and β), three intermediate chains of mass 112, 79 and 70kDa (designated IC-1, IC-2, and IC-3 respectively), and six light chains between 23 and 6kDa (Tang *et al.,* 1982; Moss *et al.,* 1992b). A determination of the molecular organisation of these polypeptides was assisted by the dissociation of 21S dynein into three smaller particles following low ionic strength-dialysis (Tang *et al.,* 1982; Sale *et al.,* 1985). Under

36

these conditions, the double-headed outer arm was shown to dissociate into two single-headed species and a cluster of three stem-associated elements (Sale *et al.*, 1985). The polypeptide composition of the two major single-headed components was then analysed. The spherical head domain was shown to consist of the α heavy chain (designated the α subunit) whereas, the 'pear-shaped' head and associated stem comprised the β heavy chain and intermediate chain 1 (designated the β/IC-1 subunit) (Tang *et al.*, 1982). Finally, the three-bead cluster associated with the base of the stem was thought to be equivalent to an intermediate chain/light chain complex comprising intermediate chains 2 and 3 (IC-2, IC-3) and at least five light chain components (Tang *et al.*, 1982; Moss *et al.*, 1992a, 1992b; Witman *et al.*, 1991).

Further investigation confirmed that the two-headed 21S particle was an α–β/IC1 heterodimer. Reconstitution experiments revealed that the α and β/IC-1 subunits could recombine in approximately equal amounts to form a partially reformed 21S molecule (Tang *et al.*, 1982), and mass analysis indicated that a single copy of each α and β heavy chain was present in the intact molecule (Bell & Gibbons, 1982). Each globular head domain was therefore shown to consist predominantly of a single heavy chain (Sale *et al.*, 1985), whereas an intermediate and light chain complex is thought to associate with the base of the stem (Witman *et al.*, 1991).

1.13.2. Function

The outer dynein arm is presumed to have a function in the cyclical microtubule-dynein ATPase reaction underlying flagella motility since selective extraction from the axoneme results in a significant reduction in flagella beat frequency (Gibbons & Gibbons, 1973) which can be restored upon reconstitution with 21S dynein (Yano & Miki-Noumura, 1981a). Similarly, the outer arm has been shown to induce the ATP-dependent translocation of microtubules from the minus to the plus end (Summers & Gibbons, 1971, Kamimura *et al.*, 1985) and possesses a microtubule-activated ATPase activity (Yokota *et al.*, 1987). The function of the individual components of the outer arm dynein has been partly investigated by the isolation of α and β/IC-1 subunits. The β/IC-1 subunit has been shown to support ATP-dependent minus-end-directed gliding of microtubules when

adsorbed onto a glass surface (Sale & Fox, 1988; Vale *et al.*, 1989). Furthermore, analysis of the amino acid sequence for the β heavy chain revealed a probable catalytic ATP-binding site and potential microtubule-binding region (Ogawa, 1991; Gibbons *et al.*, 1991). In contrast, the α subunit did not support translocation despite binding to microtubules in both the presence and absence of ATP (Moss *et al.*, 1992b). The β/IC-1 subunit was therefore thought to be the main force generating region of the molecule (Moss *et al.*, 1992a), whereas the α subunit was presumed to effect microtubule binding. In comparison, both properties were exhibited by the intact outer arm (Paschal *et al.*, 1987). Consequently, the function of the outer arm is thought to be divided between the two predominant components.

1.14. The inner arm

The inner arm of sea urchin spermatozoa has been much less intensely studied. A functional role in motility, however, has been demonstrated by the unidirectional (minus to plus end) sliding of microtubules induced by the presence of MgATP in the absence of the outer dynein arms (Fox & Sale, 1987). In contrast, a detailed investigation of the isolated inner arms has been slow due to both the difficulty of inner arm extraction and the relatively low quantity of dynein obtainable. Consequently, *in vitro* studies have been limited to an investigation of the heavy chain components remaining after the high-salt extraction of the outer dynein arm. Several heavy chains have been identified for sea urchin sperm dynein and are designated as C, Aα, Aβ, D and B (Gibbons *et al.*, 1976; Inaba *et al.*, 1988). The heavy chains Aα and Aβ are the major constituents of the 21S outer dynein arm (Tang *et al.*, 1982). In contrast, the D and B heavy chains have a currently unspecified location, whereas heavy chain C has been proposed to have an inner arm location (Yokota & Mabuchi, 1994a).

The localisation of heavy chain C to the inner dynein arm originated from the observation that a complex comprising two heavy chains (C and A), two intermediate chains (120kDa and 103kDa), and four light chains, could be routinely extracted from axonemes in which the outer arm had been previously removed (Yokota & Mabuchi, 1994a). Electron microscopy analysis of axonemes (before and after extraction) showed that removal of the

complex could be correlated with a 22% loss of inner arms. Furthermore, the C/A complex was identified as a dynein by three fundamental characteristics. Firstly, the two predominant polypeptides, C and A, were of a high molecular mass estimated to be 445kDa and 425kDa respectively. Secondly, each heavy chain was considered to possess a hydrolytic ATP-binding site since both heavy chains underwent vanadate-dependent photolysis and possessed ATPase activity. Finally, electron microscopy of the C/A complex revealed a two-headed structure and interconnecting stem similar to dyneins previously described (Goodenough & Heuser, 1984; Porter & Johnson, 1983; Sale et al., 1985). Each globular head was estimated to measure 14nm in diameter, whereas the stem was of variable size. Width and length measurements, for example, were shown to vary from 6-10nm and 25-32nm respectively (Yokota & Mabuchi, 1994a).

The C/A dynein was shown to be distinguishable from 21S outer dynein arm. Heavy chains C and A were immunologically-distinct from the two heavy chains of the 21S outer arm dynein (Aα and Aβ) despite the fact that the A heavy chain was so called because it was of similar mobility to Aα. Furthermore, the enzymatic properties were distinguishable since the ATPase activity of the C/A dynein was approximately half that of the intact 21S species (Yokota & Mabuchi, 1994b). Functionally, the C/A dynein was shown to bind and cross-link microtubules, in an ATP-insensitive manner, and exhibit a microtubule-activated ATPase activity. Taken together, these results indicated that the C/A dynein was distinct from the outer dynein arm in both function and location and most likely represents an inner arm species. The characterisation of other potential inner arm heavy chains (B and D), however, have yet to be defined.

Outer arm dynein isolated from *Tetrahymena, Chlamydomonas*, and sea urchin sperm, has been extensively studied. In comparison, the inner dynein arm is much less well-characterised due to its inherent complexity and difficulties in the extraction and yield of protein obtainable. This thesis aims to characterise 14S dynein isolated from *Tetrahymena thermophila* and reveals structural heterogeneity hitherto undescribed.

Chapter 2

Materials and Methods

This chapter describes general methods used during the project. Specialised methods which are exclusive to certain results chapters are described at the beginning of the relevant chapter.

2.1. Materials

Most of the standard reagents used were of analytical grade and supplied by either Fisons or BDH. Antifoaming reagent, proteolytic inhibitors, dibucaine hydrochloride, antichicken IgG secondary antibody, and SDS-PAGE molecular weight markers, were supplied by Sigma. Neutralised bacteriological peptone and yeast extract were obtained from Oxoid. Proteose peptone was supplied by Difco, and phosphocellulose was supplied by Whatman.

2.2. Choice of organism

The organism of choice for the extraction of dynein was a mucus-deficient strain (SB255) of the protozoan *Tetrahymena thermophila* supplied by Professor J. S. Hyams, University College, London. *Tetrahymena* was utilised as a source of dynein since the organism is multiciliated and can be grown relatively easily in large cultures. The use of a mucus-deficient strain also improved the yield of cilia by facilitating the differential centrifugation of cilia from cells.

2.3. Maintenance of *Tetrahymena thermophila*

Tetrahymena was maintained at room temperature by the weekly aseptic transfer of approximately 4 x 1ml of cells to 4 x 12ml of sterile media containing 2% proteose peptone, 0.2% glucose and 0.1% yeast extract.

2.4. Cultivation of *Tetrahymena thermophila*

Two methods of cell growth were used. Method 1 involved the inoculation of cells into a single 15 litre batch of media (carboy), while method 2 used several smaller batches of media in which to inoculate the cells. In both methods, the initial culture of *Tetrahymena* was from a stock inoculated 48 hours previously as described in section 2.3.

All sterile media was produced by autoclaving at a maintained pressure of 1.05 Kg/cm^2 for 15 minutes in the case of flask solutions, and 25-30 minutes for the 15 litre carboy.

2.4.1. Method 1

For each dynein extraction procedure, 2 x 12ml of cells were used to aseptically inoculate 2 x 750ml flasks of sterile media containing 2% neutralised bacteriological peptone, 0.2% glucose, 0.1% yeast extract and 0.1mM ferrous citrate. After inoculation, both flasks were maintained at 30°C and aerated by continuously shaking the flasks in an orbital shaker at a speed of 130 revolutions per minute for 36 hours. The cultures were then aseptically transferred, along with 300ml of a 10% sterile glucose solution, to 15 litres of sterile media containing 2% neutralised bacteriological peptone, 0.1% yeast extract and 0.1mM ferrous citrate. In order to minimise the risk of contamination, inoculations were carried out using a butane gas flame in a laminar flow cabinet. After inoculation, the culture was maintained at 30°C with continuous aeration for a further 48 hours growth (figure 2.1). Aeration was achieved by passing filtered air at a rate of 6 litres per minute, through two sterile 37mm bacterial air vents with a pore size of 0.3μm (Gelman). In cases where two carboys were utilised, a T-piece tubing was used to divide the air supply. Adequate aeration was then achieved by increasing the air flow to 12 litres per minute.

2.4.2. Method 2

This method required the preparation of twenty-three 2 litre flasks containing 750ml of media (2% neutralised bacteriological peptone, 0.2% glucose, 0.1% yeast extract and 0.1mM ferrous citrate). After sterilisation, each flask was aseptically inoculated with 12ml of cells using of a butane gas flame and laminar flow cabinet to minimise the risk of contamination. Immediately following inoculation, all flask cultures were maintained at 30°C and aerated by continuously shaking the flasks in an orbital shaker at a speed of 130 revolutions per minute for 48 hours.

STERILE BACTERIAL

OVERFLOW TUBING   AIR VENTS

COARSE
FILTRATION
UNIT

ANTIFOAM

AIR
SUPPLY

CONTINUOUS AERATION OF CULTURE

Figure 2.1. Diagrammatic representation of the cultivation of *Tetrahymena* using growth method **1** (section 2.4.1).

2.5. Measurement of cell growth

The optimal growth time for cultures of *Tetrahymena* was determined using two methods. The first was to estimate the number of cells per ml by taking cell counts at regular intervals during growth. The second method was to analyse the size and quality of the cilia pellet produced at different stages after inoculation of flask cultures.

2.5.1. Cell counts

Cell growth was measured by taking a cell count at 8-12 hourly intervals after inoculation. A sample (1ml) was aseptically removed from flask cultures using a sterile graduated pipette, and NaN_3 added (to an approximate final concentration of 5mM NaN_3) in order to reduce the movements of the organisms. Individual cells were then observed at 120 x magnification under a Leitz Wetzlar light microscope, and counted with the aid of a Neubauer haemocytometer and push-button counter. The approximate number of cells (per ml) was then estimated.

2.5.2. Analysis of the cilia pellet

Growth was also monitored by an assessment of the size and quality of cilia pellets produced from 750ml flask cultures (as described in section 2.7.1). This procedure was more commonly used to monitor the quality, rather than quantity, of the cilia produced. In both procedures, cilia pellets from cultures inoculated between 24 and 80 hours previously, were assessed by estimating the proportion of contaminating debris resulting from lysed cells. Cilia which had no debris produced white pellets, whereas those with contamination from lysed cells possessed a central black region in the pellet. The density and size of this black region increased with cultivation time. An estimation of the quantity of cilia produced was determined by taking a weight measurement.

2.6. Concentration of cells

The cell cultures were concentrated at room temperature (method 1) or 20°C (method 2) prior to the extraction of dynein (section 2.7). All centrifugation steps were carried out at 20°C using a Sorvall GSA rotor in a Sorvall RC-5B refrigerated superspeed centrifuge.

2.6.1. Method 1

A 16.5 litre culture of *Tetrahymena* was concentrated using a *Millipore Pellicon* cassette cell harvester fitted with a 0.45μm hydrophilic Durapore membrane, coarse retentate screen, and peristaltic pump. Prior to use, the concentrator was flushed through with 3 litres of deionised water and 2 litres of PBS. The concentrator was then set at a rate of 0.5 litres per minute and used to concentrate the culture, to approximately 1.5 litres, by selectively removing excess media from intact *Tetrahymena* cells. In order to ensure the maximal recovery of cells, the concentrator was flushed out with 500ml of retained media. After concentrating, the cells were centrifuged at 2,603 g for 10 minutes. Immediately after centrifugation, excess media was decanted, and the pellets of intact *Tetrahymena* cells were resuspended in 6 x 50ml quantities of remaining media.

2.6.2. Method 2

The flask cultures (23 x 750ml) were individually centrifuged at 2,603 g for 10 minutes in order to concentrate the cell mass. The individual treatment of each culture enabled the identification of contaminated flasks (fungal and/or excessive bacterial contamination only) which could then be discarded. Excess media was decanted from the cell pellets. After concentration of all the flask cultures, the resulting cells were combined and centrifuged at 2,603 g for 10 minutes. The media was decanted and the remaining pellets resuspended in 6 x 50ml volume of media.

2.7. Dynein preparation

Dynein was isolated from the cilia of *Tetrahymena thermophila* essentially using the high-salt extraction procedure described by Porter & Johnson (1983). The predominant difficulty with the dynein preparation comes from the risk of releasing proteolytic enzymes from the *Tetrahymena* cell body following deciliation. In order to minimise this problem, procedures were carried out quickly, and at 5°C. EGTA-containing buffers and protease inhibitors (PMSF and leupeptin) were also used. PMSF was prepared immediately prior to use as a 0.1M stock dissolved in ethanol. A 10μg/ml stock of leupeptin was prepared in advance and stored for up to one month at -20°C. A summary of the dynein purification procedure is shown in figure 2.2.

2.7.1. Isolation of cilia

Cilia were removed from *Tetrahymena* cells using the dibucaine method (Thompson *et al.*, 1974). Deciliation is achieved using this method as a result of a rapid increase in calcium ion concentration at the basal membrane of each cilium (Papahadjopoulos, 1972).

A 300mM stock of dibucaine hydrochloride was prepared in advance and adjusted as near to pH 7 as possible by the addition of 1M NaOH. Dibucaine hydrochloride was then added, at room temperature, to 50ml volumes of concentrated *Tetrahymena* cells (section 2.6) to a final concentration of 3mM. After 3 minutes, sterile medium was added to fill the 300ml volume of each centrifugation pot. Deciliated cells were then pelleted by centrifugation at 650 g for 4 minutes using a Sorvall GSA rotor and Sorvall RC-5B refrigerated centrifuge. The supernatant was decanted and centrifuged under the same conditions for a second time to ensure the complete removal of cells. Cellular contamination of this kind was avoided in order to protect cilia from the potential proteolytic action of cellular enzymes. After centrifugation, the resulting supernatant was centrifuged at 23,430 g for 6 minutes in order to pellet the cilia. The supernatant was discarded, and the pellet resuspended, on ice, in 2 x 40ml of wash buffer (10mM Hepes, 0.1M NaCl, 4mM $MgCl_2$ and 0.1mM EGTA, pH 7.4) containing PMSF and leupeptin at a final concentration of 0.1mM and 20μM respectively. Cilia were then pelleted by centrifuging at 17,210 g in a Sorvall SS-34 rotor for 6 minutes. Resuspension and centrifugation was then repeated such that the cilia pellets were washed a total of three times to remove traces of dibucaine hydrochloride.

2.7.2. Demembranation of cilia

Cilia were demembranated on ice in 20ml of wash buffer containing a final concentration of 0.25% of a non-ionic detergent, nonidet P40. The suspension was occasionally agitated with a Pasteur pipette to release the membranes. After 30 minutes, the demembranation solution was diluted to 80ml with wash buffer and centrifuged at 38,720 g for 6 minutes. The resulting pellet of demembranated cilia was washed three times; twice in 2 x 40ml and once in 1 x 40ml of wash buffer. At each wash, 0.1mM PMSF, 20μM leupeptin and solid DTT at a final concentration of 1mM, was added.

2.7.3. Extraction of dynein

Dynein was extracted from the resulting pellet of demembranated cilia, by the addition of 15ml of a high-salt buffer containing 10mM Hepes, 0.6M NaCl, 4mM $MgCl_2$ and 0.1mM EGTA, pH 7.4. Since the size of the cilia pellet was significant with respect to the volume of extraction buffer, an appropriate quantity of a 3M stock solution of NaCl was added, to ensure a final NaCl concentration of 0.6M. After 30 minutes, dynein-extracted cilia were pelleted by centrifugation at 38,720 g for 15 minutes. The supernatant (which contains dynein) was removed for further purification. The remaining pellet (consisting of other axonemal components, predominantly tubulin) was frozen in liquid nitrogen and stored at -70°C for use in the preparation of microtubules (section 2.10.1).

2.7.4. Purification of dynein

Dynein was separated from other axonemal proteins using a 10ml DEAE-Sephacel anion-exchange column (Pharmacia). This was routinely used at 5°C and equilibrated (prior to use) at 2ml per minute with an 80mM NaCl-Tris buffer containing 10mM Tris, 80mM NaCl, 4mM $MgCl_2$, 0.1mM EGTA and 1mM DTT, pH 8. Protein extracted by 0.6M NaCl buffer (section 7.3) was diluted with a NaCl-free Tris buffer to give a final NaCl concentration of 80mM. The diluted protein was then loaded onto the Sephacel column and washed on with 20ml of 80mM NaCl-Tris buffer. Dynein was eluted using a 200mM NaCl-Tris buffer and 2ml fractions continuously collected. Maximal protein fractions were identified spectrophotometrically at 280nm, and pooled to give a final volume of approximately 17.5ml. Following the elution of dynein, tubulin was removed from the column by the addition of 500mM NaCl-Tris buffer. Maximal fractions were again located spectrophotometrically. The concentration of protein at this stage, and at the stage prior to anion-exchange chromatography (section 2.7.3), was estimated by taking an absorbance scan between 220nm and 340nm (section 2.11.1).

2.7.5. Separation of 14S and 22S dynein

The pooled fractions eluted from the DEAE-Sephacel column using a 200mM NaCl-Tris buffer, were carefully layered onto five or six 5-25% sucrose gradients, and centrifuged for 16 hours at 100,000 g and 5°C using a SW27 Beckman rotor and Sorvall OTD65B
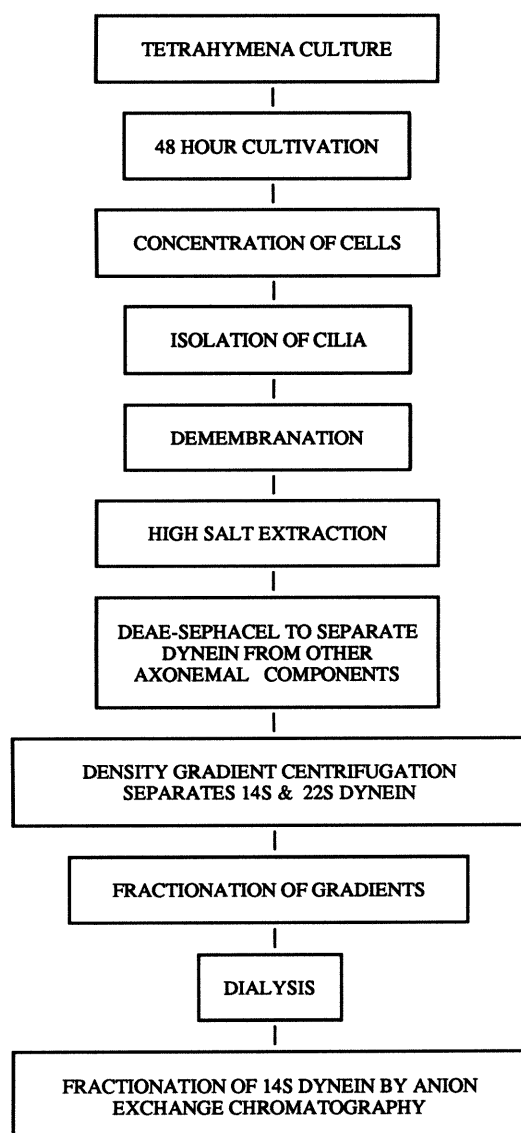
refrigerated ultracentrifuge. Sucrose gradients were prepared by freezing and thawing 31ml aliquots of a solution containing 50mM Pipes, 4mM $MgCl_2$, 0.1mM EGTA, 1mM DTT and 15% sucrose, pH 7 in 38.5ml polyallomer centrifuge tubes (25.4 x 89mm). After centrifugation, the gradients were manually fractionated into 1ml volumes. The positions of 14S and 22S dynein were determined spectrophotometrically at 280nm, and the peak fractions pooled. Sucrose was dialysed for 15 hours from 14S and 22S dynein using at least 3 x 1 litres of buffer containing 10mM Hepes, 4mM $MgCl_2$, 0.1mM EGTA, 100mM NaCl and 0.1mM DTT, pH 7.4. After dialysis, the concentration of protein was estimated by taking an absorbance scan between 220nm and 340nm (section 2.11.1)

2.7.6. Fractionation of 14S dynein using Fast Protein Liquid Chromatography

14S dynein was fractionated using fast protein liquid chromatography (FPLC). FPLC buffers **A** (10mM Hepes, 4mM $MgCl_2$, 0.1mM EGTA and 0.1mM DTT, pH 7.4) and **B** (buffer A + 1M NaCl) were filtered through a 0.2µm cellulose nitrate membrane filter (Whatman) and degassed immediately prior to use. The FPLC (Pharmacia) was coupled to a 1ml bed volume anion-exchange Mono Q HR 5/5 column (Pharmacia) and the pumps A and B filled with corresponding buffer. The functioning of the FPLC and column was routinely checked by running the elution gradient programme prior to loading 14S dynein onto the column (table 2.1). Elution gradients were produced by the differential delivery of the 1M NaCl buffer from pump B. Absorbance at 280nm, was continuously and automatically measured by a flow cell coupled to a chart recorder set at a full scale deflection of 0.2 or 0.5 absorbance units. After running the trial gradient, the column was equilibrated to 0.2M NaCl. The 14S dynein sample was then filtered through a 0.2µm Acrodisc filtration unit (Gelman) and, 25-35ml, of approximately 0.05mg/ml sample, was loaded onto the column using a 50ml capacity Superloop (Pharmacia). Once a steady baseline had been established, the elution programme was started (table 2.1) and 0.5ml fractions collected. The elution profile was monitored and all fractions kept on ice. All fractions eluted during the gradient were routinely analysed by 7.5% SDS-PAGE (section 2.12.2).

Time (minutes)	Concentration of NaCl
0	0.2M
5	0.2M*
25	0.4M*
25	1M
30	1M
30	0.2M
35	0.2M

Table 2.1. Programme used for the elution of 14S dynein fractions using FPLC (section 2.7.6). Asterisks indicate the linear gradient over which fractions are eluted.

```
          ┌─────────────────────────────┐
          │     TETRAHYMENA CULTURE      │
          └─────────────────────────────┘
                         │
            ┌──────────────────────────┐
            │    48 HOUR CULTIVATION    │
            └──────────────────────────┘
                         │
          ┌─────────────────────────────┐
          │    CONCENTRATION OF CELLS    │
          └─────────────────────────────┘
                         │
             ┌────────────────────────┐
             │    ISOLATION OF CILIA   │
             └────────────────────────┘
                         │
             ┌────────────────────────┐
             │      DEMEMBRANATION     │
             └────────────────────────┘
                         │
           ┌───────────────────────────┐
           │    HIGH SALT EXTRACTION    │
           └───────────────────────────┘
                         │
          ┌─────────────────────────────┐
          │   DEAE-SEPHACEL TO SEPARATE  │
          │      DYNEIN FROM OTHER       │
          │   AXONEMAL   COMPONENTS      │
          └─────────────────────────────┘
                         │
        ┌───────────────────────────────────┐
        │  DENSITY GRADIENT CENTRIFUGATION   │
        │     SEPARATES 14S &  22S DYNEIN    │
        └───────────────────────────────────┘
                         │
          ┌─────────────────────────────┐
          │   FRACTIONATION OF GRADIENTS │
          └─────────────────────────────┘
                         │
              ┌──────────────────┐
              │     DIALYSIS     │
              └──────────────────┘
                         │
       ┌────────────────────────────────────┐
       │  FRACTIONATION OF 14S DYNEIN BY ANION │
       │     EXCHANGE CHROMATOGRAPHY         │
       └────────────────────────────────────┘
```

Figure 2.2. Flow diagram to represent the dynein extraction procedure (section 2.7).

2.8. Concentration of 14S dynein and fractions thereof

Dynein samples were concentrated by ultrafiltration using a variety of Millipore Ultrafree filtration units with either polysulfone or low-binding cellulose membranes. Dynein samples (maximal volume of 0.4ml) were concentrated using Ultrafree-MC filter units with either 10kDa, 30kDa or 100kDa exclusion limit membranes. Filtration units were centrifuged for approximately 20 minutes at 5°C in at bench top micro-centrifuge at 11,600 g. The retentate was removed and the protein concentration estimated by absorbance at 280nm (section 2.11.1). Dynein samples (maximal volume of 2ml) were alternatively concentrated using Millipore Ultrafree-CL filter units with a polysulfone membrane of exclusion limit 30kDa. Samples were centrifuged at 5°C using a Heraeus digifuge at 5,000 g for approximately 40 minutes. The protein concentration of the retentate was estimated using absorbance at 280nm (section 2.12.1).

2.9. Gel filtration chromatography

The further purification of 14S dynein fractions was achieved using an FPLC coupled to a 24ml bed volume Superose 6 Hr 10/30 column with a separation range of 5kDa to 5000kDa. Prior to use, the column was equilibrated with buffer containing 10mM Hepes, 4mM $MgCl_2$, 0.1mM EGTA, 0.1M NaCl and 0.1mM DTT, pH 7.4, which had been filtered through a 0.2µm cellulose nitrate membrane filter (Whatman) and degassed. The dynein fraction, of approximate concentration ranging from 0.04-0.1mg/ml, was then loaded onto the column at a rate of 0.25ml per minute using a 200µl sample loop. Absorbance at 280nm was continuously monitored through a flow cell connected to a chart recorder set at a full scale deflection of 0.05 absorbance units, and 1ml fractions collected. The column was calibrated for molecular mass estimates using molecular mass standards (Sigma) as follows: thyroglobulin (669kDa), apoferritin (443kDa), β-amylase (200kDa), alcohol dehydrogenase (150kDa), bovine serum albumin (66kDa), carbonic anhydrase (29kDa), and cytochrome C (12.4kDa). The mass of the dynein fraction was estimated by extrapolation from a standard curve constructed from a graph of log molecular mass plotted as a function of the elution volume.

2.10. Microtubule preparation

Microtubules were prepared form both *Tetrahymena* axonemes (figure 2.5) and porcine brain. The preparation of microtubules from *Tetrahymena* axonemes was a modification of the methodology described by Vallee (1986). The method for microtubule preparation from brain was supplied courtesy of Dr. R. Cross, Marie Curie Research Institute, Oxted, Surrey, and incorporated the use of a phosphocellulose column to remove microtubule-associated proteins (Weingarten *et al.*, 1975). Both procedures made use of the fact that tubulin assembles to form microtubules when incubated at an elevated temperature (37°C) and in the presence of GTP. Differences between methods, however, were evident since self-assembly of microtubules does not readily occur in axonemes (Vallee, 1986). Taxol was therefore used throughout this preparation to promote and stabilise microtubules (Schiff *et al.*, 1979). In contrast, the procedure utilised for porcine brain was a modification of the well-established reversible assembly method (see Borisy *et al.*, 1975). In the absence of taxol, microtubules were purified by temperature-dependent cycles of polymerisation and depolymerisation and separated from microtubule-associated proteins by phosphocellulose chromatography. In both procedures, the formation of microtubules was monitored using transmission electron microscopy (section 3.7.1).

2.10.1. *Tetrahymena* axonemes (figure 2.3)

The axonemal pellet which remains following dynein extraction from *Tetrahymena* (section 2.7.3) was used as the tubulin source for the preparation of microtubules. At least two pellets were homogenised, using a mechanical Teflon-in-glass homogeniser, in a 3ml volume of PEM buffer containing 0.1M Pipes, 1mM EGTA and 1mM $MgCl_2$, pH 6.6. The homogenate was centrifuged at 38,720 g for 30 minutes at 2°C and the supernatant retrieved. All centrifugation steps, at this and subsequent stages, were carried out using 9ml centrifugation tubes (Sorvall), a Sorvall SS-34 rotor (with inserts), and Sorvall RC-5B refrigerated superspeed centrifuge. The concentration of tubulin in the supernatant was estimated using 1mm cuvettes by absorption at 280nm (section 2.11.1). The supernatant resulting from centrifugation was incubated at 37°C in the presence of 20μM taxol and 1mM GTP. After 30 minutes (the solution had become cloudy), 1ml of a pre-warmed

solution containing 10% sucrose, PEM buffer, 20μM taxol and 1mM GTP was used to underlay (by introducing the solution at the bottom of the tube with a Pasteur pipette) the incubating microtubule solution. This was then centrifuged at 38,720 g for 30 minutes at 25°C. The supernatant was discarded and the resulting glassy pellet retained. The pellet was re-homogenised in 0.5ml ice-cold PEM buffer containing 20μM taxol and 1mM GTP, using a 1ml Uni-Form manual homogeniser. The homogenate was then centrifuged at 38,720 g for 30 minutes at 2°C. The supernatant was removed and incubated once more at 37°C in the presence of 20μM taxol and 1mM GTP. After 30 minutes, 1ml of a pre-warmed solution containing 10% sucrose, PEM buffer, 20μM taxol and 1mM GTP was used to underlay the incubating microtubule solution as before. This was then centrifuged at 38,720 g for 30 minutes at 25°C. The microtubule pellet was used within 12 hours and stored at 5°C in the presence of NaN_3 at a final concentration of 5mM. The pellet was resuspended immediately prior to use with a 1ml Uni-Form manual homogeniser in 0.1ml of ice-cold PEM buffer.

2.10.2. Porcine brain (figure 2.4)

The brains were removed from three freshly slaughtered pigs at a local abbatoir and placed immediately into ice-cold PBS solution. They were then transported on ice to the laboratory where meninges and clots were removed. Brains were placed in a blender and homogenised for approximately 30 seconds in 300ml of Mes buffer (100mM Mes, 0.5mM $MgCl_2$, 2mm EGTA, 0.1mM EDTA, pH 6.5) containing 1mM ATP, 0.1mM GTP, 0.1mM PMSF, 20μM leupeptin and 4mM DTT. The homogenate was then centrifuged at 23,430 g for 50 minutes at 4°C and the supernatant retained. The supernatant was incubated at 37°C with a 33% volume of pre-warmed glycerol containing $MgCl_2$ and GTP at a final concentration of 5mM and 1mM respectively. After 60 minutes, the solution was immediately centrifuged at 193,000 g in a TFT. 50.38 rotor for 1 hour at 35°C.
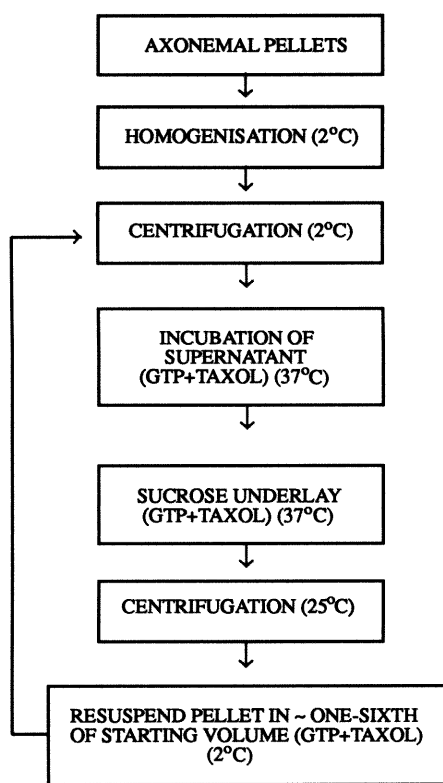
The pellets were resuspended on ice in 50ml of Pipes buffer (0.1M Pipes, 0.5mM $MgCl_2$, 2mM EGTA, 0.1mM EDTA, pH 6.8) containing 0.1mM GTP, 4mM DTT and 20μM leupeptin. Resuspension of the pellets was achieved using a mechanical Teflon-in-glass homogeniser left overnight at 5°C. The homogenate was centrifuged at 193,000 g in a

TFT. 50.38 rotor for 30 minutes at 4°C and the supernatant retained. Pre-warmed glycerol was once again added to the supernatant to give a final volume of 33%. $MgCl_2$ and GTP were also added to a final concentration of 5mM and 1mM respectively, and the solution incubated at 37°C. After 40 minutes, the solution was centrifuged using a TFT. 50.38 rotor at 244,300 g for 40 minutes at 35°C.

The pellets were resuspended in 15ml of column buffer (50mM Pipes, 1mM EGTA, 0.2mM $MgCl_2$, 0.01mM GTP, pH 6.8) containing 4mM DTT and 1mM GTP. The homogenate was maintained on ice for 40 minutes and then centrifuged for 40 minutes at 4°C using a TFT.50.38 rotor at 244,300 g. The supernatant was then loaded onto a 200ml phosphocellulose column* which had been equilibrated with column buffer containing 4mM DTT and 1mM GTP. The flow of protein solution was maintained at 0.5ml/minute using a peristatic pump attached to the top of the column. Once all the sample had been loaded onto the column, the flow of column buffer was maintained and 1.5ml fractions were collected. Tubulin was located spectrophotometrically at 280nm (section 2.11.1). Fractions with an A_{280} reading of greater than 1.0 were pooled, aliquoted into 1ml fractions, frozen in liquid nitrogen and stored at -70°C until required. Tubulin stocks were polymerised by first increasing the $MgCl_2$ and GTP content to 2mM and 1mM respectively, and then incubating the solution at 37°C. After 30 minutes, taxol was added to a final concentration of 20μM to stabilise the microtubules.

---

* The phosphocellulose column was prepared according to the manufacturer's instruction (Whatman).

```
         ┌─────────────────────────┐
         │    AXONEMAL PELLETS     │
         └─────────────────────────┘
                      ↓
         ┌─────────────────────────┐
         │  HOMOGENISATION (2°C)   │
         └─────────────────────────┘
                      ↓
         ┌─────────────────────────┐
  ┌─────→│  CENTRIFUGATION (2°C)   │
  │      └─────────────────────────┘
  │                   ↓
  │      ┌─────────────────────────┐
  │      │      INCUBATION OF      │
  │      │       SUPERNATANT       │
  │      │   (GTP+TAXOL) (37°C)    │
  │      └─────────────────────────┘
  │                   ↓
  │      ┌─────────────────────────┐
  │      │    SUCROSE UNDERLAY      │
  │      │   (GTP+TAXOL) (37°C)    │
  │      └─────────────────────────┘
  │                   ↓
  │      ┌─────────────────────────┐
  │      │  CENTRIFUGATION (25°C)  │
  │      └─────────────────────────┘
  │                   ↓
  │      ┌─────────────────────────┐
  │      │ RESUSPEND PELLET IN ~ ONE-SIXTH │
  └──────│ OF STARTING VOLUME (GTP+TAXOL)  │
         │            (2°C)                │
         └─────────────────────────┘
```
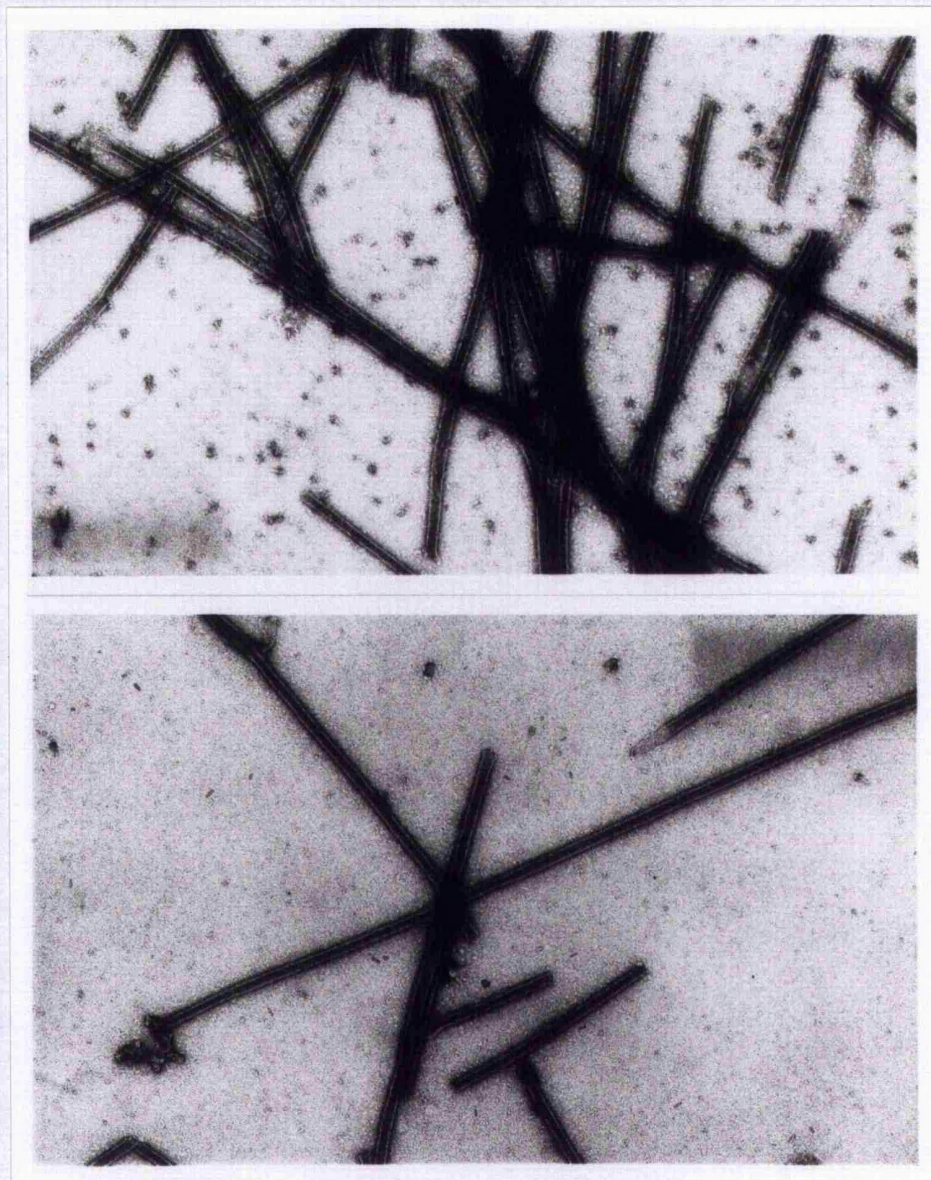
Figure 2.3. Preparation of microtubules from *Tetrahymena* axonemes (section 2.10.1).
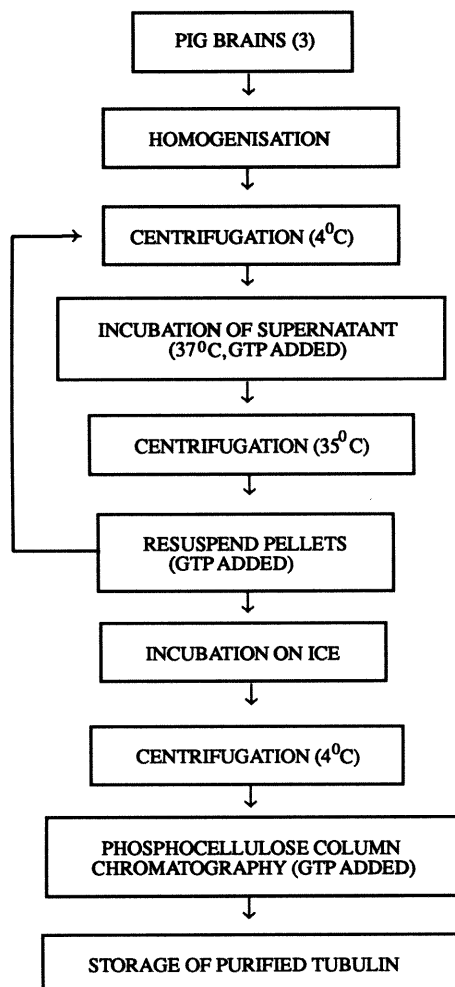
Figure 2.4. Preparation of microtubules from Porcine brain (section 2.10.2).

500nm

Figure 2.5. Negatively stained microtubules prepared from *Tetrahymena* axonemal tubulin (section 2.10.1) and visualised using electron microscopy (section 3.7.1).

2.11. Estimation of protein concentration

Two techniques were used for the estimation of protein concentration. Both techniques required a measurement of absorbance which was carried out in 1cm or 1mm quartz cuvettes using either a double-beam recording Unicam SP8-100 spectrophotometer or a Perkin-Elmer Lambda 5 double-beam recording spectrophotometer.

2.11.1. Protein absorbance spectra

An absorbance scan was taken between 220nm and 340nm. A base-line was fitted to the scan and the absorbance at 280nm was measured. Protein concentration was then calculated from the absorbance scan using the approximation that a 1mg/ml solution of protein produces an A_{280} of 1.0. Proteins solutions which contained DTT were referenced against appropriate buffer solutions containing DTT of a comparable age to that of the protein. This was necessary to minimise the absorbance effect caused by oxidised DTT (Cleland, 1964). In the oxidised state, DTT had a maximal absorbance of 283nm which, if not minimised, significantly interfered with estimates of protein concentration at 280nm.

2.11.2. Bradford assay

Protein concentration was estimated using a dye-reagent kit (Bio-Rad) developed from the method of Bradford (1976). Estimations of protein concentration were determined from the standard curve derived from a plot of absorbance (595nm) against an appropriate concentration range (μg) of bovine plasma gamma globulin. Standard curves were constructed according to the manufacturer's instruction for the Bio-Rad microassay procedure.

2.12. SDS-PAGE

SDS polyacrylamide gel electrophoresis of proteins used a modification of the technique described by Laemmli (1970).

2.12.1. Preparation of protein samples

Protein samples were typically prepared for electrophoresis by adding 60μl of protein to 35μl of sample buffer (0.18M Tris, 5.7% SDS, 29% glycerol, 0.005% bromophenol blue,

pH 6.8) and 5μl of β-mercaptoethanol. The sample was then placed immediately into boiling water for 3 minutes. Gel samples were stored at -20ºC until required.

2.12.2. Mini-gels

Mini-gels (10cm x 6cm x 1mm) were produced using the *Bio-Rad mini protean* slab gel apparatus. The percentage of acrylamide used in the resolving gel was dependent on the molecular mass of the proteins to be resolved but was typically 5%, 7.5%, or 10% (table 2.2). Once the resolving gel had been poured into the gel cast, it was immediately overlayed with isobutanol and left to set at room temperarture. The isobutanol was then removed, and the stacking gel (table 2.2) poured on top of the resolving gel. Combs to form the gel wells were then inserted. Once the gel had set, the combs were removed and the wells filled with running buffer containing 0.2M glycine, 0.02M Tris and 0.1% SDS. Protein samples were then loaded into the wells of the gel using a Gilson P20. For dynein samples, maximal amounts of protein were loaded into each well. This gave a range of protein per well from 0.5μg to 4μg. Gels were run at 40mA for approximately 60 minutes or until the bromophenol blue marker present in the gel samples (section 2.12.1) had travelled the length of the gel.

2.12.3. Gradient gels

Linear gradient gels were produced using the *Bio-Rad mini protean* apparatus by mixing equal volumes of 3% and 5% resolving gel solutions in a gradient maker, and using a peristatic pump to deliver the solution into the gel cast. The concentration of the reagents APS and TEMED were reduced from the values used in standard acrylamide gels in order to delay the onset of gel matrix formation (table 2.3). Once the resolving gel had been formed, the procedure was identical to that described in section 2.12.2.

2.12.4. Silver staining

Polyacrylamide gels were stained using a *Bio-rad* silver stain plus kit developed from the method of Gottlieb and Chavko (1987). Gels were fixed, washed and developed, according to the manufacturer's instruction, in polyethylene staining containers which were routinely cleaned with 50% nitric acid and washed in deionised water prior to use.

Staining of the gel was terminated by replacing the development reagent with 5% acetic acid. Gels were photographed within 1 hour of development.

2.12.5. Coomassie Blue stain

Polyacrylamide gels were stained for 1 hour, with agitation, in solution containing 0.1% Coomassie Brilliant Blue R250, 40% IMS (industrial methylated spirit), and 12% acetic acid. The gels were then destained in 10% acetic acid overnight or until the background had become clear.

Gel Constituents	Resolving Gel			Stacking Gel
Percentage Acrylamide	5%	7.5%	10%	4.5%
Lower Stock*	2.25ml	2.25ml	2.25ml	-
Upper Stock*	-	-	-	2.5ml
Acrylamide Solution*	1.5ml	2.25ml	3ml	1.5ml
Deionised Water	5.25ml	4.5ml	3.75ml	6ml
10% APS	40μl	40μl	40μl	30μl
TEMED	10μl	10μl	10μl	10μl

Table 2.2. Constituent solutions for 5%, 7.5% and 10% polyacrylamide gels (section 2.12.2).

Percentage Acrylamide	3%	5%
Lower Stock*	2.25ml	2.25ml
Acrylamide Solution*	0.9ml	1.5ml
Deionised Water	5.8ml	5.25ml
10% APS	20μl	20μl
TEMED	5μl	5μl

Table 2.3. Constituents for 3-5% gradient resolving gels (section 2.12.3).

---

*Lower stock consists of 1.5M Tris and 0.4% SDS, pH 8.8. Upper stock consists of 0.5M Tris, 0.4% SDS, pH 6.8. Acrylamide solution contains 30% acrylamide and 0.3% *bis*-acrylamide.

Chapter 3

The Isolation, Purification, and Structural Investigation
of Four 14S Dynein Fractions

Introduction

This chapter describes the purification of four 14S dynein fractions isolated from the cilia of *Tetrahymena thermophila*. These fractions (designated 1-4) were identified by their unique polypeptide composition, immunogenicity, and distinct molecular structures.

3.1. The isolation and purification of dynein from *Tetrahymena*

3.1.1. The dynein extraction procedure

Studies on cilia motility first began following the discovery that cilia could be successfully isolated from appropriate eukaryotic organisms. Deciliation is achieved using the relatively mild treatment of dibucaine hydrochloride (Thompson *et al.*, 1974) which does not result in lysis of the cell membrane (Satir *et al.*, 1976). Once the cilia have been successfully isolated, the membrane surrounding the cilium is solubilised using a mild detergent such as digitonin (Gibbons, 1963), Triton X-100 (Mabuchi & Shimizu, 1974), or nonidet P40 (Porter & Johnson, 1983). The components of the axoneme are then accessible, and can be separated into a soluble and an insoluble fraction using either a high-salt extraction treatment (Porter & Johnson, 1983), or a low-salt procedure involving the extensive dialysis of cilia against a low concentration of EDTA (Takahashi & Tonomura, 1978; and Gibbons, 1963). In both methods, differential centrifugation is used to separate the soluble fraction (which represented 90% of the ciliary ATPase) from the insoluble fraction (comprising the remaining 9 + 2 microtubule structure of the axoneme {section 1.4}). The ciliary ATPase, or subsequently named **dynein**, is then purified into two main types (14S and 22S) using sucrose density gradient centrifugation (Gibbons & Rowe, 1965). More recently, a column chromatography step, which separates dynein from other axonemal proteins, has been introduced prior to the density gradient centrifugation procedure (Porter & Johnson, 1983).

3.1.2. Variation between species: extractability and stability of dynein

The dynein investigated in this thesis was isolated from the multiciliated protozoan *Tetrahymena thermophila*. *Tetrahymena* cilia, along with *Chlamydomonas* and sea urchin sperm flagella, represent the most common sources of dynein for experimental

investigation (section C, chapter 1). Although the dynein extracted from these three systems share common features, species variation is apparent with respect to the extractability of dynein from the axoneme and subsequent stability of the isolated protein in solution. Dynein from sea urchin sperm flagella responds to a high-salt extraction procedure with the selective removal of the outer dynein arm (Gibbons & Gibons, 1973), whereas a similar treatment of *Tetrahymena* (Johnson & Wall, 1983) and *Chlamydomonas* (Piperno & Luck, 1979a) axonemes results in the removal of both outer and inner arms. The stability of dynein after extraction is also variable. *Chlamydomonas* outer dynein arms readily dissociate into an 18S and 12S species following extraction (Piperno & Luck, 1979a), whereas dissociation of the sea urchin sperm outer arm occurs following low ionic-strength dialysis (Tang *et al.*, 1982). In comparison, the extracted 22S outer dynein arm of *Tetrahymena* is relatively stable over a wide range of ionic strengths (Johnson, 1986). Furthermore, the yield of dynein attainable is sufficient for biochemical studies since the organism is multiciliated and can be grown in large cultures. Dynein yield is also significantly improved by the use of a mucus-deficient mutant since mucus creates significant problems in the differential centrifugation of cells from cilia.

3.2. Structure of 14S dynein isolated from *Tetrahymena*

For the reasons outlined in the previous section, *Tetrahymena* provides a useful source of axonemal dynein for biochemical analysis. Two types of dynein have been isolated from this organism and are referred to as 14S and 22S dynein. The structure of the 22S has been well-characterised and is discussed in detail elsewhere (section 1.7.1). In contrast, information regarding 14S dynein is much more limited.

3.2.1. Early investigations

Structural investigations on 14S dynein lagged far behind those of the 22S species which now has a well-defined structure (Johnson & Wall, 1983; Goodenough & Heuser, 1984). One of the main reasons for this delay was that, until the 22S species had been fully characterised, the 14S was believed to be the monomer subunit of 22S dynein (Gibbons & Rowe, 1965; Gibbons, 1966; Warner *et al.*, 1977). The 14S was originally described as a single ellipsoidal particle measuring 14nm x 9nm x 9nm, whereas the 22S species (or 30S

as it was then referred) was described as a rod, or linear polymer, of 14S subunits (Gibbons & Rowe, 1965). It was subsequently discovered, however, that the two forms of dynein were distinguishable. Differences were shown both in the enzymatic properties (Gibbons, 1966; Shimizu & Kimura, 1974) and electrophoretic profiles (Mabuchi & Shimizu, 1974; Porter & Johnson, 1983) of the two dyneins. Furthermore, particles derived from the sonication of 30S dynein, and approximating to a sedimentation coefficient of 14S, were shown to have distinguishable properties to the 14S ATPase arising from axoneme extraction (Blum & Hines, 1979). Consequently, by the mid-1980s, 14S dynein had been identified as a unique species. Nevertheless, an understanding of the structure at this time was unchanged from the ellipsoidal particle originally proposed by Gibbons & Rowe (1965).

3.2.2. Current model for the structure of 14S dynein

The present structure for 14S dynein comes from the images obtained by Marchese-Ragona *et al.* (1988) using scanning transmission electron microscopy (STEM). This technique was used following its successful application in defining the structure of 22S dynein in which unfixed and unstained dynein particles (with minimal artifacts accountable to sample preparation) were analysed (Johnson & Wall, 1983). Using this technique, in conjunction with images obtained by negative staining, Marchese-Ragona *et al.* showed that 14S dynein was a heterogeneous mixture of two populations of particles. One particle was described as a single ellipsoidal globular head (9.5nm x 14.5nm), whilst the other had a globular head domain, of equivalent dimensions, but with an additional 20-24nm tail region (figure 3.1). The two species of 14S were believed to be in roughly equal proportions, and there was a suggestion of a pit or cleft in the globular heads, indicated by the accumulation of negative stain during electron microscopy preparation.

The only other structural evidence for 14S dynein came from Toyoshima (1987a) where molecules were described as predominantly single globular particles of diameter 18nm. Toyoshima did report, however, the presence of 'C-shaped' particles thought to be indicative of a possible stalk-like appendage.
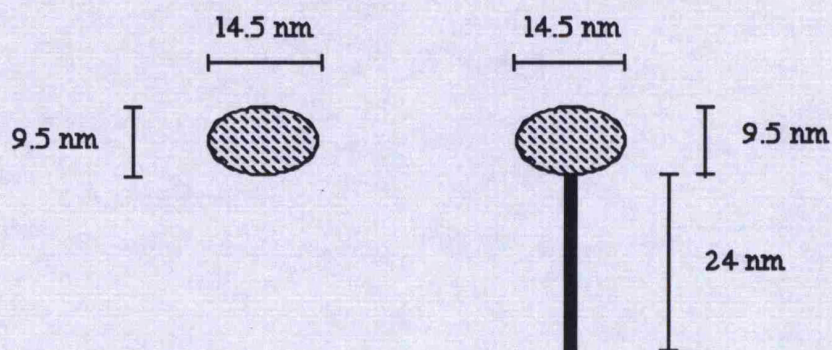
Figure 3.1. Diagrammatic representation of 14S dynein structure as proposed by Marchese-Ragona *et al.* (1988).

3.3. Polypeptide composition of 14S dynein

In addition to structural studies, the polypeptide composition of 14S dynein was investigated using SDS-PAGE. Early investigations indicated that 14S dynein consisted of **one** high molecular mass polypeptide, or heavy chain (HC), of approximate mass 460-520kDa (520kDa, Mabuchi & Shimizu, 1974; and 460kDa, Toyoshima, 1987a). In contrast, Porter and Johnson (1983) proposed that 14S dynein was composed of at least **three** heavy chains, each with an approximate mass of 300kDa. Since these initial studies, improvements in electrophoretic methods enabled a more accurate determination of polypeptide composition. In particular, Marchese-Ragona *et al.* (1988) used a 5-15% acrylamide gradient gel to resolve **two** heavy chains (which are immunologically distinct), one intermediate chain (IC) and three light chains (LC). The approximate masses of these latter polypeptide components were determined by a comparison with appropriate molecular mass standards. The mass of the single intermediate chain was estimated as 110kDa (Porter and Johnson, 1983), whereas the light chains were shown to be in the range 30-55kDa (Marchese-Ragona *et al.*, 1988). Accurate mass estimations of the two heavy chains (designated HC1 and HC2), however, have remained notoriously difficult to determine.

In contrast to this work, electrophoretic studies using 3-5% acrylamide gradient gels recently revealed at least **four** heavy chain components associated with 14S dynein (Muto *et al.*, 1994). In this study, HPLC was utilised to separate three major fractions of 14S dynein consisting of one or two heavy chain components and a light chain identified as

Tetrahymena actin. Four heavy chains were then identified by both their differing electrophoretic mobilities and by the production of different cleavage products following vanadate-dependent photolysis (see chapter 4).

3.4. Relating the polypeptide composition to the structure of 14S dynein in solution

A correlation between the polypeptide composition and structural morphology of 14S dynein has yet to be determined. In particular, the recent identification of four heavy chains (Muto *et al.* 1994) has not been interpreted with respect to electron microscopy analysis. Marchese-Ragona *et al.* (1988), however, suggested a simple interpretation based on their data resulting from 5-15% polyacrylamide gradient gels and scanning transmission electron microscopy (STEM) images. This group proposed that the two immunologically-distinct heavy chains, detected by gel electrophoresis (HC1 and HC2), were equivalent to the globular heads of the two distinct populations of 14S dynein visualised using STEM (figure 3.1). This proposal originated from the observation that the mass of each head (determined by STEM analysis) was approximately equivalent to the presumed mass of a single heavy chain (determined by SDS-PAGE). The tail-less particle was therefore suggested to be composed of a single copy of one of the heavy chains. In contrast, the head-tail structure was proposed to consist of a single copy of the remaining heavy, intermediate and light chains since the estimated molecular mass of 510kDa (using STEM analysis) could be accounted for by the presence of a single copy of one heavy chain, the 110kDa intermediate chain, and one copy of each of the three light chains (30-55kDa).

The work presented in this chapter proposes that the heterogeneity associated with 14S dynein is attributable to the presence of **four** distinct species. These species have unique structures previously undescribed for 14S dynein.

Methods

Several of the techniques relevant to this chapter have been described elsewhere. In particular, the cultivation of *Tetrahymena* (section 2.4), concentration of cells (section 2.6), and preparation of dynein (section 2.7) have been included in chapter 2. The methods described here are specifically relevant to this chapter.

3.5. Antibody (IgY) preparation from chicken eggs

Attempts at raising antibodies against fractions of 14S dynein used the methodology developed by Gassmann *et al.* (1990) for antibody production in chicken. The chickens used were hybrid egg-laying chickens of approximately 20 weeks old. Pre-immune eggs were collected and tested for antigenicity against 14S dynein fractions prior to immunization.

3.5.1. Immunization of hens

Due to the restricted yields of dynein from the extraction procedure (section 3.8.5), dynein samples from a total of three preparations were necessary for the immunization of chicken. Each dynein sample was dialysed for 16 hours in 2 x 2 liters of buffer containing 10mM Hepes, 4mM $MgCl_2$, 0.1mM EGTA, 40mM NaCl and 0.1mM DTT, pH 7.4, before being rapidly frozen in liquid nitrogen and then stored at -70^oC. Immediately prior to immunization, the relevant dynein samples were thawed and mixed thoroughly with an equal volume of complete Freund's adjuvant. Each chicken was then immunized by injecting 1.5ml of appropriate sample into the pectoral muscle. Subsequent injections of sample mixed with incomplete Freund's adjuvant were given on days 12 and 20. Eggs were labelled and collected from day 15 onwards and stored at 5^oC.

3.5.2. Extraction of antibodies from egg yolks

Antibodies were extracted from egg yolks using the technique of differential PEG precipitation (Gassmann *et al.*, 1990). The yolks were separated from four eggs which had originated from one chicken and been layed on consecutive days. After washing the yolks in deionised water, the skins were removed and an equal volume of buffer A containing 10mM Hepes, 4mM $MgCl_2$, 0.1mM EGTA, 40mM NaCl and 0.1mM DTT, pH 7.4, was

66

added. The total volume of solution at this stage was approximately 120ml. An equal volume of buffer A containing 7% PEG 6000, was then added to give a final volume of 240ml. The solution was stirred at room temperature for 30 minutes and then centrifuged at 14,000 g for 10 minutes at 4°C. The pellet was discarded and the supernatant filtered through several layers of muslin. Solid PEG 6000 was added to the supernatant to a final concentration of 12%. After mixing, the solution was centrifuged at 14,000 g for 10 minutes at 4°C. The resulting supernatant was discarded and the pellet resuspended in 40ml of buffer A. An equal volume of buffer A plus 24% PEG 6000 was then added to the resuspended pellet and mixed thoroughly before centrifuging at 14,000 g for 10 minutes at 4°C. The supernatant was again discarded and the pellet resuspended in 20ml of buffer A. This was then dialysed for 16 hours at 4°C against 2 x 1 litre of buffer A. Finally, the floating precipitate was removed by centrifugation at 14,000 g for 10 minutes at 4°C.

3.6. Immuno-blot analysis

3.6.1. Electroblotting of protein from acrylamide gels onto nitrocellulose

Protein samples were first separated by SDS-PAGE as described in section 2.12.2. After electrophoresis, the stacker gel was removed and the resolving gel immediately prepared for electroblotting. Filter papers and nitrocellulose, which had been cut to the exact dimensions of the resolving gel, were soaked in transfer buffer containing 48mM Tris, 39mM glycine, 10% methanol and 0.0375% SDS. They were then placed onto the pre-wetted positive graphite electrode of a LKB electroblotter in the following order: 9 filter papers, nitrocellulose, resolving gel, 9 filter papers. The negative electrode was then connected and the current set to 0.8mA/cm^2. The protein on the gel was left to transfer onto the nitrocellulose for 70 minutes.

3.6.2. Western blotting

After electroblotting, transfer of protein to the nitrocellulose was confirmed by staining for a few minutes with Ponceau Red solution. The nitrocellulose was rinsed in de-ionised water and then incubated, with agitation, in block buffer containing 10mM Tris, 0.9% NaCl, 0.1% Tween and 3% milk powder, overnight at 5°C. After incubation, the block

buffer was discarded and the nitrocellulose washed for 3 x 10 minutes in buffer containing 10mM Tris, 0.9% NaCl and 0.1% Tween. All wash and incubation stages, at this and subsequent points, were carried out with agitation using a R100 Luckham gyroshaker. After washing, the nitrocellulose was incubated with primary antibody diluted in block buffer for 1.5 hours at $37^{o}C$. The dilution of antibody used was 400-fold for antibodies raised in rabbit, and ranged from 5000-fold to 100-fold for those raised in chicken. Following incubation, the nitrocellulose was washed 4 x 5 minutes with PBS, and then 2 x 5 minutes in buffer containing 150mM NaCl, 50mM Tris pH 7.5. The secondary antibody was then diluted 1000-fold with block buffer, and the nitrocellulose incubated for 1 hour at room temperature. The choice of secondary antibody, was dependent on the origin of the primary antibody and had either been raised in swine against IgG of rabbit, or raised in rabbit against chicken IgY. Both secondary antibodies were coupled to alkaline phosphatase. After incubation, the nitrocellulose was washed 4 x 5 minutes with buffer containing 10mM Tris and 0.9% NaCl. The nitrocellulose was then placed in 10ml of alkaline phosphatase buffer containing 0.1M NaCl, 5mm $MgCl_2$, 0.1M Tris, pH 9.5, and developed (with agitation) by adding $66\mu l$ of nitro-blue-tetrazolium (NBT) stock (50mg dissolved in 1ml of 70% DMF), and then $33\mu l$ of 5-bromo-4-chloro-3-indolyl phosphate (BCIP) stock (50mg dissolved in 100% DMF). Development of the nitrocellulose was terminated by the addition of PBS buffer containing 20mM EDTA.

3.7. Electron microscopy

The two main electron microscopy techniques used (section 3.7.1. & 3.7.2) required the use of a high-vacuum carbon-coating unit with a Polaron E6440 power supply. The pressure in the coating unit was maintained at 6 x 10^{-7} mbar for both carbon-coating and metal-shadowing procedures. After preparation, grids were viewed in either a *Jeol 100CX* or *Siemens 102* transmission electron microscope.

3.7.1. Negative staining

Collodian coated copper grids (3.05mm x 300 square mesh) were prepared and stabilised by coating with carbon in a high-vacuum carbon-coating unit. The carbon electrode was prepared in advance by arranging two shaped carbon rods under tension, at a height of

15cm and at an angle of 90° to the grids. The grids were then glow discharged for 30 seconds, to encourage hydrophilicity, using argon gas which was ionised by applying a 1.5KV, 40mA electrical supply through two vertical electrodes. The protein sample to be investigated (dynein or microtubules), was diluted in an appropriate buffer to give a final concentration of approximately 0.01mg/ml, and then 0.01ml applied to the grids using a Gilson P20. After 5 minutes at room temperature, excess sample was removed with a filter paper by capillary action, and the grids then promptly washed using a few drops of distilled water. Excess fluid was removed with filter paper and a droplet (0.01ml) of negative stain (uranyl acetate or 1% sodium phosphotungstate) was then applied to each grid. This was removed using filter paper after a few seconds if uranyl acetate was used, and after a few minutes if sodium phosphotungstate was used. In each case, a thin film remained on the surface of the grid which was then left to air dry before viewing in the electron microscope.

3.7.2. Metal shadowing

Protein samples, of less than 0.1mg/ml, were mixed by repeated pipetting 1:1 (v/v) with glycerol (pure grade). A sheet of mica was then freshly cleaved and vertically mounted at a distance of 27cm to the direction of an artist spray gun set at a pressure of 20 psi. The glycerol and sample mixture (0.01ml) was sprayed onto the cleaved surface of the mica and immediately secured to a rotatable stage using double-sided adhesive tape. The mica was then left to dry for 10-15 minutes at 6×10^{-7} mbar in a high-vacuum carbon-coating unit. The metal electrode was prepared in advance by wrapping approximately 2cm of 0.1mm thickness platinum wire around a 6cm length of tungsten wire. This was then set at a distance of 12cm from the specimen and at an angle of 7.5°. Once the mica was dry, the stage was rotated at 90rpm (for rotary shadowing) or stationary (for unidirectional shadowing) and the specimen shadowed using the thermal evaporation of platinum. This was achieved by gradually applying a current, up to a maximum of 40A, through the tungsten over a period of 2.5 minutes. After shadowing, the specimen was stabilised by coating with carbon from a carbon electrode arranged at 90° to the stage as described previously (section 3.7.1). The mica was then scored and trimmed to enable the shadowed

replica to be floated off onto water. The floating replica samples were picked up, from below, onto 3.05mm x 300 square mesh copper grids. Excess water was then removed by touching the underside of the grid with filter paper. Grids were left to dry completely before viewing in the electron microscope.

Samples were prepared in 50% glycerol in order to assist the localisation of dynein in the electron microscope. Glycerol droplets were easily identified in the microscope and the dynein molecules located towards the periphery of the droplet.

3.7.3. Photography

Images were recorded onto Agfa Scientia E. M. film 23D56P3AH (Agfa Gevaert). Negatives were then exposed onto *Ilford* mutigrade III paper and developed using an *Ilford* multigrade processor. Scales were corrected for print enlargement, microscope calibration, and, in the case of metal shadowing, a value of 1nm was deducted as an approximation for the quantity of metal deposited on the surface of the molecule (Willison & Rowe, 1980).

Results

3.8. Preparation of dynein

The isolation and purification of four fractions of 14S dynein was achieved using the procedure outlined in figure 2.2.

3.8.1. Method of cell growth

Two methods of cell growth were used to produce large cultures of *Tetrahymena*. Method 1, which was an established technique within the laboratory (section 2.4.1), typically produced yields of 22S and 14S dynein at **(2.7 ± 1.1) mg** and **(0.8 ± 0.3) mg** respectively from 16.5 litres of cells. Although this growth method was successful for many experiments, a recurring problem with contamination and poor growth led to the need to adopt a different growth strategy. Method 2 (section 2.4.2) was therefore used and shown to eliminate most of the problems associated with method 1. The typical yield of dynein was also an improvement for this latter method, since 23 x 750ml (17.25 litres) of *Tetrahymena* culture produced **(3.5 ± 1.0) mg** of 22S and **(1.1 ± 0.4) mg** of 14S dynein (table 3.1).

Growth method	Axonemal protein	Axonemal dynein	14S dynein	22S dynein	No. of preparations
1	37.6 ± 13.4	13.8 ± 3.9	0.8 ± 0.3	2.7 ± 1.1	10
2	56.1 ± 12.4	16.0 ± 3.1	1.1 ± 0.4	3.5 ± 1.0	20

Table 3.1. A comparison of the total protein (in mg) estimated at various stages during the dynein preparation for methods 1 and 2 of cell growth (section 2.4). Data was compiled from protein determinations taken as described in sections 2.7.3 (axonemal protein), 2.7.4 (total dynein), and 2.7.5 (14S and 22S dynein).

3.8.2. Determination of optimum cell growth

Preliminary experiments involving flask cultures were carried out to determine the optimal growth rate for an inoculum of *Tetrahymena* cells (section 2.5). Cell counts were taken over a period of 4 days as described in section 2.5.1, although measurements were not taken before 24 hours of growth since the number of cells was difficult to accurately assess until a reasonable number had accumulated. A graphical representation of cell number versus time showed that the optimal number of cells was produced after approximately 72 hours of growth (figure 3.2).

The size and quality of the cilia pellet produced after different growth times was assessed (section 2.5.2). A general observation was that cultures harvested after 48 hours of growth produced cilia pellets comprising a proportion of cell debris due to a significant amount of cell death occuring after prolonged growth. Cell death presented problems in the later stages of the preparation through the release of proteolytic enzymes from lysed cells. Cells were therefore harvested after a growth period of 48 hours. This was considered the most efficient growth time since the cilia pellet produced was white in colour and largely unaffected by cell debris. Figure 3.2 shows that growth at this time was well within the exponential phase and, as a result, contamination from lysed cells and proteolytic enzymes was minimised.
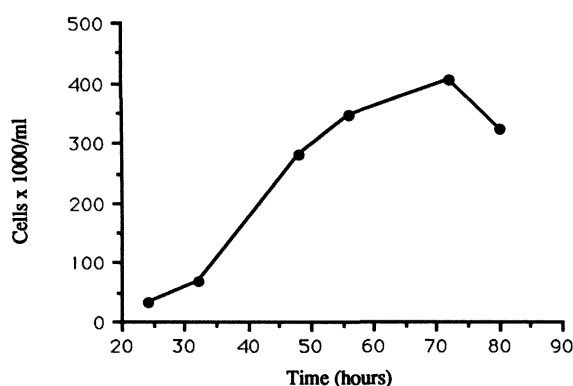
Figure 3.2. Growth curve for *Tetrahymena* determined by cell counts (section 2.5.1).

3.8.3. Extraction and purification of dynein

The extraction and purification of dynein was successfully achieved essentially using the method of Porter and Johnson, 1983 (section 2.7). The dynein preparation was routinely monitored, at various stages of the procedure, by an estimation of the protein concentration using absorbance at 280nm (section 2.11.1). Table 3.1 shows a comparison of the total protein produced at equivalent stages using growth method 1 and 2 (section 2.4). After extraction from the axoneme (section 2.7.3), dynein was separated from other axonemal proteins using anion-exchange chromatography (section 2.7.4). A typical elution profile for this column is shown in figure 3.3
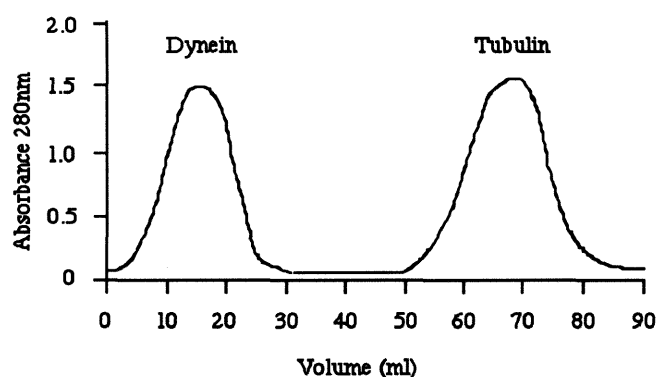
Figure 3.3. Absorbance profile of the protein eluted from a DEAE-Sephacel anion-exchange column (section 2.7.4). The first peak eluted (using a 200mM NaCl-Tris buffer) corresponds to axonemal dynein, whereas the second peak (eluted with a 500mM NaCl-Tris buffer) represents other axonemal proteins such as tubulin.

3.8.4. Isolation of 22S and 14S dynein

The two types of dynein, 22S and 14S, were separated from each other by density gradient centrifugation (section 2.7.5). The position of the 22S and 14S was determined by the manual fractionation and subsequent absorbance reading of each fraction at 280nm (section 2.11.1). A typical profile of a sucrose gradient is shown in figure 3.4.

73
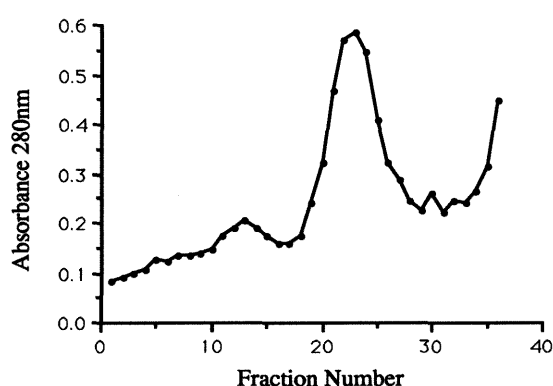
Figure 3.4. 5-25% sucrose gradient profile of 14S and 22S dynein separation (section 2.7.5). In this example, fractions 11-15 were pooled for 14S dynein and fractions 21-25 were pooled for 22S dynein.

3.8.5. Fractionation of 14S dynein

The fractionation of 14S dynein was achieved using a Mono Q HR 5/5 anion-exchange column coupled to an FPLC (section 2.7.6). Proteins were eluted using a gradient ranging from 200-400mM NaCl over a period of 20 minutes (table 2.1). These conditions enabled the sufficient separation of four major peaks of 14S dynein over a minimal time period. Attempts at improving peak separation, by reducing the steepness of the gradient, led to broadened peaks and consequently more dilute protein being eluted from the column. A typical FPLC profile is shown in figure 3.5. The identification and position of the four peaks was a reproducible feature of the profile although the resolution of peaks three and four was variable. Typical total yields of each fraction for ten representative preparations were as follows: fraction 1 (0.33 ± 0.21mg); fraction 2 (0.08 ± 0.07mg); fraction 3 (0.03 ± 0.02mg); fraction 4 (0.05 ± 0.04mg).

NaCl concentration (mM)

800 — 600 — 400 — 200

Absorbance 280nm

0.4 — 0.3 — 0.2 — 0.1

Fraction number

0   5   10   15   20   25   30

1   2   3   4
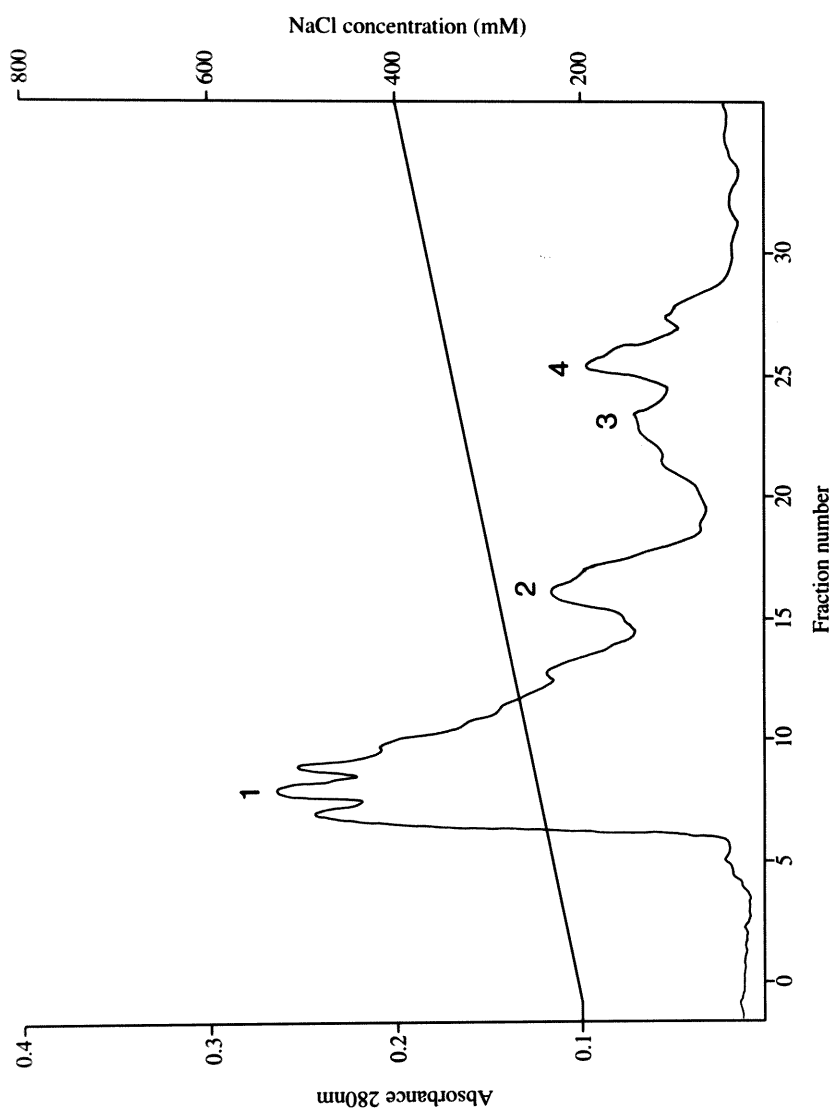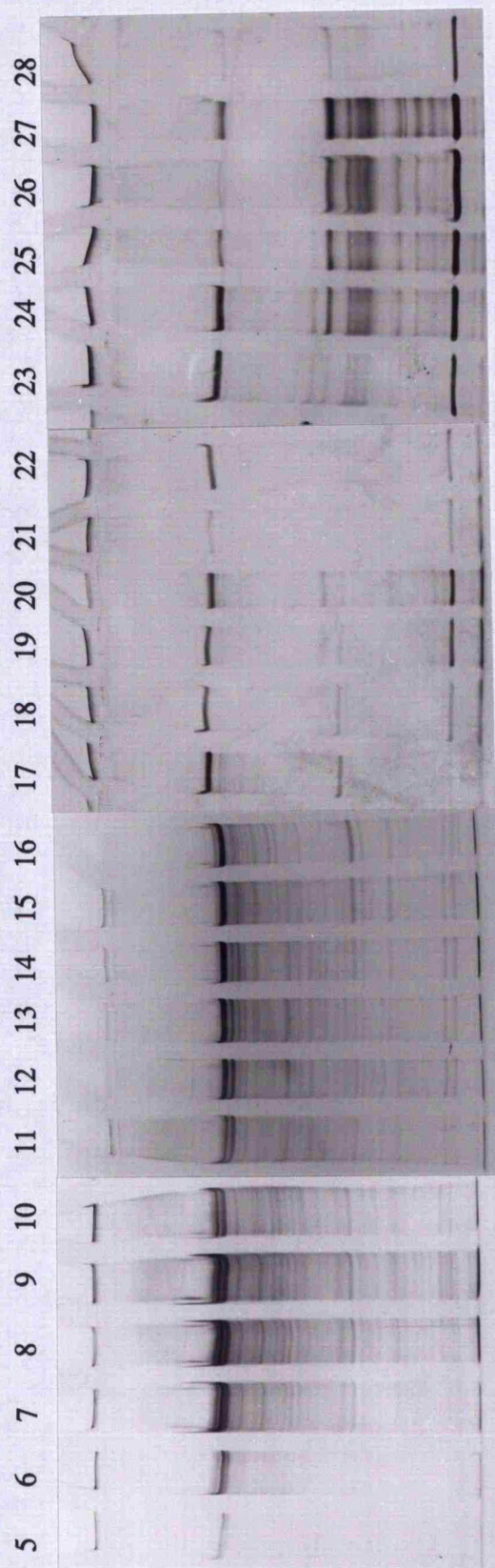
Figure 3.5. FPLC Mono Q elution profile of fractionated 14S dynein (section 2.7.6). Four main peaks (designated 1-4) were eluted over a linear NaCl gradient ranging from 200-400mM (above). The corresponding fractions (numbered 5-28) were analysed by 7.5% silver-stained SDS-PAGE (below) {section 2.12.2}.

3.9. SDS-PAGE analysis of 14S dynein fractions

Samples taken across the entire FPLC elution profile were routinely analysed by silver-stained 7.5% SDS-PAGE (section 2.12.2). This analysis enabled the identification of four different polypeptide compositions shown to coincide with the four major peaks prominent in the FPLC elution profile (figure 3.5). These four 'fractions', as they will now be referred, had unique compositions when analysed by SDS-PAGE. The most prominent feature of this analysis was the presence of one or two high molecular mass or heavy chain (HC) polypeptides which were clearly visualised using a 3-5% linear gradient gel (figure 3.6). These were referred to as HC1 and HC2 to distinguish their differing electrophoretic mobilities.

The four fractions of 14S dynein each had at least one heavy chain (figure 3.6). Fraction 1 comprised two heavy chains (HC1 and HC2); fraction 2 possessed a single heavy chain (of similar mobility to HC1); and fractions 3 and 4 each comprised a single heavy chain (of comparable mobility to HC2). In addition to heavy chain composition, SDS-PAGE analysis using 10% polyacrylamide gels revealed several lower molecular mass components associated with the four fractions (figure 3.7). In particular, fraction 4 consisted of a number of polypeptides ranging from 130kDa to 188kDa which were not apparent in fractions 1, 2, or 3 (table 3.2). Similarly, a polypeptide of approximate mass 47kDa was a prominent feature of fractions 1 and 2, but was significantly reduced and absent from fractions 3 and 4 respectively. In addition, a feature common to fractions 1, 3, and 4 was the presence of a peptide approximately 44.5kDa in mass (section 3.14.1).

Closer examination of SDS-PAGE (figure 3.7) revealed that the fractions comprised unique and similarly-sized peptides as shown in table 3.2. The prominent peptides of each fraction appeared to be associated as gel filtration chromatography did not result in the separation of heavy chain and low molecular mass polypeptides for fractions 1, 2, or a mixture of fractions 3 and 4 (figure 3.8).

Fraction 1	Fraction 2	Fraction 3	Fraction 4
-	-	-	188
-	-	-	152
-	-	-	130
105-222	102-210	102	103
-	57	-	-
-	49	-	-
47	47.5	(47.5)	-
45	-	44.5	(44.5)
-	43.5	-	-
35.5	36.5	-	-
32	-	32.2	-
30.5	31	-	-

Table 3.2. A comparison of the polypeptide composition for the prominent peptides associated with the four fractions of 14S dynein (see figure 3.7). The approximate mass (in kDa) of each peptide is indicated. Brackets indicate peptides present as low intensity bands on SDS-PAGE.
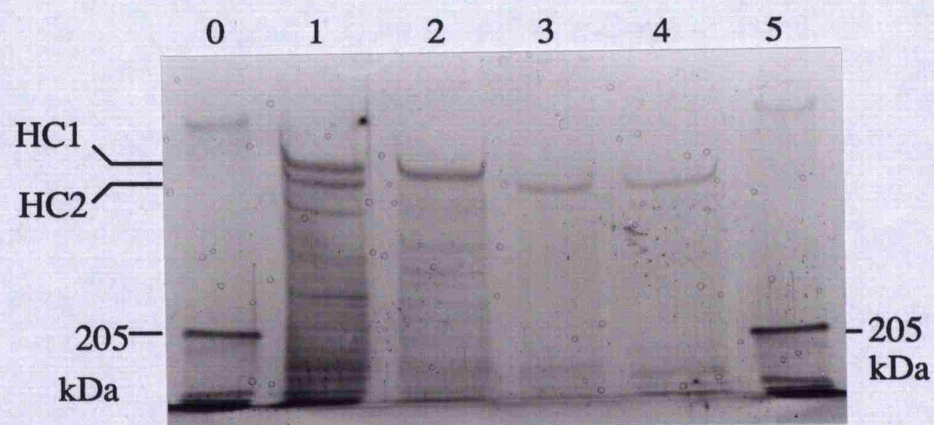
Figure 3.6. 3-5% linear gradient SDS polyacrylamide silver-stained gel of the four 14S dynein fractions. The two heavy chains are denoted HC1 and HC2. Tracks: 0 and 5, molecular mass markers; 1-4, 14S dynein fractions 1-4 respectively.
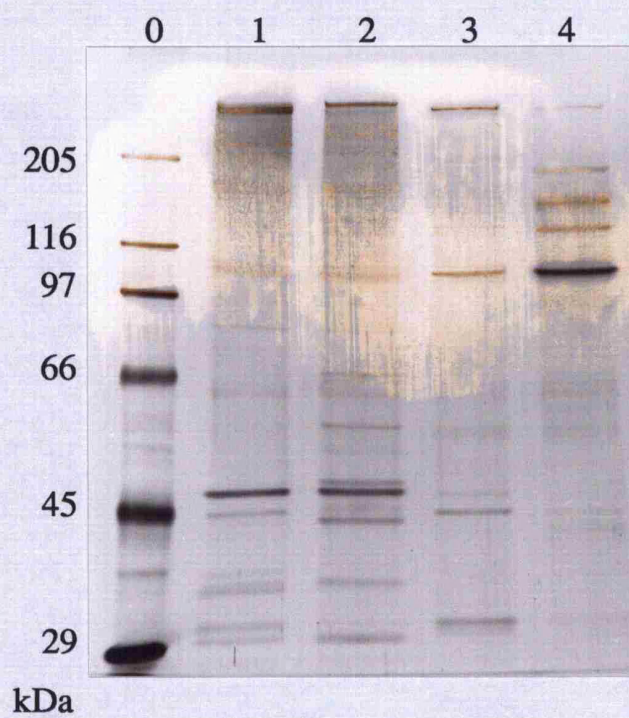
Figure 3.7. 10% polyacrylamide silver-stained gel to show the polypeptide composition of the four fractions isolated for 14S dynein. Tracks: 0, molecular mass markers; 1-4, 14S dynein fractions 1-4 respectively.
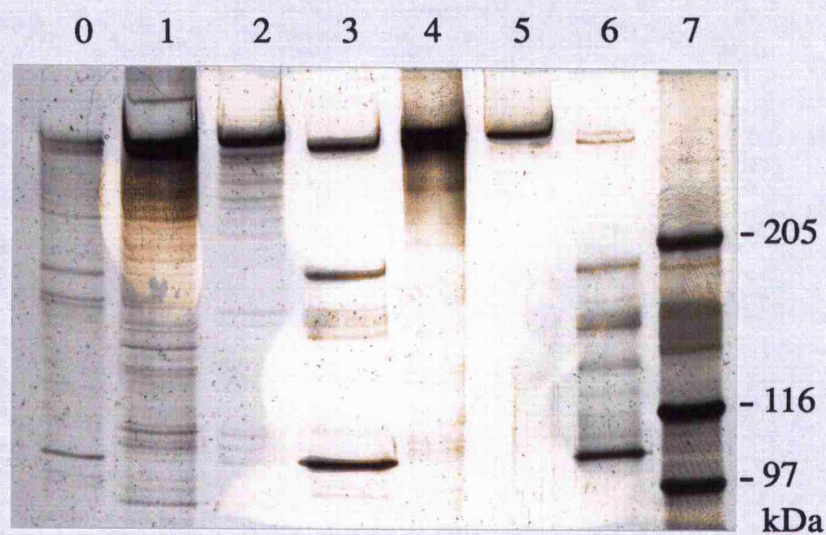
Figure 3.8. 5% SDS polyacrylamide silver-stained gel of 14S dynein fractions. Tracks: 0, unfractionated 14S; 1-3, 14S dynein fractions 1, 2, and 3/4 respectively; 4-6, fractions 1, 2, and 3/4 respectively after gel filtration chromatography; 7, molecular mass markers.

3.10. Immunoblot analysis of the four dynein fractions

The polypeptide composition of the four fractions was investigated using immuno-blot analysis. Rabbit antibodies, previously raised in the laboratory, were used to test for cross-reactivity between the polypeptide components of three of the fractions. Attempts were then made to produce antibodies (in chicken) against all four 14S fractions (section 3.5). In addition, the four fractions were investigated for the presence of tubulin and actin.

3.10.1. Antibodies raised in rabbit against three 14S dynein fractions

Antibodies raised against fractions 1, 2, and a mixed population of fractions 3 and 4 (designated fraction 3/4) were previously produced in the laboratory. These were obtained by the immunization of rabbits with the entire protein constituents of each fraction. The antibodies produced were tested for specificity with the four newly-identified 14S dynein fractions. The Western blots resulting from the incubation of these antibodies with fractions 1-4, unfractionated 14S dynein, and 22S dynein are shown in figure 3.9.

A comparison of the three antibody blots showed there to be no cross-reactivity between the heavy chains of fractions 1, 2 and 3/4. Cross-reactivity did however occur between several of the lower molecular mass components. Antibodies against fraction 1, for example, cross-reacted with a fragment greater than 205kDa and a 68kDa component associated with fraction 2. In comparison, antibodies raised against fraction 2 had affinity for a lower molecular mass component (103kDa) of fraction 4. Similarly, antibodies against fraction 3/4 responded to an 88kDa and 92kDa doublet polypeptide faintly detectable in fraction 1. The affinity of antibodies to unfractionated 14S dynein was weak, and in the case of antibodies against fraction 2, undetectable. This is most probably due to the low concentration of 14S dynein available. Attempts to concentrate dynein solutions were unsuccessful since a large proportion of the dynein was irretrievably bound to the membranes of the concentration devices tested (section 2.8). In addition, the only evidence of cross-reactivity between 14S and 22S dynein was a weak response to a 103kDa component evident in antibodies raised against fraction 3/4.

81

3.10.2. An attempt to raise chicken antibodies to the four 14S dynein fractions

The antibodies raised in rabbit showed there to be at least four distinct heavy chains associated with 14S dynein; two associated with fraction 1, and one each associated with fractions 2 and 3/4. In order to investigate the heavy chain(s) of fractions 3 and 4, however, it was necessary to raise new antibodies against all four 14S dynein fractions.

Attempts were made to raise antibodies in chicken since Gassmann *et al.* (1990) showed that immunization with as little as 20-30µg of protein could produce a high and sustained titre of specific antibodies. As an initial experiment, hens were immunized with 22S dynein, 14S dynein fraction 1 and 14S dynein fraction 2 (section 3.5.1). These proteins were chosen since they were the most concentrated and therefore considered the most likely to produce an immune response. Despite three immunizations, however, no antibodies were detected in any of the eggs which were collected and harvested in batches of four for consecutive days (section 3.5.2). Eggs up to 64 days old were tested for the presence of antibody by immuno-blot analysis (section 3.6). The detection procedure (section 3.6.2) was tested by using an antigen and antibody (kindly donated by Mr. S. Saville, Department of Genetics, Leicester University) which had been previously raised in chicken.

3.10.3. Probing the fractions for tubulin and actin

The possible association of tubulin with the four fractions of 14S dynein was investigated by immuno-blot analysis (section 3.6) since a band of approximately 50kDa (tubulin molecular mass ~ 55kDa) was apparent in fraction 2 (figure 3.7). A primary anti-tubulin antibody which had been raised in rabbit was used at a recommended 32-fold dilution (Sigma). The nitrocellulose blot resulting from this analysis is shown in figure 3.10. Anti-tubulin cross-reacted with *Tetrahymena* tubulin isolated during the dynein extraction procedure (section 2.7.4) but did not cross-react with polypeptides from any of the four fractions.

Immuno-blot analysis for actin (actin molecular mass = 42kDa, Hirono *et al.*, 1987) was only possible using mouse monoclonal actin as a primary antibody (Sigma), since antibodies against *Tetrahymena* actin were not available. This actin antibody cross-reacted

with actin obtained from rabbit muscle, but did not cross-react with any of the 14S dynein fractions (figure 3.11). This did not eliminate the possible association of actin with the fractions isolated, however, since *Tetrahymena* actin is significantly divergent from other sources of actin (Hirono *et al.*, 1987).
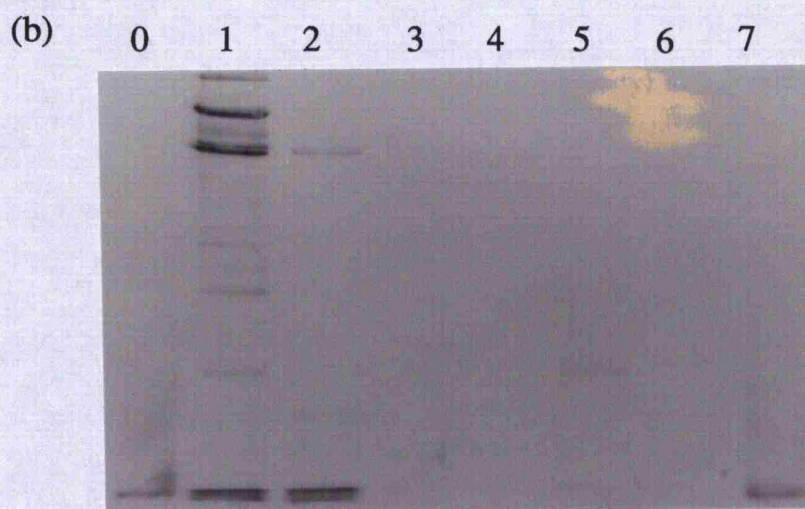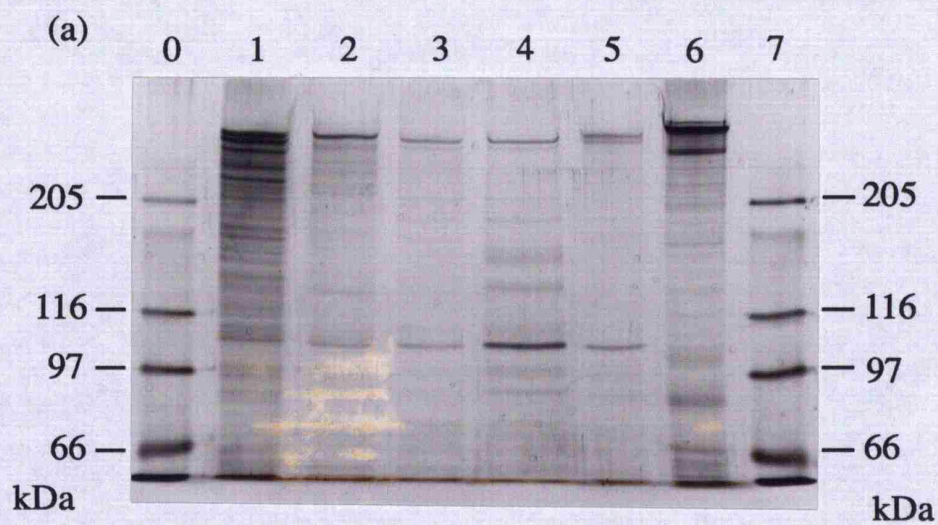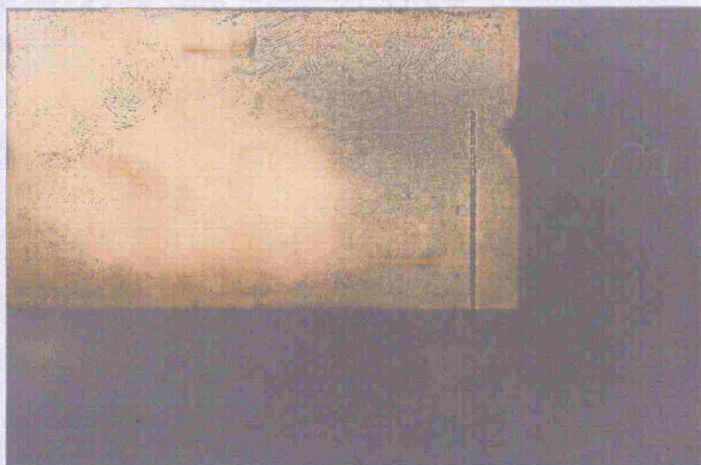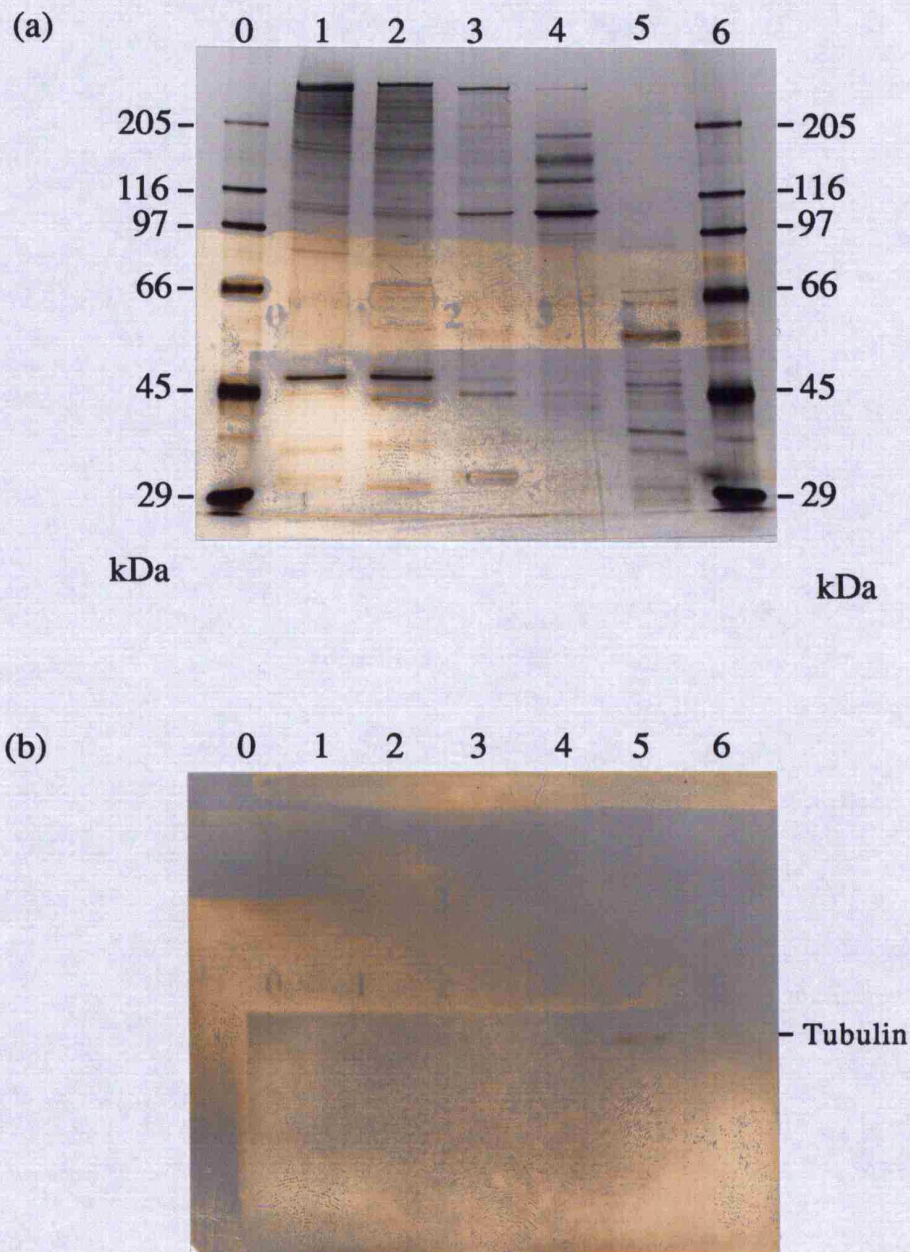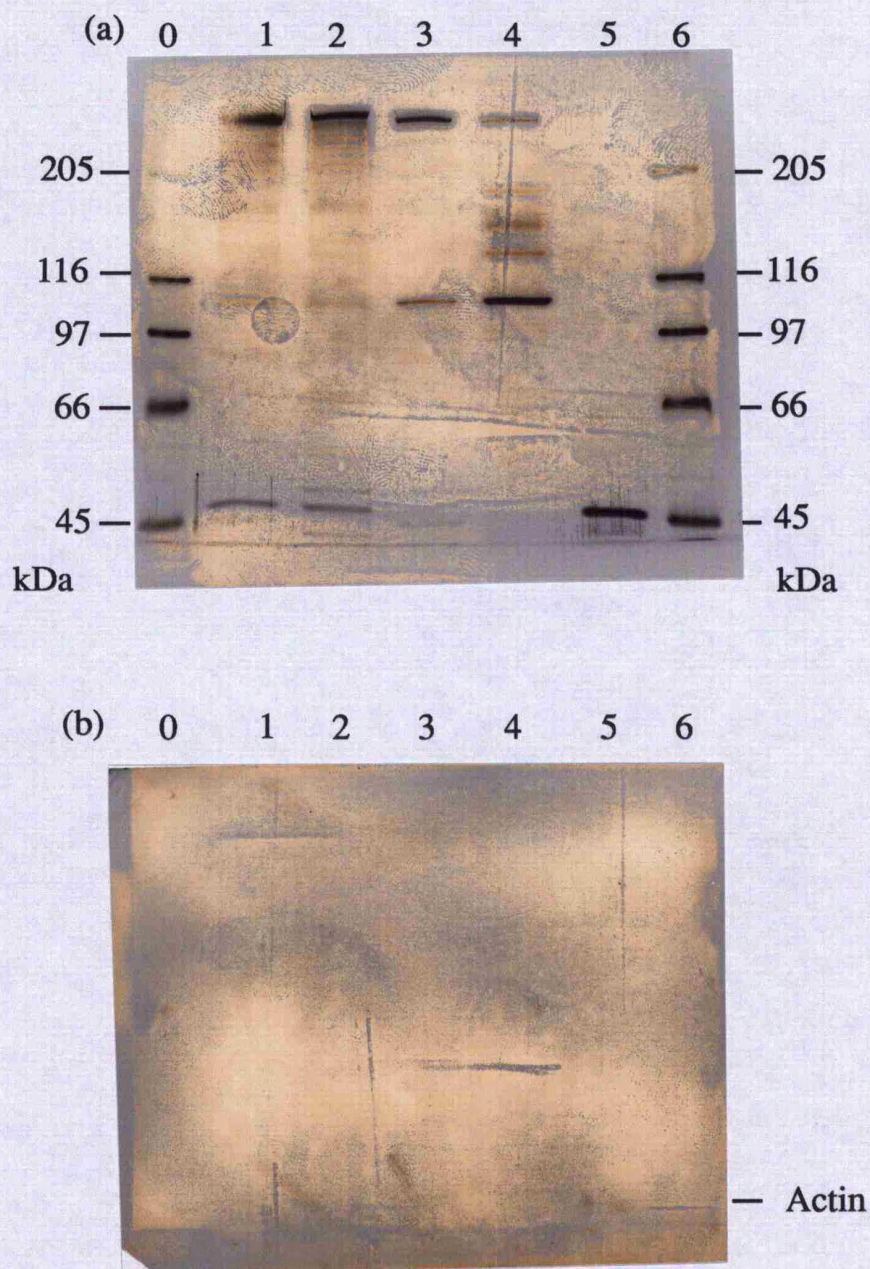
Figure 3.9. Immuno-blot analysis to investigate the four fractions of 14S dynein. Fractions were subjected to SDS-PAGE then either (a) silver-stained or transferred to nitrocellulose and Western-blotted with antibodies raised in rabbit against (b) fraction 1, (c) fraction 2, or (d) fraction 3/4. Tracks: 0 and 7, molecular mass markers; 1-4, 14S dynein fractions 1-4 respectively; 5, unfractionated 14S dynein; 6, 22S dynein.

(c)

0	1	2	3	4	5	6	7

(d)

0	1	2	3	4	5	6	7

Figure 3.10. Immuno-blot analysis to investigate the four fractions of 14S dynein. Fractions were subjected to SDS-PAGE then either (a) silver-stained or transferred to nitrocellulose and Western-blotted with antibodies against (b) **tubulin**. Tracks: 0 and 6, molecular mass markers; 1-4 14S dynein fractions 1-4 respectively; 5, *Tetrahymena* axonemal tubulin.

Figure 3.11. Immuno-blot analysis to investigate the four fractions of 14S dynein. Fractions were subjected to SDS-PAGE then either (a) silver-stained or transferred to nitrocellulose and Western-blotted with antibodies against (b) **actin**. Tracks: 0 and 6, molecular mass markers; 1-4, 14S dynein fractions 1-4 respectively; 5, rabbit actin.

3.11. Electron microscopy analysis of the four fractions

Two major electron microscopy techniques were investigated in the visualisation of 14S dynein fractions; negative-staining and metal-shadowing (sections 3.7.1 & 3.7.2). The former technique was abandoned since artifacts of the staining procedure hindered the identification of dynein molecules. Consequently, structural analysis was exclusive to the images obtained by shadowing techniques. High- and low-resolution electron micrographs of rotary- and/or unidirectionally-shadowed preparations for the four fractions are presented in figures 3.12-3.15. The molecular dimensions of the globular heads and, where appropriate, the overall length, have been determined from the direct measurement of a representative population of molecules and are summarised in table 3.3.

Fraction 1

Both unidirectionally- and rotary-shadowed images of fraction 1 indicated that the molecular structure of this fraction consists predominantly of two globular heads (figure 3.12). The heads were consistently observed together although, at low magnification (50,000 x), the nature of the interconnecting structure was unclear. At high magnification (100-130,000 x) the analysis of rotary-shadowed particles revealed the presence of a V-shaped stem emanating from the two head domains. The two head domains were shown to have an approximate diameter of (11.0 ± 2.3) nm. The length of the stem, however, was difficult to accurately determine since a basal structure was not obvious. Consequently, in comparison, the overall length of the molecule was estimated for a relatively small population of particles and has an approximate value of (25.7 ± 4.8) nm (table 3.3).

Fraction 2

Fraction 2 appeared to comprise at least three distinct structures (figure 3.13) of which two were observed as globular heads (one approximately spherical and the other ellipsoidal) with diameters of (6.5 ± 1.3) nm, and (14.4 ± 1.8) nm x (9.0 ± 1.9) nm respectively (table 3.3). The third structure appeared to be of variable size and shape and was consequently difficult to define. Later work indicated that these structures may represent aggregated forms of the fraction (section 5.8).
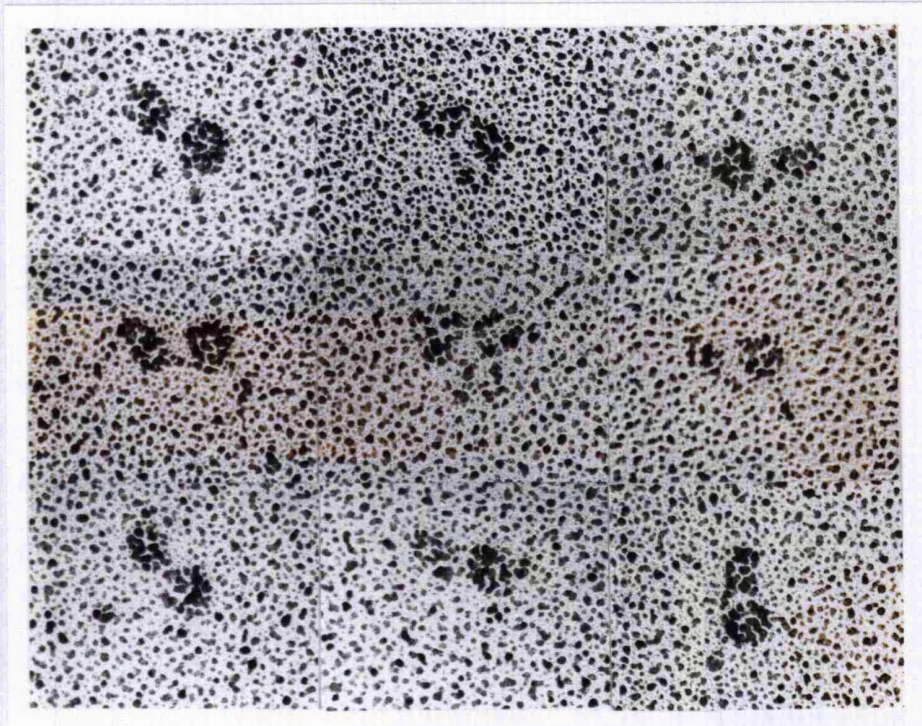
Fraction 3

Fraction 3 consisted entirely of molecules with a single globular head of approximate diameter (9.7 ± 1.5) nm (figure 3.14).
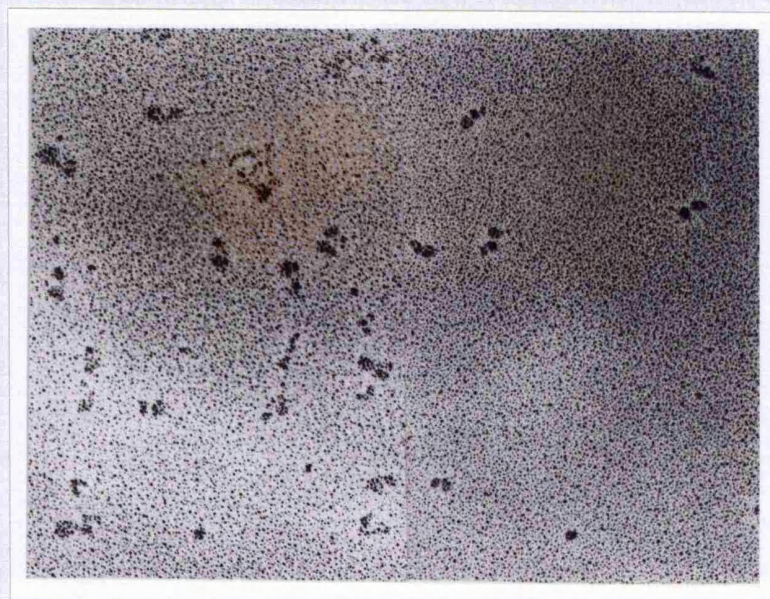
Fraction 4

Rotary-shadowed images of fraction 4 clearly defined the molecular structure of this fraction as comprising molecules with three small globular heads interconnectd via three slender stems (figure 3.15). A low magnification (50,000 x) view, using both unidirectionally- and rotary-shadowing, revealed the overall triangular arrangement of the three heads. At high magnification (100-130,000 x) the dimensions of the heads were estimated to a diameter (6.5 ± 1.7) nm (table 3.3). The overall length of the molecule was shown to be (30.9 ± 4.0) nm.
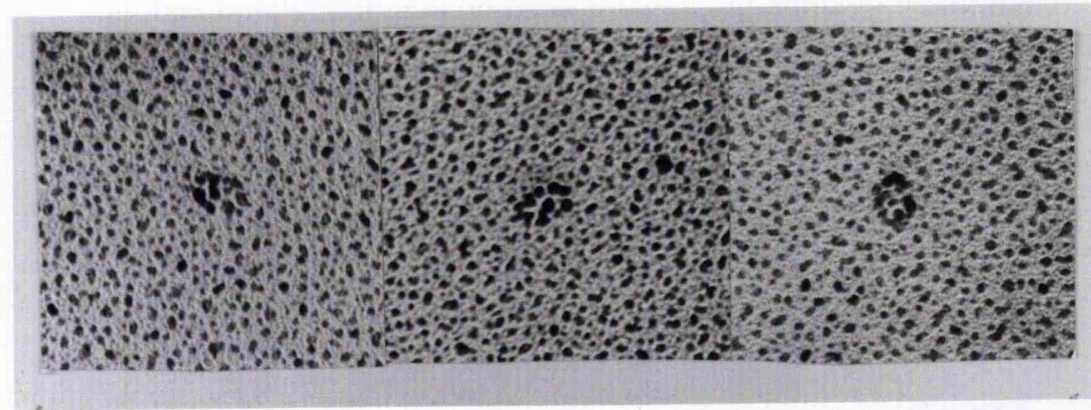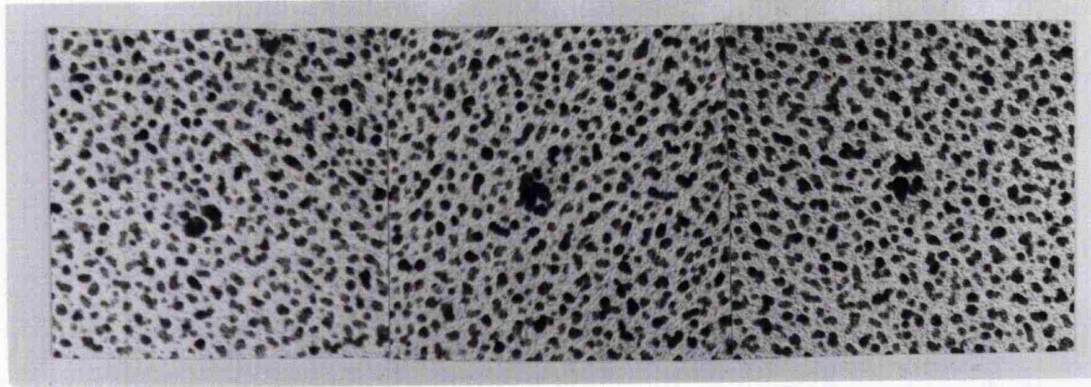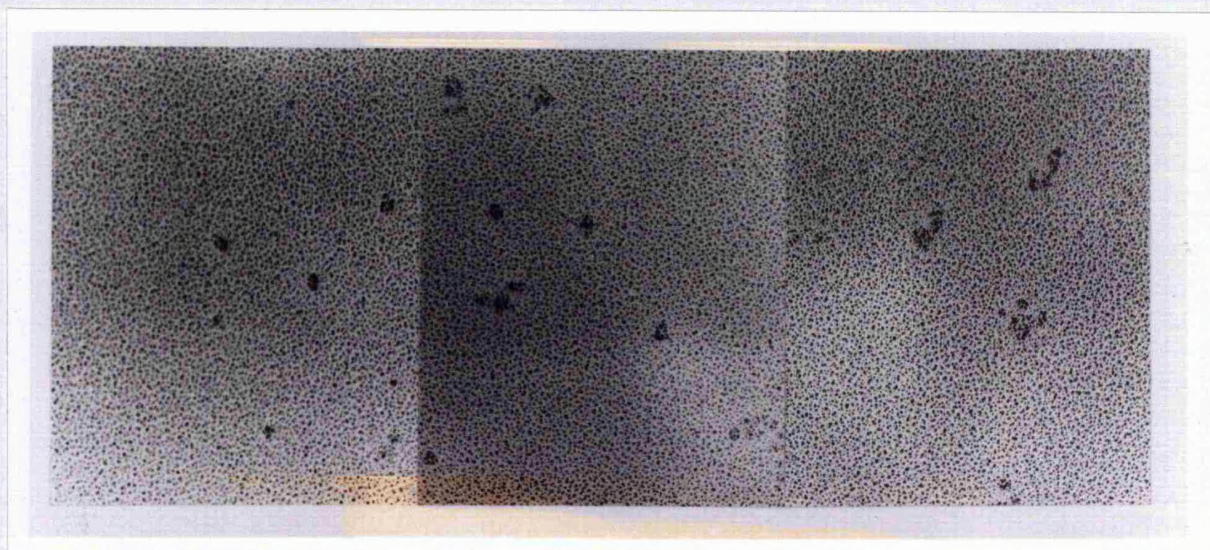
50nm

200nm

200nm

Figure 3.12. Low magnification view of rotary-shadowed (top) and unidirectionally-shadowed (below) molecules of **fraction 1** to illustrate two fields of view. High magnification view (facing page) of a montage of selected molecules in which a defined structure is apparent.
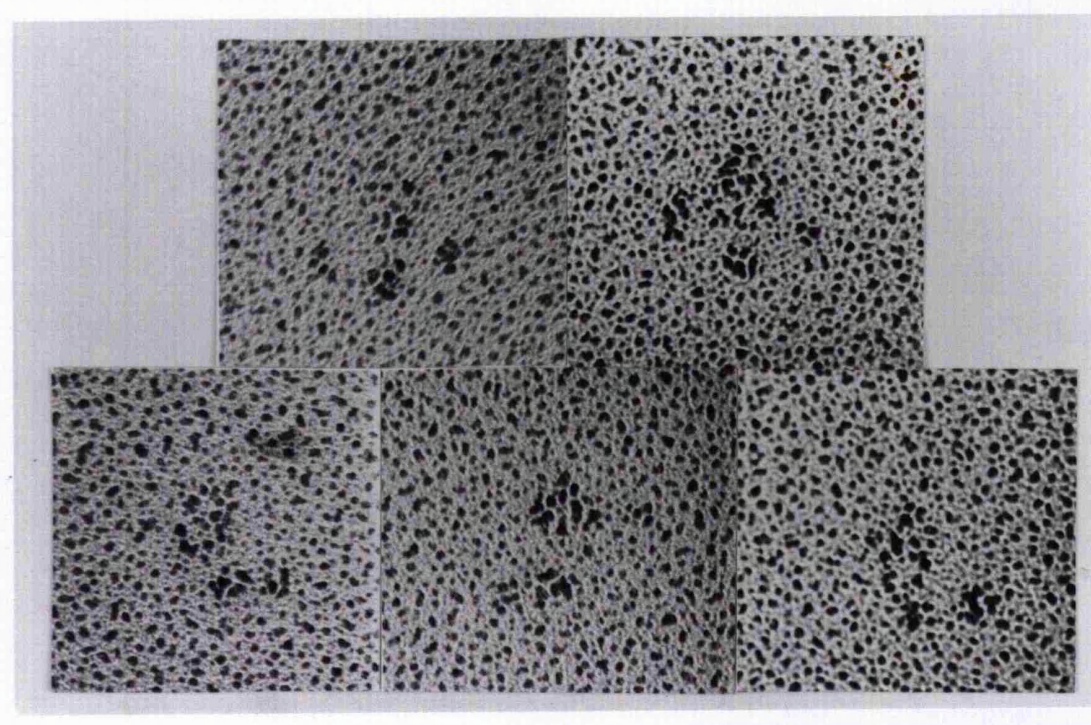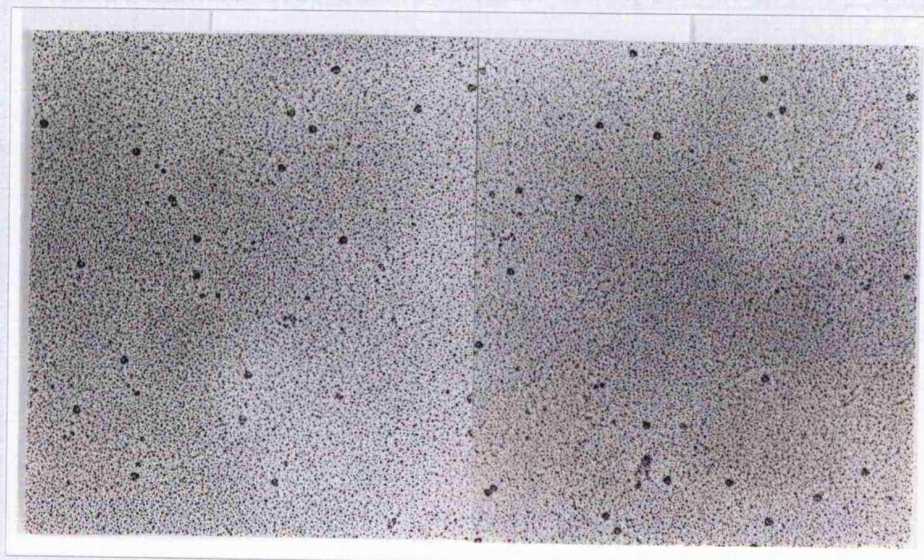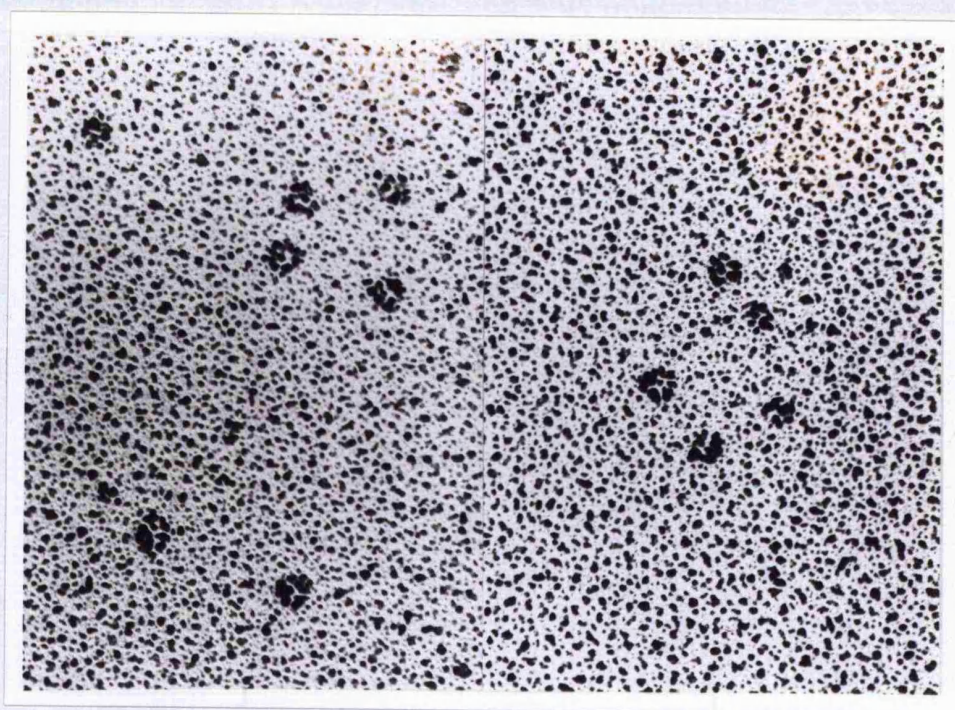
50nm

200nm

Figure 3.13. Rotary-shadowed molecules of **fraction 2.** A low magnification image, presenting three fields of view, shows at least three distinct structures (above). Two globular structures (facing page, above) and large undefined structures (facing page, below) were identified.
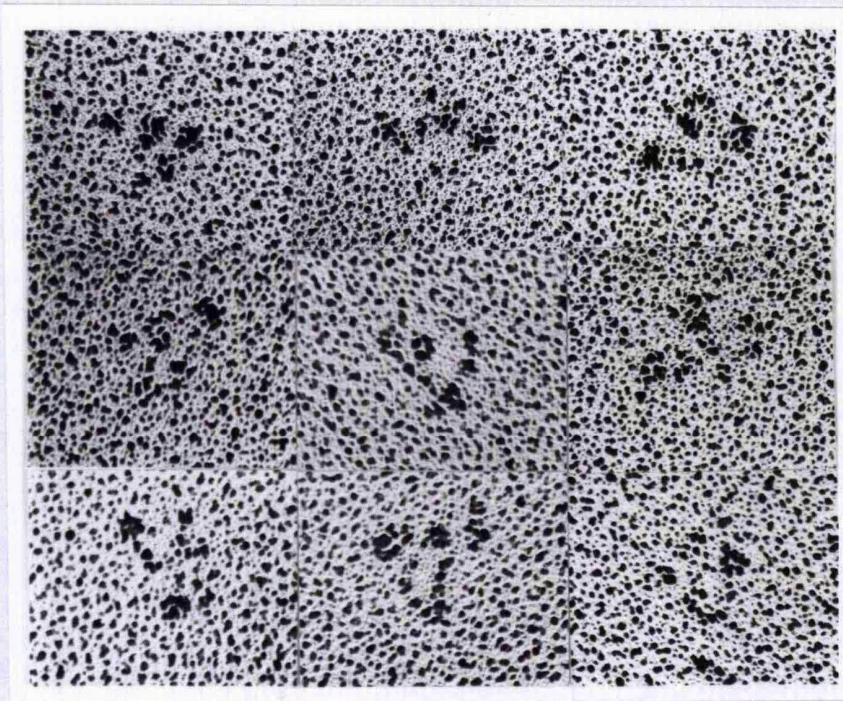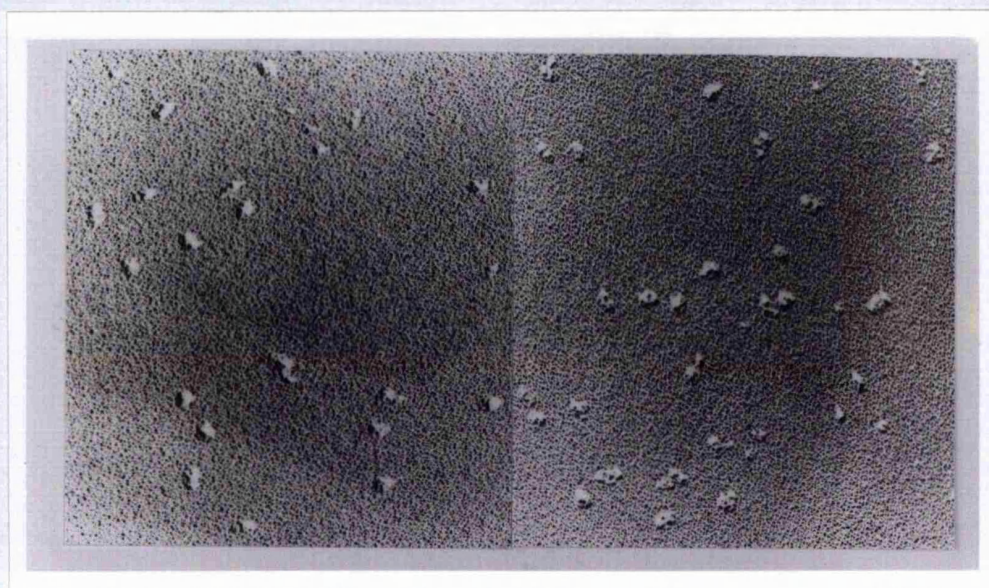
200nm

50nm

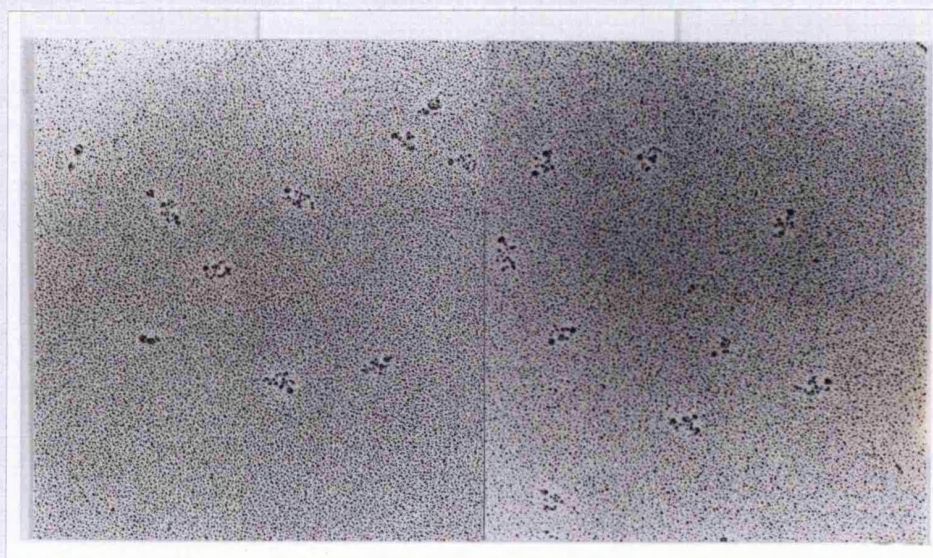**Figure 3.14.** Rotary-shadowed molecules of **fraction 3** to illustrate (top) two fields of view and (below) a high magnification image of representative molecules.

50nm

200nm

Figure 3.15. Low magnification view of rotary-shadowed (top) and unidirectionally-shadowed (below) molecules of **fraction 4** to illustrate two fields of view. High magnification view (facing page) of a montage of representative molecules.

Fraction	Diameter of head domain (nm)	Overall length of molecule
1	11.0 ± 2.3 (n = 44)	25.7 ± 4.8 (n = 16)
2	6.5 ± 1.3 (n = 14) (14.4 ± 1.8) x (9.0 ± 1.9) (n = 11)	-
3	9.7 ± 1.5 (n = 74)	-
4	6.5 ± 1.7 (n = 47)	30.9 ± 4.0 (n = 19)

Table 3.3. Molecular dimensions of the four fractions of 14S dynein.
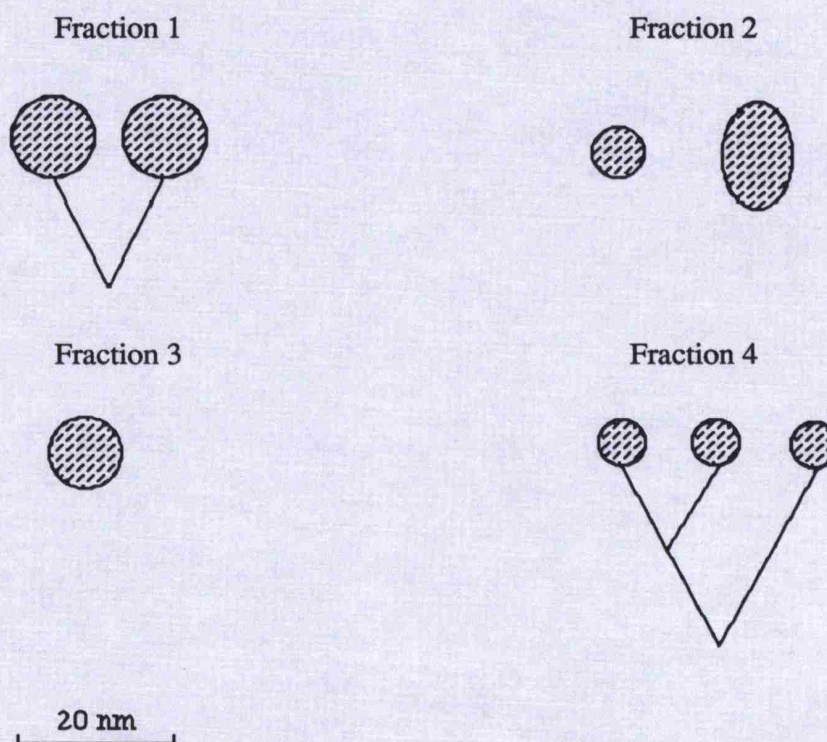
Figure 3.16. Schematic representation of the four 14S dynein fractions based upon electron microscopy analysis.

Discussion

3.12. Optimization of the dynein extraction procedure

One of the major limitations of the dynein extraction procedure concerned the relatively low yields of protein obtainable (table 3.1). In order to achieve adequate concentrations of dynein, it was essential to harvest large cultures of cells in a nutrient-rich medium. Consequently, this introduced a significant risk of fungal and/or bacterial contamination. In particular, growth method 1 was susceptible to contamination introduced either during inoculation or via the air line during aeration of the culture (section 2.4.1). These risks were minimised by inoculation in a laminar flow hood with the aid of a bunsen flame, and by the filtration of air using sterile bacterial air vents (figure 2.1). In addition, it was significantly more difficult to aseptically remove a sample for growth rate analysis from the large 15 litre culture, than from the smaller flask cultures used in growth method 2 (section 2.4.2). As a result, growth in the 15 litre culture could not be regularly monitored and, since the total yield of dyneins remained fairly constant between preparations, cells were thought to be harvested during the stationary phase of growth. Harvesting cells in the stationary phase, however, increased the proportion of debris presumably arising from a prolonged growth in which a proportion of *Tetrahymena* cells had undergone lysis (section 3.8.2). Since lysed cells give rise to the release of proteases, it was particularly important to minimise proteolysis in the dynein preparation. This was achieved by the use of EGTA to chelate calcium-activated proteases, and the use of protease inhibitors (PMSF and leupeptin) throughout the preparation (as described by Johnson, 1986). Proteases were also reduced by ensuring the deciliation process did not continue beyond three minutes since prolonged treatment can induce cell lysis (Thompson *et al.*, 1974). In addition, the effect of any remaining proteases was minimised by carrying out subsequent procedures at $5^{o}C$ (section 2.7).

The application of growth method 2 (section 2.4.2) reduced many of the problems associated with method 1 (section 2.4.1). The risk of contamination was minimised by the inoculation of smaller volumes (750ml) of media. Furthermore, the individual treatment of each flask during the concentration of cells, allowed contaminated flasks to be discarded

95

prior to the dynein preparation (section 2.6.2). Flask cultures could also be easily monitored for cell growth (section 2.5) and harvested in the exponential phase to minimise cell lysis and consequently the release of proteases (section 3.8.2). This optimisation of the dynein preparation ensured the reproducible extraction of 0.7-1.5mg of 14S dynein (table 3.1).

3.13. Heterogeneity of 14S dynein - evidence for four fractions

The 14S dynein was separated into four fractions using an anion-exchange Mono Q HR 5/5 column attached to an FPLC. Hitherto, heterogeneity of 14S dynein was thought to be due to the presence of two (Marchese-Ragona *et al.*, 1988) or three (Muto *et al.*, 1994) distinguishable fractions. Marchese-Ragona *et al.* (1988) described two morphologically different forms of 14S dynein which they were unable to separate (figure 3.1). Alternatively, Muto *et al.* (1994) isolated three fractions of 14S which differed in polypeptide composition (section 3.3).

The work presented here proposes that the heterogeneity of 14S dynein is attributable to the presence of **four** unique species. This conclusion comes from a number of observations. Firstly, four major protein peaks were reproducibly identified using anion-exchange FPLC (figure 3.5). Secondly, each of these peaks was eluted at a specific ionic strength and corresponded to a distinct polypeptide composition when analysed on polyacrylamide gels (figures 3.6 and 3.7). Thirdly, immuno-blot analysis (in conjunction with SDS-PAGE) revealed at least four distinct heavy chains; two associated with fraction 1, one associated with fraction 2, and one associated with a mixture of fractions 3 and 4 {section 3.10.1} (figure 3.9). In this study, antibodies raised in rabbit against fractions 1, 2, and a mixture of fractions 3 and 4, showed no cross-reactivity between heavy chains associated with the three fractions. The relationship between the heavy chain components of fraction 3 and 4, however, has yet to be established since attempts to raise antibodies . against all four fractions proved unsuccessful (section 3.10.2). Fourthly, each fraction showed a reproducible and unique complement of associated intermediate and low molecular mass components (figure 3.7) which were not separable by gel filtration chromatography (figure 3.8). Finally, electron microscopy observations revealed that the

four fractions had unique and distinguishable structures (figures 3.12-3.15). In summary, fraction 1 consists of two globular heads most likely attached via two stems to a common base; fraction 2 is heterogeneous and appears to consist of at least two morphologically distinct globular species; fraction 3 consists of single-headed globular molecules; and finally fraction 4 has a triangular-shaped configuration, consisting of three small globular heads connected via three prominent stems to a common base. Taken together, these results support the proposal that 14S dynein is a complex population of at least **four** species.

3.14. Comparison of the four 14S dynein fractions with previous models

The four fractions presented in this chapter can be compared with the results of previous investigations of 14S dynein.

3.14.1. Polypeptide composition

The polypeptide composition of unfractionated 14S dynein described by Marchese-Ragona *et al.* (1988) comprised **two** heavy chains (>300kDa), one intermediate chain (110kDa) and three light chains (30-55kDa). In contrast, Muto *et al.* (1994) described the existence of **four** distinct heavy chains and several light chains one of which was *Tetrahymena* actin. In agreement with this latter work, the four fractions of 14S dynein described here, show there to be **at least four** distinct heavy chains; two associated with fraction 1, and one each associated with fractions 2 and a mixture of fractions 3/4 {section 3.10.1} (figure 3.9). The association of *Tetrahymena* actin with some of the fractions is also plausible since a polypeptide of comparable mobility to actin, between 42kDa (Hirono *et al.*, 1987) and 43.5kDa (Muto *et al.*, 1994), is evident (table 3.2). The possible location of actin includes a 43.5kDa peptide evident in fraction 2, or a peptide of approximately 44.5kDa that is apparent in fractions 1 and 3, and to a lesser extent, in fraction 4. Confirmation of the association of actin, however, has yet to be established for the four fractions of 14S described here since *Tetrahymena* actin has been shown to differ significantly from rabbit actin (Hirono *et al.*, 1987). Consequently, this necessitates the use of *Tetrahymena*-specific actin antibody for immuno-blot analysis (Muto *et al.*, 1994). Other lower molecular mass polypeptides are also associated with each fraction. This complement of

peptides was thought to represent components of the four separate dynein structures and not contaminating proteins, since the peptides associated with fractions 1, 2, and a mixture of 3/4, were inseparable by gel filtration chromatography (figure 3.8).

3.14.2. Structural models

The structures proposed in this chapter for 14S dynein differ from those originally described by both Marchese-Ragona et al., (1988) and Toyoshima (1987a). In these studies, single-headed structures, some of which possessed a tail-like appendage, were identified. The dimensions of the single-headed molecule were estimated by Toyoshima (1987a) to be 18nm in diameter. In contrast, Marchese-Ragona et al., (1988) described a smaller-sized particle of dimensions 9.5nm x 14.5nm. This latter estimate is within reasonable error of the dimensions presented here for three of the newly-identified fractions, (1 {11.0nm x 11.0nm}, 2 {14.4nm x 9nm}, and 3 {9.7nm x 9.7nm}), summarised in table 3.3. Consequently, the single-headed components described here for fractions 2 and 3, may well be equivalent to the single globular domains previously described for unfractionated 14S dynein. It is also possible to envisage a relationship between fraction 1 and the head-tail structure identified by Marchese-Ragona et al. (1988). One possible interpretation, for example, is that the doubled-headed molecules described here may have been unstable under the preparation conditions used by Marchese-Ragona to produce predominantly single-headed molecules (see section 5.7).

These comparisons of structure show that although 14S dynein appears to be composed of four novel structures, similarities can be drawn between fractions 1, 2 and 3 presented here and structures previously described. Fraction 4, however, appears to be a unique, previously unidentified structure. It is comparable in overall shape to 22S dynein (figure 1.4), although the size of the heads are significantly smaller in diameter. Two of the heads for 22S dynein have been shown to measure 10nm in diameter, whereas the third has a diameter of approximately 12nm (Johnson & Wall, 1983). In contrast, the three heads of fraction 4 all measure 6.5nm (table 3.3).

3.15. Relating polypeptide composition to structure

Almost all dyneins so far described contain the same number of globular heads as heavy chains (Witman, 1989). Each head is believed to comprise the majority of a single copy of a specific heavy chain (Johnson & Wall, 1983; Witman *et al.*, 1983; Sale *et al.*, 1985), whereas the stem and base of the dynein structure are thought to represent the remaining heavy chain and a complex of intermediate and light chains respectively (King & Witman, 1990).

Using these previous observations, a relationship between polypeptide composition and the four 14S dynein structures can be speculated. SDS-PAGE analysis of fraction 1 resolved two heavy chains (figure 3.6), whilst electron microscopy investigations revealed a double-headed structure (figure 3.12). The simplest interpretation, therefore, is that each globular head comprises a single copy of a distinct heavy chain. Furthermore, the interconnecting tail structures, visible using rotary shadowing, may be equivalent to a complex of the intermediate and light chains associated with this fraction (figure 3.7). A comparable interpretation of fraction 3 is also possible since the single globular head (figure 3.14) and single heavy chain component (figure 3.6) of this fraction, suggest that each globular head is composed predominantly of a single heavy chain. In contrast, the interpretation of fractions 2 and 4 is complicated by the observation that the number of heavy chains, identified by gel electrophoresis, is not equivalent to the number of globular heads visualised by electron microscopy. Fraction 2 consists of at least two morphologically distinguishable structures (figure 3.13), whereas fraction 4 is a three-headed molecule interconnected via three stems (figure 3.15). Both fractions, however, appear to consist of a single heavy chain component (figure 3.6).

The anomaly between the number of heads and heavy chains could be interpreted in two ways. The first explanation is that each globular head is composed of a unique heavy chain, and that these heavy chains are of sufficiently similar electrophoretic mobility that they are unresolved by the electrophoretic procedures utilised (section 2.12). This interpretation consequently assumes that fraction 2 and 4 consist of two and three heavy chain components respectively which have yet to be identified. Furthermore, the single resolved heavy chain of fraction 4 could represent three **identical** heavy chains since the

heads are similarly-sized. A second interpretation is to discard the one heavy chain/one globular head domain constraint on the basis that the size of the heads in fractions 2 and 4 are significantly smaller than those described for other dyneins (section C, chapter 1). Indeed, all the heads associated with fraction 4 (figures 3.15), and at least one of the species associated with fraction 2 (figure 3.13), are appreciably smaller than, for example, the heads of 22S dynein (Johnson & Wall, 1983), and the heads of the outer dynein arms of Chlamydomonas (Goodenough & Heuser, 1984) and sea urchin sperm flagella (Sale et al., 1985). Some of these smaller-sized heads, in fractions 2 and 4, could therefore be equivalent to the lower molecular mass polypeptides identified in both fractions (table 3.2). The smaller head (6.5nm x 6.5nm) in fraction 2, for example, may well constitute intermediate and/or light chains, whereas the larger head (14.4nm x 9.0nm) may be equivalent to the single heavy chain. Similarly, intermediate and/or light chains may be equivalent to two of the three heads described for fraction 4, whereas the third head (and a significant proportion of the tail structure) may constitute the presumed single heavy chain of this fraction.

3.16. Relating 14S fractions to the inner dynein arm

The tendency to compare 14S dynein to the structure of the inner dynein arm is partly due to the comparable heterogeneity evident in both systems (section C, chapter 1). Although, the localisation of 14S dynein to the inner arm of Tetrahymena has not been proven conclusively, it is perhaps the most likely location assuming there is no great difference in the overall structure of the axoneme between Tetrahymena, Chlamydomonas and sea urchin sperm. In addition, evidence for an inner arm location is provided by the common association of actin with the inner arm (in Chlamydomonas) and 14S dynein (in Tetrahymena) {section 3.16.1}, as well as the structural similarity that is evident between the multiple species of inner dynein arm (dyad-dyad-triad array) and the heterogeneity of 14S dynein (section 3.16.2).

3.16.1. Association with actin

Indications of an inner arm location for 14S dynein come from the common association of actin with both sources of dynein. Actin is exclusively associated with a species of inner

arm (I2) identified in *Chlamydomonas* (Piperno & Luck, 1979b, 1981; Piperno *et al.*, 1990; Kagami & Kayami, 1992) and has been recently identified in three fractions of *Tetrahymena* 14S dynein (Muto *et al.*, 1994).

At least some of the fractions of 14S dynein described here are also likely to contain actin since polypeptides of corresponding size are evident (table 3.2). Conclusive evidence for this association, however, has not been possible using rabbit skeletal muscle actin antibody since this was significantly divergent from *Tetrahymena* actin to prevent cross-reactivity of immuno-blot analysis (figure 3.11). Nevertheless, assuming actin is present, two possible interpretations exist based on the knowledge that the mass predicted from amino acid sequence analysis of *Tetrahymena* actin is 42kDa (Hirono *et al.*, 1987), and the mass determined by gel electrophoresis is approximately 43.5kDa (Muto *et al.*, 1994). The first possibility is that the actin is associated with fractions 1, 3 and, to a lesser extent, 4, since a polypeptide of approximately 44.5kDa is apparent (table 3.2). In contrast, a second interpretation is that actin (43.5kDa) is associated exclusively with fraction 2. Both explanations were regarded plausible since the variability in molecular mass, between this work and others, was considered to be within the error of the gel analysis system utilised.

3.16.2 Structural comparisons

The heterogeneity of 14S dynein described here can be compared with the heterogeneity reported for inner dynein arms (section 1.12). The inner arm is composed of two distinct structures termed triads and dyads (Goodenough & Heuser, 1985). In *Chlamydomonas*, these structures have been compared to three inner arm subspecies identified by the extraction and subsequent fractionation of dynein isolated from an outer arm-deficient mutant (Goodenough *et al.*, 1987). Two species comprised a single globular head and stem, whereas the third carried two globular head domains interconnected by two stems. The double-headed species was proposed to represent the *in situ* triad (although a third head has yet to be defined), whereas the two single-headed species were suggested to participate in the formation of the dyads. In comparison, a similar analysis can be applied to the four 14S fractions described here. In this case, fraction 1 (figure 3.12) could be equivalent to the *in situ* dyad inner arms since both structures comprise two globular head

domains. Similarly, the single globular heads evident in fractions 2 and 3 (figures 3.13 & 3.14) could represent dyads either as homo- or hetero-dimers. In addition, the triad structure described *in situ* could equate to the three-headed structure of fraction 4 (figure 3.15), although the diameter of the heads for fraction 4 (6.5nm) are somewhat smaller than that determined for the proposed triad inner arm in *Chlamydomonas* (13nm). The long stem described for the triad inner arm species, however, is comparable to that evident in fraction 4. As with the *Chlamydomonas* inner arm subspecies, the long stem is thought to reflect the *in situ* morphology of the triad since this latter structure extends over the microtubule structure in the axoneme to a greater degree than either of the dyads (Goodenough & Heuser, 1985).

Assuming that 14S dynein is located to the inner dynein arm, alternative explanations exist. The four fractions may, for example, represent previously undefined species since multiple inner arm species have been predicted following the identification of two staggered rows of inner arms in *Chlamydomonas* (Muto *et al.*, 1991; Mastronarde *et al.*, 1992). One row (centrifugal) has been shown to comprise four discrete globular domains and may equate to some or all of the single-headed fractions (2 and 3). In contrast, the other row (centripetal) consists of three pairs of globular structures thought to be comparable to the dyad-dyad-triad array previously described (Goodenough & Heuser, 1985). An alternative interpretation is that the four fractions constitute a single species of inner arm yet to be defined. Avolio *et al.* (1986), for example, described one species of *Tetrahymena* inner arm which displayed a 24nm periodicity (along the length of the axoneme) equivalent to that of the outer dynein arm. Some or all of the four fractions described here may therefore be components of a larger species representing the intact inner arm. Fractions which are not part of the intricate inner arm organisation could have an alternative axonemal location such as the ciliary membrane (Dentler, 1980; Dentler *et al.*, 1980) and central pair microtubules (section 1.8.2).

Four 14S dynein fractions have been identified and isolated from the cilia of *Tetrahymena thermophila*. The fractions are unique in terms of immunogenicity, polypeptide

composition, and overall molecular structure. At least some of the fractions are likely to have an inner arm location, although the arrangement at this site has yet to be defined.

Chapter 4

Studies on the ATPase Site and Activity of the Four 14S
Dynein Fractions

Introduction

This chapter is concerned with studies on the ATPase site and activity of the four 14S dynein fractions. The chapter has been divided into two major sections entitled ATPase activity and vanadate-dependent photolysis. The first section concerns functional studies in which ATPase activity has been investigated. The second section describes the technique of vanadate-dependent photolysis which was used to highlight structural differences between the dynein fractions.

ATPase Activity

The hydrolysis of ATP is a fundamental characteristic of all motor proteins. In relation to dyneins, this reaction fuels the translocation of microtubules within the axoneme which ultimately results in bending of the intact cilium or flagellum (section 1.5). ATP hydrolysis is therefore essential to the functional role of dyneins and studies on ATPase activity can indicate important functional properties.

4.1. Dynein ATPases

The association between ATPase activity and dynein was first revealed when the 'arm-like' appendages of *Tetrahymena* axonemes were shown to possess 90% of the ATPase activity associated with these organelles (Gibbons, 1963). Preliminary studies then showed that at least two dynein ATPases could be extracted from most axonemes (including *Tetrahymena* {14S and 22S} (Gibbons & Rowe, 1965), *Chlamydomonas* {18S and 12S} (Piperno & Luck, 1979a) and sea urchin sperm {21S and 12S} (Gibbons *et al.*, 1976)), and that ATPase activity was associated with the heavy chain component of the dynein molecule.

Distinct ATPases were first identified in the outer dynein arm of sea urchin sperm flagella when the two heavy chains of this molecule were dissociated into two subunits (following a low-ionic strength dialysis) and shown to exhibit ATPase activity (Tang *et al.*, 1982). Each subunit comprised a single heavy chain and was shown to exhibit distinguishable enzymatic characteristics. Similar studies on *Chlamydomonas* outer arm and *Tetrahymena* 22S dynein also revealed multiple ATPases. Two ATPases (18S and 12S) were identified following fractionation of the *Chlamydomonas* outer arm (Piperno & Luck, 1979a),

whereas a third was revealed when two subunits of the 18S species (designated α and β) were separated as a consequence of low-ionic strength dialysis (Pfister & Witman, 1984). In comparison, three ATPases were proposed for *Tetrahymena* 22S dynein following kinetic studies in which an ATP-binding site was thought to be located within each of the three globular head domains described for this structure (Shimizu & Johnson, 1983a; Johnson & Wall, 1983). Furthermore, at least two ATPases were revealed by the proteolytic analysis of the three-headed structure of 22S dynein (Toyoshima, 1987a,b). In this study, both a two-headed (comprising the β and γ heavy chains) and a single-headed molecule (comprising the α heavy chain), produced as a result of proteolytic digestion, exhibited ATPase activity.

Several ATPases have also been identified for the inner arm. In *Chlamydomonas,* the analysis of dynein arm-deficient mutants enabled the identification of two (10-11S and 12.5S) inner arm ATPases shown to possess a single heavy chain (Piperno & Luck, 1981). In addition, a third inner arm ATPase (11S) was discovered and shown to comprise two distinct heavy chains (Goodenough *et al.*, 1987; Piperno, 1988). ATPase activity was therefore associated with the heavy chains in both inner and outer dynein arms.

4.2. Activation of ATPase activity.

The ATPase activity of dynein arms can be activated by the presence of microtubules (section 4.2.1). In addition, a number of treatments including exposure to detergent, increased concentrations of monovalent salts, EDTA, and heating have also resulted in significant activation of ATPase activity presumably due to a conformational change in the dynein structure (section 4.2.2). Both observations are thought to reflect a physiological increase in activity that is presumed to occur during motility.

4.2.1. Microtubule activation

The activation of dynein by microtubules occurs as a consequence of the ATP-cyclical interaction through which cilia bending is ultimately achieved (section 1.5.2). Dynein arms attach and detach from microtubules in an ATP-sensitive manner to cause the relative sliding of outer doublet microtubules in the axoneme (section 1.4). During this reaction,

105

microtubules activate dynein ATPase activity by accelerating the release of products (ADP and P_i) from the ATP hydrolysis sites of the dynein molecule (Omoto & Johnson, 1986). Activation by microtubules was first demonstrated in sea urchin 21S outer arm dynein (Gibbons & Fronk, 1979). In this study, ATPase activity was shown to increase 6-fold when 21S dynein was recombined with axonemes in which the dynein arms had been selectively removed. This activation was later shown to be associated with the presence of the outer doublet microtubules (Yokota *et al.*, 1987). Activation has also been demonstrated in the presence of purified microtubules. *Tetrahymena* 22S dynein, for example, was shown to be activated 3-10 fold by purified and repolymerised microtubules originating from bovine brain or *Tetrahymena* axonemes (Omoto & Johnson, 1986). In contrast, a similar study involving *Tetrahymena* 14S revealed a level of activation (3-fold) appreciably less than that exhibited with dynein-depleted axonemes (Shimizu *et al.*, 1992; Warner & McIlvain, 1986). This phenomenon, however, was thought to be due to a difference in the microtubule concentration around each dynein molecule, since the use of a chemical cross-linking reagent (which prevents the ATP-dependent release of dynein from the dynein-microtubule complex) enhanced the level of activation to a maximum of 10-fold (Shimizu *et al.*, 1992).

4.2.2. Latency

The specific ATPase activity of outer arm dynein ATPases was shown to be affected by the conditions up to and following extraction from the axoneme. Studies in sea urchin sperm flagella showed that 21S outer arm dynein had a low specific ATPase activity when removed from the axoneme by high-salt extraction (Gibbons & Fronk, 1979). This so-called 'latent activity dynein' (termed LAD-1) was able to restore motility when recombined with outer arm-deficient axonemes (Gibbons & Fronk, 1979). The term 'latent' arose to reflect the fact that activity could be activated approximately 10-fold following exposure to an increased concentration of monovalent salt (up to 1M), Triton X-100 solution, EDTA, or heating. Under these conditions, the dynein was no longer capable of restoring function in flagella and was consequently thought to be irreversibly modified (Gibbons & Gibbons, 1979). Latent ATPase activity was also demonstrated in

Tetrahymena 22S dynein. In this case, the activation was less pronounced (2-fold) and occurred (in the isolated dynein) following exposure to monovalent salt, sulphydryl reagents, an increased temperature, and ageing (Gibbons, 1966; Blum & Hayes, 1974). Activation under these conditions was thought to be due either to the loss of a subunit or component that regulates ATPase activity, or alternatively, as a consequence of a change in the conformation of the dynein molecule (Gibbons & Fronk, 1979). Both interpretations originated from the observation that the sedimentation coefficient (and presumably mass) was shown to decrease following exposure to Triton X-100 (Gibbons & Fronk, 1979). In addition, evidence in support of a conformational change was provided by an analysis of salt concentration on the conformation and ATPase activity of *Tetrahymena* 22S dynein (Wells *et al.*, 1990). In this study, an increase in monovalent salt concentration (from 40mM to 600mM) was shown to result in a 2.7-fold activation of ATPase activity. Furthermore, under these conditions both the sedimentation coefficient and mass of the molecule was shown to decrease. This decrease was considered to reflect a conformational change. In particular, the presence of 40mM NaCl was thought to induce self-association of the dynein molecule to form dimers and was coincident with a decrease in ATPase activity (Wells *et al.*, 1990). A conclusive relationship between conformation and ATPase activity, however, remains to be established.

4.3. Localisation of ATP-hydrolysis sites

Each globular head domain of the dynein molecule has been shown to possess a catalytic site for ATP binding and hydrolysis. This association was first proposed following kinetic analysis of *Tetrahymena* 22S dynein in which three ATP-binding sites were associated with the three-headed 22S molecule (Shimizu & Johnson, 1983a). As a result, the proposal of a single hydrolytic ATP-binding site located within each globular head domain was first considered. This hypothesis was then confirmed by a number of independent studies.

The use of ATP analogues provided a direct means for the identification of ATP-binding sites. In particular, the radioactive photoaffinity analogue 8-azido ATP ($8-N_3ATP$) was shown to competitively inhibit ATP hydrolysis by its interaction with nucleotide-binding sites. Studies involving this analogue showed that the *Chlamydomonas* 12S outer arm

dynein has an ATP-binding site located exclusively in the single heavy chain component (γ) of this dynein (Pfister *et al.*, 1984). This was concluded since radiolabelled analogue was shown to incorporate specifically into the heavy chain component and not into either of the two associated light chains. Similar, studies on the 18S subunit of the outer arm showed that both α and β heavy chains possessed single ATP-binding sites (King *et al.*, 1989). In comparison, investigations with sea urchin dynein indicated a site of ATP-hydrolysis in each of the two heavy chains of the flagellar dynein (Pratt, 1986). Consequently, an ATP hydrolysis site was located in all cases to the dynein heavy chain. Conclusive evidence for the localisation of an ATP-hydrolysis site within dynein heavy chains was produced following the determination of the heavy chain amino acid sequences for the α , β (Mitchell & Brown, 1994), and γ (Wilkerson *et al.*, 1994) heavy chains of *Chlamydomonas*, and the β heavy chain of sea urchin sperm (Gibbons *et al.*, 1991; Ogawa, 1991). In all sequences, the heavy chain was shown to possess four putative ATP-binding sites (or P-loops) which are thought to represent nucleotide binding regions since the consensus sequence GXXXXGKT/S resembles that identified in several other nucleotide-metabolising enzymes (Walker *et al.*, 1982). In particular, one site (designated **P1**) shows absolute conservation within the dynein heavy chain sequences currently known, and is consequently thought to represent a site for catalytic ATP binding. It has yet to be established, however, whether any of the three remaining P-loop motifs participate in nucleotide binding.

Vanadate-dependent Photolysis

Another method for the localisation of potential ATP hydrolysis sites has been achieved using the technique of vanadate-dependent photolysis. This procedure can be used since a site of cleavage designated V1 has been shown to reside within the hydrolytic domain of the dynein heavy chain (Gibbons *et al.*, 1991; Ogawa, 1991; Mitchell & Brown, 1994; Wilkerson *et al.*, 1994). In addition, vanadate-dependent photolysis has been used to indicate structural differences between dynein heavy chains, as well as to provide more accurate determinations of heavy chain molecular mass, and enable the construction of heavy chain linear peptide maps.

4.4. Two types of vanadate-dependent photolysis

Dynein heavy chains can be cleaved at specific sites when subjected to UV irradiation in the presence of vanadate. Two specific sites of cleavage have been reported and are termed V1 and V2. The V1 site has been shown to occur at, or near, the hydrolytic site of ATP binding (section 4.4.1), whereas the location of the V2 site is unclear (section 4.4.2). The conditions under which V1 and V2 photolysis occur were originally defined during initial investigations on vanadate-dependent photolysis. In these studies, V1 photolysis of the heavy chains was shown to require low ($10\mu M$) concentrations of inorganic vanadate (V_i) and the presence of both magnesium ions (Mg^{2+}) and ATP (Lee-Eiford *et al.*, 1986). In contrast, cleavage at the V2 site required larger concentrations of V_i ($100-150\mu M$) and, in order to inhibit cleavage at the V1 site, the presence of manganese ions (Mn^{2+}) (Tang & Gibbons, 1987). In addition, V2 cleavage was inhibited by the presence of ATP. Since these original definitions, a differential requirement for nucleotide has been reported. Certain heavy chains have been reported to undergo V1 photolysis in the absence of ATP whereas, ATP-dependent inhibition of V2 cleavage is not always apparent (section 4.6.2). These differences are thought to reflect structural variation (which may be related to functional differences) between dynein heavy chains.

4.4.1. V1 photolysis

The cleavage of dynein heavy chains by UV irradiation was first reported in the isolated outer dynein arm of sea urchin sperm flagella (Lee-Eiford *et al.*, 1986). This investigation showed that when dynein was irradiated at 254nm in the presence of 50μM MgATP and 100μM V_i, the α and β dynein heavy chains of the outer arm, were each specifically cleaved to produce two similarly-sized fragments, termed **cleavage peptides** (228kDa and 200kDa). As well as this specific cleavage, however, an amount of non-specific cleavage was also apparent. Subsequent studies then showed that non-specific cleavage could be significantly reduced by a change in wavelength from 254nm to 365nm (Gibbons *et al.*, 1987a). This had the effect of optimising the photolysis reaction since the yield of cleavage peptides increased from 63% to 90% (Lee-Eiford *et al.*, 1986; Gibbons *et al.*, 1987a).

The specific sites at which cleavage occurred were later termed the V1 sites (Gibbons *et al.*, 1987a). The V1 site has been located at (or in close proximity to) the proposed ATP-hydrolysis site of the dynein heavy chain (Gibbons *et al.*, 1991; Ogawa, 1991; Wilkerson *et al.*, 1994; Mitchell & Brown, 1994). Analysis of the amino acid sequence showed that the V1 site mapped closely to the highly conserved nucleotide-binding consensus sequence termed P1 (section 4.3). Furthermore, preliminary evidence to indicate this location came from the initial observations that cleavage was dependent upon the presence of MgATP, and that dynein ATPase activity was completely inactivated following photolysis (Lee-Eiford *et al.*, 1986). Similarly, V1 cleavage was shown to be prevented if ATPase activity (and consequently the hydrolysis site) was disrupted by denaturing agents (Gibbons *et al.*, 1987a).

4.4.2. V2 photolysis

Cleavage of dynein heavy chains at one or more V2 sites was first demonstrated in the outer dynein arm of sea urchin sperm. In this study, the α and β heavy chains were shown to cleave at a region 100kDa removed from the V1 site (Tang & Gibbons, 1987). This site (termed V2) was originally thought to be in close proximity to the hydrolytic ATP-binding

site (Tang & Gibbons, 1987). Both V1 and V2 sites were therefore considered to have a similar location within the tertiary structure of the heavy chain.

Support for this initial location of the V2 site was thought to be provided by a number of observations. Firstly, the hydrolysis site was indicated by the ATP-induced inhibition of V2 photolysis. This suggested that the reaction could only proceed if the hydrolysis site was unoccupied (Tang & Gibbons, 1987). Secondly, studies using ATP analogues (as probes for the ATP hydrolysis site) revealed that two distant regions of the heavy chain primary structure could bind ATP. In sea urchin sperm, for example, the photoaffinity ATP analogue 8-N_3ATP was shown to differentially label the cleavage peptides arising from V2 photolysis of the α and β heavy chains (Tang & Gibbons, 1987). The β heavy chain incorporated label in both cleavage peptides, whereas only the larger cleavage peptide was labelled following photolysis of the α heavy chain. In comparison, similar studies in *Chlamydomonas* outer arm dynein revealed that the α heavy chain incorporated label on the larger (C-terminus) of two cleavage peptides, whereas both products were labelled for the β heavy chain (King *et al.*, 1989). Taken together these data were interpreted to suggest that two distant regions in the heavy chain structure could form a single ATP hydrolysis site. Indeed, the 100kDa difference in distance between the V1 and V2 sites was thought to arise due to the presence of a loop within the heavy chain tertiary structure (King *et al.*, 1989).

More recently, analysis of heavy chain amino acid sequences has enabled an alternative interpretation for the location of V2 sites (Gibbons *et al.*, 1991; Ogawa, 1991; Wilkerson *et al.*, 1994; Mitchell & Brown, 1994). The identification of four nucleotide-binding site consensus sequences (P-loops) suggest that the V1 and V2 sites may be localised to different regions of the heavy chain. Although the V1 site has been mapped to the most highly conserved sequence (P1), the location of the V2 sites (with respect to the three remaining P-loops) is less defined. In the β heavy chain of sea urchin sperm, for example, a P-loop termed P4 (which is conserved amongst axonemal dyneins) is closely mapped to the single V2 cleavage site of this heavy chain (Gibbons *et al.*, 1991). Similarly, two of the three V2 sites identified in the α heavy chain of *Chlamydomonas* map closely with P-loops 3 and 4 (Mitchell & Brown, 1994). In contrast, however, other sites show less

coincidence. In *Chlamydomonas*, the third site of V2 cleavage in the α heavy chain is located 12kDa C-terminal to P4. Similarly, the single V2 site associated with the β heavy chain, and the two V2 sites associated with the γ heavy chain, have been mapped to regions **between** P-loop motifs (Mitchell & Brown, 1994; Wilkerson *et al.*, 1994). Consequently, a relationship between P-loops and V2 sites has yet to be established.

4.5. Mechanism of vanadate-dependent photolysis

Vanadate was recognised as an inhibitor of ATPase activity long before the phenomenon of photolysis was reported and, in dynein, was first demonstrated in the outer arm of sea urchin sperm flagella (Gibbons *et al.*, 1978). Kinetic experiments then showed that inorganic vanadate (V_i) acts as a phosphate analogue resulting in the formation of a dynein.ADP.V_i complex which prevents further ATP hydrolysis (Shimizu & Johnson, 1983b). Vanadate is thought to occupy the γ phosphate location of ATP to form ADP.V_i (Shimizu & Johnson, 1983b). In this way, the V_i and β phosphate are coordinated with a divalent cation (Mg^{2+} or Mn^{2+}), within the hydrolytic site, in a manner similar to that of the β and γ phosphates of ATP (Shimizu & Furusawa, 1986). Irradiation of the dynein.ADP.V_i complex was later shown to result in cleavage of the dynein heavy chains at the V1 site (Lee-Eiford *et al.*, 1986; Gibbons *et al.*, 1987a). Irradiation (at 365nm) causes the excitation of monomeric V_i which ultimately catalyses the cleavage of a peptide bond localised within the hydrolytic site {section 4.5.1} (Gibbons *et al.*, 1987a, 1991). In contrast, cleavage at the V2 site generally occurs in the absence of nucleotide, and involves an interaction between oligomeric vanadate species and target sites within the heavy chain sequence (section 4.5.2).

4.5.1. V1 photolysis

The site of V1 photolysis has been mapped to the P1 consensus sequence in dynein heavy chains from both *Chlamydomonas* and sea urchin sperm (section 4.4.1). In sea urchin sperm, the amino acid proline in this sequence (GXXXXGKT/S; where X = proline) was proposed as the likely point of cleavage in the photolysis reaction on the basis of a comparison with vanadate-dependent photolysis in myosin and adenylate kinase (Gibbons *et al.*, 1991). In myosin, for example, the point of scission was localised specifically to a

serine residue (GESGAGKT) within an almost identical consensus sequence (Cremo *et al.*, 1989). Similarly, a comparable location was identified in adenylate kinase but in this case a proline (GGPGSGKG) was identified as the point of scission (Cremo *et al.*, 1992). By analogy, a conserved proline was considered the most likely point of scission in dynein heavy chains and is present in all P1 sequences so far determined (Gibbons *et al.*, 1991; Wilkerson *et al.*, 1994; Mitchell & Brown, 1994).

4.5.2. V2 photolysis

The sites for V2 photolysis in dynein are less well defined although the chromophore responsible for cleavage has been indicated as oligomeric (in particular trimeric) vanadate (Tang & Gibbons, 1987; King & Witman, 1987). In contrast with V1 photolysis, **oligomeric** V_i species are thought to interact directly with V2 sites to cause scission of a peptide bond. This interpretation is based upon the observation that higher concentrations of V_i (in which oligomeric species predominate) are required for V2 photolysis to occur (Tang & Gibbons, 1987), and that oligomeric V_i (specifically tetravanadate) has been implicated in the V2 cleavage of myosin (Cremo *et al.*, 1990). In this latter study, cleavage at the V1 and V2 sites occurred in the presence of high concentrations of V_i (1mM), and was shown to involve tetrameric V_i which bound, or was considered to bind, to the V2 and V1 sites respectively. Cleavage at the V1 site was then shown to be partially inhibited by the presence of a divalent transition metal (Co^{2+}) which was thought to form a tight complex between V_i, the transition metal, and the hydrolytic (V1) site. As a result, V2 cleavage in myosin was studied in isolation from cleavage at the V1 site, and was localised to a lysine-rich region in which one or more serine residues were implicated in the cleavage reaction (Cremo *et al.*, 1990). By analogy, plausible cleavage points within the dynein heavy chains include a serine residue in P4 of the sea urchin β heavy chain (Gibbons *et al.*, 1991), and a serine in P3 and P4 of the *Chlamydomonas* α heavy chain (Mitchell & Brown, 1994). The exact position of these sites within the dynein heavy chains, however, has yet to be defined (section 4.4.2). Consequently, the possible localisation of V2 site(s) to the ATP-hydrolysis site cannot be discarded since the differing location of the V1 and V2 sites (100kDa in the primary structure) may be in close

proximity in the tertiary structure as a result of extensive heavy chain folding (King *et al.*, 1989).

4.6. Applications of vanadate-dependent photolysis

4.6.1 A tool for identifying dyneins?

Vanadate-dependent photolysis has been described as a property characteristic of most or all dynein ATPases. Although **inhibition** by inorganic vanadate (V_i) had been demonstrated in other ATPases, such as rabbit skeletal myosin (Goodno, 1979), heavy chain cleavage was initially regarded as a feature unique to dyneins. Following the discovery of V2 photolysis, however, cleavage was demonstrated in ATPases other than dyneins. Investigations on rabbit skeletal myosin showed that irradiation in the presence of 1mM V_i resulted in cleavage at three specific sites within the heavy chain (Mocz, 1989). Similarly, adenylate kinase from chicken muscle was shown to undergo photolysis at a single site in the presence of 0.25mM V_i (Cremo *et al.*, 1992). Furthermore, transition metals other than V_i were shown to promote cleavage. Both iron (III) and rhodium (III) were shown to promote heavy chain cleavage in the outer dynein arm of sea urchin sperm flagella (Mocz & Gibbons, 1990). Despite these exceptions, vanadate-dependent photolysis is still often utilised as a diagnostic tool for the presence of cytoplasmic and axonemal dyneins.

4.6.2. Determination of structural differences

One of the major applications of vanadate-dependent photolysis, has been in the determination of structural variation, which is thought may reflect functional differences, between dynein heavy chains. The analysis of cleavage peptides has indicated differences in the number and location of V1 and V2 sites. Differences have also been implicated by the differential requirement for nucleotide in the photolysis reaction.

V1 photolysis revealed that dynein heavy chains have a single V1 site located within 50kDa of the heavy chain midpoint. In the presence of nucleotide, the heavy chains from *Tetrahymena* 22S dynein (Marchese-Ragona *et al.*, 1989), *Chlamydomonas* (King & Witman, 1987; 1988) and sea urchin sperm outer dynein arm (Gibbons *et al.*, 1987a) were

each cleaved to produced two cleavage peptides (table 4.1). Variations within this site, however, were indicated by a differential requirement for nucleotide. In *Chlamydomonas*, the α and γ heavy chains were cleaved at the V1 site regardless of the absence or presence of MgATP, whereas cleavage of the β heavy chain was dependent upon nucleotide. Similarly, in *Tetrahymena* 22S dynein only the β heavy chain (and not the α or γ) underwent cleavage at the V1 site in the absence of MgATP.

Source of dynein	α	β	γ
Sea urchin sperm flagella outer arm	228 200	228 200	-
Chlamydomonas outer arm	290 190	255 185	235 180
Tetrahymena 22S	232 185	225 195	242 161

Table 4.1. Mass of cleavage peptides (in kDa) produced as a result of V1 photolysis in the presence of nucleotide for the outer dynein arm of sea urchin sperm flagella (Gibbons *et al.*, 1987a), *Chlamydomonas* (King & Witman, 1987, 1988), and *Tetrahymena* 22S dynein (Marchese-Ragona *et al.*, 1989). The heavy chains from each dynein source are denoted α, β, and γ.

Dynein heavy chains were also shown to differ significantly with respect to the number and location of V2 photolysis sites. In the absence of nucleotide, three and two V2 sites were identified in the α and γ heavy chains respectively of the *Chlamydomonas* outer dynein arm (King & Witman, 1987, 1988). In contrast, single V2 sites were located in the α and β heavy chains of sea urchin sperm outer arm (Tang & Gibbons, 1987), the β heavy chain of *Chlamydomonas* outer arm (King & Witman, 1987; 1988), and all three heavy chains associated with *Tetrahymena* 22S dynein (Marchese-Ragona *et al.*, 1989). Table 4.2 summarises the cleavage peptides produced by V2 photolysis in the absence of nucleotide.

V2 photolysis in the presence of nucleotide revealed additional variation between heavy chains. Under these conditions, the α and β heavy chains of sea urchin sperm flagella (Tang & Gibbons, 1987), and the three heavy chains of *Chlamydomonas* outer dynein arm (King & Witman, 1987; 1988), did not undergo cleavage. In contrast, V2 photolysis of all three heavy chains associated with *Tetrahymena* 22S dynein were unaffected by the presence of nucleotide (Marchese-Ragona *et al.*, 1989).

Source of dynein	α	β	γ
Sea urchin sperm flagella outer arm	260 170	255 175	-
***Chlamydomonas* outer arm**	(250, 230) & (280, 200) & (290, 190)	260 180	(215, 200) & (250, 165)
***Tetrahymena* 22S**	237 178	240 175	218 205

Table 4.2. Mass of cleavage peptides (in kDa) produced as a result of V2 photolysis in the absence of nucleotide for the outer dynein arm of sea urchin sperm flagella (Tang & Gibbons, 1987), *Chlamydomonas* (King & Witman, 1987, 1988), and *Tetrahymena* 22S dynein (Marchese-Ragona *et al.*, 1989). The heavy chains from each dynein source are denoted α, β, and γ. Brackets indicate pairs of peptides produced in the photolysis reaction where more than one V2 site exists.

4.6.3. Estimations of heavy chain mass

Another major use for vanadate-dependent cleavage is in the estimation of heavy chain molecular mass. The mass predicted for dynein heavy chains has been notoriously difficult using gel electrophoresis due to the inadequacy of the technique, and lack of appropriate standards, in the high (200-500kDa) molecular mass range. By comparison, the vanadate-cleavage technique has enabled more accurate determination of heavy chain mass based on the assumption that new peptides appearing after UV irradiation originate from the dynein heavy chain. A summation of the cleavage peptides give a more accurate approximation of the heavy chain mass (from which they originated) since the cleavage

116

peptides are of appreciably smaller size. Cleavage at both the V1 and V2 sites enable two determinations of heavy chain mass (table 4.3).

Source of dynein	α	β	γ
Sea urchin sperm flagella outer arm	V1 = 428 V2 = 430	V1 = 428 V2 = 430	-
Chlamydomonas outer arm	V1 = 480 V2 = 480	V1 = 440 V2 = 440	V1 = 415 V2 = 415
Tetrahymena 22S	V1 = 417 V2 = 415	V1 = 420 V2 = 415	V1 = 403 V2 = 423

Table 4.3. Mass estimates (in kDa) for the heavy chains of the outer dynein arm of sea urchin sperm flagella (Gibbons *et al.*, 1987a; Tang & Gibbons, 1987), *Chlamydomonas* (King & Witman, 1987, 1988), and *Tetrahymena* 22S dynein (Marchese-Ragona *et al.*, 1989). The heavy chains from each dynein source are denoted α, β, and γ. Mass estimates have been calculated from a summation of the cleavage peptides resulting from V1 or V2 photolysis.

The accuracy with which heavy chain molecular masses have been estimated using vanadate-dependent methods, can be compared with data from other work. The complete amino acid sequence for the β heavy chain from sea urchin sperm flagella, for example, predicted a heavy chain mass of 512kDa (Ogawa, 1991). Similarly, the complete sequence for the β (Mitchell & Brown, 1994) and γ (Wilkerson *et al.*, 1994) heavy chains of *Chlamydomonas* predicted masses of 520kDa and 513kDa respectively. A comparison with vanadate-dependent photolysis revealed the relative inadequacy of SDS-PAGE, in the high molecular mass region (>200kDa), since this technique underestimated heavy chain mass. Nevertheless, the vanadate estimates are all within 100kDa of that predicted by amino acid sequence data.

4.6.4. Construction of linear peptide maps

Vanadate-dependent photolysis has also been a useful tool in the construction of linear peptide maps which describe sites of structural and functional interest within the dynein heavy chain. In general, maps incorporate data from vanadate-dependent and proteolytic

cleavage experiments as well as primary sequence determination. From these studies, two important characteristics of the dynein heavy chain structure have emerged. Firstly, the V2 site has been localised within the larger V1 cleavage peptide in all the heavy chains associated with the outer dynein arm of *Chlamydomonas* and sea urchin sperm, as well as *Tetrahymena* 22S dynein (King & Witman, 1987, 1988; Tang & Gibbons, 1987; Marchese-Ragona *et al.*, 1989). Secondly, the orientation of the V1 and V2 sites has been localised towards the amino- and carboxyl-terminus respectively in heavy chains associated with both *Chlamydomonas* and sea urchin sperm (Gibbons *et al.*, 1991, Ogawa, 1991; Wilkerson *et al.*, 1994; Mitchell & Brown, 1994).

Methods

This section describes methods exclusive to this chapter. General preparative techniques have been described elsewhere. In particular, the preparation of dynein (section 2.7) and microtubules (sections 2.10) have been included in chapter 2.

4.7. ATPase assay

ATPase activity was investigated using a linked assay in which ATP hydrolysis was coupled to the oxidation of NADH (Emes and Rowe, 1978). This assay works on the principle that, providing the linking enzymes and intermediate substrates are in excess, the production of NAD is proportional to ATPase activity (figure 4.1). The ATPase activity of dynein is measured as the rate of decrease in absorbance at 340nm caused by the oxidation of NADH. All assays were carried out at a constant temperature of 23°C in micro-cuvettes with a volume capacity of 150μl. The decrease in absorbance was monitored at a rate of 5mm per minute, using either a Perkin-Elmer Lambda 5 double-beam or a Unicam SP8-100 spectrophotometer attached to a chart recorder. Each series of assays were routinely calibrated by the addition of 4μl aliquots of 1mM ADP to the assay mix in the absence of dynein. The reduction in absorbance caused by a known quantity of ADP was then determined and used to calculate the production of ADP (μmoles) per minute per mg of dynein.
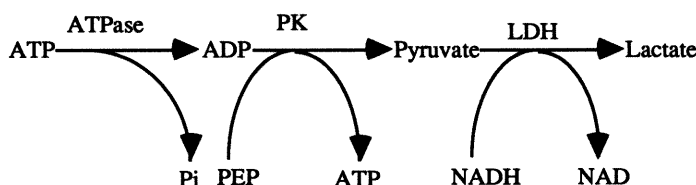
Figure 4.1. Pathway by which ATPase hydrolysis is coupled to the oxidation of NADH.

4.7.1. Dynein ATPase activity

Dynein samples were dialysed for 16 hours in 2 x 2 litres of buffer (10mM Hepes, 4mM MgCl$_2$, 0.1mM EGTA and 0.1mM DTT, pH 7.4) containing a final concentration of either 40mM or 600mM NaCl. The assay was prepared directly in the cuvette by adding 100µl of dynein (ranging in concentration from 0.04-0.1mg/ml) to 12µl of an assay mixture to give a final volume of 400µM PEP, 250µM NADH and 1% (v/v) PK/LDH (700/1000 units ml^{-1}). A fixed volume (26µl) of the dialysate was then added so that the final assay volume (once the MgATP had been added) was 150µl. Before the addition of MgATP, the assay mixture was monitored for 5 minutes until a steady baseline was achieved. The ATPase activity was then initiated by the addition, and subsequent mixing, of MgATP at a final concentration of 400µM. The rate of decrease in absorbance at 340nm was recorded for approximately 20 minutes.

In addition, ATPase activity was recorded for dynein samples dialysed for 16 hours in 2 x 2 litres of buffer containing 10mM Hepes, 1mM MnCl$_2$, 0.1mM EGTA and 40mM NaCl, pH 7.4. The assay procedure was then identical to that described previously with the exception that the assay was initiated by the addition of **MnATP**.

4.7.2. The effect of microtubules on dynein ATPase

The linked assay (figure 4.1) was also used to measure the ATPase activity of dynein samples in the presence of purified porcine brain microtubules. Microtubules were prepared in advance and repolymerised prior to use (section 2.10.2). Dynein samples were dialysed for 16 hours in 2 x 2 litres of buffer containing 10mM Hepes, 4mM MgCl$_2$, 0.1mM EGTA, 40mM NaCl and 0.1mM DTT, pH 7.4.

Microtubules were pre-incubated with the dynein sample for 10 minutes at 23°C. The weight ratio of microtubules to dynein was 333:1 and 667:1 for 22S dynein, and 360:1, 800:1, and 1400:1, for each of the four 14S fractions. A small volume of 3M NaCl was added at this stage to maintain the final NaCl concentration at 40mM. A fixed volume (127µl) of the pre-incubated solution was then transferred to the micro-cuvette and 12µl of the assay mixture (as described in section 4.7.1) added. The assay was then monitored at 340nm for 20-30 minutes in order for a linear rate to be established. ATPase activity was

then initiated by the addition, and subsequent mixing, of MgATP at a final concentration of 400µM. The rate of decrease in absorbance at 340nm was recorded for approximately 20 minutes. As a control experiment, the absorbance was monitored for an equivalent concentration of microtubules in the absence of dynein. This rate was subsequently deducted from those in which dynein was present, before using an ADP calibration to calculate the production of ADP per minute per mg of dynein. In addition, the rate of each dynein fraction was recorded in the absence of microtubules to determine whether activation had occurred.

4.8. Vanadate-dependent photolysis

Two types of vanadate-dependent photolysis (V1 and V2) have been described for dynein (section 4.4) both of which were used to investigate differences between the 14S dynein fractions. Due to a restriction on the total available sample, it was not possible to investigate V1 and V2 cleavage, in the presence and absence of ATP, on a single preparation. Photolysis conditions were initially optimised for fraction 1. These experiments revealed that use of the recommended photolysis irradiation buffer described by Tang & Gibbons (1987), had no detectable advantages over the buffer used in the dialysis of 14S fractions (see below). Consequently, this latter buffer was utilised in all photolysis reactions.

4.8.1. Preparation of vanadate

Prior to each experiment, a 200mM stock solution of sodium orthovanadate was prepared. The solution was boiled, until colourless, and adjusted to pH 10 by the addition of acetic acid or sodium hydroxide to destroy oligomeric species of the vanadate ion (Wells and Bagshaw, 1984).

4.8.2. V1 photolysis

Dynein samples were dialysed for 16 hours in 2 x 2 litres of buffer containing 10mM Hepes, 4mM $MgCl_2$, 0.1mM EGTA, 40mM NaCl and 0.1mM DTT, pH 7.4. As a control experiment, 100µl of each dynein sample was removed after dialysis. To the remaining dynein sample, sodium orthovanadate, pH 10, was added to a final concentration of 10µM.

In cases where the effect of ATP was investigated, MgATP at a final concentration of 50μM, was also added at this stage. After adequate mixing, these samples along with the control (dynein only), were aliquoted out (100μl) into the wells of a micro-titre plate. A hand-held UVGL-58 lamp was then set at a height of 5mm above the plate which was placed on ice. The samples were then irradiated at 365nm for 0, 5, 20 and 60 minutes. The control experiment of dynein only, was irradiated for 100 minutes. Gel samples were prepared immediately after irradiation and subsequently analysed by 7.5% and 12% SDS-PAGE (section 2.12).

4.8.3. V2 photolysis

Dynein samples were dialysed for 16 hours in 2 x 2 litres of buffer free from both magnesium and DTT (10mM Hepes, 1mM MnCl$_2$, 0.1mM EGTA and 40mM NaCl pH 7.4). As with V1 photolysis, 100μl of each dynein sample was removed after dialysis as a control experiment. Vanadate was then added to the remaining samples at a final concentration of 150μM. When the presence of ATP was also investigated, MnATP, at a final concentration of 250μM, was also added at this stage. After adequate mixing, these samples, along with the control (dynein only), were aliquoted (100μl) into the wells of a micro-titre plate and irradiated as described previously (section 4.8.2) for 0, 20, 60, 100, 140 and 180 minutes. Gel samples were prepared immediately following irradiation and subsequently analysed by 7.5% and 12% SDS-PAGE (section 2.12).

4.8.4. Estimation of molecular mass

Mass estimates were achieved by extrapolation of a standard curve which was constructed from a log-linear plot of mass versus distance travelled on SDS-PAGE, using high molecular mass standards obtained from Sigma. Mass standards were as follows: rabbit skeletal myosin (205kDa); β-galactosidase (116kDa); phosphorylase B (97.4kDa); bovine plasma albumin (66kDa); ovalbumin (45kDa) and carbonic anhydrase (29kDa).

Results

ATPase Activity

4.9. ATPase activity

The ATPase activities of unfractionated 14S dynein and fractions thereof, as well as 22S dynein, were determined in the presence of **40mM NaCl** (and magnesium ions) using the linked assay procedure described in section 4.7.1. Specific activities were expressed as μmol ADP/minute/mg dynein (table 4.4). In all dynein preparations, fraction 2 exhibited the highest specific activity, and the four fractions showed a consistent trend in which activity decreased in the order **2>3>1>4**.

Dynein sample	Mean specific activity	Standard error	No. of preparations
Fraction 1	0.12	0.01	10
Fraction 2	0.30	0.02	10
Fraction 3	0.15	0.01	10
Fraction 4	0.10	0.02	10
14S (unfractionated)	0.15	0.01	10
22S	0.25	0.02	7

Table 4.4. Specific ATPase activity (expressed as μmol ADP/min/mg dynein) for the four fractions of 14S, unfractionated 14S, and 22S dynein. The mean value was derived from a number of individual dynein preparations.

A general observation with all four of the 14S fractions under these conditions was that the specific activity increased over time. Over a period of nine days following the dynein preparation procedure, the ATPase activity of fractions 3 and 4, in particular, showed an appreciable enhancement of activity (table 4.5).

123

Fraction	Days after dynein preparation			% increase in activity
	4	7	9	
1	0.12	0.17	0.16	33
2	0.28	0.29	0.31	11
3	0.13	0.18	0.24	85
4	0.10	0.21	0.22	120

Table 4.5. ATPase activity (expressed as μmol ADP/min/mg dynein) recorded for the four fractions over a period of nine days following the extraction of dynein.

4.9.1. Effect of increasing ionic strength

The effect, on ATPase activity, of increasing the ionic strength was investigated by extensively dialysing the four fractions in buffer containing 600mM NaCl (section 4.7.1). Table 4.6 shows that in all cases, the specific activity of the four 14S fractions decreased. In particular, the activity of fractions 3 and 4 was undetectable by the assay system utilised.

Dynein fraction	1		2	
	40mM	600mM	40mM	600mM
1	0.09	0.03	0.15	0.11
2	0.34	0.18	0.31	0.19
3	0.16	-	0.12	-
4	0.05	-	0.11	-
22S	0.14*	0.38*		

Table 4.6. Specific ATPase activity (expressed as μmol ADP/min/mg) of the four fractions of 14S dynein in the presence of 40mM or 600mM NaCl. The activities are shown for two individual dynein preparations. Asterisk indicates data which has been previously published for 22S dynein (Wells *et al.*, 1990).

4.9.2. ATPase assay in the presence of manganese ions

ATPase assays were carried out in the presence of manganese ions {Mn^{2+}} (at the same concentration that supports V2 photolysis) instead of magnesium ions {Mg^{2+}}. The specific ATPase activity was determined for the four fractions which had been dialysed in 40mM NaCl buffer containing either Mg^{2+} or Mn^{2+} (section 4.7.1). Table 4.7 shows the percentage increase in specific activity in the presence of Mn^{2+}. Under these conditions, the ATPase activity associated with fraction 1 increased, whereas fractions 2, 3, and 4 had a reduced activity.

Dynein fraction	Mean % increase in specific activity	Standard error (%)	No. of preparations
1	+73	43.9	3
2	-54	4.0	3
3	-56	5.8	3
4	-23	14.4	3

Table 4.7. Measurement of the percentage increase in ATPase activity (expressed as μmol ADP/min/mg dynein) as a result of substituting Mn^{2+} for Mg^{2+} in the standard assay procedure (section 4.7.1). The specific activity is given for three individual dynein preparations.

4.9.3. ATPase assay in the presence of microtubules

Preliminary investigations involving 22S dynein established conditions under which ATPase activity could be successfully activated by the presence of microtubules purified from porcine brain and free of microtubule-associated proteins {MAPs} (section 2.10.2). Table 4.8 shows the specific activity of 22S dynein in the presence and absence of microtubules. Under these conditions, an increase in ATPase activity was associated with an increase in the weight ratio of microtubules to dynein.

Assay	Specific activity
22S only	0.33
Ratio microtubules to 22S (by weight) 333:1	0.47
Ratio microtubules to 22S (by weight) 667:1	0.59

Table 4.8. Preliminary investigations to show activation of 22S dynein in the presence of MAP-free microtubules. Specific activity is expressed as μmol ADP/min/mg dynein.

In contrast, two experiments with 14S dynein revealed no activation of any of the fractions in the presence of porcine brain microtubules. A second microtubule preparation, however, did show an activation of the ATPase activity associated with fraction 1 (table 4.9). This activation was not apparent at the microtubule to dynein ratio quoted for unfractionated 14S dynein in which a 2-3 fold activation was reported at a weight ratio of approximately 375:1 (Shimizu *et al.*, 1992). In comparison, fraction 1 showed a 2.8-fold enhancement of activity at a weight ratio of 800:1. No other fractions showed a significant increase in activity in the presence of microtubules.

Fraction	Dynein only	Ratio of microtubules to dynein (by weight)		
		360:1	800:1	1400:1
1	0.08	0.07 ± 0.01	0.22 ± 0.01	0.76 ± 0.23
2	0.15	0.04 ± 0.02	0.13 ± 0.04	0.21 ± 0.04
3	0.14	0.07 ± 0.01	0.09 ± 0.01	0.18 ± 0.03
4	0.05	0.07 ± 0.01	0.05 ± 0.01	0.08 ± 0.02

Table 4.9. Microtubule activation of fraction 1. Specific activity is expressed as μmol ADP/min/mg dynein.

Vanadate-dependent Photolysis

Vanadate-dependent photolysis results in the specific cleavage of dynein heavy chains to produce cleavage peptides. One feature of the reaction was the differential silver-staining intensity of the cleavage peptides produced. In general, the larger-sized cleavage peptide stained more intensely than the smaller fragment (figures 4.2-4.10). This observation was in agreement with a previous report of differential silver-staining (in the cleaved γ heavy chain of *Chlamydomonas*) in which differences in intensity were not considered to reflect a significant difference in the quantity of cleavage peptide produced (King & Witman, 1988).

4.10. Control experiments for vanadate-dependent photolysis

Irradiation of the four fractions, for a maximum of 100 minutes in the absence of ATP and vanadate, produced no cleavage peptides (figure 4.2). Analysis by 12% SDS-PAGE revealed the stability of peptides in both the high and low molecular mass range. The polypeptide composition of these fractions was identical to those which had not been irradiated but had been treated as described for V1 or V2 photolysis (section 4.8). These latter controls were run in lane 2 of figures 4.3-4.10.

4.11. V1 photolysis

V1 cleavage (section 4.8.2) of the four 14S dynein fractions in the presence of nucleotide resulted in the production of cleavage peptides which were subsequently analysed by 7.5% (figures 4.3a-4.6a) and 12% SDS-PAGE (data not shown). The requirement for nucleotide was also investigated (figures 4.3b-4.6b). A low percentage gel was chosen in order to assist the separation of cleavage peptides. Figures 4.3-4.6 show SDS-PAGE analysis of the four 14S dynein fractions after V1 photolysis in either the (a) presence or (b) absence of MgATP. The estimated molecular masses (section 4.8.4) of all the cleavage peptides appearing after irradiation are shown in table 4.10 in which the V1 data is summarised for all four fractions.

127

Fraction 1 (figure 4.3)

The two heavy chains of fraction 1 gradually decreased in intensity as a result of increased irradiation exposure at 365nm in the presence of MgATP and 10μM vanadate (figure 4.3a). This decrease in heavy chain intensity was concomitant with the appearance of five new peptides of estimated masses 230, 225, 152, 148, and 140kDa. The intensity of the new peptides was variable, although the 148kDa and 140kDa peptides always appeared as faint bands. The 225kDa peptide showed similar mobility to a peptide present in the preirradiated sample. Nevertheless, the marked increase in intensity of this peptide, with irradiation time, indicates this to be a cleavage product of one of the heavy chains.

In the absence of MgATP, the intensity of both heavy chains remained equivalent from 0 to 60 minutes of irradiation (figure 4.3b). No cleavage products were evident during this time.

Fraction 2 (figure 4.4)

Three new peptides of approximate masses 232, 152 and 147kDa, appeared after V1 photolysis in the presence of MgATP (figure 4.4a). The 232kDa peptide was always more intensely-stained than either of the remaining peptides.

As with fraction 1, no cleavage products were evident in the absence of MgATP and the heavy chain intensity was unchanged from 0 to 60 minutes of irradiation (figure 4.4b).

Fraction 3 (figure 4.5)

Irradiation of fraction 3 in the presence of 10μM vanadate resulted in a decreased intensity of the heavy chain in both the presence and absence of MgATP. In the presence of MgATP, one prominent cleavage peptide of approximate masses 232kDa appeared concomitantly with the decrease in heavy chain intensity (figure 4.5a). In addition, two peptides of approximate masses 140kDa and 135kDa were evident after 20 minutes of irradiation. These latter peptides (particularly that of 135kDa) were appreciably less intensely-stained than the 232kDa peptide.

In the absence of MgATP, the intensity of the heavy chain decreased although only a single new peptide of estimated mass 228kDa, was detectable (figure 4.5b). Heavy chain intensity also decreased at a slower rate than when nucleotide was present. The heavy

chain was prominent even after 60 minutes of irradiation in the absence of MgATP, whereas at an equivalent time point in the presence of nucleotide, the heavy chain was completely cleaved. Similarly, in the presence of nucleotide, a 103kDa peptide apparent in the preirradiated sample, decreased in intensity after irradiation. This was not observed when MgATP was omitted from the irradiation buffer.

Fraction 4 (figure 4.6)

As with fraction 3, cleavage products were evident after irradiation, in the presence of $10\mu M$ vanadate, in either the absence or presence of MgATP. In the presence of nucleotide, the decrease in intensity of the heavy chain was concurrent with the appearance of **two** new peptides of approximate masses 228kDa and 138kDa (figure 4.6a). A **third** peptide of 133kDa, which was detectable in the preirradiated sample, may also have increased in intensity.

In the absence of MgATP, **two** new peptides of estimated masses 225kDa and 140kDa were detected (figure 4.6b). Cleavage of the heavy chain also occurred at a reduced rate when nucleotide was omitted from the irradiation buffer. As with fraction 3, the heavy chain was almost completely cleaved after 60 minutes of irradiation in the presence of nucleotide, whereas the heavy chain was still prominent at an equivalent time point in the absence of MgATP.

Fraction No.	V1 (+ ATP) (a)	V1 (- ATP) (b)
1 (figure 4.3)	230 225 152 148 140	No Cleavage
2 (figure 4.4)	232 152 147	No Cleavage
3 (figure 4.5)	232 140 135	228
4 (figure 4.6)	228 138 133	225 140

Table 4.10. V1 cleavage of 14S dynein fractions in both the presence and absence of nucleotide. The estimated masses of cleavage peptides are given in kDa (section 4.8.4). The corresponding figure number, in the (a) presence or (b) absence of ATP, are indicated for all four fractions.
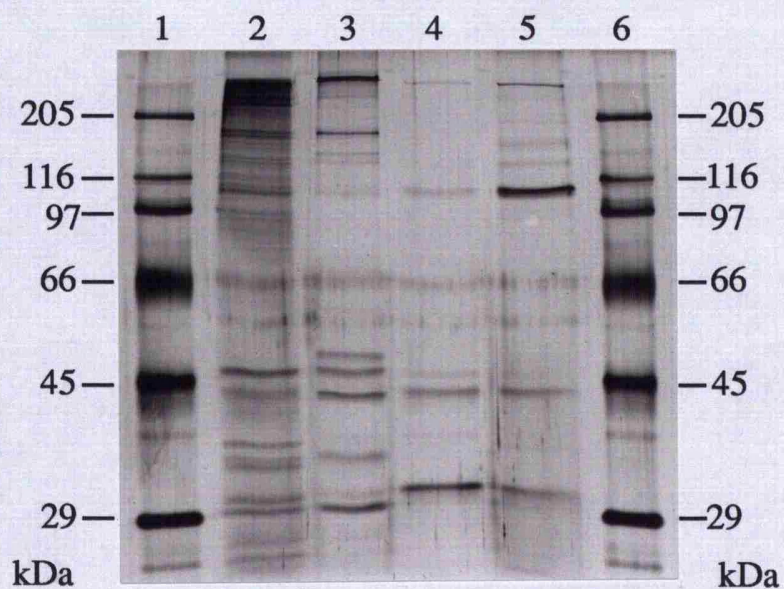
Figure 4.2. 12% SDS-PAGE analysis of the four fractions of 14S dynein after irradiation in the absence of vanadate and MgATP. Tracks: 1 and 6, molecular mass markers; 2-5, 14S dynein fractions 1-4 respectively which had been irradiated at 365nm for 100 minutes.
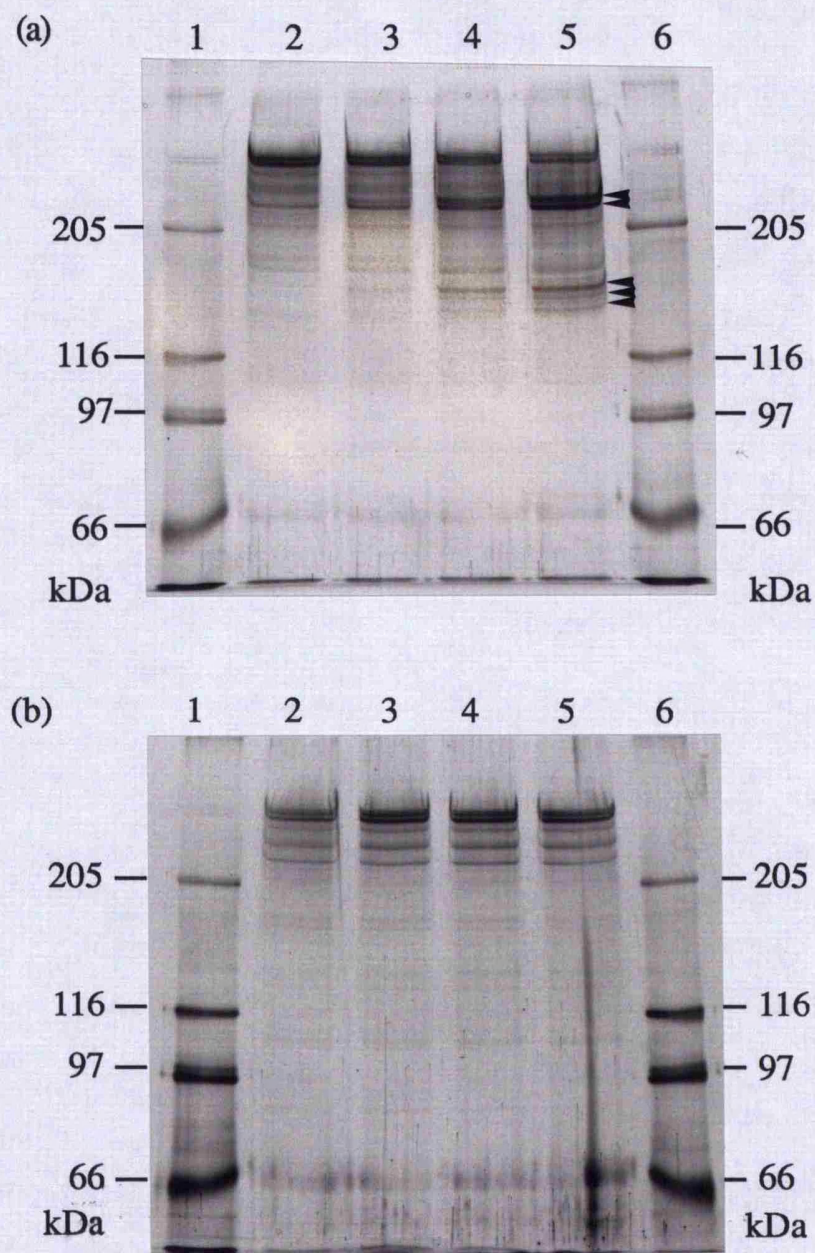
Figure 4.3. 7.5% SDS-PAGE analysis of **fraction 1** following **V1** photolysis in the (a) presence and (b) absence of MgATP. Tracks: 1 and 6, molecular mass markers: 2-5, fraction 1 after irradiation (365nm) for 0, 5, 20, and 60 minutes respectively. Cleavage products are marked with arrows.
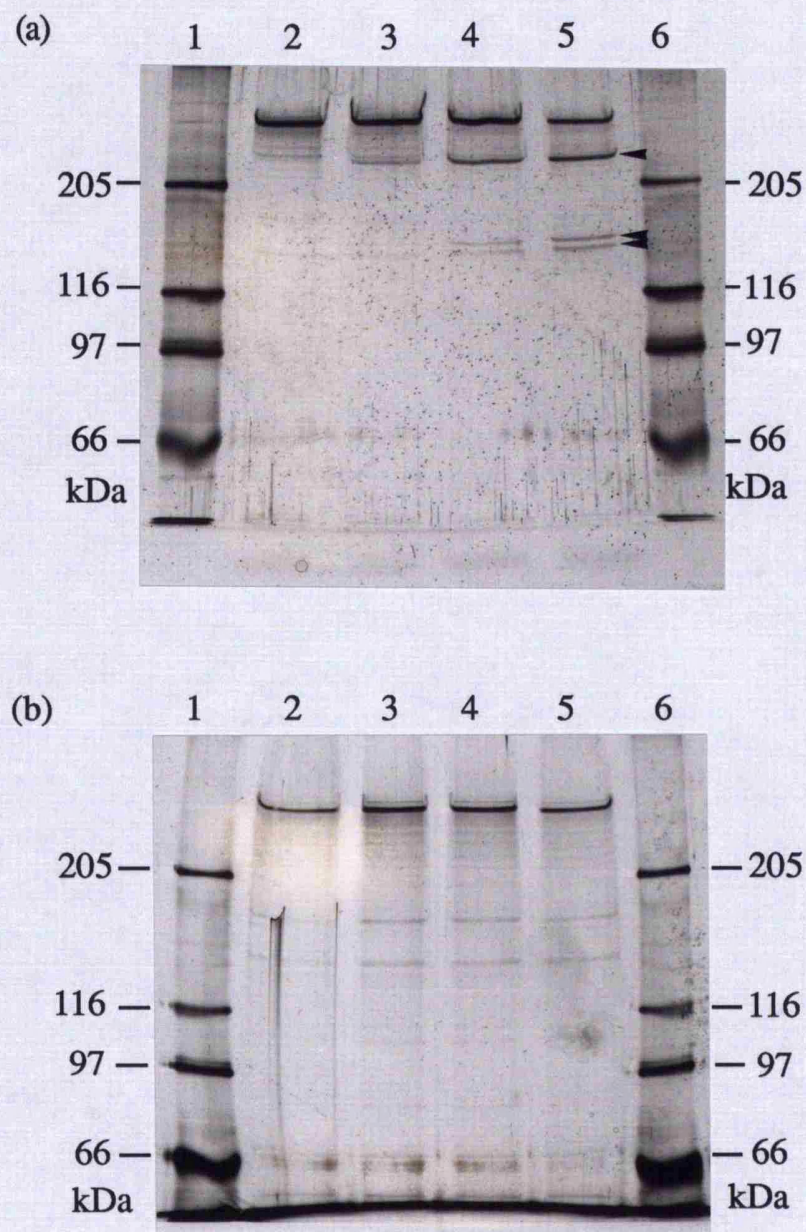
Figure 4.4. 7.5% SDS-PAGE analysis of **fraction 2** following **V1** photolysis in the (a) presence and (b) absence of MgATP. Tracks: 1 and 6, molecular mass markers: 2-5, fraction 2 after irradiation (365nm) for 0, 5, 20, and 60 minutes respectively. Cleavage products are marked with arrows.
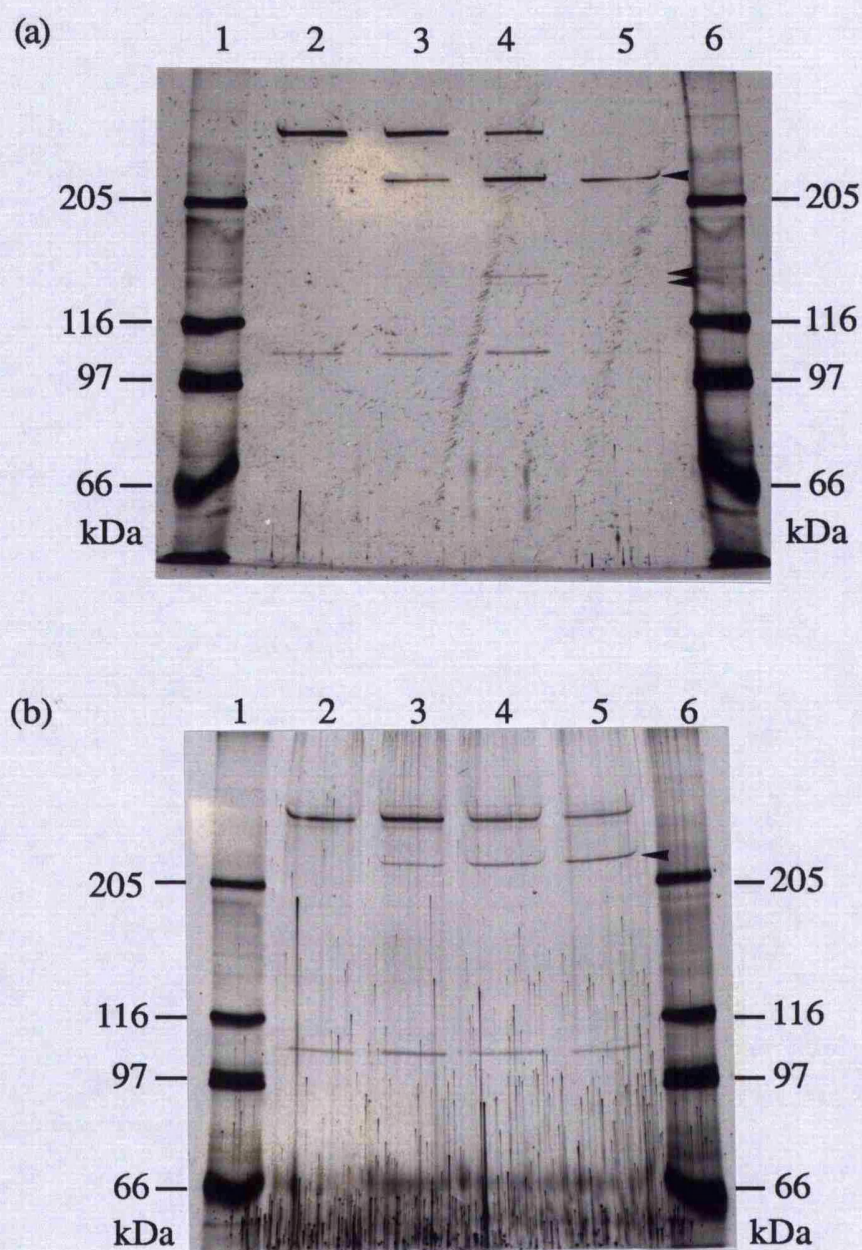
Figure 4.5. 7.5% SDS-PAGE analysis of **fraction 3** following **V1** photolysis in the (a) presence and (b) absence of MgATP. Tracks: 1 and 6, molecular mass markers: 2-5, fraction 3 after irradiation (365nm) for 0, 5, 20, and 60 minutes respectively. Cleavage products are marked with arrows.
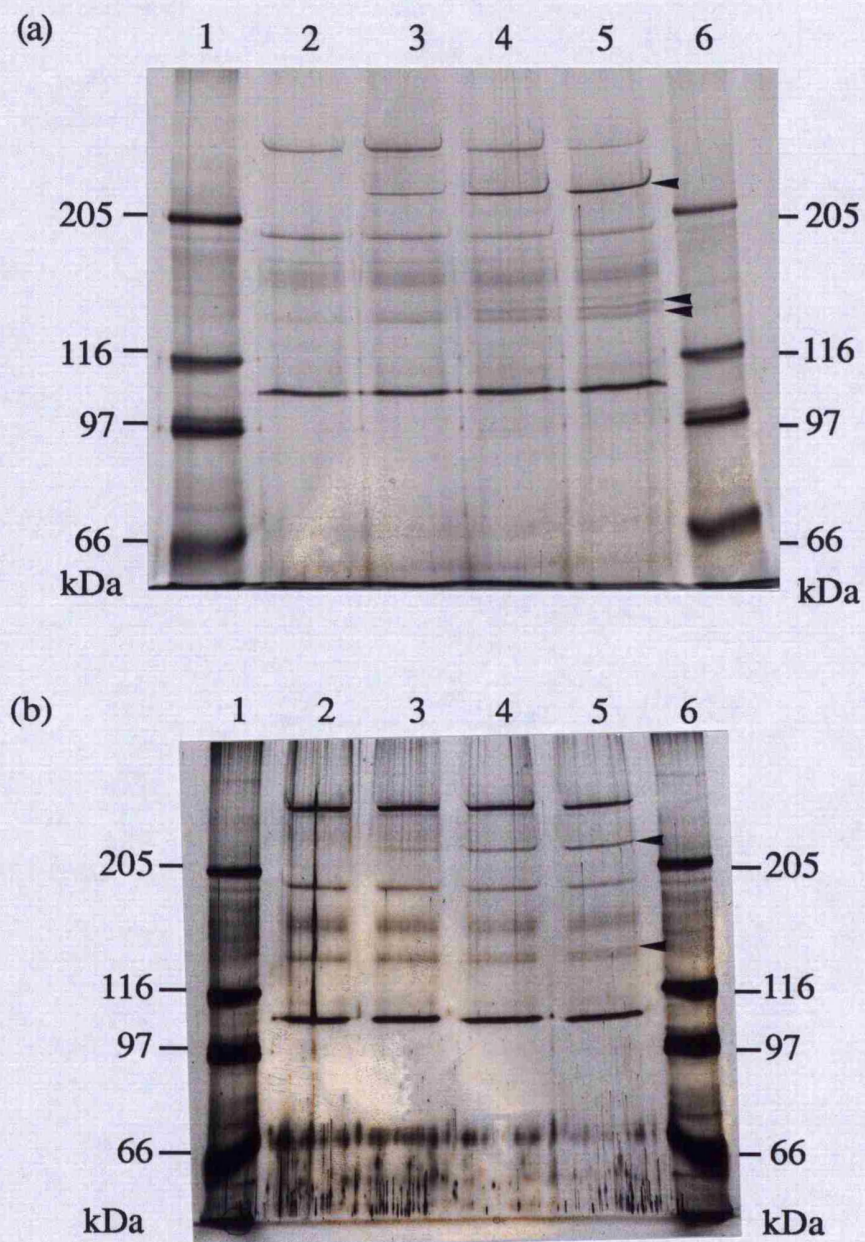
Figure 4.6. 7.5% SDS-PAGE analysis of **fraction 4** following **V1** photolysis in the (a) presence and (b) absence of MgATP. Tracks: 1 and 6, molecular mass markers: 2-5, fraction 4 after irradiation (365nm) for 0, 5, 20, and 60 minutes respectively. Cleavage products are marked with arrows.

4.12. V2 photolysis

V2 photolysis of the four 14S dynein fractions in the absence of nucleotide resulted in the production of cleavage peptides as identified by 7.5% (figures 4.7b-4.10b) and 12% SDS-PAGE. The presence of ATP was also investigated (figures 4.7a-4.10a). The approximate masses (section 4.8.4) of new peptides appearing after irradiation are shown in table 4.11 which summarises the V2 data for all four fractions.

Fraction 1 (figure 4.7)

The appearance of **four** peptides, of approximate masses 218, 211, 173, and 168kDa, coincided with the decrease in heavy chain intensity observed after irradiation in the absence of MnATP (figure 4.7b).

In the presence of MnATP, no cleavage products were evident and the intensity of both heavy chains remained equivalent for time periods or irradiation between 0 and 100 minutes (figure 4.7a). The staining intensity of the entire fraction after 180 minutes of irradiation, however, was significantly reduced, although no cleavage peptides were detected.

Fraction 2 (figure 4.8)

Two prominent peptides of approximate masses 213kDa and 170kDa, were apparent after irradiation in the absence of MnATP (figure 4.8b).

In the presence of MnATP, no new peptides were produced, and the intensity of the heavy chain remained unchanged even after 180 minutes of irradiation (figure 4.8a).

Fraction 3 (figure 4.9)

The heavy chain of fraction 3 decreased in intensity after 100 minutes of irradiation in the absence of MnATP (figure 4.9b). This decrease in the heavy chain was concomitant with the appearance of **one** prominent peptide of estimated mass 167kDa.

In the presence of MnATP, **two** major peptides of approximate masses 160kDa and 121kDa became apparent after irradiation (figure 4.9a). The summation of these two peptides, however, was appreciably lower than the estimated molecular mass of the intact heavy chain (see discussion). This discrepancy prompted further analysis of the gel which

revealed the presence of a faint peptide of approximately 98kDa which appeared after 60-100 minutes of irradiation. All peptides were difficult to detect after 180 minutes of irradiation in the presence of nucleotide since the intensity of peptides significantly decreased.
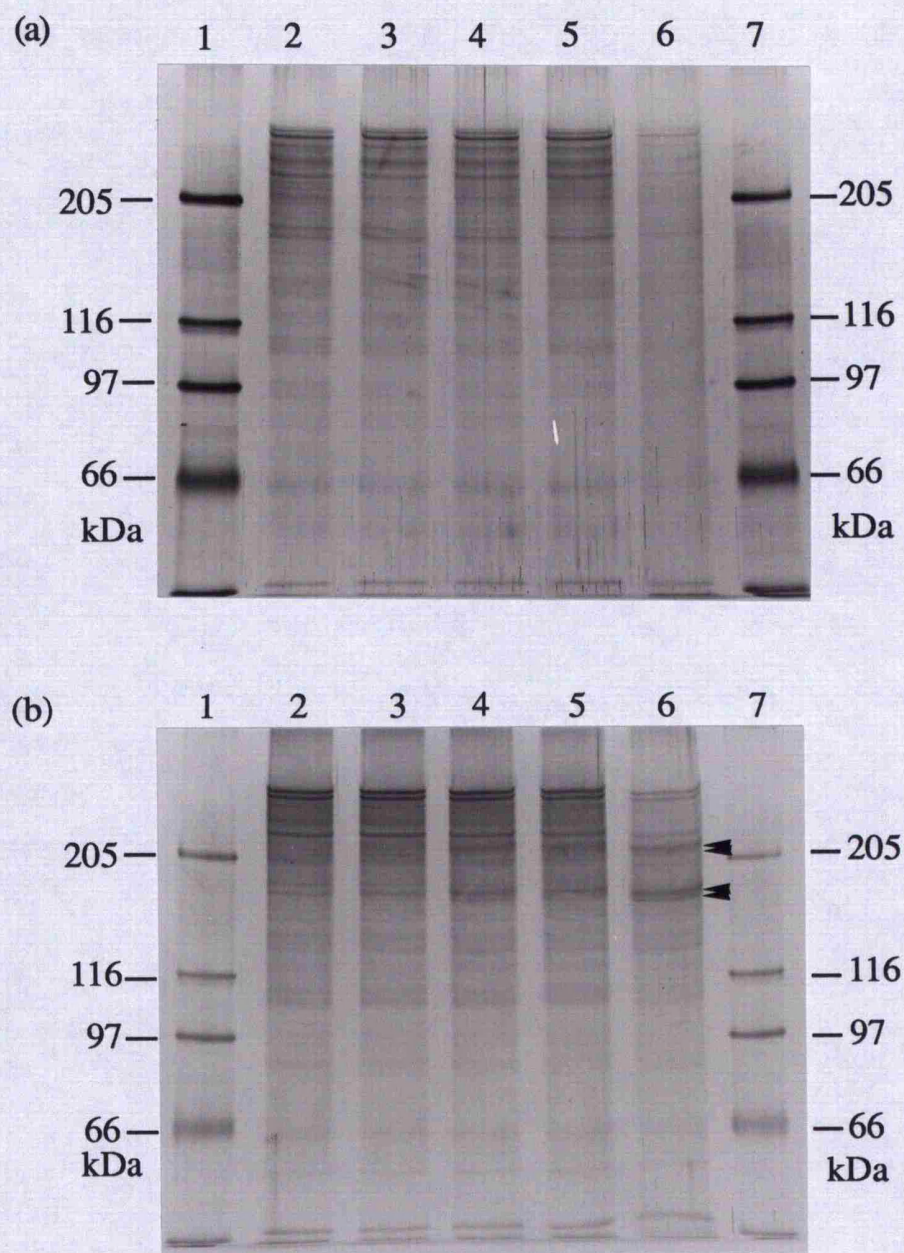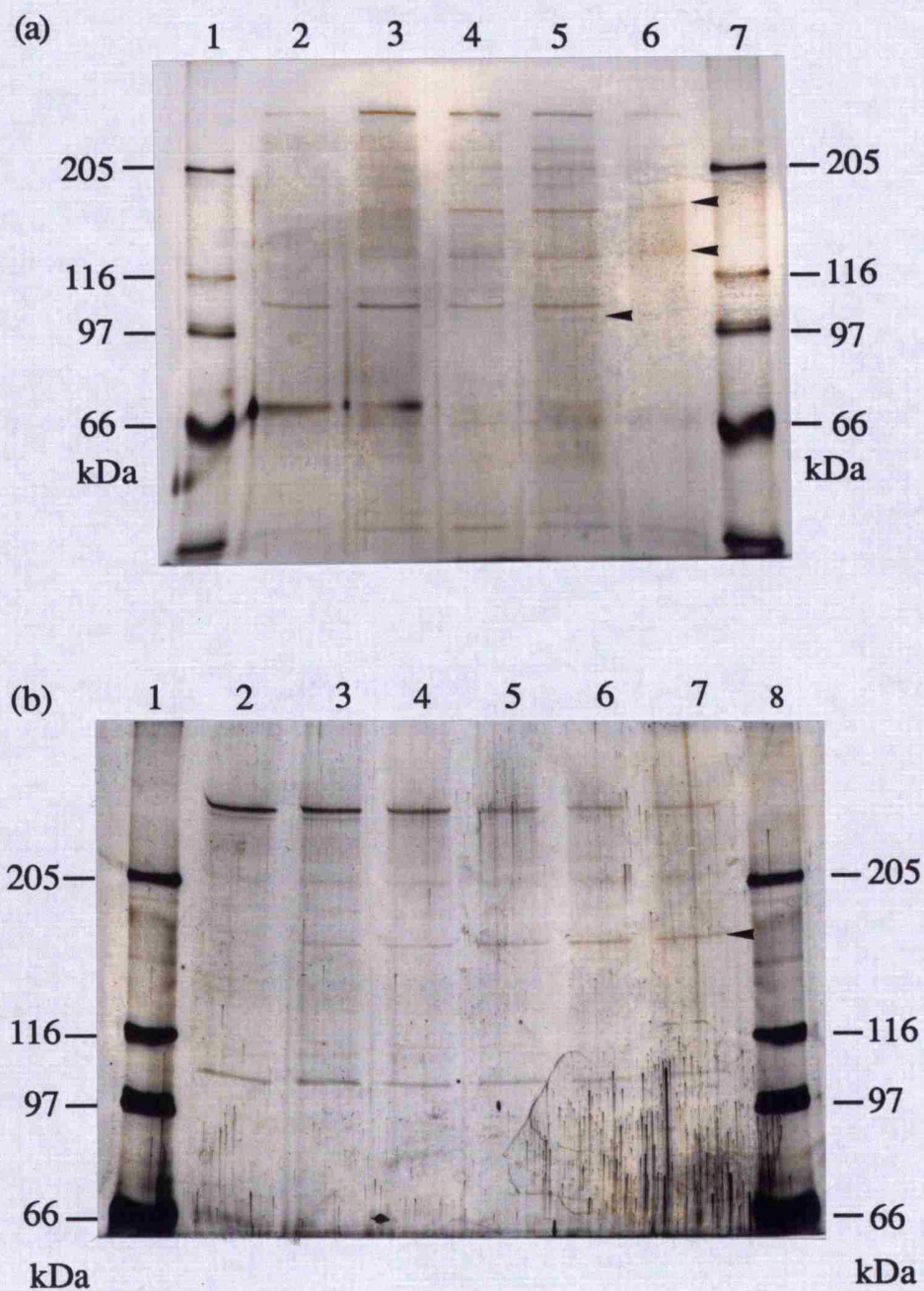
Fraction 4 (figure 4.10)

The single heavy chain of fraction 4 decreased in intensity after irradiation in the absence of MnATP (figure 4.10b). **One** prominent peptide of approximate mass 163kDa appeared concomitantly with the decrease in heavy chain.

In the presence of MnATP, **two** peptides of masses 200kDa and 158kDa were detected (figure 4.10a). In addition, a 103kDa peptide present in the pre-irradiated sample, showed a significant decrease in intensity after irradiation in the presence of MnATP which was not obvious when nucleotide was omitted.

Fraction No.	V2 (+ ATP) (a)	V2 (- ATP) (b)
1 (figure 4.7)	No cleavage	218 211 173 168
2 (figure 4.8)	No cleavage	213 170
3 (figure 4.9)	160 121 (98)	167
4 (figure 4.10)	200 158	163

Table 4.11. V2 cleavage of 14S dynein fractions in both the presence and absence of MnATP. The estimated masses of cleavage peptides are given in kDa (section 4.8.4). The corresponding figure number, in the (a) presence or (b) absence of ATP, are indicated for all four fractions.

Figure 4.7. 7.5% SDS-PAGE analysis of **fraction 1** following **V2** photolysis in the (a) presence and (b) absence of MnATP. Tracks: 1 and 7, molecular mass markers: 2-6, fraction 1 after irradiation (365nm) for 0, 20, 60, 100, and 180 minutes respectively. Cleavage products are marked with arrows.
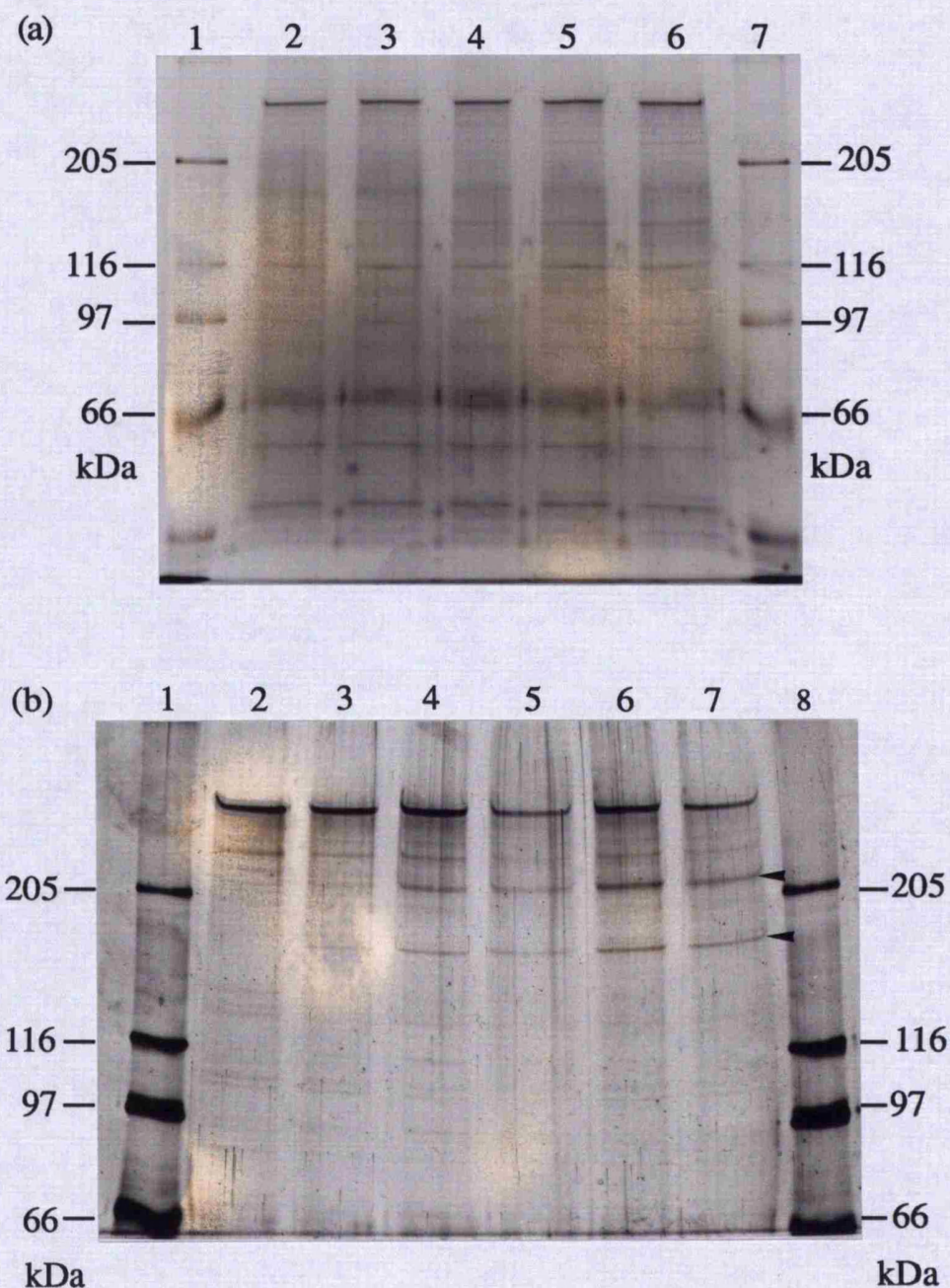
Figure 4.8. 7.5% SDS-PAGE analysis of **fraction 2** following **V2** photolysis in the (a) presence and (b) absence of MnATP. (a) Tracks: 1 and 7, molecular mass markers: 2-6, fraction 2 after irradiation (365nm) for 0, 20, 60, 100, and 180 minutes respectively. (b) Tracks: 1 and 8, molecular mass markers; 2-7 fraction 2 after irradiation (365nm) for 0, 20, 60, 100, 140, and 180 minutes respectively. Cleavage products are marked with arrows.

Figure 4.9. 7.5% SDS-PAGE analysis of **fraction 3** following **V2** photolysis in the (a) presence and (b) absence of MnATP. (a) Tracks: 1 and 7, molecular mass markers: 2-6, fraction 3 after irradiation (365nm) for 0, 20, 60, 100, and 180 minutes respectively. (b) Tracks: 1 and 8, molecular mass markers; 2-7 fraction 2 after irradiation (365nm) for 0, 20, 60, 100, 140, and 180 minutes respectively. Cleavage products are marked with arrows.
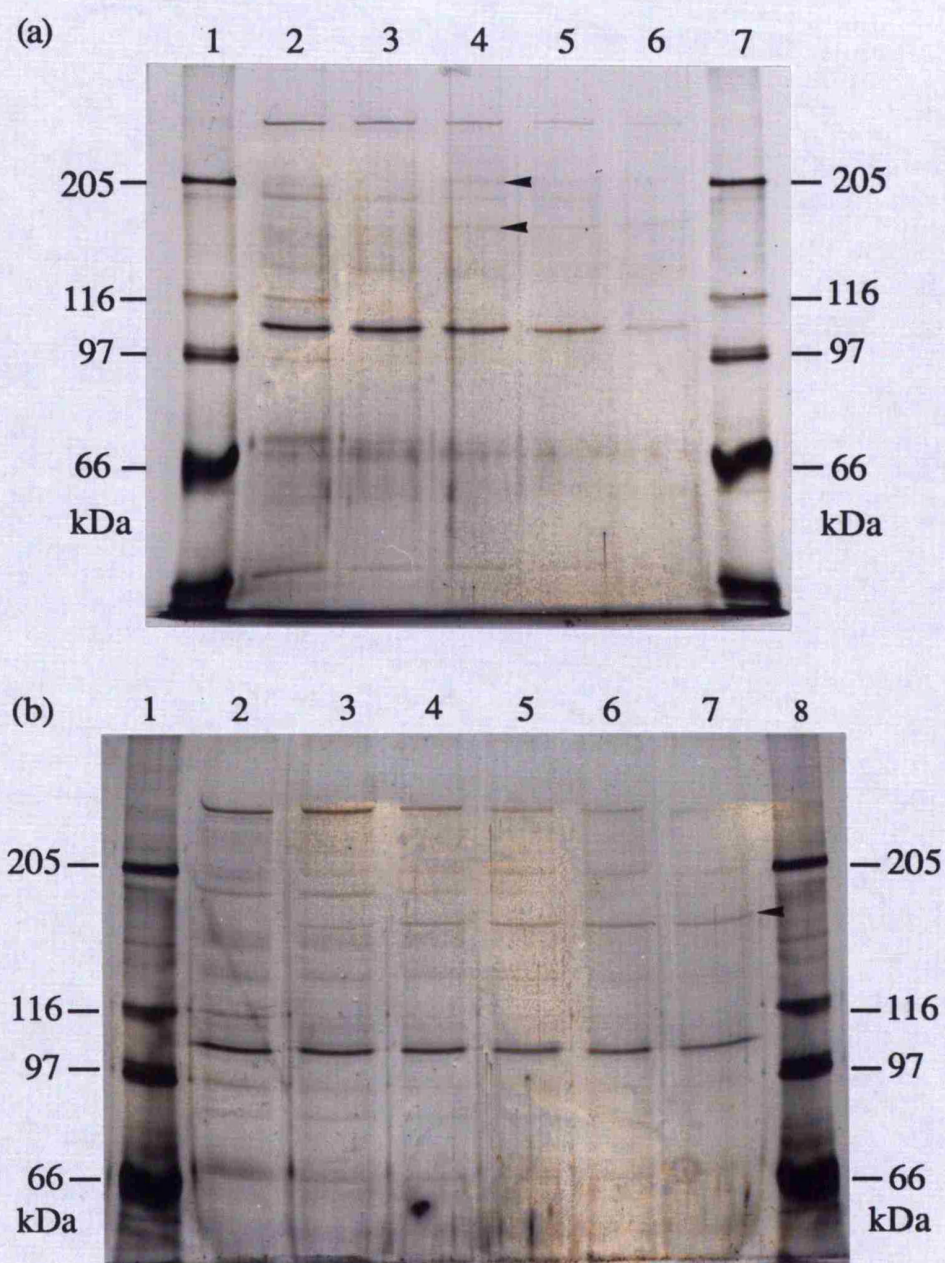
Figure 4.10. 7.5% SDS-PAGE analysis of **fraction 4** following **V2** photolysis in the (a) presence and (b) absence of MnATP. (a) Tracks: 1 and 7, molecular mass markers: 2-6, fraction 4 after irradiation (365nm) for 0, 20, 60, 100, and 180 minutes respectively. (b) Tracks: 1 and 8, molecular mass markers; 2-7 fraction 2 after irradiation (365nm) for 0, 20, 60, 100, 140, and 180 minutes respectively. Cleavage products are marked with arrows.

ATPase activity

4.13. ATPase activity in the presence of 40mM NaCl

All four fractions of 14S dynein exhibited ATPase activity. The specific activity showed a consistent trend which, in order of decreasing activity, was **fraction 2 >> fraction 3 > fraction 1 > fraction 4**. In particular, fraction 2 had an activity (0.30 μmol ADP/min/mg dynein) 2-3 fold greater than the remaining fractions 1 (0.12), 3 (0.15), and 4 (0.10) {table 4.4}. It does not appear likely that any of the fractions were activated as a consequence of separation, since the total activity[*] associated with the four fractions (0.07 μmol ADP/min) was less than that of the unfractionated dynein (0.17 μmoles ADP/minute). This observation is in contrast to a study in *Chlamydomonas* in which fractionation of 18S dynein (into α and β/IC1) resulted in the activation of the β/IC1 subunit (Pfister & Witman, 1984). In addition, the specific activity associated with the four fractions was shown to increase over time (table 4.5). In particular, the activity of fractions 3 and 4 increased approximately 2-fold after a total of nine days at 5°C, whereas the activation of fractions 1 and 2 was less pronounced. This response to ageing distinguished fractions 1 and 2 from fractions 3 and 4, and may be comparable to the latency described previously (section 4.2.2) for sea urchin 21S outer arm dynein (Gibbons & Fronk, 1979) and *Tetrahymena* 22S dynein (Gibbons, 1966; Blum & Hayes, 1974).

4.14. Effect of increasing ionic strength

The effect of increasing ionic strength was investigated in order to compare the four 14S dynein fractions with 22S dynein. The ATPase activity associated with 22S dynein (in the presence of 40mM NaCl) was previously shown to be activated 2.7-fold in the presence of 600mM NaCl (Wells *et al.*, 1990). In contrast, the four fractions differed from 22S in that ATPase activity was significantly inhibited under these conditions (table 4.6). In particular, the activity of fractions 3 and 4 was undetectable by the assay system utilised. These observations are compatible with studies involving unfractionated 14S dynein in

---

[*] see section 3.8.5 for average total yield (in mg) of the four fractions per dynein preparation, and table 3.1 for total yield of unfractionated 14S dynein.

which increasing monovalent salt concentration (up to 0.4M) was shown to cause a decrease (of 45%) in activity (Gibbons, 1966). The effect of monovalent salt on ATPase activity may arise due to the loss of a subunit which regulates ATPase activity, or as a consequence of a change in molecular conformation (see chapter 5).

4.15. ATPase activity in the presence of manganese ions

All four fractions supported ATP hydrolysis in the presence of manganese ions {Mn^{2+}} (table 4.7). This suggested that Mn^{2+} could successfully substitute for magnesium {Mg^{2+}} in the coordination of ATP in the hydrolytic site, and that MnATP was a suitable substrate for ATP hydrolysis. These data also suggested that, for all four fractions, the inhibition of V1 cleavage by Mn^{2+} is likely to be the result of an interaction between Mn^{2+} and the hydrolytic (or V1) site (section 4.5).

The presence of Mn^{2+} also revealed differences in the ATPase activity of the four fractions which were considered to indicate structural variation within the site of ATP hydrolysis. Fraction 1 was readily distinguished from fractions 2, 3 and 4 since this fraction was associated with an increase in ATPase activity (compared with the presence of MgATP) and was considered to reflect a favourable coordination of MnATP within the catalytic site. In contrast, the ATPase activity observed for fractions 2, 3 and (to a lesser extent) 4 was shown to decrease (table 4.7).

4.16. Effect of microtubule presence on ATPase activity - preliminary studies

Preliminary studies on the effect of microtubules on the ATPase activity of 22S dynein, revealed a 1.8-fold activation at a microtubule to dynein weight ratio of 667:1 (table 4.8). Similar investigations on the four 14S dynein fractions, however, proved inconclusive. Two experiments showed that no fractions were activated by the presence of microtubules, whereas studies using a second microtubule preparation indicated that fraction 1 was activated at a microtubule to dynein weight ratio between 800:1 and 1400:1 (table 4.9). This potential activation suggests that fraction 1 interacts with microtubules in an ATP-sensitive manner. The lack of activation in the preceding preparation may well be related to the purity of the microtubules, since contamination from microtubule-associated proteins (MAPs) has been shown to prevent 14S dynein from binding to microtubules and

144

thus inhibit microtubule-activation of ATPase activity (Marchese-Ragona & Johnson, 1989; Shimizu et al., 1992).

The four 14S dynein fractions have distinct ATPase properties. In summary, fraction 1 is distinguishable from other fractions with respect to its differential response to Mn^{2+} (section 4.15) and potential activation by the presence of microtubules (section 4.16). Fraction 2 has an activity 2-3 fold greater than that of the other fractions (section 4.13). Finally, fractions 3 and 4 are distinguishable from 1 and 2 in their time-dependent activation (section 4.13) and response to high ionic strength (section 4.14).

Vanadate-Dependent Photolysis

V1 photolysis is presumed to occur at the hydrolytic ATP-binding site of dynein heavy chains (section 4.4.1). The conditions which support cleavage at this site require low concentrations of vanadate ($10\mu M$) and the presence of both Mg^{2+} and ATP (Lee-Eiford *et al.*, 1986). In contrast, V2 photolysis requires Mn^{2+} (to inhibit cleavage at the V1 site) and a higher concentration of vanadate ($100\text{-}150\mu M$), and is typically inhibited by Mg^{2+} and ATP (Tang & Gibbons, 1987). Variation on these original conditions have been reported and in particular, the presence or absence of ATP has been shown to have a differential effect on photolysis. These differences are thought to reflect structural (and possible functional) variation between dynein heavy chains (King & Witman 1987, 1988; Marchese-Ragona *et al.*, 1989).

The four fractions of 14S dynein have been investigated using V1 and V2 photolysis. Both types of cleavage were demonstrated in all four fractions using the standard conditions outlined by early studies (Gibbons *et al.*, 1987a; Tang & Gibbons, 1987). These data indicated that all four fractions are dynein ATPases which share the characteristic property of vanadate-dependent cleavage (section 4.6.1). Structural variation between the fractions was then demonstrated by an analysis of the number and approximate mass of cleavage peptides, as well as investigations on the requirement and affect of ATP in the photolysis reaction. Analysis of the cleavage peptides also enabled estimations of the heavy chain molecular mass associated with each fraction (section 4.19). Finally, these data were used to construct linear peptide maps in which the possible orientation of the V1 and V2 sites on the dynein heavy chain was considered (section 4.20).

4.17. V1 photolysis

All four fractions of 14S dynein supported V1 photolysis in the presence of MgATP (figures 4.3a-4.6a). Five cleavage peptides were associated with the photolysis of fraction 1, whereas fractions 2, 3, and 4 each produced three cleavage peptides (table 4.10). In the absence of ATP, fractions 1 and 2 did not undergo photolysis (figures 4.3b & 4.4b). The intensity of the heavy chains of these fractions remained unchanged, and no cleavage peptides were detected even after 60 minutes of irradiation. In contrast, fractions 3 and 4

146

did undergo photolysis in the absence of ATP (figures 4.5b & 4.6b) although fewer cleavage peptides were evident (table 4.10). In particular, the cleavage peptides deficient in fractions 3 and 4 (in the absence of MgATP) were shown to correspond to one (fraction 4) or both (fraction 3) of two closely-migrating cleavage peptides designated **doublets**. These doublet peptides (with a maximal difference in mobility of 5kDa) were associated with all four fractions in the presence of MgATP and can be summarised as follows: fraction 1 (152kDa and 148kDa), fraction 2 (152kDa and 147kDa), fraction 3 (140kDa and 135kDa) and fraction 4 (138kDa and 133kDa).

The doublets most likely arise due to the existence of two independent cleavage sites within a single heavy chain. These were considered to represent either two different ATP-binding sites or, alternatively, two distinct cleavage points within a single hydrolytic site. In either case, the doublets were thought to be structurally related (*ie* differ by only 5kDa) since the presence of three unique cleavage peptides per heavy chain was inconsistent with data from V1 photolysis in the absence of MgATP (table 4.10), and heavy chain mass estimates using V2 photolysis (section 4.19).

An interesting comparison of the data presented here can be made with previous observations involving unfractionated 14S dynein (Marchese-Ragona *et al.*, 1991). This previous study showed that the two heavy chains described for the 14S were cleaved under V1 photolysis conditions to produce four cleavage peptides of masses 232, 225, 220, 155kDa. These were concluded to represent complimentary pairs of peptides in which each of the two heavy chains was thought to have a single V1 site of cleavage. This group acknowledged, however, that the predicted heavy chain masses for 14S exceeded those of the three (α, β and γ) 22S heavy chains and was inconsistent with their relative electrophoretic mobilities on SDS-PAGE (Marchese-Ragona *et al.*, 1988, 1989). This discrepancy was interpreted at this time as a consequence of anomalous electrophoretic mobilities of the 14S cleavage peptides (Marchese-Ragona *et al.*, 1991). The data presented here, however, reveals that the peptides described previously reflect some, but not all, of the cleavage peptides associated with each of the four fractions (table 4.10). This interpretation comes from the observation that comparably-sized peptides are associated with V1 photolysis of fraction 1 (230, 225, and 152kDa), fraction 2 (232,

152kDa), fraction 3 (232kDa), and fraction 4 (228kDa). In addition, cleavage peptides which were not identified by the Coomassie Blue staining procedure utilised by Marchese-Ragona *et al.* (1991) have also been described (table 4.10). Consequently, the pairing of peptides in the previous study is misleading since more than two heavy chains (and more than four cleavage peptides) have been associated with 14S dynein (section 3.14.1).

4.18. V2 photolysis

All four fractions produced cleavage peptides under V2 photolysis conditions in the absence of ATP (figures 4.7b-4.10b). Fraction 1 produced four cleavage peptides, fraction 2 produced two such peptides, and fractions 3 and 4 were each cleaved to produce a single detectable cleavage peptide (table 4.11). Furthermore, fractions 1 and 2 did not undergo photolysis in the presence of MnATP (figures 4.7a and 4.8a) whereas both fractions 3 and 4 (figures 4.9a and 4.10a) were cleaved under these conditions.

These data showed that each heavy chain associated with fractions 1 and 2 had a single site of V2 cleavage which could not be cleaved in the presence of nucleotide, presumably due to the occupation of ATP-binding site(s). Fraction 1 produced four cleavage peptides which most likely corresponds to cleavage at a single site within each of the two heavy chains associated with this fraction. Similarly, the two cleavage peptides detected for fraction 2 indicates a single site of cleavage within a single heavy chain. In contrast, the interpretation of fractions 3 and 4 was ambiguous since the number of detectable cleavage peptides was variable. Only one cleavage peptide was detected in each fraction in the absence of ATP, whereas in the presence of nucleotide, at least three cleavage peptides were associated with fraction 3, and two associated with fraction 4 (table 4.11). This discrepancy could be interpreted in three ways. Firstly, it was possible that in these fractions, cleavage in the absence of ATP, occurred at a site exactly in the centre of the heavy chain to produce two equivalently-sized cleavage products. This was considered unlikely, however, since the presence of one similarly-sized cleavage peptide in both the presence and absence of MnATP, suggested that V2 cleavage occurs at the same site(s) under both conditions (fraction 3 = 160/167kDa; fraction 4 = 158/163kDa; see table 4.11). A second interpretation was that cleavage peptides comparable to those found in the

148

presence of ATP were simply undetected by the silver-staining system utilised. Thirdly, it was considered likely that multiple cleavage sites (which are specifically susceptible to photolysis in the absence of ATP) produced low molecular mass peptides which went undetected even after analysis by 12% SDS-PAGE (data not shown). As a result of this complexity, the simplest interpretation of fractions 3 and 4 was based upon the data derived for V2 photolysis in the presence of MnATP. These data suggested that fraction 3 may have been cleaved at two V2 sites (to produce three peptides), and fraction 4 was cleaved at one V2 site (to produce two cleavage peptides).

4.19. Estimates of heavy chain mass: V1 and V2 photolysis

The results from V1 and V2 cleavage were used to estimate heavy chain molecular mass (section 4.6.3). Table 4.12 summarises these data which were based upon the following assumptions. Firstly, the doublet peptides described for V1 photolysis in the presence of MgATP (section 4.17) were considered to be structurally related since the combined mass attributable to three unique peptides greatly exceeded those predicted for the same heavy chains by V2 photolysis. Furthermore, these masses would exceed the values derived for the three heavy chains (α, β, and γ) of 22S dynein (417kDa, 420kDa and 403kDa respectively) which is contrary to the observation that 14S heavy chains have a higher mobility than 22S when analysed by SDS-PAGE (Marchese-Ragona *et al.*, 1989). Consequently, since the doublet peptides were presumed to be structurally related (and differ by only 5kDa), only one was used in the determination of molecular mass. Secondly, for fractions 3 and 4, the results of V2 photolysis in the presence of MnATP were taken to represent the cleavage peptides on the basis that multiple sites and/or detection of cleavage peptides were considered to complicate the analysis of these fractions (section 4.18).

| Fraction	Mass of heavy chain(s) estimated by V1	Mass of heavy chain(s) estimated by V2
1	747 (743) *	770*
2	384 (379)	383
3	372 (367)	379
4	366 (361)	358

Table 4.12. Molecular mass estimates (in kDa) for the heavy chains for each fraction of 14S dynein determined by V1 or V2 photolysis. Mass estimates shown in brackets represent values derived using the alternate peptide of the doublet pair (section 4.17). Asterisk indicates fraction 1 is given as a combined summation of the two heavy chains since the origin of the cleavage products is unknown.

4.20. Construction of linear peptide maps

The above interpretation enabled the construction of linear peptide maps for the dynein heavy chains associated with each fraction (figure 4.11). Although the position of the V1 and V2 cleavage sites cannot be conclusively determined from these data, previous observations shown in other dynein species enabled likely orientations to be considered (section 4.6.4). The V2 site, for example, has been localised within the larger V1 cleavage peptide for all heavy chains studied so far (King & Witman, 1987, 1988; Tang & Gibbons, 1987; Marchese-Ragona et al., 1989). Similarly, the V1 site has been mapped closer to the amino-terminus than the carboxyl-terminus in the primary heavy chain structure in both *Chlamydomonas* (α, β, and γ) and sea urchin sperm (β) heavy chains (Gibbons et al., 1991, Ogawa, 1991; Mitchell & Brown, 1994; Wilkerson et al., 1994). This orientation has also been suggested for the three heavy chains of *Tetrahymena* 22S as a consequence of proteolytic analysis (Marchese-Ragona et al., 1989). Based upon these observations, figure 4.11 shows a likely arrangement of cleavage peptides within the intact heavy chain(s) for each fraction. These linear peptide maps show both V1 and V2 cleavage sites with respect to the amino- (N) and carboxyl-terminals (C). Although the interpretation of fraction 1 was further complicated by the unknown origin of the cleavage peptides, the

most likely arrangement is that the 230kDa and 152kDa cleavage peptides of this fraction originate from one heavy chain, whereas the other heavy chain comprises the 225kDa and 148kDa cleavage peptides.
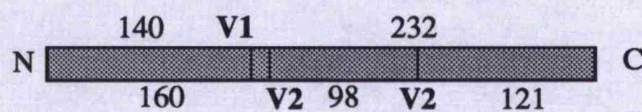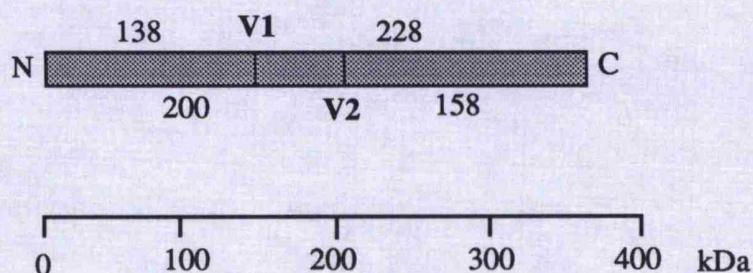
Fraction 1
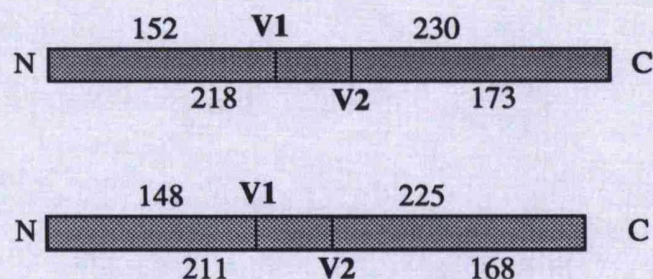
Fraction 2
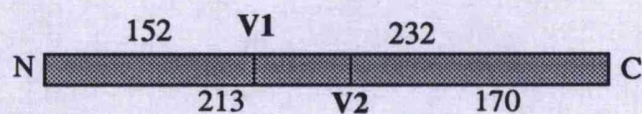
Fraction 3

Fraction 4

Figure 4.11. Peptide map showing one possible orientation of cleavage peptides from both V1 and V2 photolysis experiments. The maps were constructed according to the rules outlined in section 4.20.

4.21. Conclusions

V1 and V2 photolysis revealed both similarities and differences between the four 14S dynein fractions. V1 experiments showed that the four fractions were dynein ATPases which share homology with other dynein species in that each possessed a single V1 site located near the midpoint of the heavy chain sequence (figure 4.11). In this respect, the four fractions are similar to each other, 22S dynein from *Tetrahymena*, and outer arm dyneins from *Chlamydomonas* and sea urchin sperm (Gibbons *et al.*, 1987a; King & Witman, 1987, 1988; Marchese-Ragona *et al.*, 1989).

Structural variation between the fractions was indicated by a number of observations. Firstly, fractions 1 and 2 were readily distinguished from fractions 3 and 4 with respect to the V1 site of cleavage (*ie* the proposed hydrolytic ATP-binding site) {section 4.5.1}. The V1 photolysis of fractions 1 and 2 required MgATP (presumably to form a MgADP.V_i complex within the hydrolytic site), whereas the presence of Mg^{2+} and V_i alone was sufficient for photolysis in fractions 3 and 4 (section 4.17). Secondly, fractions 1 and 2 were readily distinguished from fractions 3 and 4 since V2 cleavage was inhibited by ATP in the former fractions (table 4.11). This suggested that (unlike fractions 3 and 4) occupation of ATP-binding site(s) in fractions 1 and 2 protects the V2 site from cleavage (section 4.18). Thirdly, the fractions were distinguished by the location of V2 sites which was demonstrated by the differing mobilities of the cleavage peptides (table 4.11). Finally, an analysis of the V2 cleavage peptides indicated that fractions 1, and 2, comprised a single V2 site, fraction 4 comprised at least one site, and fraction 3 was thought to possess two V2 sites (figure 4.11).

Chapter 5

Hydrodynamic Investigations of 14S Dynein Fractions

Introduction

The size, shape and interaction of macromolecules such as proteins can be studied using the technique of analytical ultracentrifugation. This procedure provides accurate measurements of biophysical characteristics such as sedimentation coefficients and absolute molecular mass. Furthermore, centrifugation techniques provide information concerning the purity, homogeneity, and interaction parameters of the protein analysed. The work presented in this chapter has been carried out using the recently developed Beckman Optima XL-A analytical ultracentrifuge. This has enabled the study of proteins at low concentration by using scanning absorption optics at wavelengths in the far UV.

The first analytical ultracentrifuge was developed in the 1920's by Svedberg and was originally used for the study of colloidal gold suspensions. Its application to biochemistry was established following experiments on haemoglobin where the, then unexpectedly, large molecular mass and homogeneity of this protein was first reported. Consequently, the analytical ultracentrifuge became the most important tool in the characterisation of proteins until the 1970's. After this time, the centrifuge became largely replaced by alternative, simpler to use and relatively inexpensive techniques such as gel electrophoresis and gel filtration chromatography. These latter techniques were preferentially utilised until the mid-1980's, after which time serious limitations of the techniques became apparent (see Bowen & Rowe, 1970; Rowe, 1984; Schachman, 1992).

Two significant limitations of these simpler techniques are particularly relevant to the determination of dynein molecular mass. Firstly, measurements of mass are largely dependent upon the prior knowledge of well-characterised proteins with masses in a comparative range to those under analysis. These molecular mass standards are required, for example, in the calibration of polyacrylamide gels in electrophoresis techniques. The use of such standards, however, is particularly inappropriate for dyneins since the unusually high molecular masses of some polypeptide components cannot be accurately determined due to the lack of appropriate standards, and inadequacy of electrophoresis, in the high molecular mass region. Heavy chain components of *Tetrahymena* 22S dynein, for example, have been approximated to have masses ranging from 360kDa (Warner *et al.*,

1977) to 560kDa (Mabuchi & Shimizu, 1974) using this technique. A second serious limitation concerns the overall configuration of protein molecules in solution. Techniques such as gel filtration chromatography, for example, enable the Stokes radius of the molecule to be determined (equation 5.9) but require prior calibration with proteins which tend to be of a typically globular nature (Rowe, 1984). This method is consequently highly inappropriate for the analysis of dyneins since the unique 'bouquet' structure described for outer dynein arms (figure 1.4) has an appreciable deviation from the typically globular conformation of proteins used to calibrate columns. The overall configuration of proteins can have severe consequences on the determination of mass. A rod-shaped protein, for example, will travel the length of a gel filtration column at a much slower speed than an equivalently-massed globular protein. The increased frictional forces attributable to the rod shape cannot be assessed and the consequent reduction in speed can only be interpreted with respect to the globular molecular mass standards. Limitations of this type resulted in a renewed interest in the analytical ultracentifuge since this technique requires no calibration and, for mass determination, makes no assumptions with respect to protein shape. The revival of the analytical ultracentrifuge resulted in significant improvements in the available technology.

5.1. The analytical ultracentrifuge - Optima XL-A

The recent development of the Optima XL-A analytical ultracentrifuge has enabled proteins to be investigated at concentrations of a few μg per ml (see Giebeler, 1992). This is achieved by the use of scanning absorption optics in which proteins can be analysed at wavelengths in the far UV. Absorption optics rely upon the ability of solutions to absorb light and, for proteins, optimal absorptions typically occur at 280nm and in the region 205-230nm. This latter region provides at least five times the absorption values at 280nm and, as a result, enhances the level of measurable absorption for proteins of low concentration. Dynein is therefore particularly suited to this new technology since present purification methods result in relatively low protein concentrations. The four 14S dynein fractions, for example, had very low absorption at 280nm but could be successfully monitored in the far UV (figure 5.8).

In order to monitor the dynein fractions in this way, the solution to be analysed is placed in specially designed cells which are optically accessible, water-tight, and resistant to stress and distortion by vacuum and centrifugal force (figure 5.1). A simple cell has a 12mm optical pathlength and consists of a centrepiece comprising two sectors; one for the protein solution and one for the appropriate solvent. This arrangement enables the reference (solvent) and sample (protein solution) sectors of the cell to be directly compared and translated into an absorbance value attributed only to the protein under investigation. The type of cell utilised is dependent upon the experiment. As discussed later, there are two types of investigation; sedimentation velocity and sedimentation equilibrium (section 5.2). Velocity experiments generally involve the use of double-sector cells in which a single dynein sample can undergo investigation (figure 5.2). Three such cells can be analysed during a single experimental run. In contrast, equilibrium studies utilised three six-channel centrepieces (figure 5.2). These cells take a shorter column length and were used in order to reduce the time taken to reach equilibrium as well as to increase the number of samples investigated during a single experiment. In general, the longer the column length of solution in the cell the greater the accuracy of the data. This relationship arises since the column length determines the number of solution traces that can be analysed. Longer column lengths, however, can require an impractical amount of time to reach equilibrium (section 5.2.2). The short column length (1.5mm) of the six-channel cell is therefore a compromise between data accuracy and time expenditure.

Normally, the solvent or solution is placed in a sector-shaped compartment. This shape is designed to prevent non-radial distributions of molecules which would occur in a parallel-sided cell as a result of collisions with the cell walls. The sector shape, however, does introduce the phenomenon of radial dilution in sedimentation velocity experiments (section 5.2.1). Radial dilution refers to the progressive decrease in absorbance apparent as protein molecules travel down the sector-shaped cell. This decrease is due to the effective dilution of molecules as they are forced to occupy a progressively increasing volume.
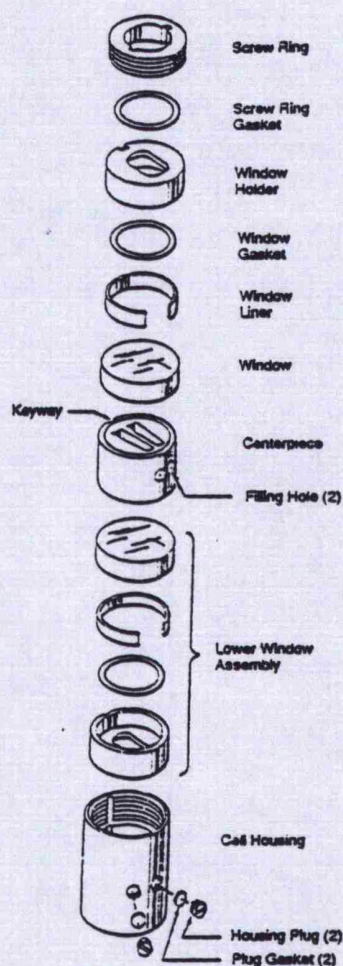
Figure 5.1. The assembly of an analytical ultracentrifuge cell as used in the Optima XL-A (from Beckman, Optima XL-A Users' Manual).
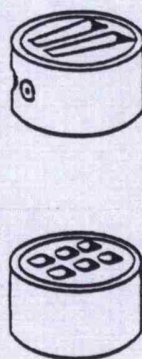
Figure 5.2. A standard double-sector centrepiece (top) and six-channel centrepeice (below) used in sedimentation velocity and equilibrium experiments respectively (from Beckman, Optima XL-A Users' Manual).

5.2. Sedimentation techniques

Two major analytical ultracentrifugation techniques can be applied to the study of dynein in solution; sedimentation equilibrium and sedimentation velocity. The fundamental difference between the techniques resides in the centrifugal force exerted on the solution to be analysed. Velocity experiments require a force sufficient to cause the progressive sedimentation of the protein. In contrast, equilibrium studies require a reduced centrifugal force in which solute particles are distributed throughout the sample volume until the forces of sedimentation and diffusion are equal (section 5.2.2). Differences between the required centrifugal force are achieved by selecting an appropriate speed of centrifugation. Velocity experiments are generally performed at speeds of 20,000-50,000 rpm, whereas equilibrium studies require a reduced speed and, for dynein samples, is typically 5000 rpm. The relationship between centrifugal force and rotor speed is demonstrated by equation 5.1 (from van Holde, 1971).

$$F_c = rm\omega^2 \tag{5.1}$$

where F_c = centrifugal force, m = mass, r = radial distance from centre of rotation, and ω = angular velocity of the rotor (radians/second).

Both velocity and equilibrium experiments rely upon the accurate measurement of several parameters to determine reliable values for sedimentation coefficient and mass respectively. Table 5.1 illustates which parameters are important to each type of experiment and describes how these values are determined. Of particular note, is the value for the partial specific volume ($\bar{v}$) which is approximated to 0.73 ml/g. Ideally, $\bar{v}$ is derived from a knowledge of the protein composition obtainable from sequence data or amino acid analysis. The 14S dynein fractions under investigation, however, have an unknown composition and must therefore be assigned an approximate value. The value of 0.73 ml/g comes from the observation that many proteins agree within one per cent of this figure (Ralston, 1993). Nevertheless, one per cent errors in $\bar{v}$ are responsible for three per cent differences in the determination of molecular mass.

157

Parameter	Velocity	Equilibrium
Temperature/Speed	Accurately maintained by Optima XL-A	
Partial Specific Volume $(\bar{v})$	Approximated to 0.73 ml/g	
Density of Solvent (ρ)	Measured by densitometry (g/ml)	
Viscosity of Solvent (η)	Measured by viscometry (g/ml)	-
Baseline Offset (E)	-	Accurately determined by overspeeding centrifuge at end of run

Table 5.1. The determination of parameters in sedimentation equilibrium and sedimentation velocity.

5.2.1. Sedimentation velocity

Sedimentation velocity experiments result in the determination of the sedimentation coefficient (designated s) for the protein under analysis. This value is defined as the ratio of velocity to centrifugal field strength (equation 5.2) and is expressed in units of seconds. The value 1 x 10^{-13} seconds is commonly encountered in velocity experiments and has been termed the Svedberg unit (designated S). The sedimentation coefficient provides information regarding the size and shape of proteins and is related through the mass (g/mol) and frictional coefficient (g/sec) by equation 5.2 (from Ralston, 1993).

$$s = \frac{v}{\omega^2 r} = \frac{M(1-\bar{v}\rho)}{N_a f} \qquad (5.2)$$

where s = sedimentation coefficient, v = velocity, M = molecular mass, $\bar{v}$ = partial specific volume, N_a = Avogadro's constant, f = frictional coefficient, ρ = density of solvent.

The underlying principle of the velocity experiment is to sediment the protein under investigation at a rate which can be easily monitored over time. The progression of protein from the meniscus to the cell base is typically visualised as a sharp boundary between the depleted region and the uniform concentration of sedimenting solute. Figure 5.3 illustrates the characteristics of a typical trace produced for 14S dynein fraction 1 (see 'results and

discussion'). The position of the boundary is monitored at regular time intervals and traces overlayed to show the progressive movement of solute towards the base of the cell (figure 5.4). A prominent feature of the velocity trace is the decrease in absorbance at the plateau region as the boundary progresses down the cell. This is due to the phenomenon of radial dilution which is a direct consequence of the sector-shaped compartment of the centrepiece (section 5.1).

The sedimentation coefficient is derived from the solution traces by measuring the rate of movement of the boundary midpoint. The midpoint is directly digitised with respect to the meniscus and cell base with the aid of a graphics tablet (section 5.4.2). This rate of change in boundary position can then be related to the sedimentation coefficient by equation 5.3 (from Ralston, 1993).

$$\ln\left(\frac{r_{bnd}}{r_m}\right) = s\omega^2 t \qquad (5.3)$$
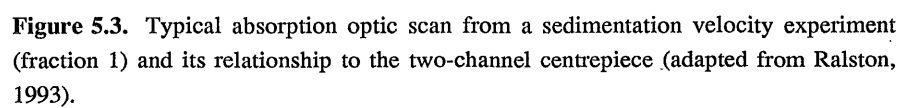
where r_{bnd} = radial position of the boundary midpoint and r_m = radial position of the meniscus, t = time in seconds.

Sedimentation coefficients derived in this way are routinely converted to standard conditions using equation 5.4 (from Ralston, 1993). This ensures that sedimentation coefficients measured in a variety of buffers of different viscosity and density and run at different temperatures, can be directly compared by correcting to the standard solvent water at 20°C. This standardised sedimentation coefficient is denoted $s_{20,w}$.

$$s_{20,w} = s_{obs}\left(\frac{\eta_{T,w}}{\eta_{20,w}}\right)\left(\frac{\eta_s}{\eta_w}\right)\left(\frac{1-\bar{v}\rho_{20,w}}{1-\bar{v}\rho_{T,s}}\right) \qquad (5.4)$$
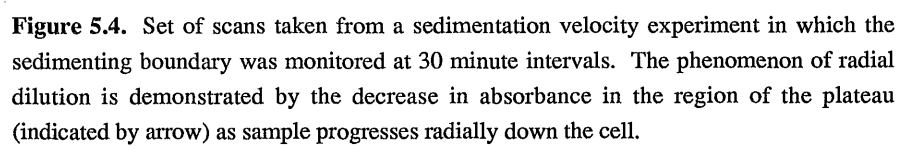
where s_{obs} = measured sedimentation coefficient in the experimental solvent at the experimental temperature (in Kelvin), ,$\eta_{T,w}$ = viscosity of water at the experimental temperature, $\eta_{20,w}$ = viscosity of water at 20°C, η_s and η_w = viscosities of solvent and water respectively at a common temperature, $\rho_{20,w}$ = density of water at 20°C, $\rho_{T,s}$ = density of solvent at the experimental temperature.
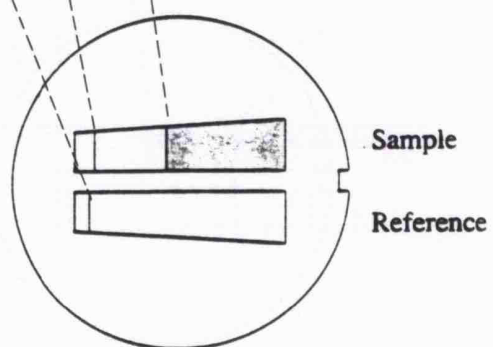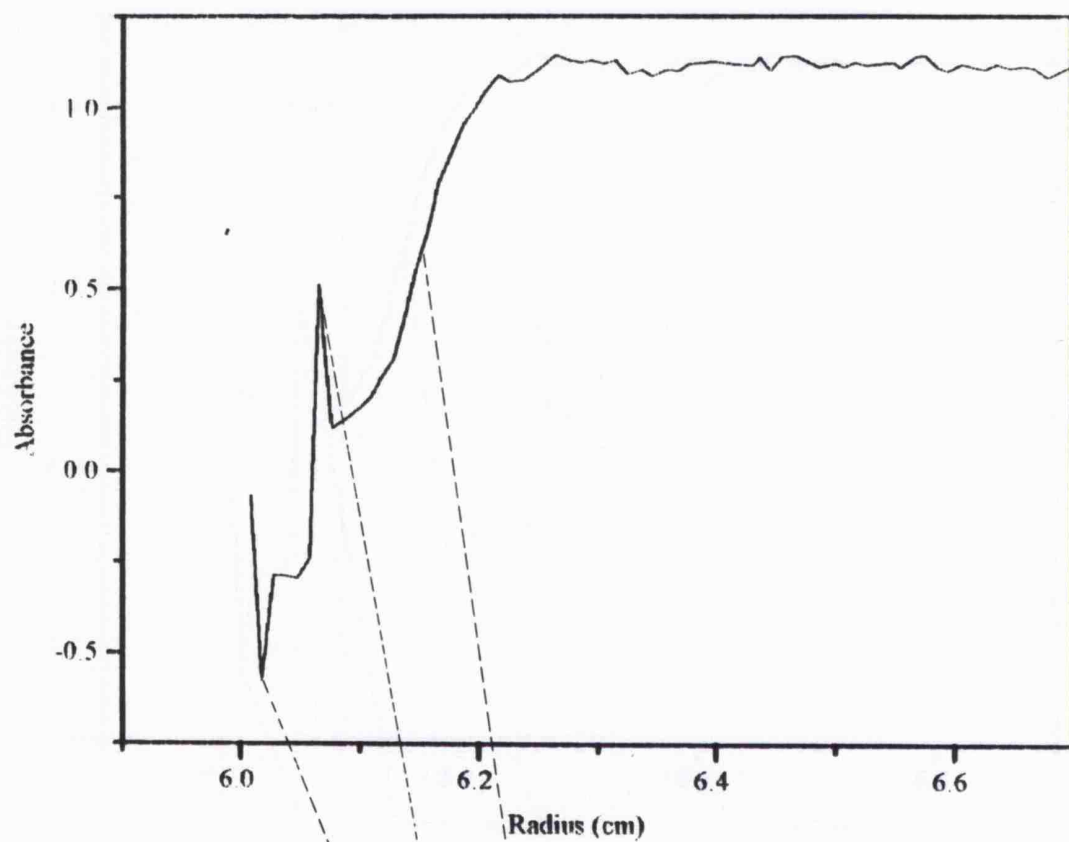
Figure 5.3. Typical absorption optic scan from a sedimentation velocity experiment (fraction 1) and its relationship to the two-channel centrepiece (adapted from Ralston, 1993).

Radius (cm)
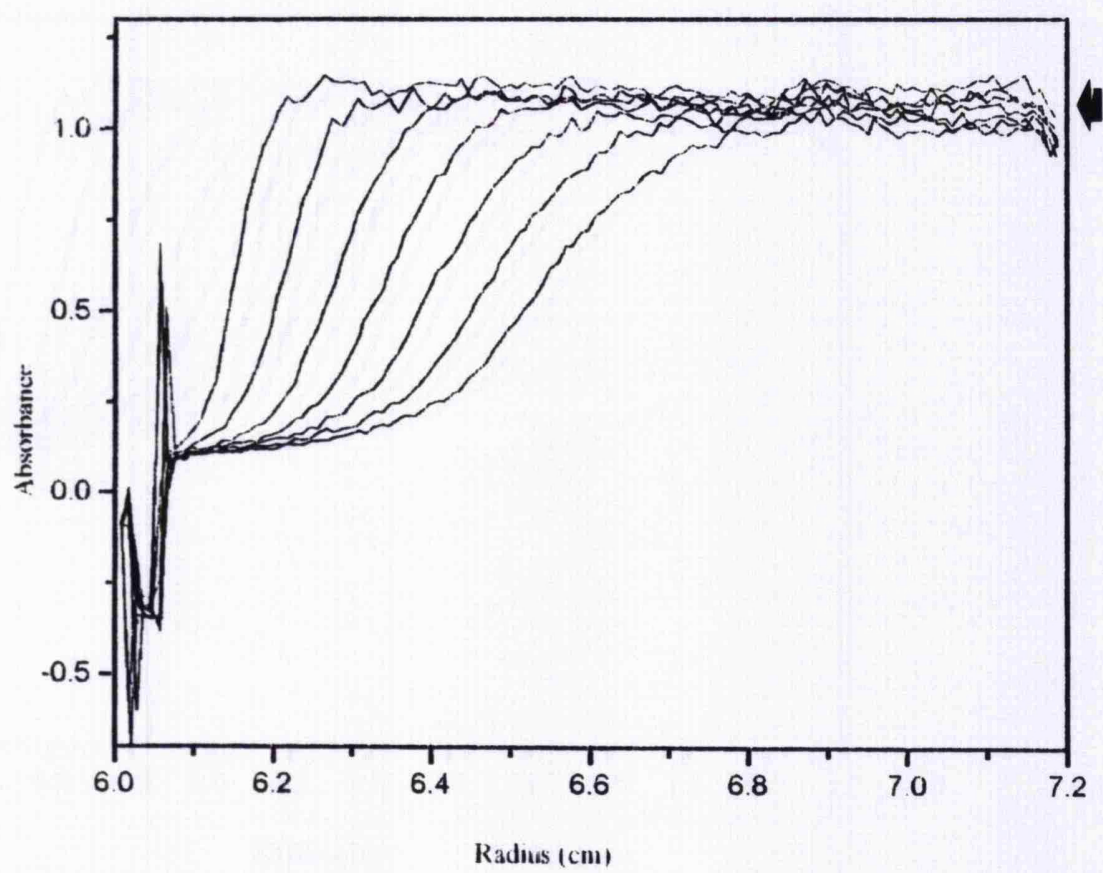
Figure 5.4. Set of scans taken from a sedimentation velocity experiment in which the sedimenting boundary was monitored at 30 minute intervals. The phenomenon of radial dilution is demonstrated by the decrease in absorbance in the region of the plateau (indicated by arrow) as sample progresses radially down the cell.

5.2.2. Sedimentation equilibrium

Sedimentation equilibrium studies enable the determination of absolute molecular mass. This is achieved by an analysis of the protein distribution throughout the sample volume at the point of equilibrium. At equilibrium, sedimentation and diffusion forces are balanced and the protein distribution remains unchanged. This point is determined when absorption scans taken at intervals during the run perfectly overlay one another. A typical scan is shown in figure 5.5.

The centrifugation time taken to reach equilibrium is related to the column length of the cell utilised via equation 5.5. Appropriate column lengths are selected in order to reduce the experimental time without severely affecting data accuracy. Column lengths which are too short, for example, do not provide a sufficient solute distribution to enable an accurate determination of mass. In contrast, column lengths which are too long make impractical constraints on experiment time. In the case of the 14S dynein fractions under investigation, the time taken to reach equilibrium was approximated since the amino acid sequence molecular mass (designated M) is unknown. All fractions were approximated within a similar mass range and as a consequence could be investigated in a single run. This had advantages in that all four fractions were derived from the same preparation procedure and underwent identical treatment.

$$E_T = \frac{0.7 \times H^2 \times \sqrt[3]{M}}{3 \times 10^5} \qquad (5.5)$$

where E_T = time taken to reach equilibrium in seconds, M = sequence molecular mass, and H = solution column length in cm (from Beckman, Optima XL-A Users' Manual).

Analysis of the solute distribution at equilibrium enables a determination of the whole cell weight-average apparent molecular mass of the protein under investigation. This mass is independent of knowledge regarding shape and represents an *apparent* weight-average molecular mass of all components in the cell. As a result, this value includes any contaminants or fragmented molecules that become part of the solute distribution. Consequently, effects such as aggregation will result in greater discrepancy between the apparent and absolute molecular mass.

The apparent weight-average molecular mass is determined directly from experimental data using nonlinear least squares regression analysis. This procedure minimises the sum of the squares of the residuals between the data points and the fitted function by means of the Marquardt algorithm (Smith, 1992). The model assumed for analysis of the 14S dynein fractions is that of a single non-interacting ideal species (Lamm, 1929). Using this model, the software calculates a molecular mass with fitting equation 5.6 based on a plot of absorbance versus radius of the cell (figure 5.6).
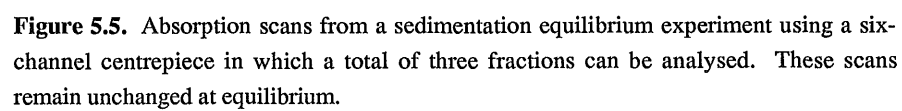
$$A_r = A_o \exp\left[\frac{(1-\rho)\omega^2}{2RT} \times M(r^2 - r_o^2) \right] + E \qquad (5.6)$$

where A_r = absorbance at radius r, A_o = absorbance at reference radius r_o, exp = exponent, $\bar{v}$ = partial specific volume of the macromolecule, ρ = density of the solvent, ω = angular velocity of the rotor, E = baseline offset, M = molecular weight, R = gas constant, T = temperature in Kelvin.

The accuracy with which data fits the determination of mass can be tested by an analysis of a plot of the residuals. The residuals represent the differences between the experimental data points and those at the corresponding points on the curve calculated using the model equation (5.6). These values are calculated by subtracting the absorbance of the fitted curve from the absorbance of data along the radius of the cell. Data which fit the curve is observed as a random distribution with low margins of error. In contrast, poor fitting data may show large errors in the residuals or, in some cases, show a systematic trend indicative of phenomenons such as aggregation (figure 5.7).

As with velocity experiments, conditions such as the temperature and speed are accurately maintained throughout the experiment (table 5.1). The baseline offset (E) is also accurately determined by overspeeding the rotor at the end of the run until the solute has pelleted. The value E is then read as the absorbance remaining following depletion of solute from the meniscus. This procedure minimises the erroneous results attributable to absorbing particles or molecules left undistributed in the gradient. Finally, the value $\bar{v}$ is approximated to 0.73 ml/g and thus may be a source of error (section 5.2).
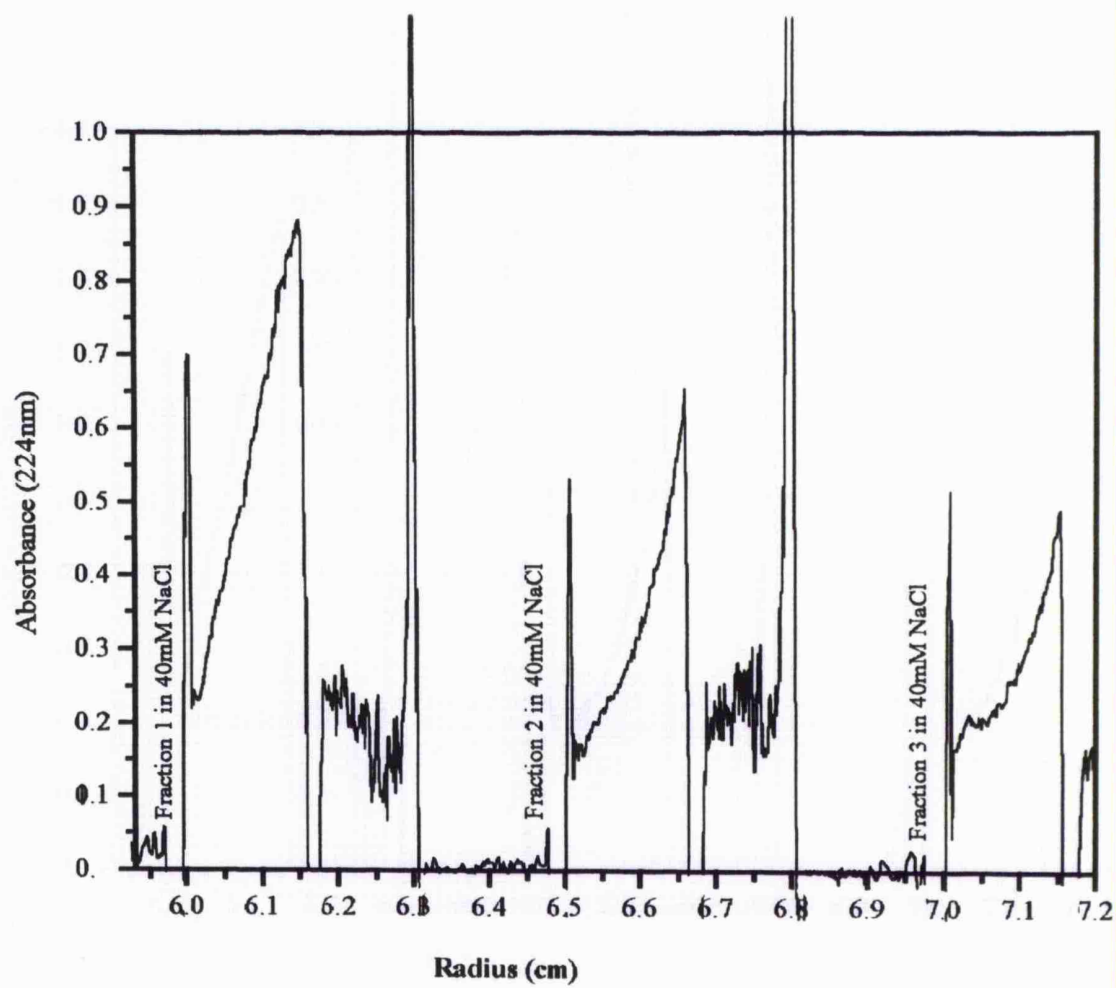
Figure 5.5. Absorption scans from a sedimentation equilibrium experiment using a six-channel centrepiece in which a total of three fractions can be analysed. These scans remain unchanged at equilibrium.
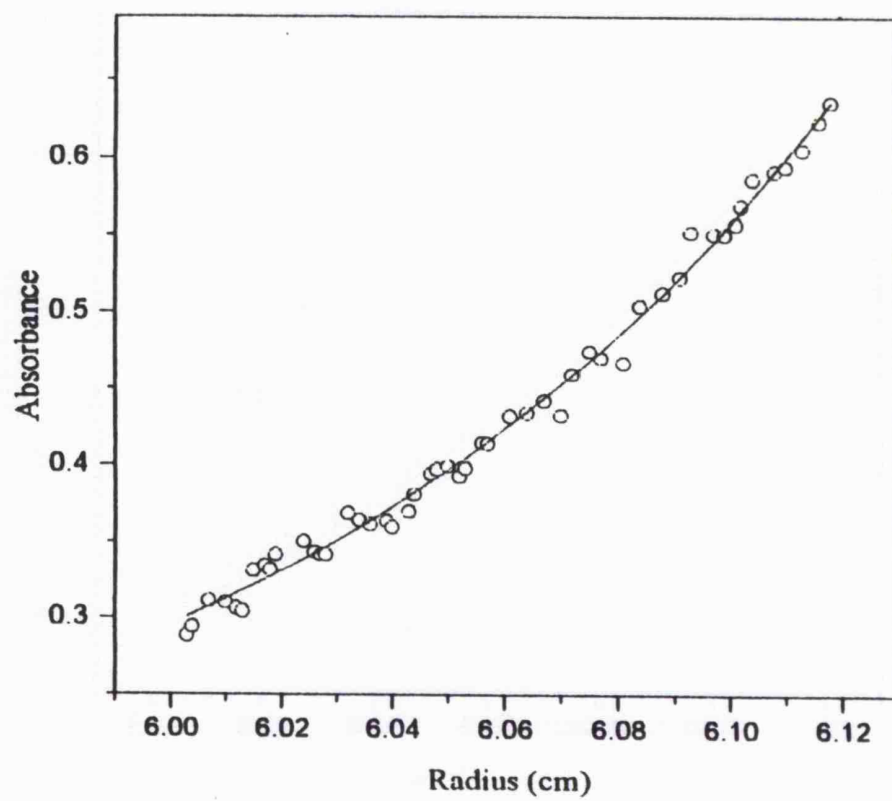
Figure 5.6. Graph showing a typical absorbance versus radius plot for a sedimentation equilibrium experiment (fraction 1). The position of the curve is calculated assuming a single species model (section 5.2.2).
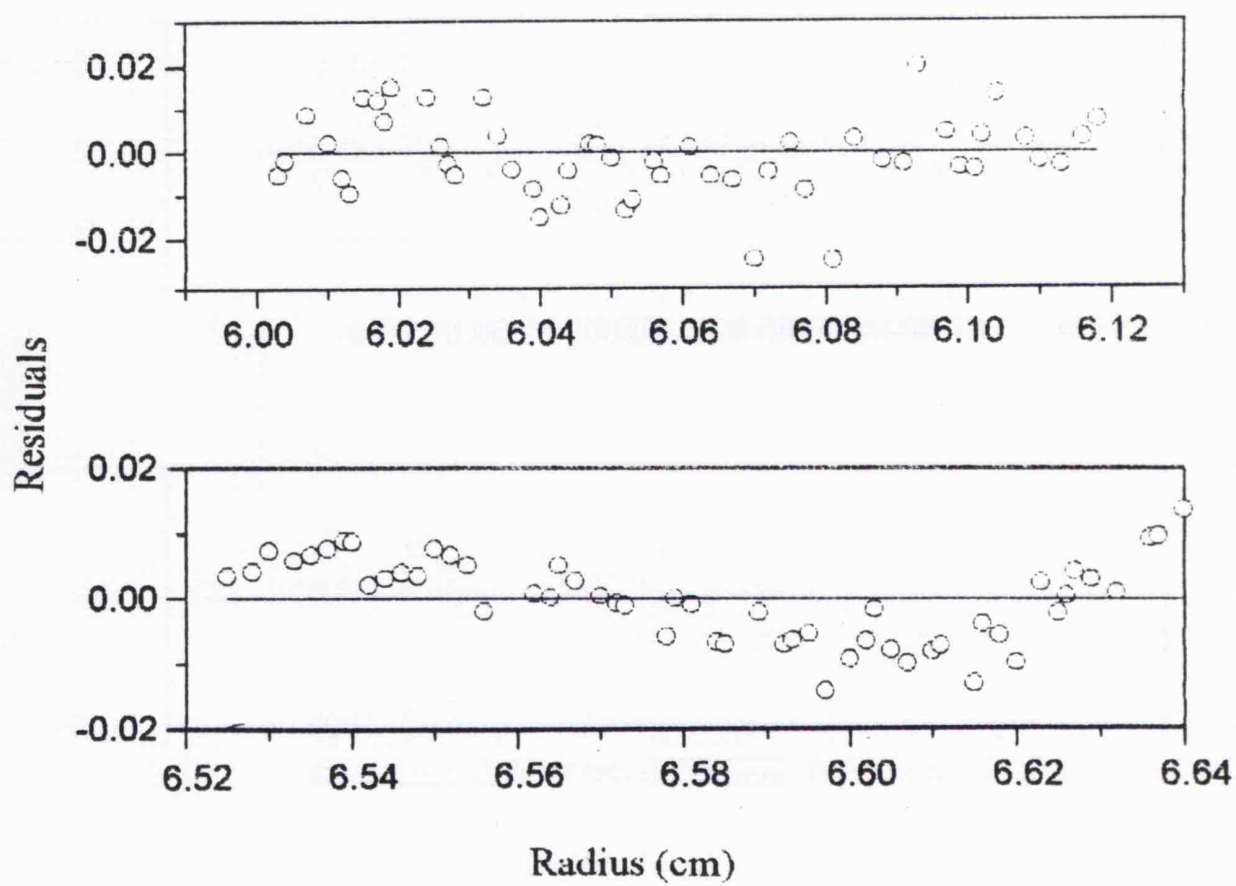
Figure 5.7. Graphical representation of the goodness of fit for data from a sedimentation equilibrium experiment. The zero line is equivalent to the fit calculated assuming a single species model (section 5.2.2). Data showing a good fit with the calculated value are visualised as a random distribution (top), whereas the systematic distribution (below) is indicative of an aggregating system.

<u>5.2.3. Sample heterogeneity</u>

Both sedimentation velocity and equilibrium techniques can provide information with respect to the purity and homogeneity of the dynein sample analysed. Equilibrium studies for example, provide a determination of the whole cell weight-average apparent molecular mass which reflects all components involved in the equilibrium distribution. This value can then be compared with an approximate estimation of the 'expected' monomer mass based on independent but less accurate data such as electron microscopy dimensions or gel electrophoresis. Large deviations from the monomer mass may reflect a self-associating system, heterogeneity or sample impurity.

Sedimentation velocity experiments also provide an assessment of sample homogeneity. Homogeneous proteins generally produce a single sedimenting boundary under velocity conditions, whereas the presence of multiple boundaries indicates other sedimenting species or contaminants. It is possible, however, that several species present in the protein solution under investigation are of sufficiently similar size and shape that only a single sedimenting boundary is apparent. Similarly, a system undergoing reversible self-association can resemble a single species (Roark & Yphantis, 1969).

5.3. Construction of models

Electron microscopy provides an invaluable insight into the structure of a protein since the overall shape and approximate size of molecules can be determined by an analysis of a representative population. One significant limitation, however, is apparent by the very nature of the technique (section 3.7). Molecules which are adsorbed to a mica surface, for example, no longer reflect the conformation, and hydrated size of the protein **in solution**. Furthermore, artefacts introduced by the shadowing procedure used to visualise molecules can lead to erroneous estimates of molecular dimensions and subsequent estimations of mass. In contrast, the quantities measurable by hydrodynamic techniques provide information as to the size, shape and interaction of the protein as it exists in solution. Consequently, the two techniques taken together enable an optimal analysis. Furthermore, these data provide the basis on which potential models for the protein structure can be constructed.

Simple, low-resolution models for proteins can be constructed using appropriately-sized spheres or beads to represent the molecule visualised using electron microscopy. The model has two constraints; firstly, the size of the beads must agree with the dimensions imposed by electron microscopy analysis; and secondly, the total anhydrous volume of spheres must agree with the mass and partial specific volume according to equation 5.7 (see Tanford, 1961).

$$V_a = \frac{M\bar{v}}{N_a}$$ (5.7)

where V_a = anhydrous volume of a sphere, M = mass, $\bar{v}$ = partial specific volume.

Once constructed, coordinates and radii of the bead model are used as input for computer software known as TRV(Translation, Rotation, and Viscosity) written by Garcia de la Torre (1989). This programme was developed and extended largely from the work of Kirkwood (1954) and Bloomfield et al, (1967) and enables the calculation of hydrodynamic parameters for any bead model. Each bead in the model is treated as a sphere of finite size since these structures are well-defined mathematically and exact equations exist to describe their behaviour in solution (Kirkwood, 1954; Bloomfield et al., 1967). Kirkwood's original description of 'irreversible processes in solutions of macromolecules' described the hydrodynamic behaviour of molecules in solution using models comprising identical beads (Kirkwood 1954). This analysis, however, was limited to simple structures since models were restricted to equally-sized and non-overlapping beads. Subsequently, Bloomfield et al. (1967) modified the theory to enable more complex models to be analysed by incorporating beads of variable size.

The theory of Kirkwood and Bloomfield is the basis behind the TRV bead-modelling software (Garcia de la Torre, 1989) utilised for the analysis of the 14S dynein fractions. These fractions are particularly well-suited to this analysis since models can be relatively easily constructed from an array of different sized beads. The two unknown parameters of hydration and conformation for the model can then be analysed to provide the most likely interpretation of molecular conformation.

5.3.1. Hydration

Hydration is an important consideration in the analysis of bead models since this factor can have significant affects on certain hydrodynamic parameters. The term 'hydration' (designated δ) generally refers to the amount of water 'bound' to protein molecules (Kuntz & Kauzmann, 1974). This amount includes water molecules 'carried along' with the protein as a consequence of the interaction with polar or charged amino acids (particularly on the protein surface) capable of forming hydrogen bonds. In addition, hydration refers to water molecules entrapped within the protein. The level of hydration can effect the density, volume, and shape associated with protein molecules and, as a result, has significant influence on the sedimentation coefficient. An exact value for hydration, however, is difficult to measure (Kuntz & Kauzmann, 1974) or theoretically quantify (Squire & Himmel, 1979). Nevertheless, the hydrated volume of any bead model can be calculated (equation 5.8) when the mass and partial specific volume have been defined and a level of hydration has been imposed (see Tanford, 1961). Values for hydration have been shown to be in the range 0.27-0.78 g water/g protein (Squire & Himmel, 1979), although, in practice, a level of 0.3g water/g protein is generally considered reasonable.

$$V_h = \frac{M}{N_a}(\bar{v} + \delta) \qquad (5.8)$$

where M = protein mass, and N_a = Avogadro's constant.

5.3.2. Conformation

Conformation is another important consideration in the analysis of bead models since the sedimentation coefficient is influenced by the conformation of molecules in solution. The frictional coefficient, for example, is dependent upon the size and shape of a given molecule and for a sphere can be determined via Stokes' equation (5.9).

$$f = 6\pi\eta r \qquad (5.9)$$

where η = viscosity of the solvent.

Frictional coefficients for molecules deviating from sphericity can be expressed in terms of the frictional ratio f/f_o (where f is the experimentally-determined frictional coefficient

and f_o is the theoretical frictional coefficient of a sphere of equivalent volume to the anhydrous molecule under analysis). This ratio reflects the fact that a highly elongated structure has a frictional coefficient greater than a molecule of equivalent mass favouring a more compact conformation (see Bowen & Rowe, 1970).

The relationship between the frictional and sedimentation coefficient is demonstrated in equation 5.2. Experimentally, the frictional coefficient is preferentially determined from both sedimentation and diffusion measurements since diffusion is related to friction via equation 5.10 (see van Holde, 1971).

$$D = \frac{RT}{N_a f} \qquad\qquad (5.10)$$

where D = diffusion coefficient (cm^2s^{-1}).

The effect of conformation on the sedimentation coefficient is investigated by the analysis of a number of plausible bead models. With respect to multiple-headed dyneins, for example, conformation can be analysed by varying the angle between the stems to which the heads are attached. The effect of conformation on the sedimentation coefficient can then be investigated.

This chapter is concerned with the hydrodynamic investigation of the four 14S dynein fractions described in chapter 3. Sedimentation equilibrium and sedimentation velocity experiments have been used to provide information with respect to the mass and sedimentation coefficients of each fraction in the presence of 40mM and 600mM NaCl. Structural models have then been proposed which encompass data from both hydrodynamic and electron microscopy studies.

Methods

5.4. Analytical ultracentrifugation

All experiments were carried out using an Beckman Optima XL-A analytical ultracentrifuge with scanning absorption optics. This is fitted with a xenon-pulsed light source and monochromator which enables the accurate selection of an appropriate wavelength (see Giebeler, 1992).

5.4.1. Preparation of 14S dynein fractions

The four fractions of 14S dynein were dialysed for 16 hours against 2 x 2 litres of buffer containing 10mM Hepes, 4mM $MgCl_2$, 0.1mM EGTA, 0.1mM DTT, pH 7.4, and 40mM or 600mM NaCl . After dialysis, the protein concentrations of the fractions were estimated by absorbance at 280nm (section 2.11.1). The concentration of the four fractions was typically in the range 40-100µg/ml. This corresponded to absorbance values well below the recommended minimum of 0.3 absorbance units for analytical ultracentrifugation using scanning absorption optics (Beckman, Optima XLA User Manual). As a result, all ultracentrifugation experiments were performed in the far UV where a significantly greater absorbance was recorded (figure 5.8). The optimal wavelength was determined for each fraction using the wavelength scanning facility on the ultracentrifuge and was typically in the region 215-230nm.

5.4.2. Sedimentation velocity

The use of double-sector cells enabled a maximum of three 14S dynein fractions to be analysed during each experiment. The three cells were prepared by loading dialysate (380µl) into the reference sector, and the dynein fraction to be analysed (360µl) into the sample sector of each cell. The cells were placed in a pre-cooled An-60 Ti rotor and installed into the XL-A. The rotor was run at 25,000 rpm for approximately five hours at 5°C. During this time, the position of the sedimenting boundaries for each fraction was recorded at 30 minute intervals. The sedimentation coefficient was subsequently evaluated from the resulting traces by a measurement of the midpoint of each sedimenting boundary. These positions were digitised directly from the traces using an Apple Graphics Tablet

linked to an Apple II+ microcomputer. The programme utilised calculates the sedimentation value corrected for rotor expansion, reference to reference calibration and true rotor speed (A. J. Rowe). The resulting sedimentation coefficient was corrected to standard conditions using equation 5.4.

5.4.3. Sedimentation equilibrium

The use of three six-channel centerpieces enabled a total of nine samples to be analysed during each experiment. Each cell had a column length of 1.5mm which minimises the time taken to reach equilibrium (equation 5.5) without severely reducing data accuracy. The cells were prepared by loading 65μl of each dynein fraction into the three sample sectors of each cell. The appropriate dialysate (70μl) was then loaded into the corresponding reference sectors of the cells. The rotor (An-60 Ti) was run at 5000 rpm for approximately 48 hours at 5°C. The samples were scanned at eight-hourly intervals after starting the run, recording the absorbance at 0.01mm intervals along the length of each cell. The point of equilibrium was identified when traces of absorbance versus cell radius could be overlayed to show no change in sample distribution. After scanning, the baseline position (E) for each sample was determined by increasing the rotor speed to 40,000 rpm until all solute was depleted from the meniscus. Equilibrium data were analysed using the Origin Ideal 1 programme available on Optima XL-A Data Analysis Software Version 2.0. Data from absorbance scans were manipulated by the software to produce a nonlinear least squares regression analysis of absorbance versus cell radius distributions. The nature of the fit was graphically represented by a plot of the residuals.

5.4.4. Density and viscosity measurements

The density and viscosity of solvents were determined, relative to water at 20°C, using a precision density metre Anton-Paar DMA 02C and an Ostwald viscometer (with a Townson & Mercer water bath providing temperature control to $\pm$ 0.02°C) respectively.

5.5. Bead modelling

Bead models for 22S dynein were constructed using previously published electron microscopy (Johnson & Wall, 1983; Goodenough & Heuser, 1984) and hydrodynamic data

(Wells *et al.*, 1990). In comparison, models for the four 14S dynein fractions were constructed on the basis of original data derived from both electron microscopy and hydrodynamic analysis (see 'results & discussion' and chapter 3).

The construction of each bead model was subject to two constraints. Firstly, the dimensions for each globular head domain (and where applicable stem length) were restricted to within one standard deviation of the mean value derived from electron microscopy data (see table 3.3). Secondly, the specific dimensions utilised in each model were optimised to give a total volume in agreement with the experimentally-derived mass and assigned value (0.73 ml/g {section 5.2}) for the partial specfic volume (equation 5.7). Consequently, models were constructed which provided the optimal fit for both dimension and mass data. In addition, fractions which could be approximated to a single sphere (*ie* fractions 2 and 3) were tested for compatibility with dimension data and the experimentally-derived sedimentation coefficient using Stokes' law (equation 5.9).
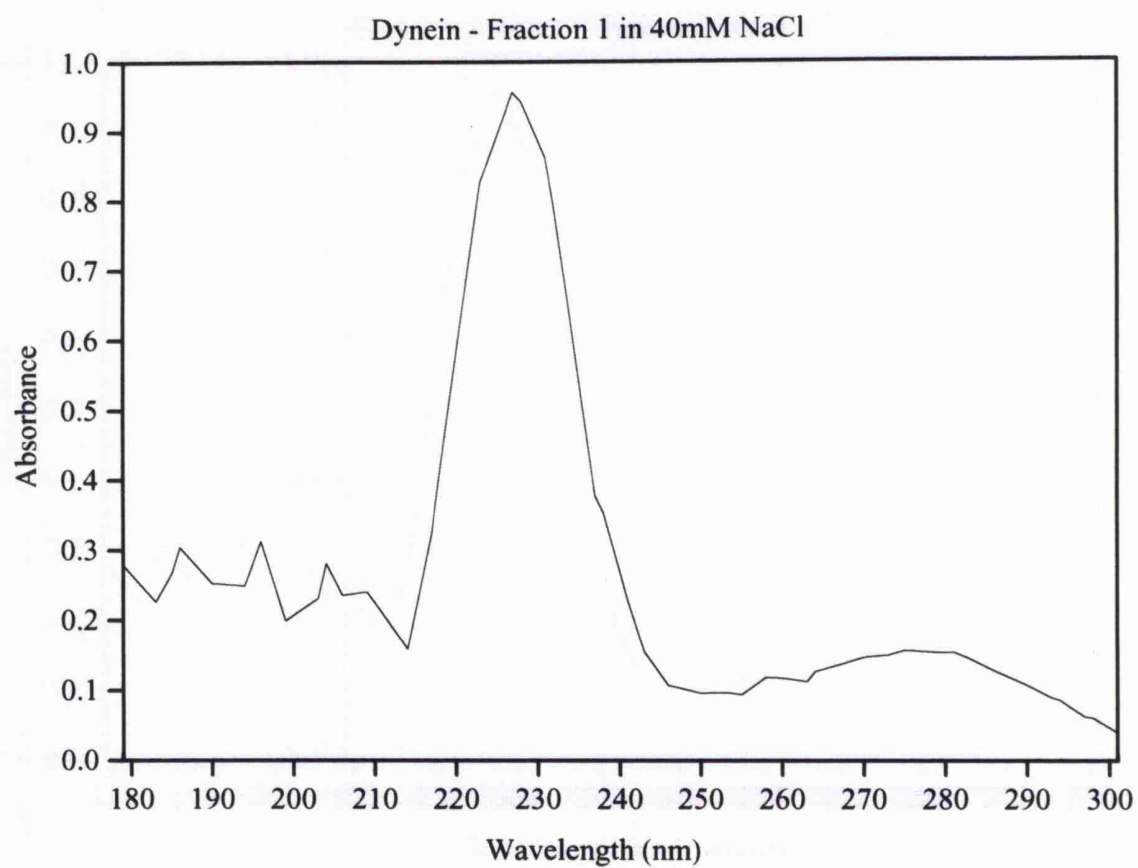
After construction, models were used as input for a modified version of the FORTRAN programme TRV (Garcia de la Torre, 1989) using a Silicon Graphics Instruments mainframe computer (section 5.3). The input data required included the number, radius, coordinates, and mass of each bead in the model, as well as an approximation for the partial specific volume (0.73ml/g), and an imposed level of hydration (Garcia de la Torre, 1989). Furthermore, where appropriate, the coordinates of each bead were calculated (using the software) for a given angle between the stems on which the head domains are attached.
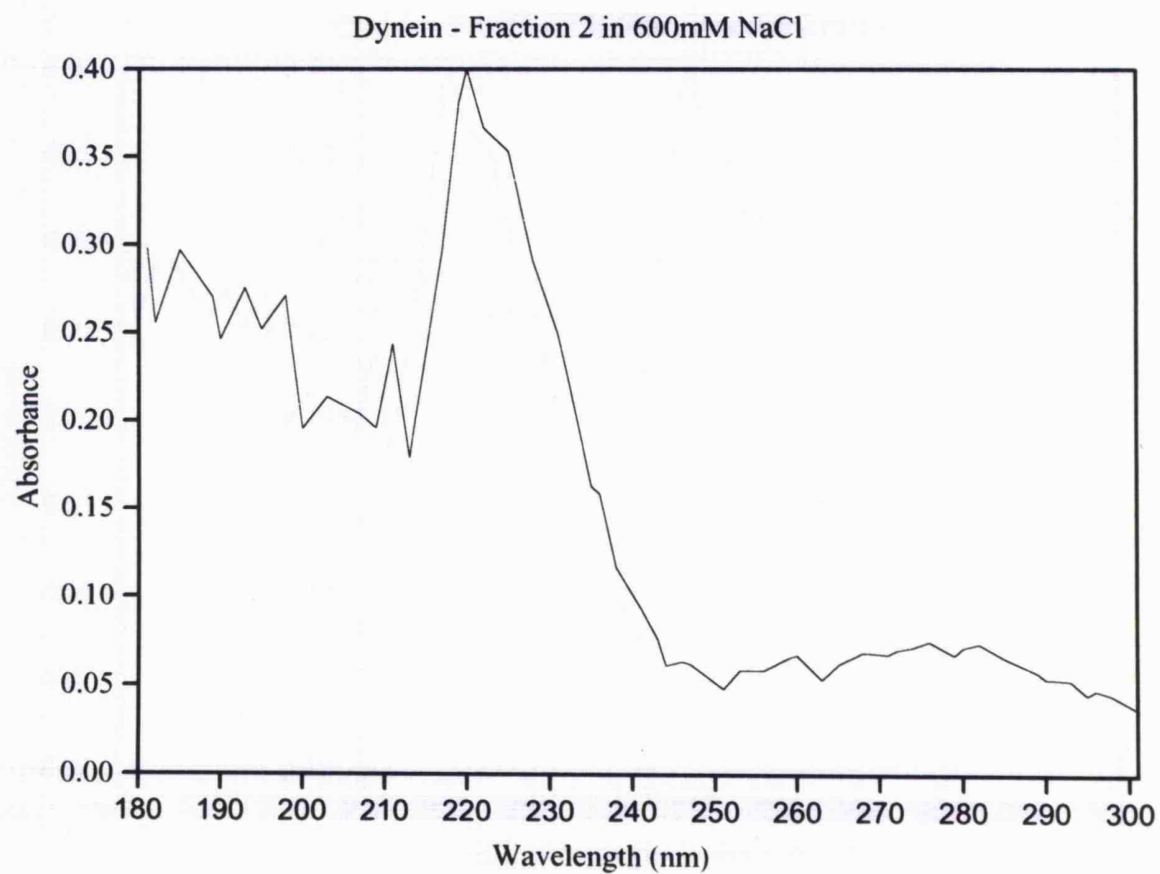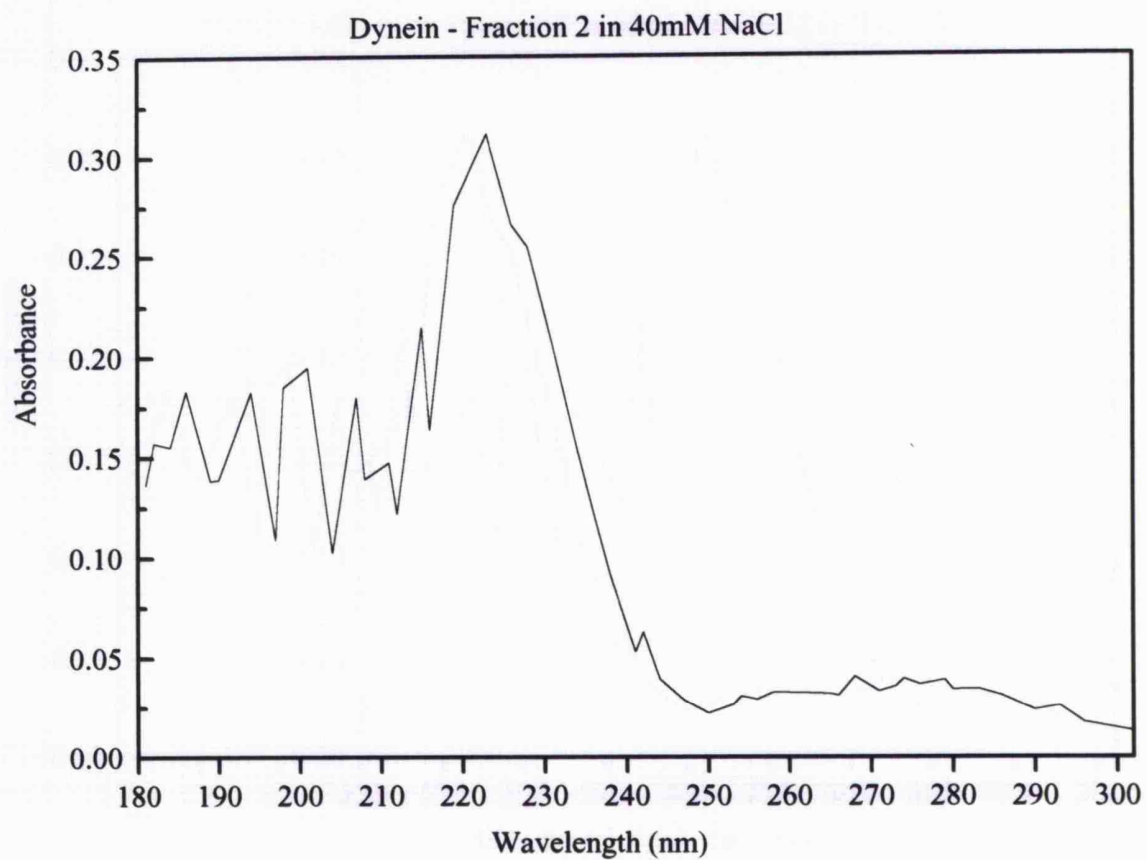
The output generated from the models included the frictional ratio (section 5.3.2), and the frictional-, diffusion- and sedimentation coefficients. In particular, the sedimentation coefficient was important to the analysis of 14S dynein fractions since the theoretical value generated for the bead model could be directly compared to the value derived experimentally. In addition, the effect of the two unknown parameters, hydration and conformation, was investigated. The effect of hydration on the sedimentation coefficient was analysed by modelling over a range of hydration levels from 0.0 to 0.5 g water/ g protein. Similarly, where conformation was of importance (see models for 22S dynein and fractions 1 and 4), the effect on the sedimentation coefficient was investigated by varying
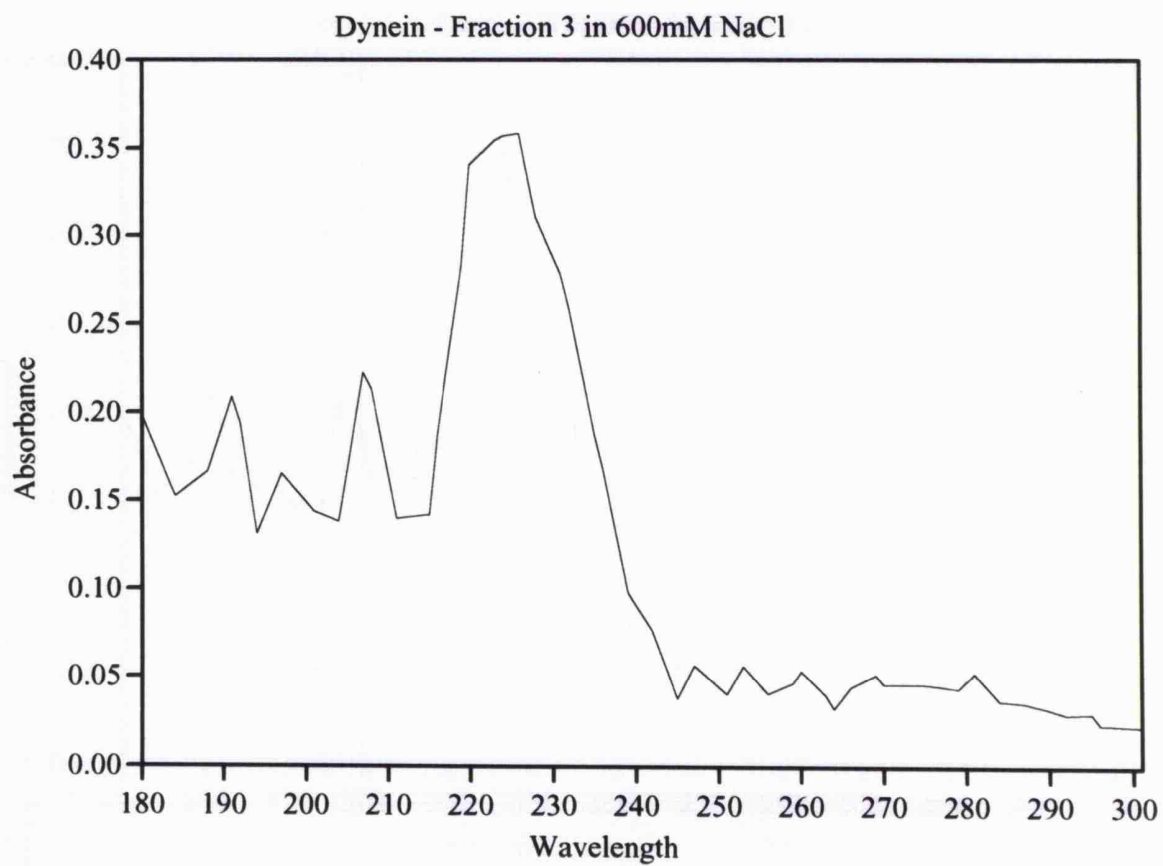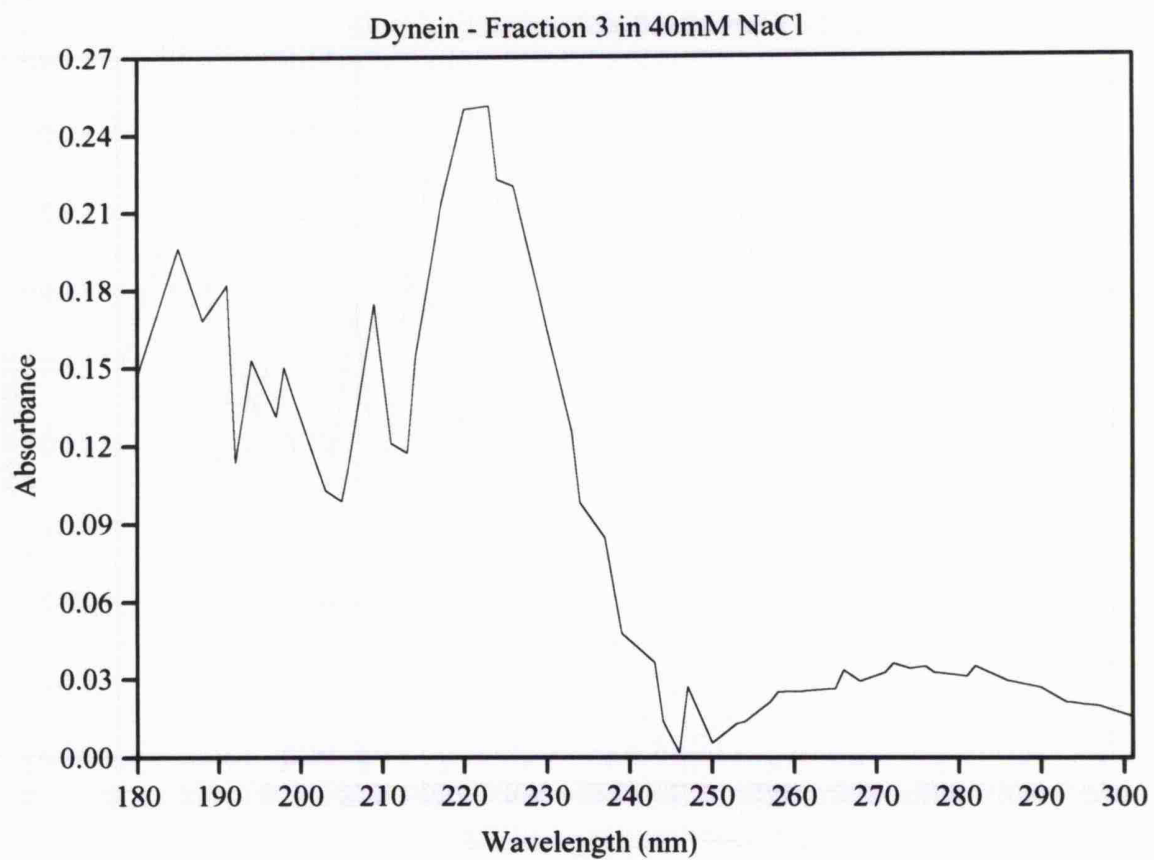
the angle between the stems. It was considered that an optimal model had been produced when the experimentally-derived sedimentation coefficient was reproduced for the model at a reasonable level of hydration (section 5.3.1).
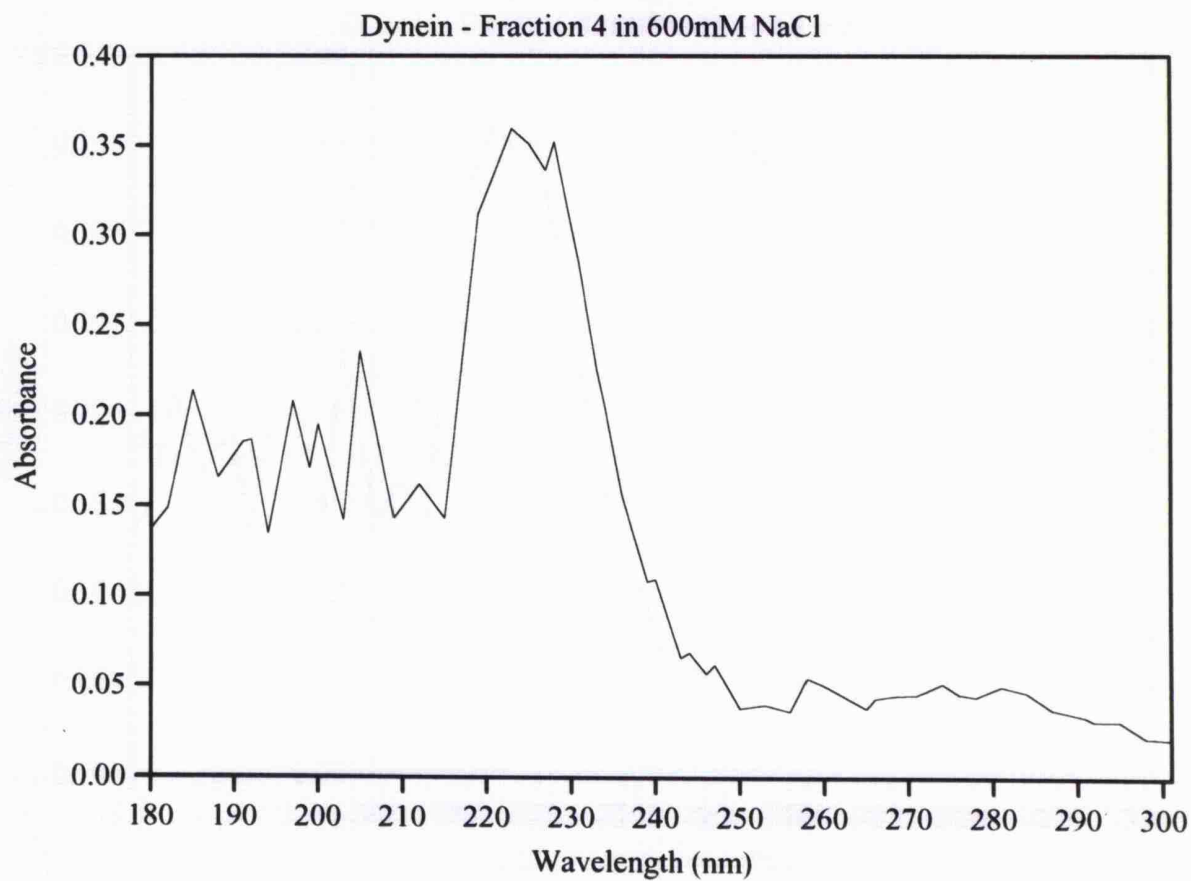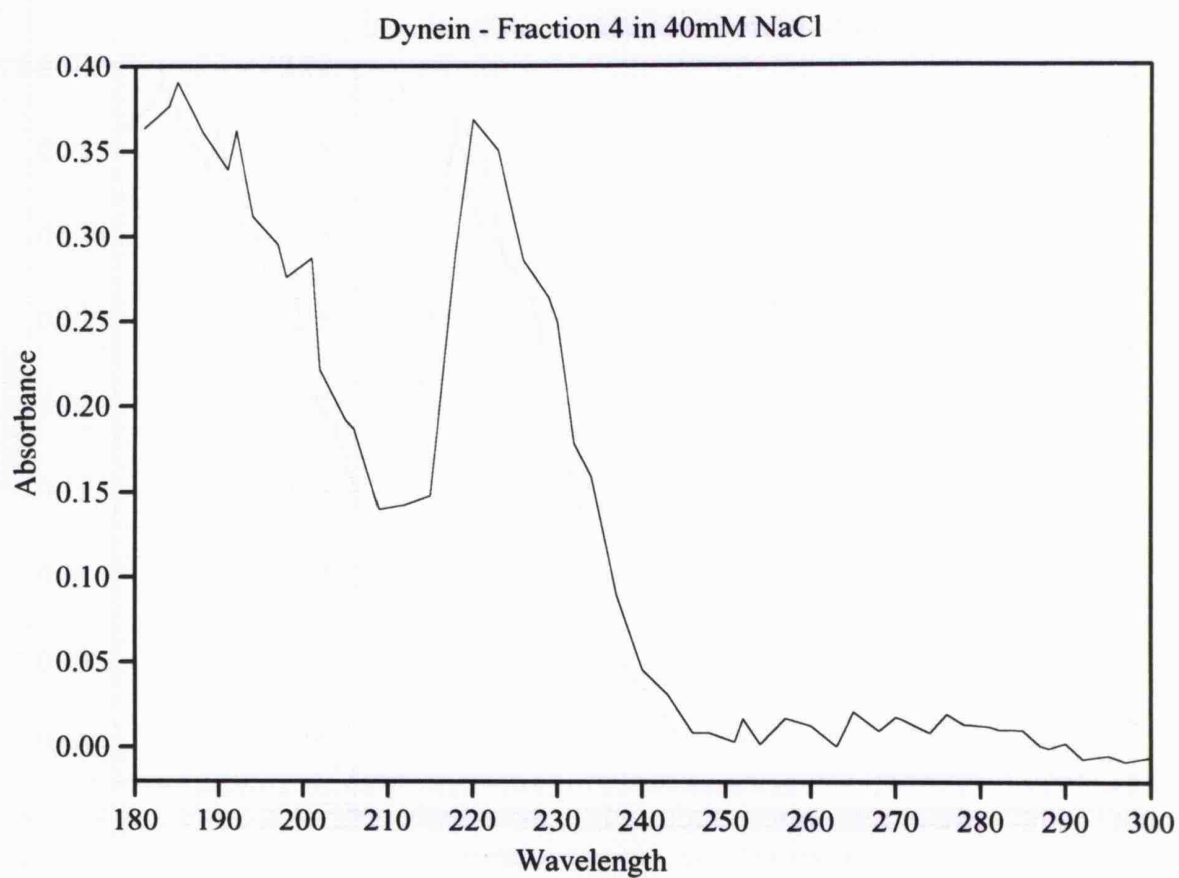
Figure 5.8. Absorbance profiles for the four 14S dynein fractions in the presence of 40mM and 600mM NaCl determined using the wavelength scanning facility on the Optima XL-A.

Dynein - Fraction 1 in 40mM NaCl

Dynein - Fraction 1 in 600mM NaCl

Dynein - Fraction 2 in 40mM NaCl

Dynein - Fraction 2 in 600mM NaCl

Dynein - Fraction 3 in 40mM NaCl

Dynein - Fraction 3 in 600mM NaCl

Dynein - Fraction 4 in 40mM NaCl

Dynein - Fraction 4 in 600mM NaCl
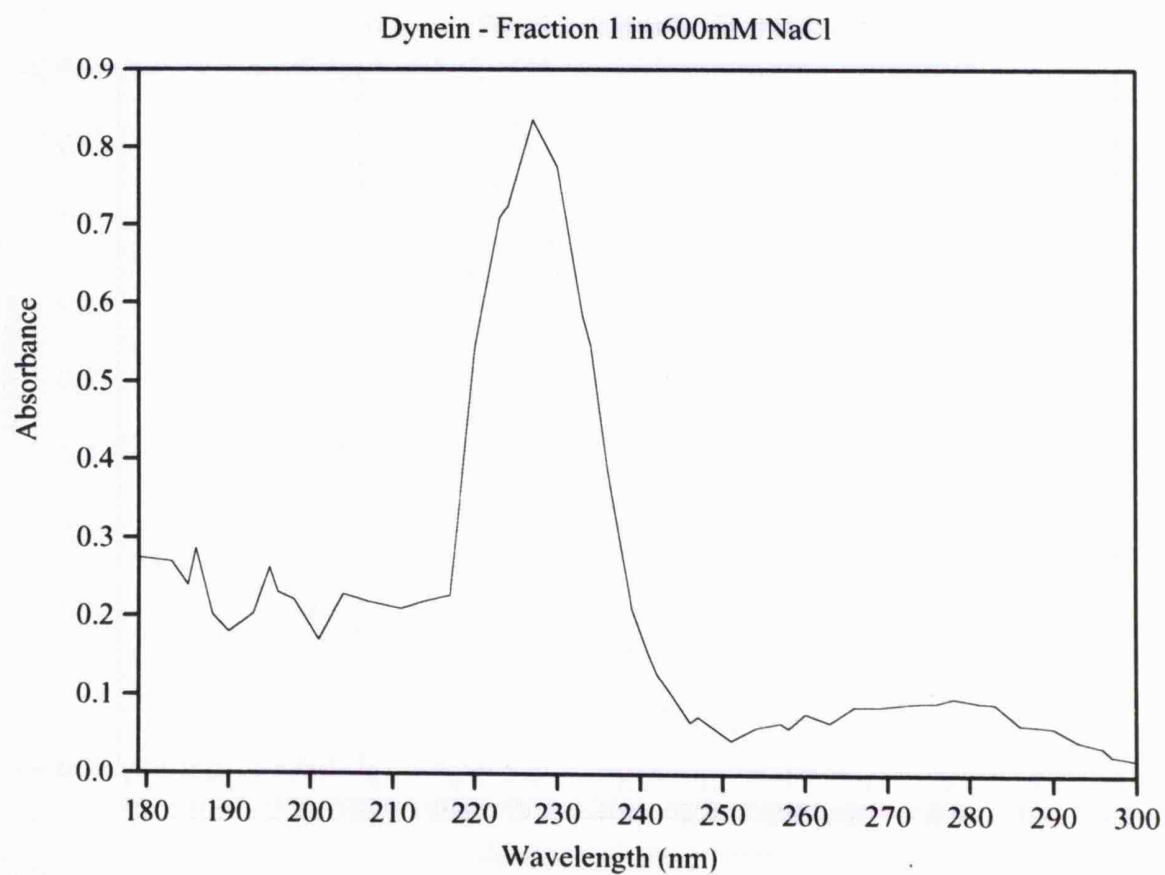
Results and Discussion

This section presents the experimental data derived from hydrodynamic investigations and relates this to the electron microscopy images presented in chapter 3. Hydrodynamic data for all the fractions is summarised in the form of two tables representing sedimentation equilibrium and velocity experiments respectively (tables 5.2 & 5.3). The four 14S dynein fractions are considered in turn and their analysis is demonstrated by the presentation of solution traces (velocity) and graphs of absorbance versus cell radius (equilibrium). The relationship between hydrodynamic and electron microscopy data is then discussed using the technique of bead modelling (section 5.3). The application and usefulness of this technique was justified by a preliminary investigation of the well-characterised *Tetrahymena* 22S dynein.

5.6. Application of bead-modelling to 22S dynein

The structure of 22S dynein is now well-established and the molecular dimensions have been determined by electron microscopy analysis (Johnson & Wall, 1983). Two of the heads have been shown to measure 10nm in diameter whereas the third is slightly larger and has an estimated diameter of 12nm. In addition, the tail for the two smaller heads has an estimated thickness of 2nm whilst that of the larger head measures 3-4nm. Finally, the overall length of the molecule has been approximated to 35nm (Johnson & Wall, 1983). In contrast, hydrodynamic investigations of 22S dynein have been less well-defined. The sedimentation coefficient, for example, has been previously reported as 30S (Gibbons & Rowe, 1965), 21-22S (Mitchell & Warner, 1981; Clutter *et al.*, 1983), and more recently 24.3S (Wells *et al.*, 1990). Similarly, mass estimates have varied from 1.64 x 10^6 Da using sedimentation equilibrium analysis (Wells *et al.*, 1990) to 1.96 x 10^6 Da using scanning transmission electron microscopy techniques (Johnson & Wall, 1983). These apparent inconsistencies are thought to be due both to the accuracy of the experimental procedure utilised, and to the possible variation related to the ability of 22S dynein to dimerise in the presence of 40mM NaCl (Wells *et al.*, 1990). This self-association phenomenon is thought to be prevented under higher salt conditions (600mM NaCl) in which the isolated 22S behaves as a single 'monomer' (three-headed) species. Consequently, hydrodynamic

176

investigations in the presence of 600mM NaCl were considered to more accurately reflect the properties of the monomer 22S molecule and the values of 1.64×10^6 Da and 24.3S have been used for the mass and sedimentation coefficient respectively (Wells *et al.*, 1990).

Information from both electron microscopy and hydrodynamic investigations have been utilised to construct bead models which best incorporate all the available data (section 5.5). Since the precise angle between the stems (on which the globular head domains were attached) was undefined, three possible conformations (60°, 80°, and 100°) have been investigated (figure 5.9). The three models were then tested using the bead modelling software (TRV) in which the sedimentation coefficient was determined as a function of hydration (section 5.3.1). Figure 5.10 shows a graphical representation of the predicted sedimentation coefficients for the three individual models. The published experimental value of 24.3S intercepts all three models at levels of hydration ranging from 0.2 to 0.5 g water/g protein. In particular, the model comprising an angle of 80 degrees was considered optimal since this corresponded to an intermediate level of hydration within the range acceptable (section 5.3.1). In conclusion, the hydrodynamic bead modelling approach works well when applied to 22S dynein and provides a feasible interpretation for the structure of this protein in solution.
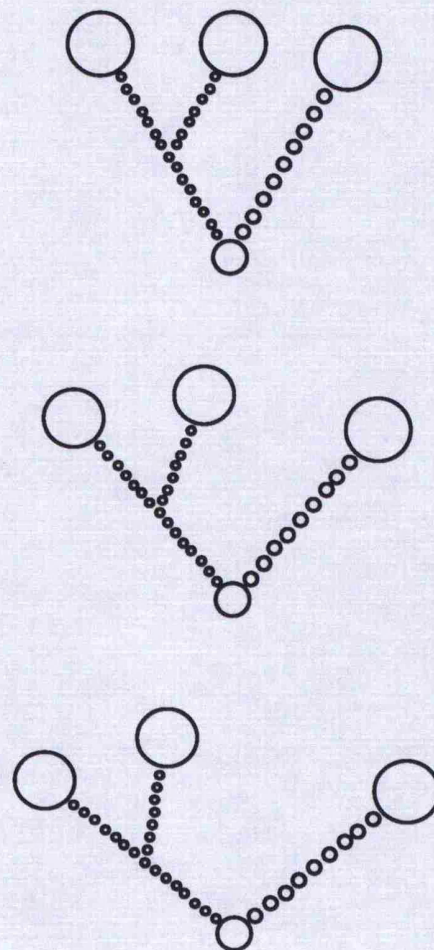
Figure 5.9. Bead models used in the investigation of 22S dynein structure. The three models differ with respect to the angle between the stems on which the globular head domains are located. Angles of 60° (top), 80° (middle) and 100° (below) were investigated.
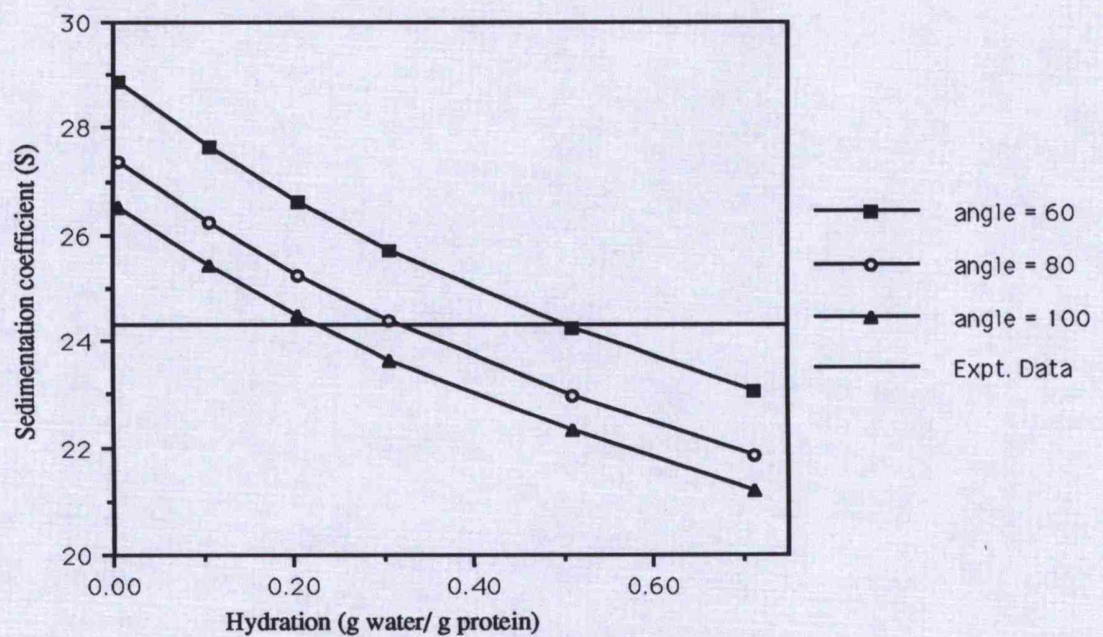
Figure 5.10. Graphical representation of the sedimentation coefficient as a function of hydration for three models (60°, 80°, and 100°, angle between stems) of 22S dynein. For each model, the effect of hydration on the sedimentation coefficient was predicted and directly compared with the value determined experimentally using sedimentation equilibrium (designated expt. data).

5.7. Sedimentation analysis and bead modelling of fraction 1

Sedimentation equilibrium and velocity experiments revealed that, in the presence of 40mM NaCl, fraction 1 has a mean molecular mass of (654 ± 75) kDa and a sedimentation coefficient of (20.1 ± 0.3) S (tables 5.2 & 5.3 respectively). Analysis of a representative equilibrium trace indicated that a plot of the residuals was relatively random with low margins of error (figure 5.11). Velocity traces revealed a clearly defined single sedimenting boundary (figure 5.13). Both techniques therefore produced data indicative of a single species showing no self-association (section 5.2). It was then considered likely that this proposed single species was equivalent to the single predominant structure described previously (at an equivalent ionic strength) using electron microscopy techniques (section 3.11). In these studies, fraction 1 was shown to consist of a double-headed molecule interconnected via two stalk-like appendages (figure 3.12).

This interpretation was tested by modelling the molecular structure of fraction 1 based upon the constraints imposed by hydrodynamic and electron microscopy data (section 5.5). Three bead models were constructed in which the precise angle separating the stems was defined as 40, 60, and 80 degrees (figure 5.14). The models were constructed on the basis of two imposed constraints. Firstly, the total mass attributed to each model was restricted to the mean mass (654kDa) determined using sedimentation equilibrium analysis (table 5.2). Secondly, each head domain was approximated to a sphere of diameter 8.96nm and the overall length constrained to 19nm. These values were within one standard deviation of the mean dimensions (estimated from electron microscopy data, see table 3.3) and, though somewhat low, were necessary in order that the mass and volume of beads in the model were compatible (section 5.5). Furthermore, since the diameter of the stems was difficult to measure with any degree of accuracy, it seemed reasonable to assume that the relative sizes of heads and tails could be approximated to the 22S model (section 5.6). Consequently, the diameter of the beads used to construct the tail were approximated to a size of 2nm. The predicted sedimentation coefficients for the three fraction 1 models (plotted as a function of hydration) were then compared to the experimentally derived value of 20.1S (figure 5.15). All three models were shown to intercept with the experimental value at levels of hydration between 0.06 and 0.46 g water/g protein and

therefore represented a plausible interpretation of fraction 1. In particular, an intermediate value for hydration (section 5.3.1) corresponding to an angle between 40 and 60 degrees was considered to represent the most likely conformation. The two-headed interpretation of fraction 1 is therefore a feasible model for this fraction as it exists in the presence of 40mM NaCl.

In the presence of **600mM NaCl**, both the mass and sedimentation coefficient of fraction 1 decreased by approximately 30 per cent to give a mean mass of **(451 ± 65) kDa** and a sedimentation coefficient of **(13.6 ± 0.5) S** (tables 5.2 & 5.3 respectively). Surprisingly, as with the conditions of 40mM NaCl, both equilibrium and velocity data indicated components of sufficiently similar mass and size that behaviour was identical to that expected for a single non-aggregating species system (figures 5.12 & 5.13). The simplest interpretation of these data is that 600mM NaCl conditions disrupt the structure of the proposed two-headed molecules (which exist in the presence of 40mM NaCl) to produce molecules with predominantly single heads. Protein dissociation and/or denaturation could be possible explanations since under these conditions significant reductions occur in size, mass, and enzymatic activity (section 4.9.1).

One obvious discrepancy in this interpretation, however, is evident from a comparison of the experimentally-derived masses for the two possible conformations. The mass of the presumed single-headed or 'monomer' molecule (451kDa), for example, is not equal to half the value derived for the dimer (654kDa). This discrepancy can be explained in two ways. Firstly, dissociation and/or denaturation of dimeric molecules may produce particles which, though hydrodynamically similar, are not true monomers. The so-called 'monomer' value of 451kDa may therefore reflect the average mass of a mixed population of particles. This interpretation assumes, however, that the particles predominating in the presence of 600mM NaCl, are similar enough to go undetected as separate components by hydrodynamic analysis. A second, and perhaps more likely, interpretation is that monomer and dimer conformations exist in a state of equilibrium as a result of reversible self-association (section 5.2.3). The association is presumed to be reversible since evidence for two components is not apparent in either velocity traces (figure 5.13) or residual plots

(figure 5.12). Reversible self-association will affect the mass (and consequently the interpretation of bead models) since the experimentally-derived mass will not accurately reflect either the monomer or dimer conformation. Instead, the mass will reflect a state of equilibrium between monomer and dimer species which is influenced by the concentration of NaCl. Evidence in support of this interpretation is indicated by a comparison of the mass associated with the two-headed molecule (654kDa) with estimates of heavy chain mass (derived by vanadate-dependent photolysis {section 4.19}). In this case, the estimated mass of the heavy chains (743-770kDa) is greater than that predicted for the dimer by hydrodynamic analysis (table 4.12). The hydrodynamic determination of the presumed dimeric mass may therefore be an underestimate due to a monomer-dimer state of equilibrium.

In conclusion, the two-headed structure of fraction 1 evident in the presence of 40mM NaCl can be adequately modelled on the basis of electron microscopy and hydrodynamic data. Limitations of the model, however, exist since the mean dimensions derived from electron microscopy data were inconsistent with the experimentally determined mass. This discrepancy could be explained in two ways. Firstly, the estimation of molecular dimensions was susceptibile to error. Secondly, the possibility of reversible self-association would prevent the accurate determination of either the dimer or monomer mass. Since the extent of reversible self-association was unknown, a minimal dimension value (within one standard deviation of the mean) was imposed on the construction of bead models. In this way, the mass and dimension data were compatible. Based on these data, an optimal model was produced in which the angle separating the two stems was shown to be intermediate between 40 and 60 degrees.
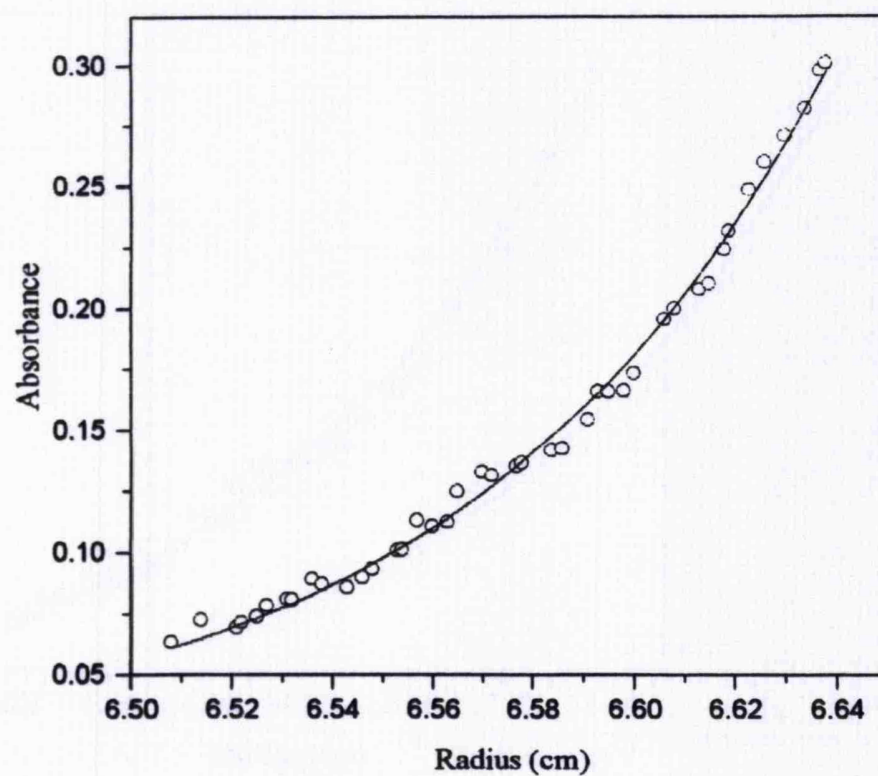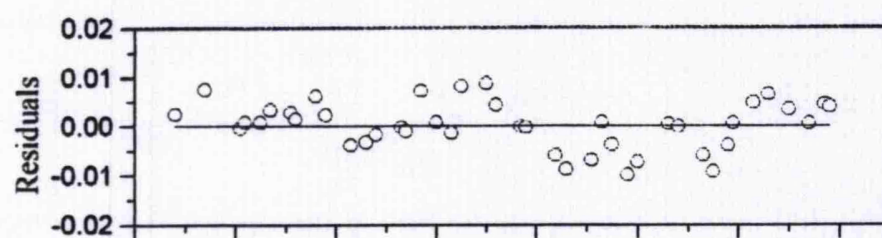
Figure 5.11. Sedimentation equilibrium analysis of fraction 1 in the presence of 40mM NaCl. The calculated mass for this distribution was 673kDa. The randomly-distributed residuals indicate a good fit with that expected for a single ideal species (section 5.2.2). Equilibrium experiments were carried out at a rotor speed of 5000 rpm and a temperature of 5°C.
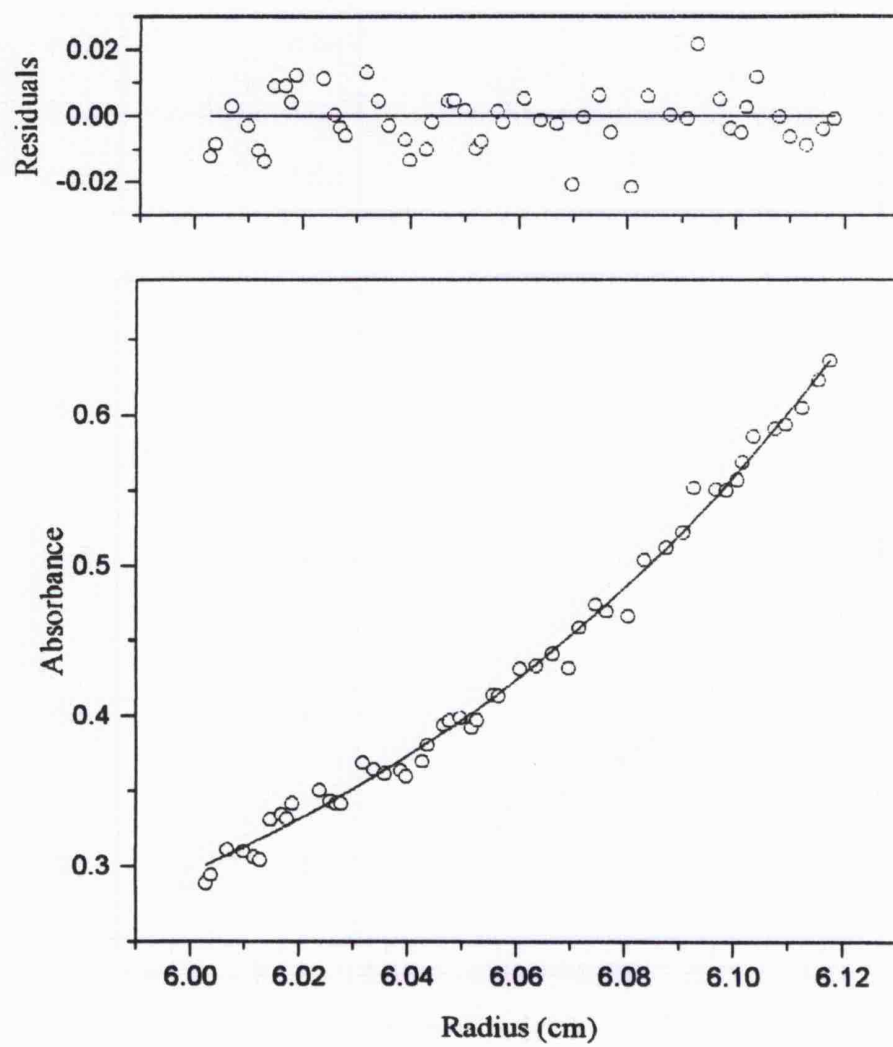
Figure 5.12. Sedimentation equilibrium analysis of fraction 1 in the presence of 600mM NaCl. The calculated mass for this distribution was 499kDa. The randomly-distributed residuals indicate a good fit with that expected for a single ideal species (section 5.2.2). Equilibrium experiments were carried out at a rotor speed of 5000 rpm and a temperature of 5°C.
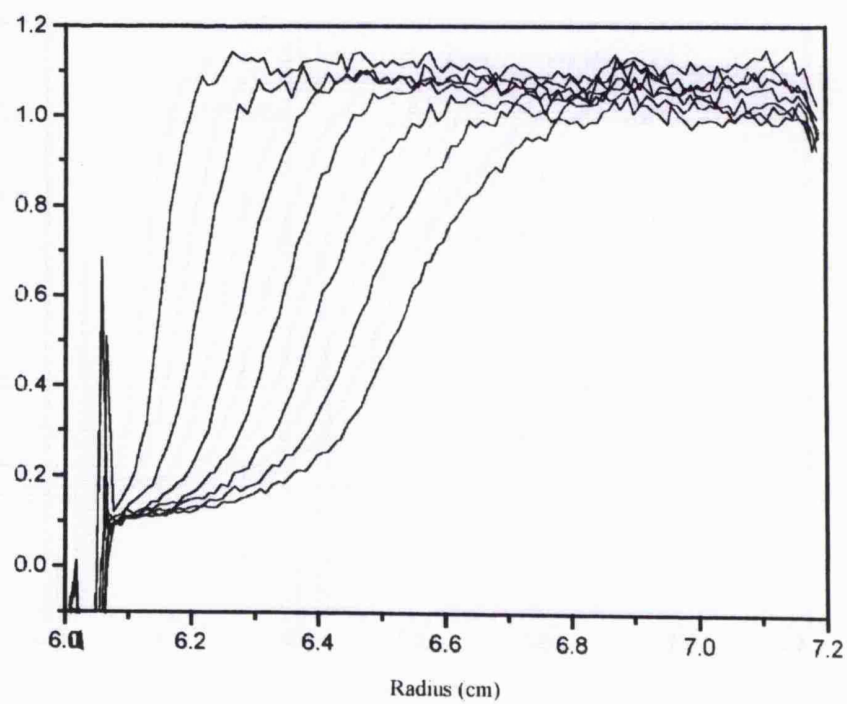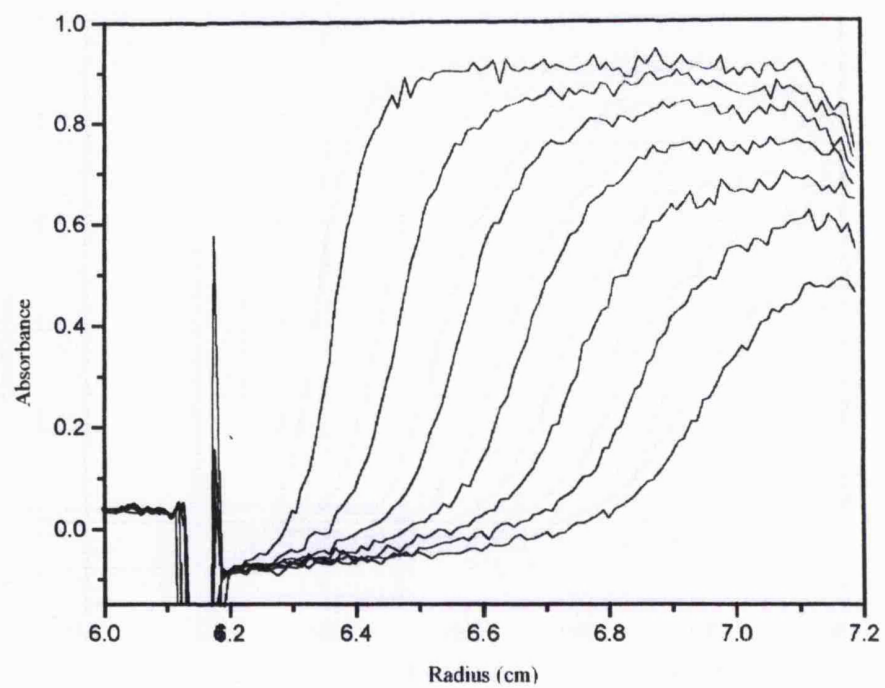
Figure 5.13. Sedimentation velocity traces for fraction 1 in the presence of 40mM NaCl (top) and 600mM (below) NaCl. At 40mM NaCl, the single sedimenting boundary has an $s_{20,w}$ of (20.1 ± 0.1) S, whereas under conditions of 600mM NaCl this value is reduced to (13.9 ± 0.1) S. Traces were recorded at 30 minute intervals at a rotor speed of 25,000 rpm and a temperature of 5°C.
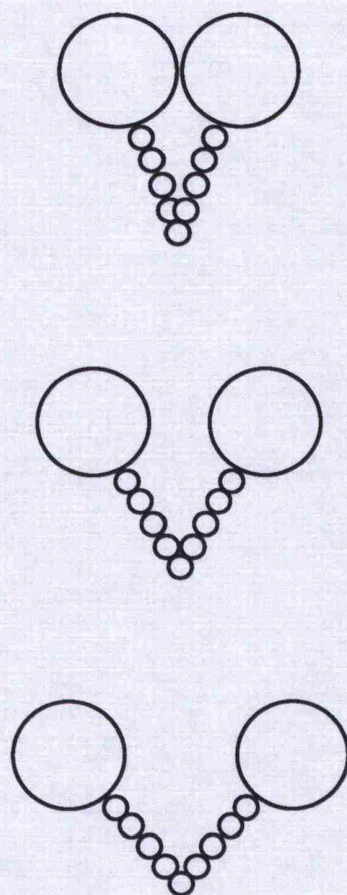
Figure 5.14. Bead models used in the structural investigation of fraction 1. The three models differ with respect to the angle between the globular head domains. Angles of 40° (top), 60° (middle) and 80° (below) were investigated.
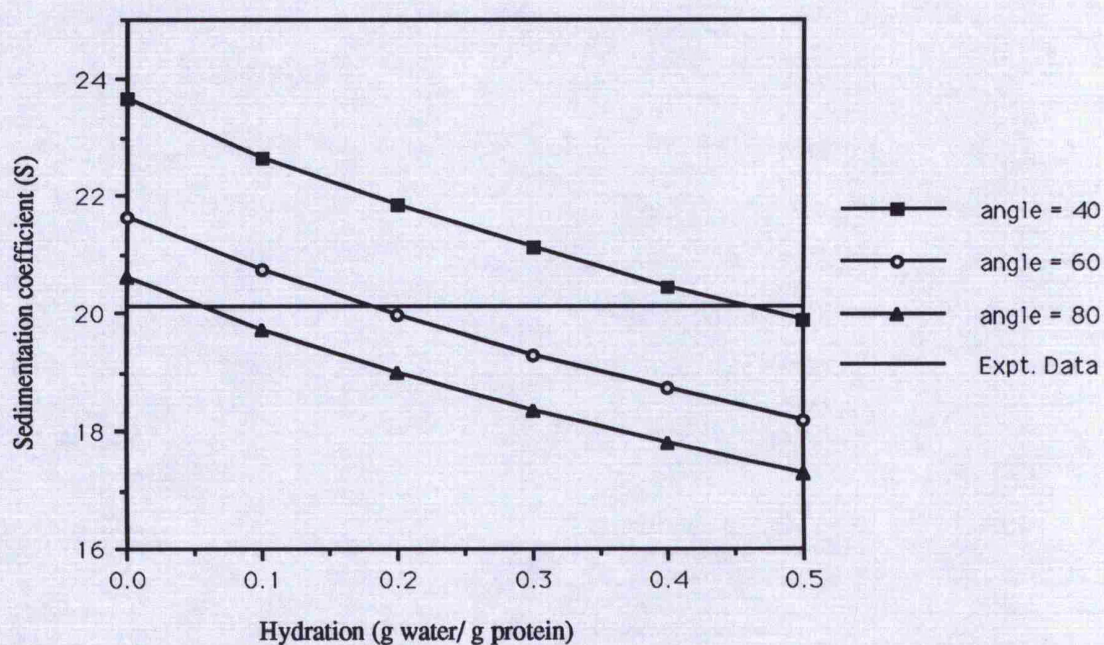
Figure 5.15. Graphical representation of the sedimentation coefficient as a function of hydration for models of fraction 1. For each model, the effect of hydration on the sedimentation coefficient was predicted and directly compared with the value determined experimentally using sedimentation equilibrium (designated expt. data).

5.8. Sedimentation analysis and bead modelling of fraction 2

In the presence of **40mM NaCl**, fraction 2 was shown to comprise at least <u>two</u> components. The relationship of these components was uncertain since it was impossible to distinguish between the presence of different molecular species and stable aggregation states. Nevertheless, heterogeneity was identified by three independent experimental procedures.

Firstly, heterogeneity was indicated by the variability in mass associated with different preparations of the fraction in which estimates varied from **616kDa** to **966kDa** (table 5.2). Analysis of equilibrium data showed that a plot of the residuals exhibited a systematic distribution (figure 5.16) indicative of an associating or heterogeneous system (section 5.2.2). Secondly, an analysis of sedimentation velocity traces clearly indicated at least two sedimenting components (figure 5.18). The predominant sedimenting component had a sedimentation coefficient of **(16.6 $\pm$ 0.2) S**, whereas that of a second component was measured for two different experiments as (6.8 $\pm$ 0.3) S and (9.9 $\pm$ 0.9) S (table 5.3). Finally, aggregation and/or heterogeneity was indicated by the electron microscopy analysis (section 3.11). Aggregated species may well be represented by the large structures of variable size and shape previously described (figure 3.13). Similarly, sample heterogeneity was indicated by the identification of at least two types of approximately ellipsoidal structures.

In the presence of **600mM NaCl**, the level of apparent heterogeneity decreased and both the mass and sedimentation coefficient were reduced (tables 5.2 & 5.3). Analysis of equilibrium data revealed that a plot of the residuals was more random (figure 5.17) and the mean mass was reduced to **(485 $\pm$ 56) kDa**. In comparison, the two sedimenting boundaries described for velocity traces in the presence of 40mM NaCl, were no longer evident in the corresponding trace at 600mM NaCl (figure 5.18). Furthermore, the trace more closely resembled that of a single sedimenting species with a reduced sedimentation coefficient of **(13.2 $\pm$ 0.6) S**.

The interpretation of these data is complicated by the unknown heterogeneity of the fraction. It is uncertain, for example, whether the two components evident in velocity traces in the presence of 40mM NaCl represent stable aggregation states or distinct

molecular species (figure 5.18). Nevertheless, the identification of only one sedimenting boundary in the presence of 600mM NaCl can be interpreted in two ways. Firstly, the two components predominant at 40mM NaCl could dissociate to produce several smaller hydrodynamically equivalent particles which behave as a single species. Secondly, the concentration of NaCl could effect the equilibrium state of a reversibly-associating system. In this latter case, reversible association can affect the mass (by favouring for example a monomeric rather than a dimeric conformation) but still resemble a single ideal species at low-to-moderate K_a values (Roark & Yphantis, 1969). A similar interpretation can be applied to equilibrium data. In the presence of 40mM NaCl, evidence for a reversibly-associating system is indicated by the range of masses exhibited within different preparations of the fraction (table 5.2). In contrast, a single species is evident in the presence of 600mM NaCl. As with velocity, this apparent single species may either arise as a consequence of dissociation, or as the result of a change in the equilibrium state of a reversibly-associating system.

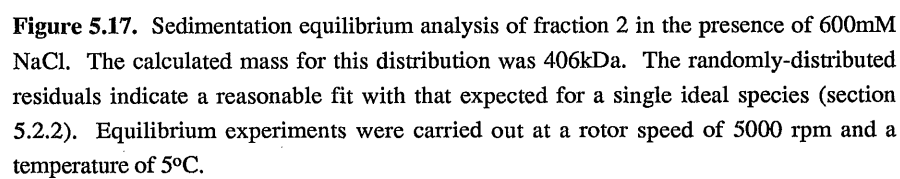In conclusion, fraction 2 is a complex heterogeneous system in which at least two components can be identified. It is unclear, however, whether these components represent distinct molecular species or aggregates. As a result, it was difficult to define this fraction further. In addition, attempts to construct bead models were unsatisfactory on the basis that both the mass and specific structure were undefined.
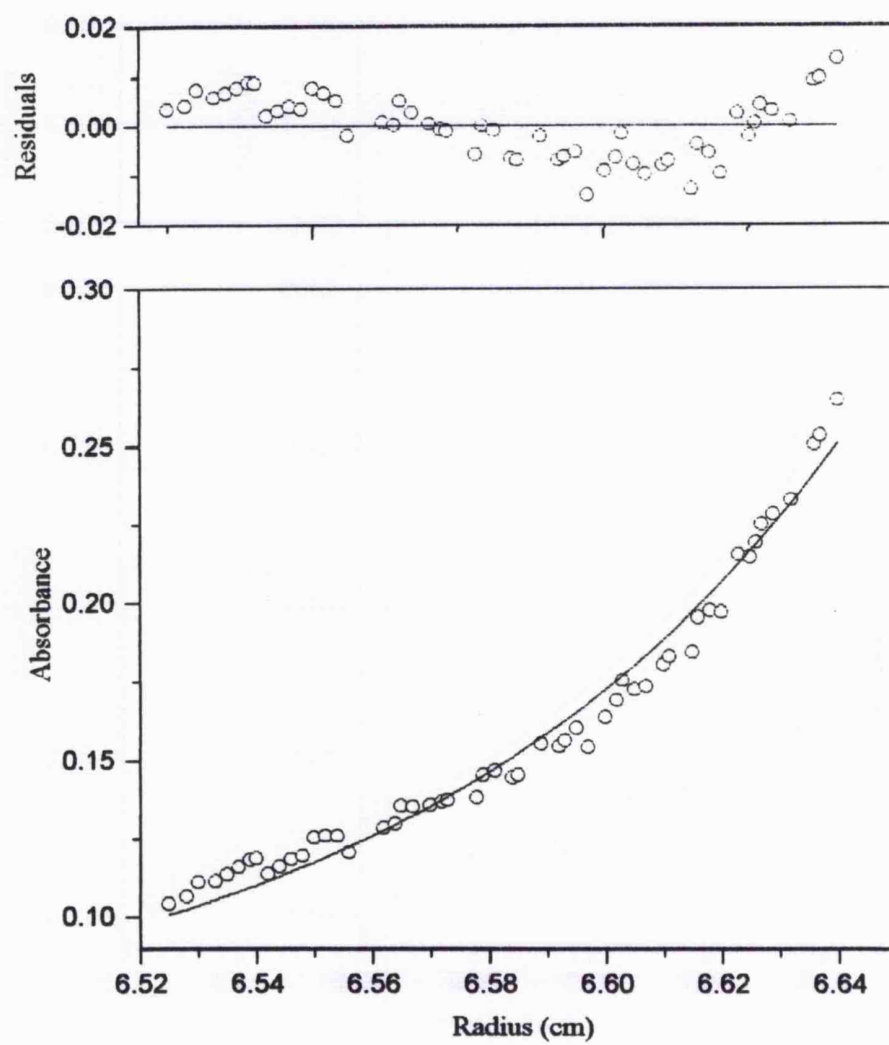
Figure 5.16. Sedimentation equilibrium analysis of fraction 2 in the presence of 40mM NaCl. The calculated mass for this distribution was 664kDa. The systematic distribution of residuals indicate a poor fit with that expected for a single ideal species (section 5.2.2). Equilibrium experiments were carried out at a rotor speed of 5000 rpm and a temperature of 5°C.
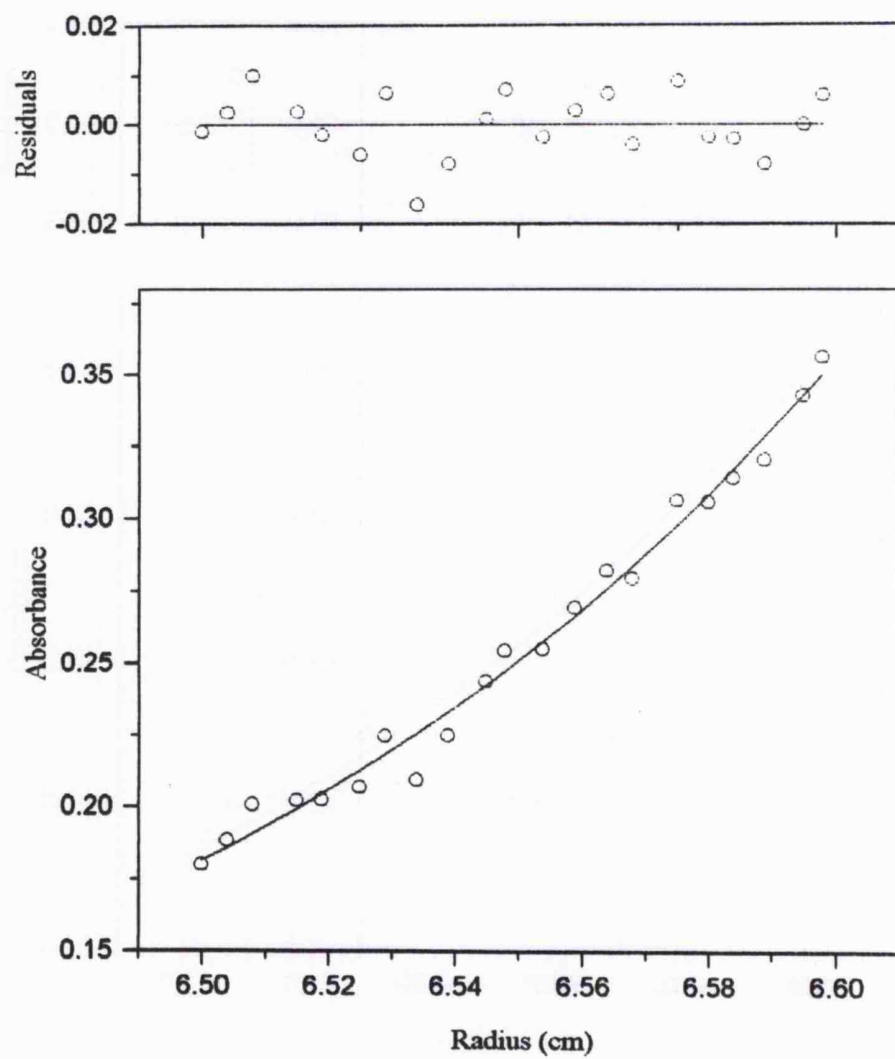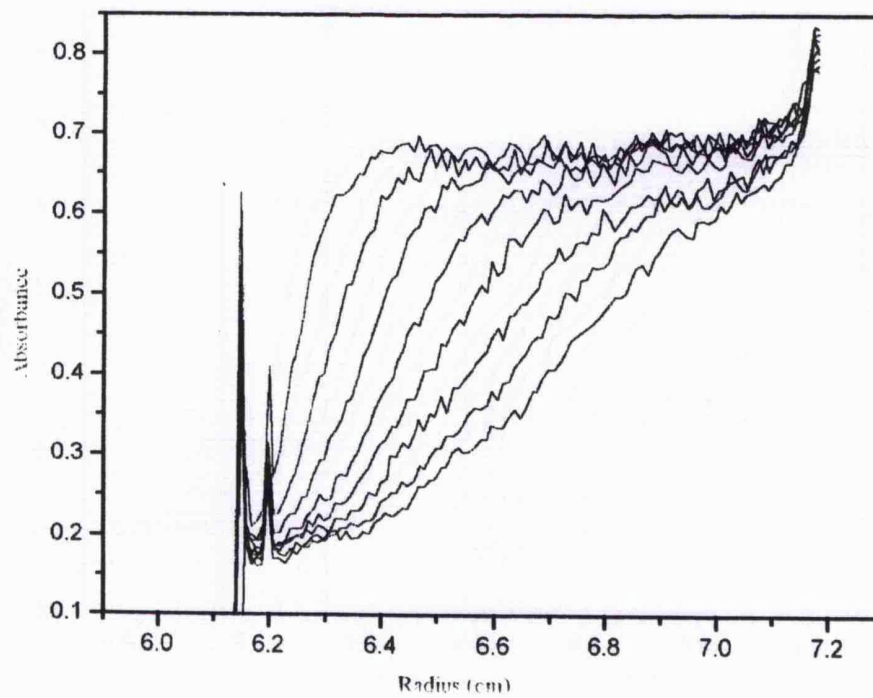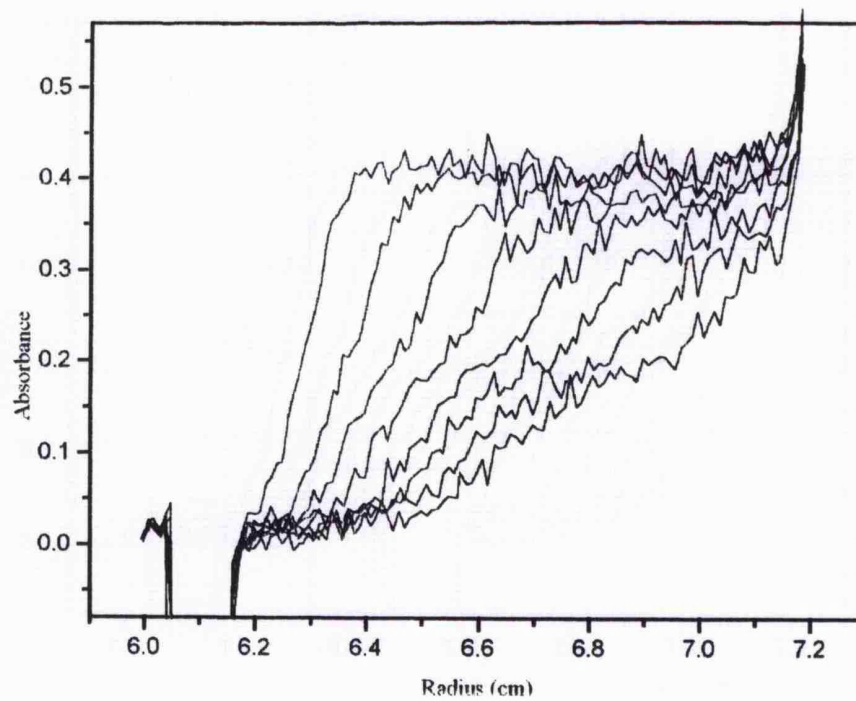
Figure 5.17. Sedimentation equilibrium analysis of fraction 2 in the presence of 600mM NaCl. The calculated mass for this distribution was 406kDa. The randomly-distributed residuals indicate a reasonable fit with that expected for a single ideal species (section 5.2.2). Equilibrium experiments were carried out at a rotor speed of 5000 rpm and a temperature of 5°C.

Figure 5.18. Sedimentation velocity traces for fraction 2 in the presence of 40mM NaCl (top) and 600mM (below) NaCl. At 40mM NaCl, the predominant sedimenting boundary has an $s_{20,w}$ of (16.4 ± 0.5) S, whereas the slower sedimenting component was calculated to be (6.8 ± 0.3) S. Under conditions of 600mM NaCl, a single boundary was apparent with an $s_{20,w}$ of (14.0 ± 0.3) S. Traces were recorded at 30 minute intervals at a rotor speed of 25,000 rpm and a temperature of 5°C.

5.9. Sedimentation analysis and bead modelling of fraction 3

The mean mass of fraction 3 was estimated as **(701 ± 20) kDa** in the presence of **40mM NaCl** (table 5.2). Analysis of a representative equilibrium trace indicated that a plot of the residuals was random with low margins of error and indicative of a single species with no detectable aggregation (figure 5.19). Velocity traces (figure 5.21) indicated the presence of one variable component which, for two independent preparations, had a calculated sedimentation coefficient of (13.1 ± 0.5) S and (16.7 ± 0.4) S (table 5.3).

In the presence of **600mm NaCl**, the weight-average molecular mass of fraction 3 was reduced to **(478 ± 25) kDa** (table 5.2). Sedimentation equilibrium data gave poor fits and indicated a range of masses deviating from that predicted for a single non-associating species. This was particularly evident in a plot of the residuals which exhibited a systematic non-random distribution (figure 5.20). In comparison, the velocity trace in the presence of 600mM NaCl was difficult to interpret (due to a low signal-to-noise ratio) and may have included a number of sedimenting components (figure 5.21). The main sedimenting boundary decreased to a value of approximately **(10.8 ± 0.4) S** (table 5.3). Taken together, these results could be interpreted in two ways. Firstly, it was possible that in the presence of 600mM NaCl fraction 3 underwent dissociation since both the mass and sedimentation coefficient were reduced. Furthermore, this level of dissociation may be variable since an analysis of the residual plot for equilibrium showed a systematic distribution (figure 5.20). Secondly, fraction 3 could exhibit reversible self-association in which the state of equilibrium is influenced by the concentration of NaCl.

Using electron microscopy, the predominant structure for fraction 3 in the presence of 40mM NaCl was identified as a single globular head which could be roughly approximated to a sphere (figure 3.14). This structure was simulated using a simple single-bead model (figure 5.22). Two possible models were then tested in which hydrodynamic data derived from the <u>same</u> dynein preparation were utilised to minimise error introduced by the variable sedimentation coefficient (table 5.3). Models were therefore constructed on the basis of a mass of 720kDa and a sedimentation coefficient of (16.7 ± 0.4) S. The first model (designated monomer) was constrained to a mean diameter 9.4nm, in accordance with electron microscopy data (table 3.3), and a mass of 360kDa which was exactly half
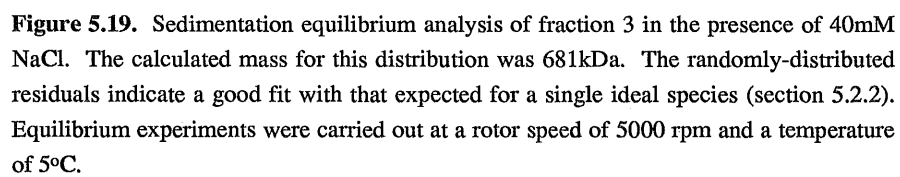
the value determined by sedimentation equilibrium analysis (table 5.2). This latter value was selected since a single bead model of 720kDa required a diameter of 11.86nm which is outside the standard deviation of the mean dimension value (9.7 ± 1.5nm). Furthermore, this molecular mass was also rejected on the basis that a single spherical molecule would give a correspondingly large sedimentation coefficient of approximately 29S (see equations 5.9 & 5.2) which was very much greater than the experimental value of 16.7S (table 5.3). The 'monomer' model gave a predicted range of sedimentation coefficients with respect to hydration as shown in figure 5.23 (top). The experimentally determined value (16.7S) was shown to intercept the modelled data at a point between 0.2 and 0.3 g water/g protein which corresponds to an acceptable level of hydration (section 5.3.1). This model therefore seems to agree with sedimentation velocity data but is based upon the assumption that the mass is exactly half that of the experimentally derived value.

A second model (designated dimer) was then tested which constrained the electron microscopy dimension as before (9.4nm diameter), but this time constrained the mass to the experimental value of 720kDa by using two (360kDa) beads to represent a dimer (figure 5.22). This model produced much greater values for the sedimentation coefficient which were outside the range of the experimental data (figure 5.23). Indeed, in order for the modelled sedimentation coefficient to match that of 16.7S, an unusually high level of hydration (greater than 0.5 g water/g protein) was predicted (section 5.3.1). Both models were therefore inconsistent with at least one experimental parameter; the mass in the case of the monomer model, and the sedimentation coefficient with respect to the dimer model. A third interpretation was therefore considered in which the behaviour of the molecule was presumed to be affected by the experimental conditions. Equilibrium conditions may favour the dimeric conformation (corresponding to a mass of 720kDa), whereas velocity experiments promote the monomer state (with a corresponding sedimentation coeffcient of 16.7S). Evidence in support of this interpretation, however, has yet to be produced. Nevertheless, it is possible that the distinct procedures of equilibrium and velocity affect interactions between dynein molecules. Equilibrium experiments, for example, were run for considerably longer amounts of time (at least 11 hours) than the 4-5 hour velocity experiments. In addition, the hydrostatic pressure exerted on the protein solution was

194

significantly greater for velocity experiments than for equilibrium runs, because of the higher velocities used, and may affect the equilibrium state of an associating system (Harrington & Kegeles, 1973).

In conclusion, the structure of fraction 3 predominating in the presence of 40mM NaCl can be analysed with the use of bead models. A unique model, however, is difficult to produce.
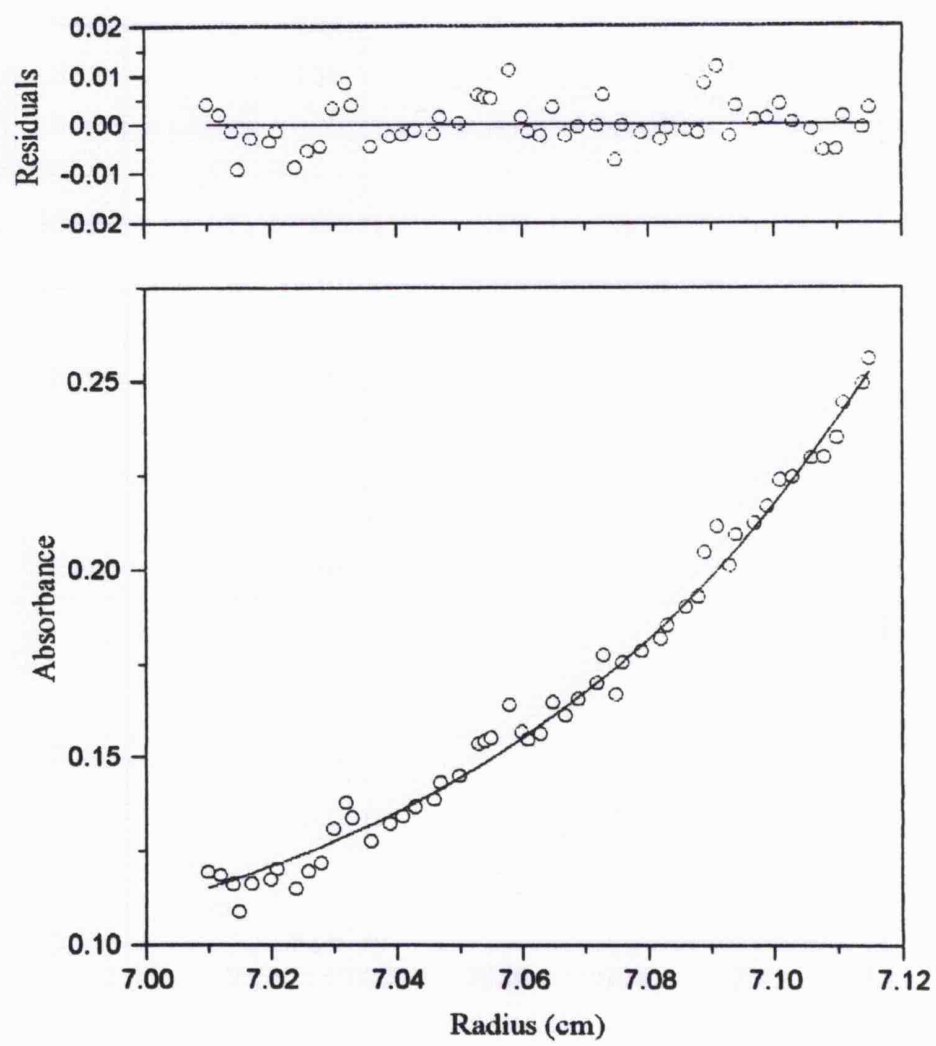
Figure 5.19. Sedimentation equilibrium analysis of fraction 3 in the presence of 40mM NaCl. The calculated mass for this distribution was 681kDa. The randomly-distributed residuals indicate a good fit with that expected for a single ideal species (section 5.2.2). Equilibrium experiments were carried out at a rotor speed of 5000 rpm and a temperature of 5°C.
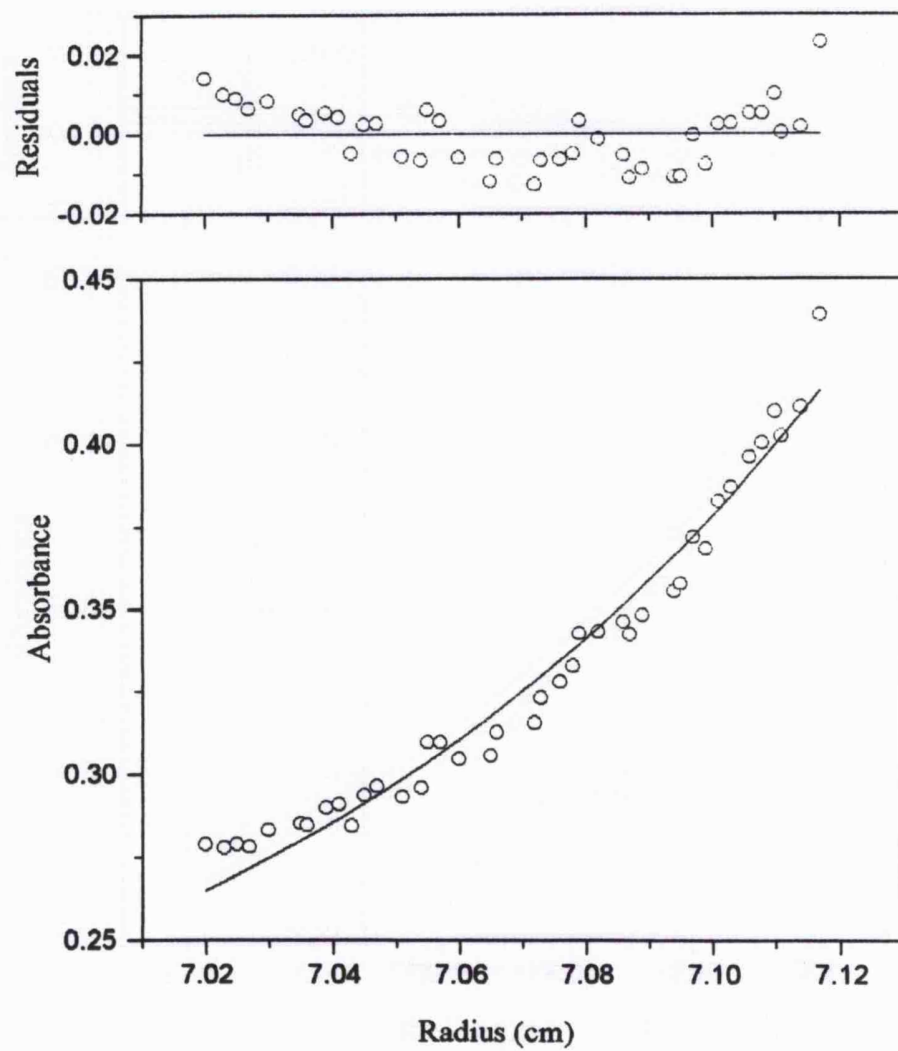
Figure 5.20. Sedimentation equilibrium analysis of fraction 3 in the presence of 600mM NaCl. The calculated mass for this distribution was 453kDa. The systematic distribution of residuals indicate a poor fit with that expected for a single ideal species (section 5.2.2). Equilibrium experiments were carried out at a rotor speed of 5000 rpm and a temperature of 5°C.
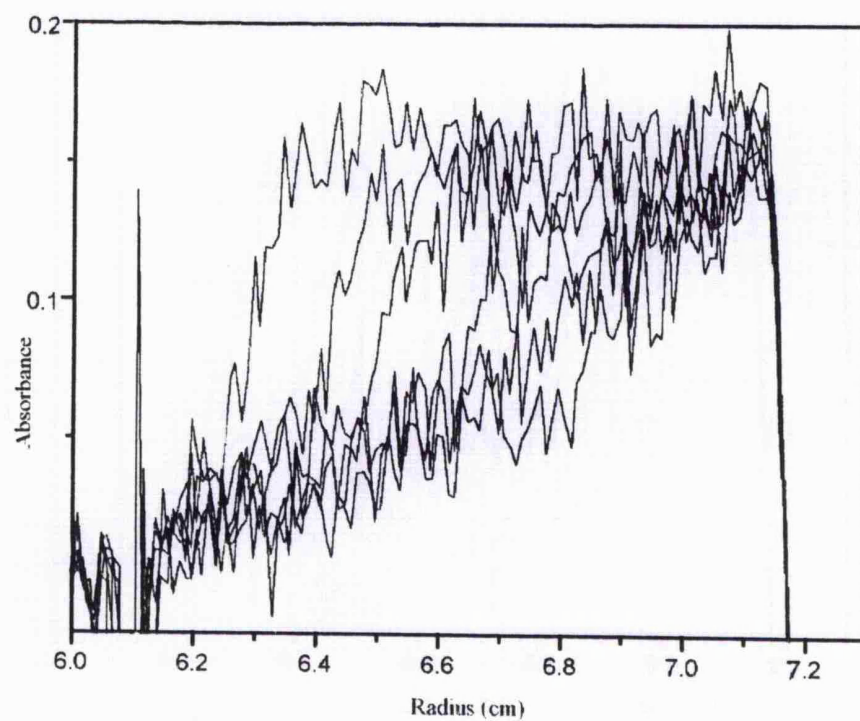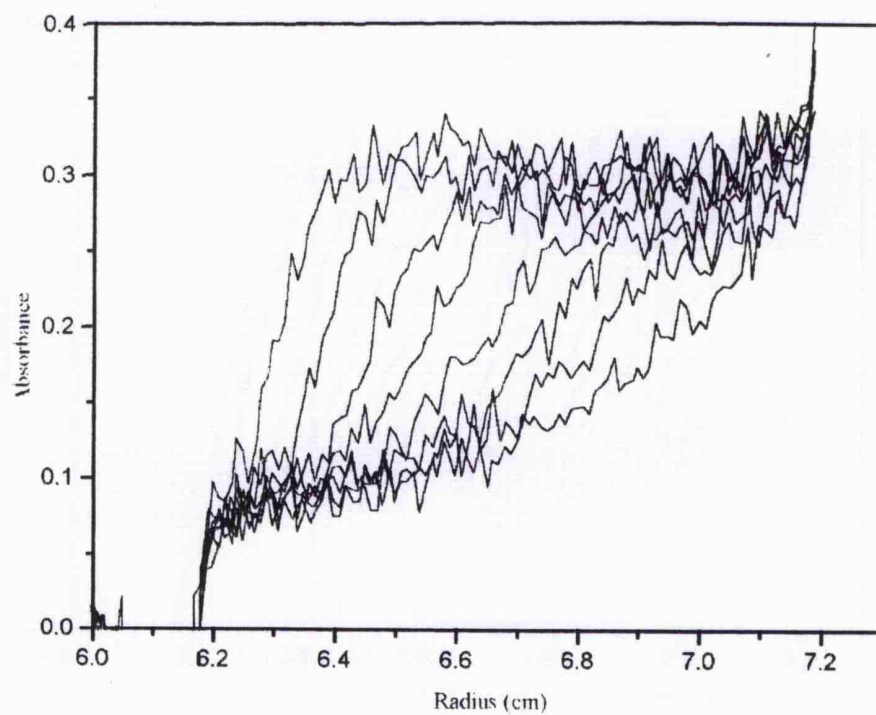
Figure 5.21. Sedimentation velocity traces for fraction 3 in the presence of 40mM NaCl (top) and 600mM (below) NaCl. At 40mM NaCl, the single sedimenting boundary has an $s_{20,w}$ of (16.7 ± 0.4) S, whereas under conditions of 600mM NaCl this value is reduced to (10.8 ± 0.4) S. Traces were recorded at 30 minute intervals at a rotor speed of 25,000 rpm and a temperature of 5°C
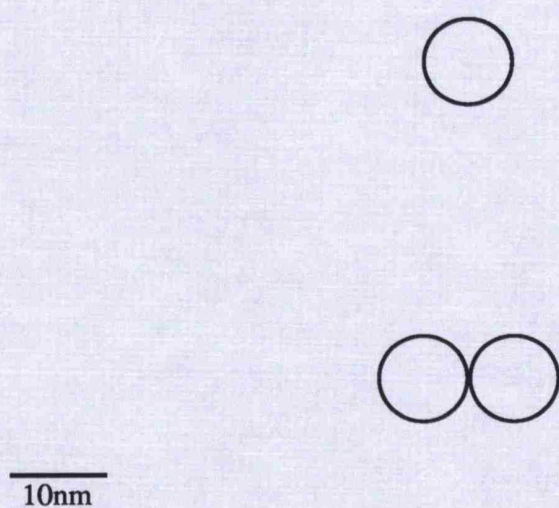
Figure 5.22. Bead models used in the structural investigation of fraction 3 assuming a monomer (top) and dimer (below) model.
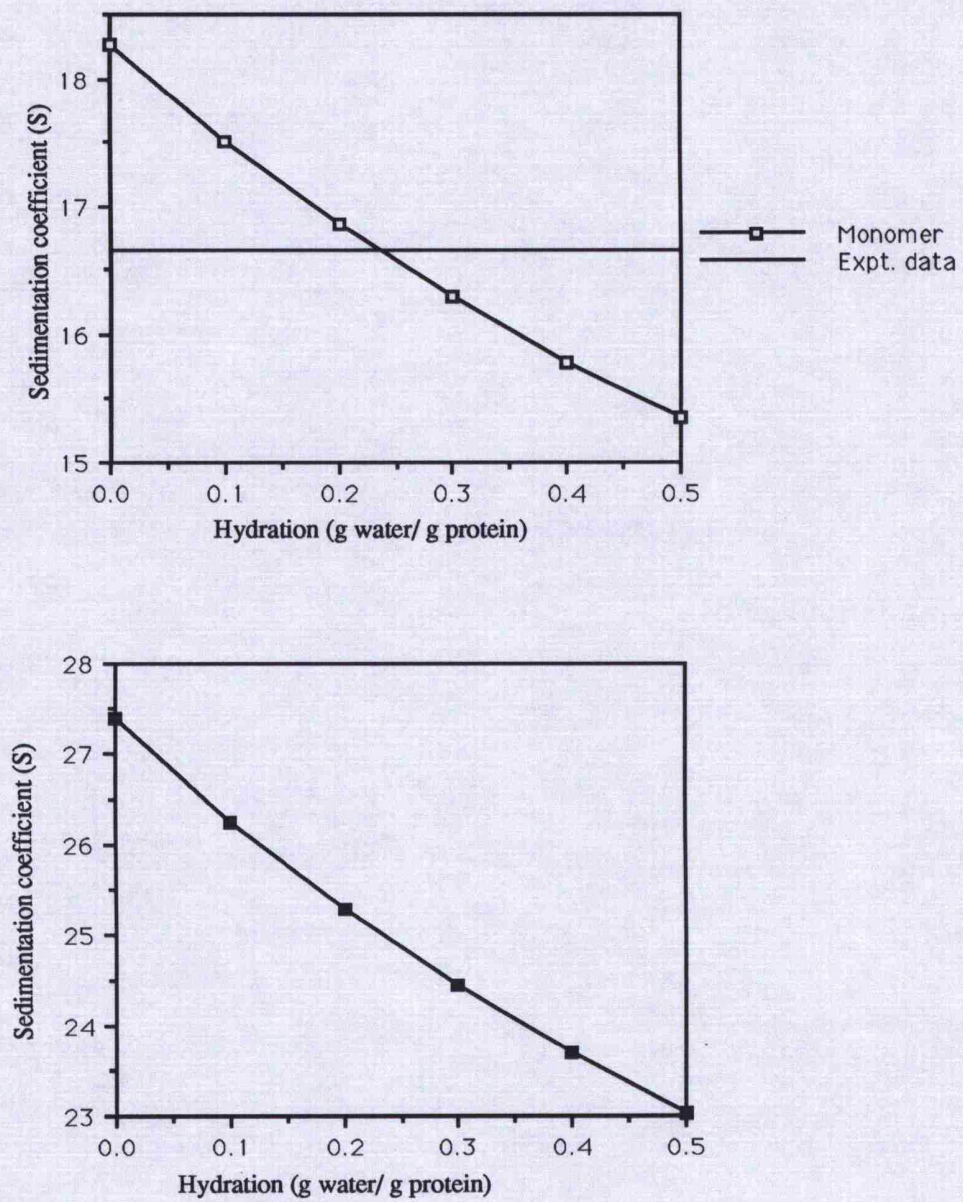
Figure 5.23. Graphical representation of the sedimentation coefficient as a function of hydration for fraction 3 assuming a monomer (top) and dimer (below) model.

5.10. Sedimentation analysis and bead modelling of fraction 4

Sedimentation equilibrium analysis revealed that in the presence of **40mM NaCl** the mass of fraction 4 was estimated as **(527 ± 2) kDa** (table 5.2). These data produced random residual plots with acceptable margins of error (figure 5.24). In contrast, velocity experiments (figure 5.26) showed greater variation and for two independent dynein preparations the sedimentation coefficient was determined as (13.2 ± 0.6) S and (16.0 ± 0.2) S (table 5.3). The variation in sedimentation coefficient was thought to reflect changes in the overall conformation of molecular structure and was investigated by hydrodynamic bead modelling (see below).

In the presence of **600mM NaCl**, both the mass and sedimentation coefficient decreased to **(386 ± 65) kDa** and **(10.4 ± 0.4) S** respectively. As with other fractions, this decrease was thought to indicate either dissociation of the components predominating in the presence of 40mM NaCl, or a change in the equilibrium state of a reversibly-associating system. In the case of dissociation, the particles produced were required to be of sufficiently similar mass and size that they behaved as a single species since at equilibrium a plot of the residuals was random with reasonable margins of error (figure 5.25). The presence of a single sedimenting boundary in velocity traces, however, was difficult to conclude due to the high signal-to-noise ratio (figure 5.26). Nevertheless, the equilibrium data at least, could also be interpreted as a reversible self-associating system as described for fractions 1, 2, and 3.
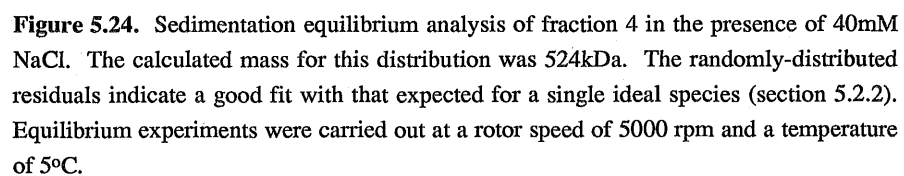
The effect of molecular conformation on the sedimentation coefficient was investigated using bead models based upon both electron microscopy and hydrodynamic data in the presence of 40mM NaCl (figure 3.15). The bead model utilised in the molecular interpretation of fraction 4 was comparable to that of 22S dynein with the obvious exception of size (figure 5.27). The bead size of each head was assigned a diameter of 6.5nm, and the overall length of the molecule estimated as 31nm, in agreement with the mean value determined by electron microscopy analysis (table 3.3). The stems, however, were much more difficult to measure with any degree of accuracy and it seemed reasonable to assume that the relative sizes of heads and tails could be approximated to the 22S model (section 5.6). Consequently, the beads used to construct the tail were assigned

a diameter of 2nm and 3nm for the small and large stalks respectively (figure 5.27). In addition, the mass of the model was constrained to 524kDa, and the experimentally derived sedimentation coefficient used in the analysis, (13.2 ± 0.6) S, was consistent with the same dynein preparation (tables 5.2 & 5.3). In this way, variation of the sedimentation coefficient between dynein preparations was minimised. Three models were investigated which differed with respect to the angle between the head domains (figure 5.27). Figure 5.28 shows a graphical representation of the predicted sedimentation coefficients for the three models plotted as a function of hydration. The models tested show that an angle of 30 degrees between the stems (on which the head domains were attached) would require a hydration of 0.4 g water/g protein slightly above the average for most proteins (section 5.3.1). In contrast, an angle of 45 degrees requires a slightly lower hydration level of 0.14 g water/g protein. Consequently, an intermediate and more acceptable value for hydration would be provided by a model in which the angle separating the stems is between 30 and 45 degrees. In conclusion, an optimal model can be produced for the structure of fraction 4 in the presence of 40mM NaCl which is consistent with all the available experimental data.

5.11. A comparison of the fractions

The four fractions of 14S dynein have hydrodynamic properties which can be compared in a number of respects. Firstly, the mass and sedimentation coefficient associated with the fractions were shown to reduce in the presence of 600mM NaCl when compared with 40mM NaCl conditions (tables 5.2 & 5.3). Secondly, this reduction was thought to be the result of either dissociation (in which particles of equivalent hydrodynamic properties were formed), or as a result of a NaCl-induced change in the state of equilibrium of a reversibly-associating system. Thirdly, fraction 2 was distinguishable from the other fractions with respect to its inherent complexity (section 5.8). In particular, the possible existence of aggregates and/or multiple dynein components or species make further interpretation of this fraction difficult. Finally, fractions 1, 4, and to some extent fraction 3, were analysed to produce plausible low resolution structural models which incorporate data from both hydrodynamic and electron microscopy analysis (figures 5.14, 5.22, 5.27).
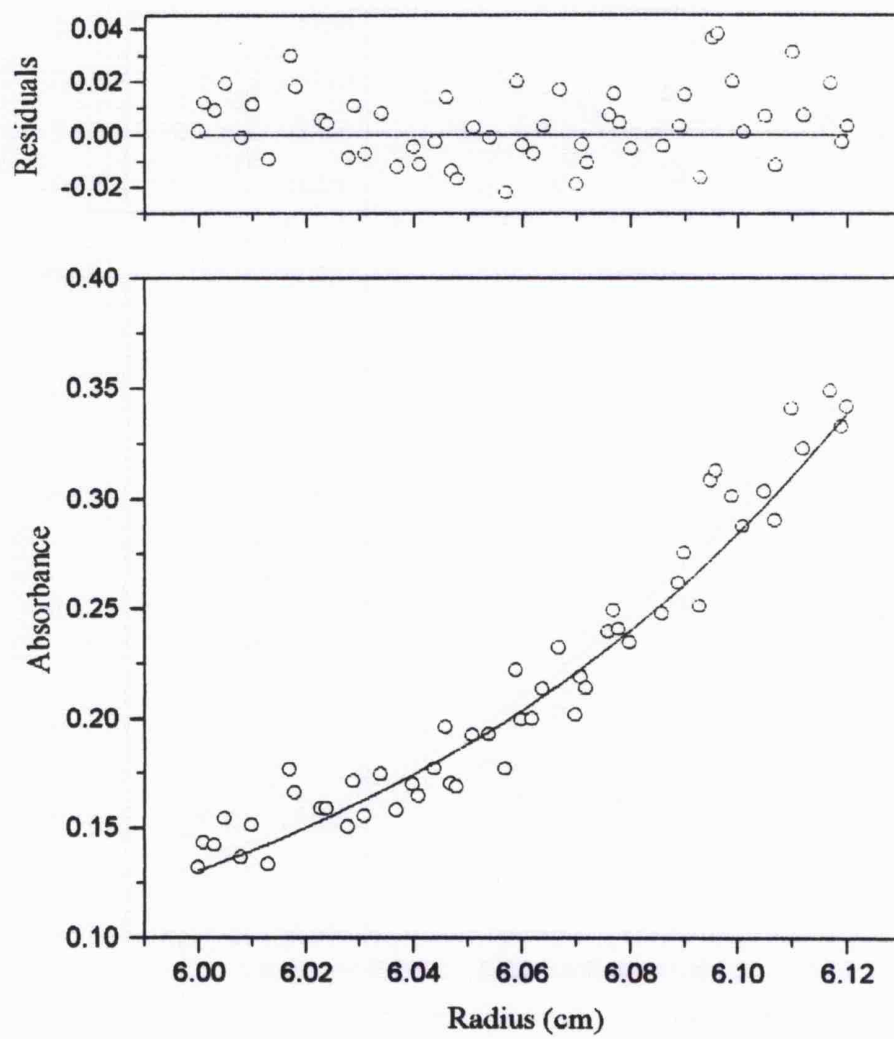
Figure 5.24. Sedimentation equilibrium analysis of fraction 4 in the presence of 40mM NaCl. The calculated mass for this distribution was 524kDa. The randomly-distributed residuals indicate a good fit with that expected for a single ideal species (section 5.2.2). Equilibrium experiments were carried out at a rotor speed of 5000 rpm and a temperature of 5°C.
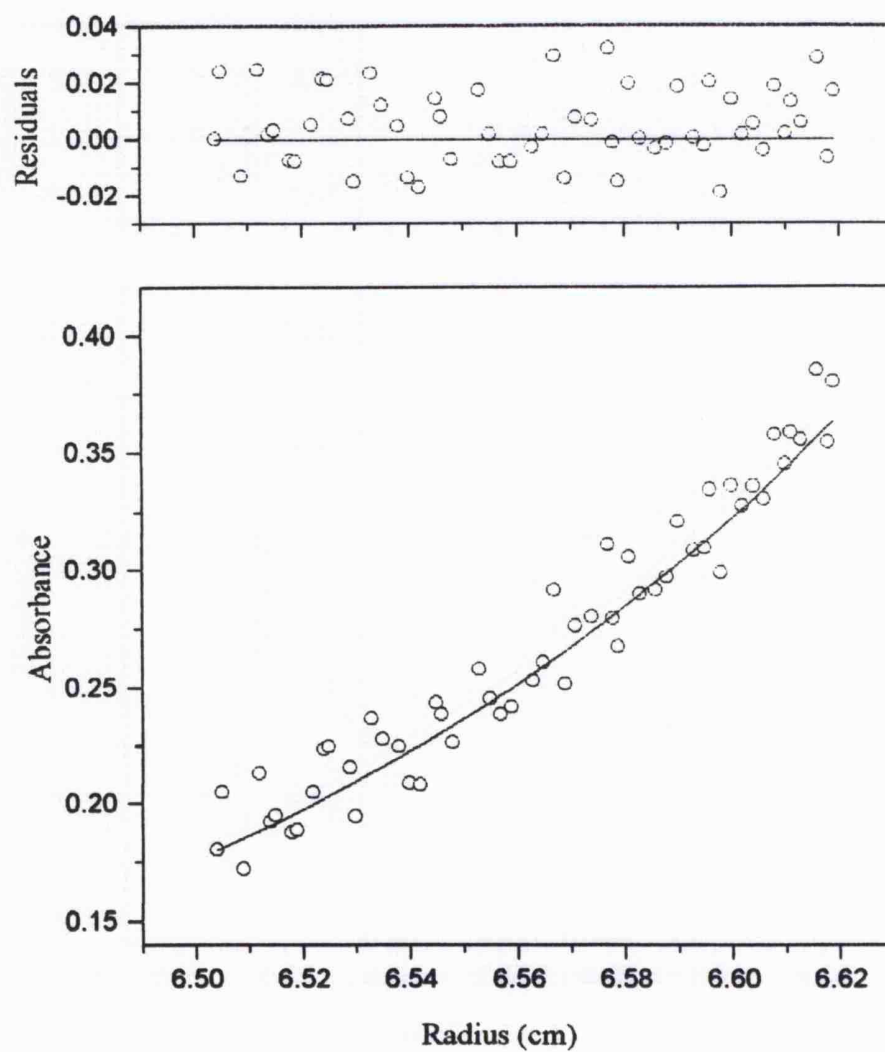
Figure 5.25. Sedimentation equilibrium analysis of fraction 4 in the presence of 600mM NaCl. The calculated mass for this distribution was 340kDa. The randomly-distributed residuals indicate a good fit with that expected for a single ideal species (section 5.2.2). Equilibrium experiments were carried out at a rotor speed of 5000 rpm and a temperature of 5°C.
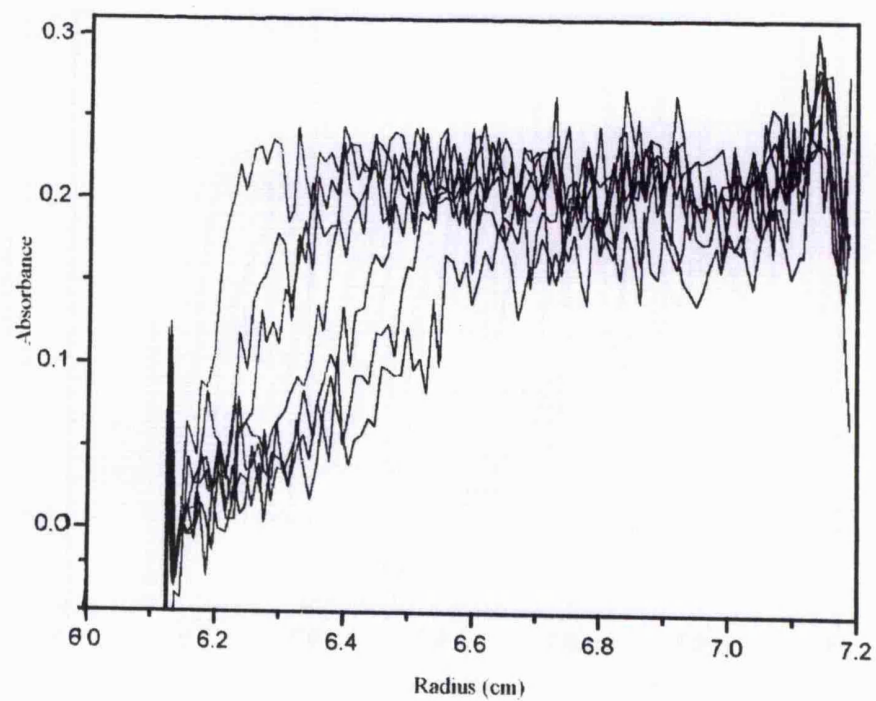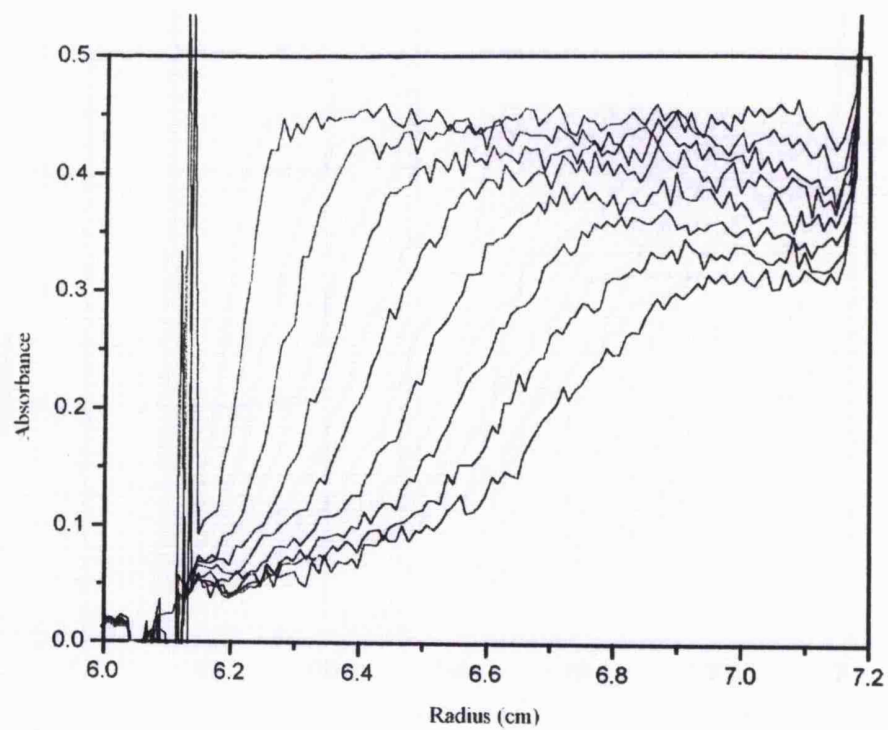
Figure 5.26. Sedimentation velocity traces for fraction 4 at 40mM NaCl (top) and 600mM (below) NaCl. At 40mM NaCl the single sedimenting boundary has an $s_{20,w}$ of (16.0 ± 0.2) S, whereas under conditions of 600mM NaCl this value is reduced to (10.4 ± 0.2) S. Traces were recorded at 30 minute intervals at a rotor speed of 25,000 rpm and a temperature of 5°C.
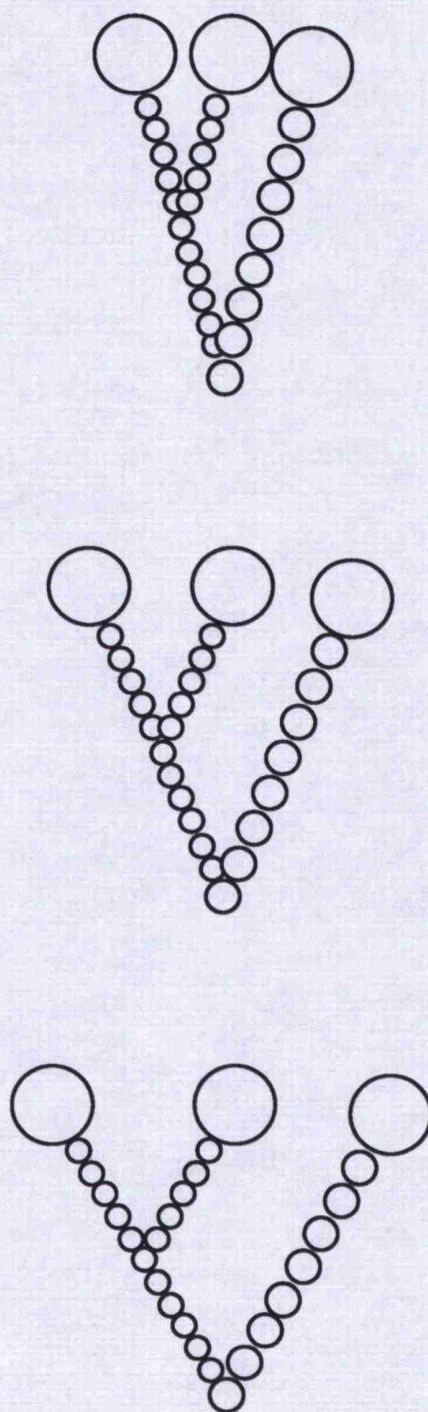
10nm

Figure 5.27. Bead models used in the structural investigation of fraction 4. The three models differ with respect to the angle between the globular head domains. Angles of 30° (top), 45° (middle) and 60° (below) were investigated.
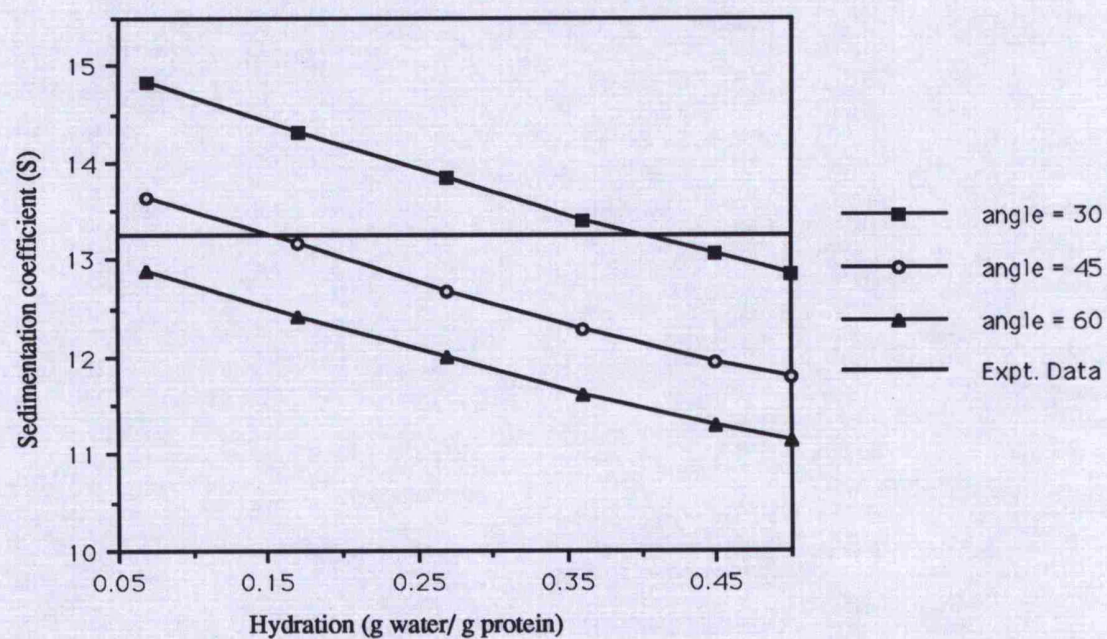
Figure 5.28. Graphical representation of the sedimentation coefficient as a function of hydration for models of fraction 4.

Fraction	[NaCl] (mM)	1	2	3	4	5	6	Mean	SE*
1	40	723	591	673	722	559	-	654	75
	600	499	-	-	-	476	377	451	65
2	40	616	938	966	814	664	-	-	-
	600	-	486	-	-	564	406	485	56
3	40	-	681	-	-	720	-	701	20
	600	-	453	-	-	503	-	478	25
4	40	-	524	-	529	-	-	527	2
	600	-	340	-	-	432	-	386	65

Table 5.2. Experimental data for sedimentation equilibrium studies of the four fractions of 14S dynein. The mass for each fraction is expressed in kDa. Numbers indicate different experiments.

---

* Values for the standard error have not been given where genuine variation exists between dynein preparations.

Fraction	[NaCl] (mM)	1	2	3	4	Mean	SE*
1	40	20.1 ± 0.1	20.5 ± 0.2	19.6 ± 0.1	-	20.1	0.3
	600	13.9 ± 0.1	13.2 ± 0.1	-	-	13.6	0.3
2	40	17.0 ± 0.4 & 9.9 ± 0.9	16.4 ± 0.5 & 6.8 ± 0.3	16.5 ± 0.9	-	16.6 -	0.2 -
	600	12.1 ± 0.3	14.0 ± 0.3	-	13.5 ± 0.1	13.2	0.6
3	40	13.1 ± 0.5	16.7 ± 0.4	-	-	-	-
	600	-	-	-	10.8 ± 0.4	-	-
4	40	13.2 ± 0.6	16.0 ± 0.2	15.5 ± 1.3	13.2 ± 0.3	-	-
	600	-	-	-	10.4 ± 0.4	-	-

Table 5.3. Experimental data for sedimentation velocity studies of the four fractions of 14S dynein. The sedimentation coefficient is expressed in Svedberg (S) units. Numbers indicate different experiments.

* Values for the standard error have not been given where genuine variation exists between dynein preparations.

Chapter 6

Discussion

The aim of this thesis has been to investigate 14S dynein isolated from *Tetrahymena thermophila*. The conclusions to be drawn from each chapter have been discussed in the relevant section. This chapter presents a general summary of the overall conclusions and aims to address overlapping areas which have not been presented elsewhere.

6.1. General structure

Four unique structures (designated 1-4) have been identified following the fractionation of 14S dynein using anion-exchange FPLC. Four unique fractions were apparent by electron microscopy analysis and are summarised in figure 3.16 (see table 3.3 for molecular dimensions). Fraction 1 comprises two globular heads interconnected via two stems (figure 3.12); fraction 2 consists of at least two distinguishable globular structures (figure 3.13); fraction 3 is a single globular head (figure 3.14); and fraction 4 comprises three globular head domains interconnected via three stems to a base (figure 3.15).

The fractions were further characterised using hydrodynamic techniques in which the mass and sedimentation coefficients were determined (tables 5.1 & 5.2). These parameters were then utilised, in conjunction with electron microscopy data, in the construction of bead models to represent the fractions. Models which incorporated all the available data, were produced for fractions 1 (section 5.7), 4 (section 5.10), and to some extent fraction 3 (section 5.9). In contrast, the complexity of fraction 2 (in both the presence of aggregation states and/or heterogeneity) prevented the satisfactory analysis of this fraction using the bead modelling approach (section 5.8). A summary of the overall structure of the fractions, determined using both electron microscopy and hydrodynamic techniques, is presented in figure 6.1.

The four structures presented here for 14S dynein are contrary to those described previously by Marchese-Ragona *et al.*, (1988), in which 14S was described as an inseparable mixture of two populations of particles (figure 3.1). The 14S fractions described here, however, can be compared with structures proposed for the *in situ* inner arm dyneins of *Tetrahymena, Chlamydomonas,* and sea urchin sperm, where two morphologically-distinct forms of inner arm, termed triads (comprising three globular heads) and dyads (comprising two globular heads), have been described (Goodenough &

Heuser, 1985). It is possible that fractions 1, 2, and 3 may be involved in the formation of the dyad inner arm subspecies, whereas fraction 4 may be equivalent to the triad (section 3.16.2).
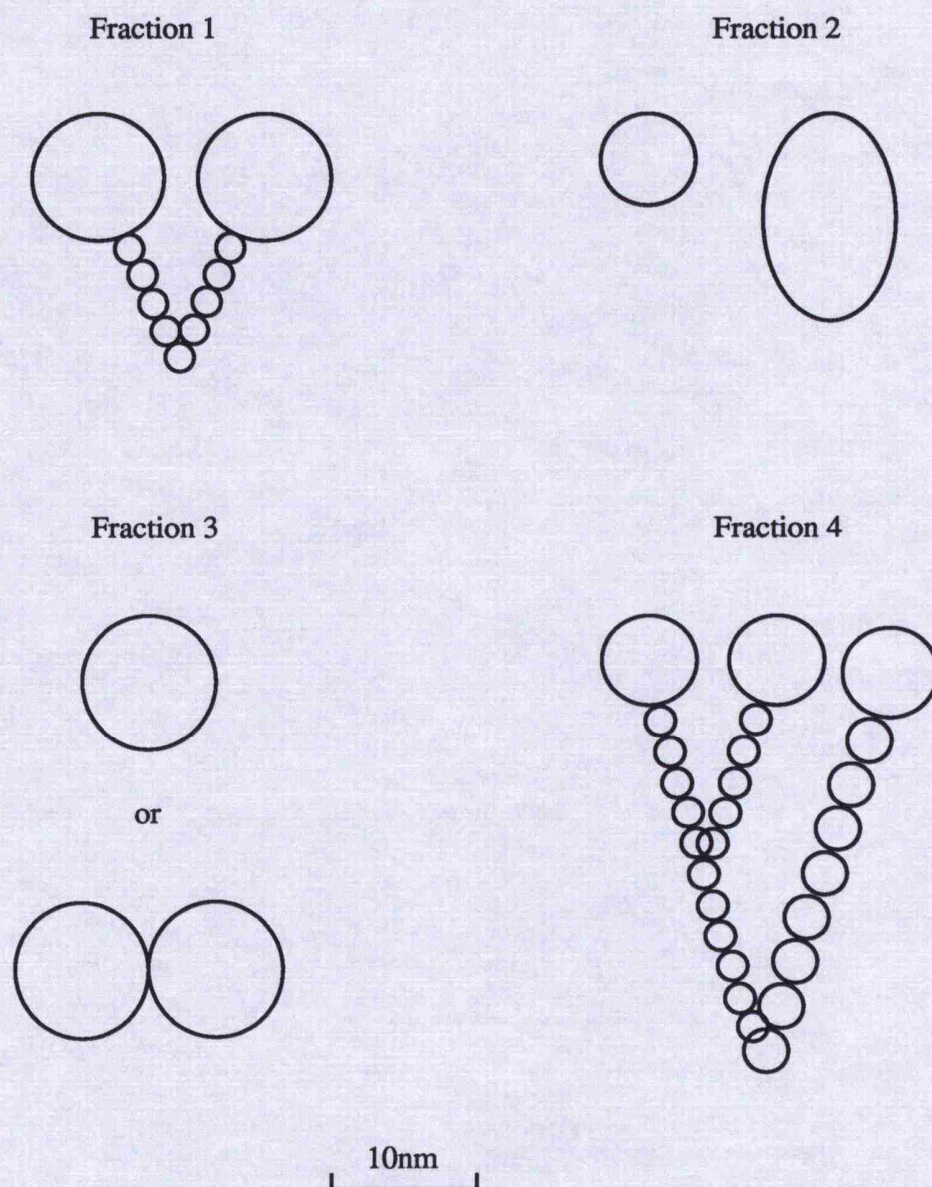
Figure 6.1. Schematic diagram of the structures proposed for the four fractions of 14S dynein. The models were constructed on the basis of both electron microscopy and (with the exclusion of fraction 2) hydrodynamic data. The approximate angle of the stems in fractions 1 and 4 are 50° and 38° respectively in accordance with the most plausible bead models produced (sections 5.7 & 5.10).

6.2. Polypeptide composition

All four 14S fractions comprise at least one heavy chain component. Fraction 1 has two heavy chains, whereas fractions 2, 3, and 4, each possess a single heavy chain as shown by 3-5% SDS-PAGE (figure 3.6). At least **four** heavy chains are immunologically-distinct; two associated with fraction 1, one associated with fraction 2, and one associated with a mixture of fractions 3 and 4 (figure 3.9){section 3.10.1}. The presence of four immunologically-distinct heavy chains is in agreement with the work recently presented by Muto *et al.* (1994) in which four heavy chains were described and identified as unique on the basis of the cleavage fragments produced following vanadate-dependent photolysis. The presence of at least four heavy chains, however, is contrary to the **two** heavy chains previously described for unfractionated 14S dynein (Marchese-Ragona *et al.*, 1988).

The approximate mass of the heavy chains was determined using the technique of vanadate-dependent photolysis (section 4.19). The two heavy chains of fraction 1 gave a combined mass of 743-770kDa, whereas the single detectable heavy chains of fractions 2, 3, and 4, were estimated as 379-384kDa, 367-379kDa, and 358-361kDa respectively (table 4.12). These values are consistent with the general observation that 14S dynein heavy chains are of greater electrophoretic mobility than the three heavy chains of 22S dynein (α, β, and γ) which have estimated masses of 417, 420, and 403kDa respectively (Marchese-Ragona *et al.*, 1989). These data are contrary, however, to the predicted heavy chain estimates for **two** previously described 14S heavy chains (determined using vanadate-dependent photolysis) in which the pairing of cleavage peptides produced values of 445-457kDa for the one heavy chain and 375-387kDa for the other (Marchese-Ragona *et al.*, 1991).

In addition to heavy chain composition, the four fractions each have a unique complement of intermediate and light chains (summarised in table 3.2) which can be compared with the previous report of one intermediate chain (110kDa) and three light chains (30-55kDa) for unfractionated 14S dynein (Marchese-Ragona *et al.*, 1988). The single intermediate chain described previously is likely to be equivalent to a prominent peptide of approximately 103kDa identified in fractions 3 and 4 (figure 3.7). Furthermore, this peptide can be compared with a 110kDa peptide identified as specific to inner dynein arm species in

212

Chlamydomonas (Huang *et al.*, 1979; Goodenough *et al.*, 1987). In addition, a light chain recently identified as actin (43.5kDa) in three 14S fractions separated by Mono Q HPLC (Muto *et al.*, 1994) could also correspond to a 43.5kDa band identified in fraction 2, or alternatively, a 44.5kDa band identified in fractions 1, 3, and, to a much lesser extent, fraction 4 (table 3.2). As with the 110kDa intermediate chain, actin has been reported as a polypeptide unique to inner dynein arm subspecies in *Chlamydomonas* (Huang *et al.*, 1979; Piperno & Luck, 1979b; Goodenough *et al.*, 1987; Piperno, 1988).

6.3. A comparison of the four fractions of 14S dynein

The heavy chains associated with the four fractions of 14S dynein were shown to have both structural similarities and differences using the technique of vanadate-dependent photolysis. All fractions were shown to exhibit homology with each other, and other dynein species, in that each possessed a single V1 site located near the midpoint of the heavy chain (figure 4.11). By analogy with other dyneins, this site is thought to represent the hydrolytic ATP-binding site (P1), since the V1 site has been mapped to the P1 consensus sequence following amino acid sequencing of the three heavy chains of *Chlamydomonas* (Mitchell & Brown, 1994; Wilkerson *et al.*, 1994), and the β heavy chain of sea urchin sperm (Ogawa, 1991; Gibbons *et al.*, 1991). In contrast, the four fractions differed from one another with respect to the differential requirement for nucleotide in the photolysis reaction, fractions 1 and 2 being readily distinguishable from fractions 3 and 4 (sections 4.17 & 4.18). Structural variation was also indicated by the number and location of V2 cleavage sites. In particular, two sites of V2 cleavage were identified for fraction 3, whereas fractions 1, 2, and 4 exhibited cleavage at a single V2 site (figure 4.11).

All four fractions exhibited ATPase activity (table 4.4). The greatest activity in the presence of 40mM NaCl, was associated with fraction 2 and, in order of decreasing activity, followed the trend: **fraction 2** (0.30μmol ADP/min/mg dynein) >> **fraction 3** (0.15μmol ADP/min/mg dynein) > **fraction 1** (0.12μmol ADP/min/mg dynein) > **fraction 4** (0.10μmol ADP/min/mg dynein). It is unknown whether the specific activities of the four fractions reflect their relative activites *in situ* and the possibility that some fractions are activated or inactivated by the extraction and separation procedure cannot be discarded.

Nevertheless, differences between the fractions are demonstrated by their response to the substitution of Mn^{2+} for Mg^{2+} in the ATPase assay procedure (section 4.15), to the presence of microtubules (section 4.16), and to an increase in ionic strength (section 4.14). An increase in ionic strength (from 40mM NaCl to 600mM NaCl) affected both the ATPase activity and the structure of the four fractions. In terms of structure, the mass and sedimentation coefficient (derived for the four fractions in the presence of 40mM NaCl) was shown to decrease in the presence of 600mM NaCl (table 6.1). In all cases, the reduction was thought to be attributable either to dissociation (in which particles of equivalent hydrodynamic properties were derived), or as a result of a NaCl-induced change in the state of equilibrium of a reversibly-associating system (sections 5.7-5.10). Under these conditions, the specific ATPase activity of the four fractions was also shown to decrease (section 4.9.1). In particular, no activity was detected for fractions 3 and 4 in the presence of 600mM NaCl (table 6.1).

Fraction	40mM NaCl			600mM NaCl		
	Mass	$s_{20,w}$	ATPase	Mass	$s_{20,w}$	ATPase
1	654	20.1	0.15	451	13.6	0.11
2	616-966	16.6	0.31	485	13.2	0.19
3	701	(a)	0.12	478	(a)	(b)
4	527	(a)	0.11	386	(a)	(b)

Table 6.1. Summary of the change in mass (in kDa), sedimentation coefficient (in Svedbergs), and ATPase activity (in μmol ADP/min/mg dynein) exhibited for the four fractions as a result of increasing the ionic strength from 40mM to 600mM NaCl. Data are not given where (a) genuine variation between dynein preparations exists or (b) levels of activity are undetected.

The physiological significance of these structural and functional changes in the four fractions of 14S dynein is unclear. A comparison with functional studies on unfractionated 14S dynein, however, indicate that low ionic-strength conditions are required for maximal activity. In particular, the translocation of microtubules *in vitro* (by unfractionated 14S

214

dynein) has been shown to require an optimal buffer of low ionic-strength {5mM KCl} (Vale & Toyoshima, 1988) since motility is drastically reduced at higher salt concentrations {100mM NaCl} (Moss *et al.*, 1992a). Similarly, the specific ATPase activity of unfractionated 14S dynein was shown to decrease by 45% on the addition of 0.4M KCl (Gibbons, 1966). Taken together, these results suggest that the functional activity of 14S dynein (and fractions thereof) is inhibited by an increase in ionic strength. Whether this functional inhibition is a direct consequence of the observed changes in structure and/or conformation in all four fractions, however, has yet to be established.

6.4. Further work

The work presented in this thesis has shown that 14S dynein consists of four unique fractions and has implied that some fractions at least, may represent species of inner dynein arm. A progression from this work could therefore involve the localisation of the fractions within the axoneme. This could be achieved using immunogold labelling providing that antibodies specific for the four fractions can be obtained. Transverse- and longitudinal-sections of demembranated cilia could then be examined to determine whether any of the four fractions are localised (a) to the inner arm and (b) differentially along the length of the axoneme as seen for inner arm species in *Chlamydomonas* (Piperno & Ramanis, 1991). This localisation may then give some indication as to the possible function of the four fractions. Function could then be investigated using *in vitro* motility assays in which dynein-induced translocation of microtubules can be monitored. These studies would assist in the functional characterisation of the four fractions and enable a comparison with previous reports of microtubule translocation in the inner arm subspecies of *Chlamydomonas* (Kagami & Kamiya, 1992).

The work presented here suggests that the heterogeneity of 14S dynein is attributable to four distinct fractions. These fractions can be compared to some of the multiple inner arm species previously reported. The significance of multiple dyneins within the axoneme has yet to be established, although this inherent complexity may reflect the diversity of movement exhibited in the motile cilium.

Chapter 7

Bibliography

Adams, G. M. W., Huang, B., Piperno, G. and Luck, D. J. L. (1981). Central-pair microtubular complex of *Chlamydomonas* flagella: polypeptide composition as revealed by analysis of mutants. *J. Cell Biol.* **91**, 69-76.

Alberts, B., Bray, D., Lewis, J., Raff, M., Roberts, K. and Watson, J. D. (1983). Molecular Biology of the Cell. Garland Publications, Inc.

Allen, R. D., Metuzals, J., Tasaki, I., Brady, S. T. and Gilbert, S. P. (1982). Fast axonal transport in squid giant axon. *Science* **218**, 1127-1128.

Amos, L. A. (1987). Kinesin from pig brain studied by electron microscopy. *J. Cell Sci.* **87**, 105-111.

Amos, L. A. and Amos, W.B. (1991). Molecules of the Cytoskeleton. Macmillan Education Ltd.

Attwell, G. J., Bricker, C. S., Schwandt, A., Gorovsky, M. A. and Pennock, D. G. (1992). A temperature-sensitive mutation affecting synthesis of outer arm dyneins in *Tetrahymena thermophila. J. Protozool.* **39**, 261-266.

Avolio, J., Glazzard, A. N., Holwill, M. E. J., and Satir, P. (1986). Structures attached to doublet microtubules of cilia: computer modeling of thin-section and negative-stain stereo images. *Proc. Nat. Acad. Sci. USA,* **83**,4804-4808.

Bagshaw, C. (1993). Muscle Contraction. Second edition. Chapman and Hall.

Barkalow, K., Hamasaki, T. and Satir, P. (1994). Regulation of 22S dynein by a 29-kD light chain. *J. Cell Biol.* **126**, 727-735.

Bell, C. W. and Gibbons, I. R. (1982). Structure of the dynein-1 outer arm in sea urchin sperm flagella. II. Analysis by proteolytic cleavage. *J. Biol. Chem.* **257**, 516-522.

Bernstein, M. and Rosenbaum, J. L. (1994). Kinesin-like proteins in the flagella of *Chlamydomonas. Trends Cell Biol.* **4**, 236-240.

Bloom, G. S. and Endow, S. A. (1994). The discovery of kinesin: an historical perspective. *Protein profile* **1**, 1059-1061.

Bloomfield, V., Dalton, W.O. and van Holde, K. E. (1967). Frictional coefficients of multisubunit structures. I. Theory. *Biopolymers* **5**, 135-148.

Blum, J. J. and Hayes, A. (1974). Effect of *N*-ethylmaleimide and of heat treatment on the binding of dynein to ethylenediaminetetraacetic acid extracted axonemes. *Biochem.* **13**, 4290-4298.

Blum, J. J., Hayes, A., Jamieson, G. A. and Vanaman, T. C. (1980). Calmodulin confers calcium sensitivity on ciliary dynein ATPase. *J. Cell Biol.* **87**, 386-397.

Blum, J. J. and Hines, M. (1979). Biophysics of flagellar motility. *Quat. Rev. Biophys.* **12**, 103-180.

Borisy, G. G., Marcum, J. M., Olmsted, J. B., Murphy, D. B. and Johnson, K. A. (1975). Purification of tubulin and associated high molecular weight proteins from porcine brain and characterisation of microtubule assembly *in vitro*. *Ann. N.Y. Acad. Sci.* **253**, 107-132.

Bowen, T. J. and Rowe, A. J. (1970). An Introduction to Ultracentrifugation. John Wiley and Sons Inc.

Bradford, M. M. (1976). A rapid and sensitive method for the quantitation of microgram quantities of protein utilizing the principle of protein-dye binding. *Anal. Biochem.* **72**, 248-254.

Brady, S. T. (1995). A kinesin medley: biochemical and functional heterogeneity. *Trends Cell Biol.* **5**, 159-164.

Brady, S. T., Lasek, R. J. and Allen, R. D. (1982). Fast axonal transport in extruded axoplasm from squid giant axon. *Science* **218**, 1129-1131.

Chilcote, T. J. and Johnson, K. A. (1990). Phosphorylation of *Tetrahymena* 22S dynein. *J. Biol. Chem.* **28**, 17257-17266.

Cleland, W. W. (1964). Dithiothreitol, a new protective reagent for SH groups. *Biochem.* **3**, 480-482.

Clutter, D., Stimpson, D., Bloomfield, V. and Johnson, K. A. (1983). The structure of *Tetrahymena* dynein in solution. *J. Cell Biol.* **97**, 197 (abstr).

Cremo, C. R., Grammer, J. C. and Yount, R. G. (1989). Direct chemical evidence that serine-180 in the glycine-rich loop of myosin binds ATP. *J. Biol. Chem.* **264**, 6608-6611.

Cremo, C. R., Long, G. T. and Grammer, J. C. (1990). Photocleavage of myosin subfragment 1 by vanadate. *Biochem.* **29**, 7982-7990.

Cremo, C. R., Loo, J. A., Edmonds, C. G. and Hatlelid, K. M. (1992). Vanadate catalyzes photocleavage of adenylate kinase at proline-17 in the phosphate-binding loop. *Biochem.* **31**, 491-497.

Crossley, E. M., Hyman, S. C. and Wells, C. (1991). Axonemal dynein from *Tetrahymena*. *J. Cell Sci.* **S14**, 117-120.

Darnell, J., Lodish, H. and Baltimore, D. (1986). Molecular Cell Biology. Scientific American, Inc.

Dentler, W. L. (1980). Microtubule-membrane interactions in cilia. I. Isolation and characterisation of ciliary membranes from *Tetrahymena pyriformis*. *J. Cell Biol.* **84**, 364-380.

Dentler, W. L., Pratt, M. M. and Stephens, R. E. (1980). Microtubule-membrane interactions in cilia. II. Photochemical crosslinking of bridge structures and the identification of a membrane-associated dynein-like ATPase. *J. Cell Biol.* **84**, 381-403.

Dillman, J. F. and Pfister, K. K. (1994). Differential phosphorylation *in vivo* of cytoplasmic dynein associated with anterogradely moving organelles. *J. Cell Biol.* **127**, 1671-1681.

Emes, C. H. and Rowe, A. J. (1978). Frictional properties and molecular weight of native and synthetic myosin filaments from vertebrate skeletal muscle. *Biochim. Biophys. Acta* **537**, 125-144.

Endow, S. A. and Titus, M. A. (1992). Genetic approaches to molecular motors. *Ann. Rev. Cell Biol.* **8**, 29-66.

Fox, L. A. and Sale, W. S. (1987). Direction of force generated by the inner row of dynein arms on flagellar microtubules. *J. Cell Biol.* **105**, 1781-1787.

Garcia De La Torre, J. (1989). Hydrodynamic properties of macromolecular assemblies. In *Dynamic Properties of Biomolecular Assemblies* (ed. A. J. Rowe and S. E. Harding),pp. 3-31. Royal Society of Chemistry.

Gardner, L. C., O'Toole, E., Perrone, C. A., Giddings, T. and Porter, M. E. (1994). Components of a "dynein regulatory complex" are located at the junction between the radial spokes and the dynein arms in *Chlamydomonas* flagella. *J. Cell Biol.* **127**, 1311-1325.

Gassmann, M., Thommes, P., Weiser, T. and Hubscher, U. (1990). Efficient production of chicken egg yolk antibodies against a conserved mammalian protein. *FASEB J.* **4**, 2528-2532.

Gibbons, B. H. and Gibbons, I. R. (1973). The effect of partial extraction of dynein arms on the movement of reactivated sea-urchin sperm. *J. Cell Sci.* **13**, 337-357.

Gibbons, B. H. and Gibbons, I. R. (1974). Properties of flagellar "rigor waves" formed by abrupt removal of adenosine triphosphate from actively swimming sea urchin sperm. *J. Cell Biol.* **63**, 970-985.

Gibbons, B. H. and Gibbons, I. R. (1979). Relationship between the latent adenosine triphosphatase state of dynein 1 and its ability to recombine functionally with KCl-extracted sea urchin sperm flagella. *J. Biol. Chem.* **254**, 197-201.

Gibbons, I. R. (1963). Studies on the protein components of cilia from *Tetrahymena pyriformis*. *Proc. Nat. Acad. Sci. USA* **50**, 1002-1010.

Gibbons, I. R. (1966) Studies on the adenosine triphosphatase activity of 14S and 30S dynein from cilia of *Tetrahymena*. *J. Biol. Chem.* **241**, 5590-5596.

Gibbons, I. R. (1981). Cilia and flagella in eukaryotes. *J. Cell Biol.* **91**, 107s-124s.

Gibbons, I. R., Cosson, M. P., Evans, J. A., Gibbons, B. H., Houck, B., Martinson, K. H., Sale, W. S. and Tang, W. Y. (1978). Potent inhibition of dynein adenosinetriphosphatase and of the motility of cilia and sperm flagella by vanadate. *Proc. Nat. Acad. Sci. USA.* **75**, 2220-2224.

Gibbons, I. R. and Fronk, E. (1979). A latent adenosine triphosphatase form of dynein 1 from sea urchin sperm flagella. *J. Biol. Chem.* **254**, 187-196.

Gibbons, I. R., Fronk, E., Gibbons, B. H. and Ogawa, K. (1976). Multiple forms of dynein in sea urchin sperm flagella. In *Cell Motility book C*. (ed. R. Goldman, T. Pollard, and J. Rosenbaum), pp. 915-932. Cold Spring Harbor Laboratory.

Gibbons, I. R., Gibbons, B. H., Mocz, G. and Asai, D. J. (1991). Multiple nucleotide-binding sites in the sequence of dynein β heavy chain. *Nature* **352**, 640-643.

Gibbons, I. R., Lee-Eiford, A., Mocz, G., Phillipson, C. A., Tang, W, Y. and Gibbons, B. H. (1987a). Photosensitized cleavage of dynein heavy chains. *J. Biol. Chem.* **262**, 2780-2786.

Gibbons, I. R. and Rowe, A. J. (1965). Dynein: a protein with adenosine triphosphatase activity from cilia. *Science* **149**, 424-425.

Gibbons, I. R., Shingyoji, C, Murakami, A. and Takahashi, K. (1987b). Spontaneous recovery after experimental manipulation of the plane of beat in sperm flagella. *Nature* **325**, 351-352.

Giebeler, R. (1992). The Optima XL-A: a new analytical ultracentrifuge with a novel precision absorption optical system. In *Analytical Ultracentrifugation in Biochemistry and Polymer Science* (ed. S. E. Harding, A. J. Rowe, and J. C. Horton), pp. 16-25. Royal Society of Chemistry.

Gilbert, S. P. and Johnson, K. A. (1993). Expression, purification and characterisation of the *Drosophila* kinesin motor domain produced in *Escherichia coli*. *Biochem.* **32**, 4677-4684.

Gill, S. R., Schroer, T. A., Szilak, I., Steuer, E. R., Sheetz, M. P. and Cleveland, D. W. (1991). Dynactin, a conserved, ubiquitously expressed component of an activator of vesicle motility mediated by cytoplasmic dynein. *J. Cell Biol.* **115**, 1639-1650.

Goldstein, L. S. B. (1991). The kinesin superfamily: tails of functional redundancy. *Trends Cell Biol.* **1**, 93-98.

Goodenough, U. W., Gebhart, B., Mermall, V., Mitchell, D. R. and Heuser, J. E. (1987). High pressure liquid chromatography fractionation of *Chlamydomonas* dynein extracts and characterisation of inner-arm dynein subunits. *J. Mol. Biol.* **194**, 481-494.

Goodenough, U. and Heuser, J. (1984). Structural comparison of purified dynein proteins with *in situ* dynein arms. *J. Mol. Biol.* **180**, 1083-1118.

Goodenough, U. W. and Heuser, J. E. (1985). Substructure of inner dynein arms, radial spokes, and the central pair/projection complex of cilia and flagella. *J. Cell Biol.* **100**, 2008-2018.

Goodno, C. C. (1979). Inhibition of myosin ATPase by vanadate ion. *Proc. Nat. Acad. Sci.* **76**, 2620-2624.

Goodson, H. V., Kang, S. J. and Endow, S. A. (1994). Molecular phylogeny of the kinesin family of microtubule motor proteins. *J. Cell Sci.* **107**, 1875-1884.

Gottlieb, M. and Chavko, M. (1987). Silver staining of native and denatured eukaryotic DNA in agarose gels. *Anal. Biochem.* **165**, 33-37.

Hammer, J. A. (1991). Novel myosins. *Trends Cell Biol.* **1**, 50-56.

Harrington, W. F. and Kegeles, G. (1973). Pressure effects in ultracentrifugation of interacting systems. *Meth. Enzy.* **27**, 306-345.

Hirokawa, N., Pfister, K. K., Yorifuji, H., Wagner, M. C., Brady, S. T. and Bloom, G. S. (1989). Submolecular domains of bovine brain kinesin identified by electron microscopy and monoclonal antibody decoration. *Cell* **56**, 867-878.

Hirokawa, N., Sato-Yoshitake, R., Kobayashi, N., Pfister, K. K., Bloom, G. S. and Brady, S. T. (1991). Kinesin associates with anterogradely transported membranous organelles *in vivo. J. Cell Biol.* **114**, 295-302.

Hirokawa, N., Sato-Yoshitake, R., Yoshida, T. and Kawashima, T. (1990). Brain dynein (MAP 1C) localises on both anterogradely and retrogradely transported membranous organelles *in vivo. J. Cell Biol.* **111**, 1027-1037.

Hirono, M., Endoh, H., Okada, N., Numata, O. and Watanabe, Y. (1987). *Tetrahymena* actin; cloning and sequencing of the *Tetrahymena* actin gene and identification of its gene product. *J. Mol. Biol.* **194**, 181-192.

Hollenbeck, P. J. (1989). The distribution, abundance and subcellular localization of kinesin. *J. Cell Biol.* **108**, 2335-2342.

Holzbaur, E. L. F., Hammerback, J. A., Paschal, B. M., Kravit, N. G., Pfister, K. K. and Vallee, R. B. (1991). Homology of a 150K cytoplasmic dynein-associated polypeptide with the *Drosophila* gene *Glued. Nature* **351**, 579-695.

Holzbaur, E. L. F., Mikami, A., Paschal, B. M. and Vallee, R. B. (1994). Molecular characterisation of cytoplasmic dynein. In *Microtubules* (ed. J. S. Hyams and C. W. Lloyd), pp. 251-267. Wiley-Liss, Inc.

221

Hosokawa, Y. and Miki-Noumura, T. (1987). Bending motion of *Chlamydomonas* axonemes after extrusion of central-pair microtubules. *J. Cell Biol.* **105**, 1297-1301.

Huang, B., Piperno, G. and Luck, D. J. L. (1979). Paralysed flagella mutants of *Chlamydomonas reinhardtii* defective for axonemal doublet microtubule arms. *J. Biol. Chem.* **254**, 3091-3099.

Huang, B., Ramanis, Z. and Luck, D. J. L. (1982). Suppressor mutations in *Chlamydomonas* reveal a regulatory mechanism for flagellar function. *Cell* **28**, 115-124.

Hyams, J. S. (1985). Binding of *Tetrahymena* dynein to axonemes of *Marsilea vestita* lacking the outer dynein arm. *J. Cell Sci.* **73**, 299-310.

Inaba, K., Mohri, T. and Mohri, H. (1988). B-band protein in sea urchin sperm flagella. *Cell Motil. Cytoskel.* **10**, 506-517.

Jamieson, G. A., Vanaman, T. C. and Blum, J. J. (1979). Presence of calmodulin in *Tetrahymena. Proc. Nat. Acad. Sci. USA* **12**, 6471-6475.

Johnson, K. A. (1983). The pathway of ATP hydrolysis by dynein. *J. Biol. Chem.* **258**, 13825-13832.

Johnson, K. A. (1985). Pathway of the microtubule-dynein ATPase and the structure of dynein: a comparison with actomyosin. *Ann. Rev. Biophys. Biophys. Chem.* **14**, 161-188.

Johnson, K. A. (1986). Preparation and properties of dynein from *Tetrahymena* cilia. *Meth. Enzy.* **134**, 306-317.

Johnson, K. A. and Wall, J. S. (1983). Structure and molecular weight of the dynein ATPase. *J. Cell Biol.* **96**, 669-678.

Kagami, O. and Kamiya, R. (1992). Translocation and rotation of microtubules caused by multiple species of *Chlamydomonas* inner-arm dynein. *J. Cell Sci.* **103**, 653-664.

Kamimura, S., Yano, M. and Shimizu, H. (1985). ATP hydrolysis coupled to microtubule sliding in sea-urchin sperm flagella. *J. Biochem.* **97**, 1509-1515.

Kamiya, R., Kurimoto, E. and Muto, E. (1991). Two types of *Chlamydomonas* flagellar mutants missing different components of inner-arm dynein. *J. Cell Biol.* **112**, 441-447.

Kamiya, R. and Okamuto, M. (1985). A mutant of *Chlamydomonas reinhardtii* that lacks the flagella outer dynein arm but can swim. *J. Cell Sci.* **74**, 181-191.

King, S. M., Haley, B. E. and Witman, G. B. (1989). Structure of the α and β heavy chains of the outer arm dynein from *Chlamydomonas* flagella. *J. Biol. Chem.* **264**, 10210-10218.

King, S. M., Wilkerson, C. G. and Witman, G. B. (1991). The M_r 78,000 intermediate chain of *Chlamydomonas* outer arm dynein interacts with α-tubulin *in situ*. *J. Biol. Chem.* **266**, 8401-8407.

King, S. M., Wilkerson, C. G. and Witman, G. B. (1992). Molecular cloning and domain analysis of the M_r 78,000 intermediate chain of *Chlamydomonas* outer arm dynein. *Mol. Biol. Cell* **3**, 2a (abstr).

King, S. M. and Witman, G. B. (1987). Structure of the α and β heavy chains of the outer arm dynein from *Chlamydomonas* flagella: masses of chains and sites of ultraviolet-induced vanadate-dependent cleavage. *J Biol. Chem.* **262**, 17596-17604.

King, S. M. and Witman, G. B. (1988). Structure of the γ heavy chain of the outer arm dynein from *Chlamydomonas* flagella. *J. Cell Biol.* **107**, 1799-1808.

King, S. M. and Witman, G. B. (1990). Localisation of an intermediate chain of outer arm dynein by immunoelectron microscopy. *J. Biol. Chem.* **265**, 19807-19811.

King, S. M. and Witman, G. B. (1994). Multiple sites of phosphorylation within the α heavy chain of *Chlamydomonas* outer arm dynein. *J. Biol. Chem.* **269**, 5452-5457.

Kirkwood J. G. (1954). The general theory of irreversible processes in solutions of macromolecules. *J. Polymer Sci.* **12**, 1-14.

Koonce, M. P., Grissom, P. M. and McIntosh, J. R. (1992). Dynein from *Dictyostelium*: primary strucure comparisons between a cytoplasmic motor enzyme and flagellar dynein. *J. Cell. Biol.* **119**, 1597-1604.

Kuntz, I. D. and Kauzmann, W. (1974). Hydration of proteins and polypeptides. In *Advances in Protein Chemistry, Vol. 28* (ed. C. B. Anfinsen, J. T. Edsall, and F. M. Richards), pp. 239-345. Academic press.

Laemmli, U. K. (1979). Cleavage of structural proteins during the assembly of the head of bacteriophage T4. *Nature* **227**, 680-685.

Lamm, O. (1929). Die differentialgleichung der ultrazentrifugierung. *Ark. Mat. Astron. Fys.* **21B**, 1-4.

Lanford, G. M. (1995). Actin- and microtubule-dependent organelle motors: interrelationships between the two motility systems. *Curr. Opin. Cell Biol.* **7**, 82-88.

Lasek, R. J. and Brady, S. T. (1985). Attachment of transported vesicles to microtubules in axoplasm is facilitated by AMP-PNP. *Nature* **316**, 645-647.

Lee-Eiford, A., Ow, R. A. and Gibbons, I. R. (1986). Specific cleavage of dynein heavy chains by ultraviolet irradiation in the presence of ATP and vanadate. *J. Biol. Chem.* **261**, 2337-2342.

Lin, S. X. H. and Collins, C. A. (1992). Immunolocalisation of cytoplasmic dynein to lysosomes in cultured cells. *J. Cell Sci.* **101**, 125-137.

Lin, S. X. H. and Collins, C. A. (1993). Regulation of the intracellular distribution of cytoplasmic dynein by serum factors and calcium. *J. Cell Sci.* **105**, 579-588.

Ludmann, S. A., Schwandt, A., Kong, X., Bricker, C. S. and Pennock, D. G. (1993). Biochemical analysis of a mutant *Tetrahymena* lacking outer dynein arms. *J. Euk. Microbiol.* **40**, 650-660.

Mabuchi, I. and Shimizu, T. (1974). Electrophoretic studies on dyneins from *Tetrahymena* cilia. *J. Biochem.* **76**, 991-999.

Marchese-Ragona, S. P., Facemyer, K. C. and Johnson, K. A. (1989). Structure of the α−, β−, and γ−heavy chains of 22S outer arm dynein obtained from *Tetrahymena* cilia. *J. Biol. Chem.* **264**, 21361-21368.

Marchese-Ragona, S. P., Facemyer, K. C. and Johnson, K. A. (1991). Structural studies of the dynein ATPase's. *Sixth international congress of spermatology* **75**, 403-406.

Marchese-Ragona, S. P. and Johnson, K. A. (1989). Structure and subunit organisation of the soluble dynein particle. In *Cell Movement Vol. 1.* (ed. F. D. Warner, P. Satir, and I. R. Gibbons), pp. 37-48. Alan R. Liss, Inc., New York.

Marchese-Ragona, S. P., Wall, J. S. and Johnson, K. A. (1988). Structure and mass analysis of 14S dynein obtained from *Tetrahymena* cilia. *J. Cell Biol.* **106**, 127-132.

Margolis, R. L. and Job, D. (1994). Microtubule stabilization. In *Microtubules* (ed. J. S. Hyams and C. W. Lloyd), pp. 221-228.Wiley-Liss, Inc.

Marks, D. L., Larkin, J. M. and McNiven, M. A. (1994). Association of kinesin with the Golgi apparatus in rat hepatocytes. *J. Cell Sci.* **107**, 2417-2426.

Mastronarde, D. N., O'Toole, E. T., McDonald, K. L., McIntosh, J. R. and Porter, M. E. (1992). Arrangement of inner dynein arms in wild-type and mutant flagella of *Chlamydomonas. J. Cell Biol.* **118**, 1145-1162.

Mikami, A., Paschal, B. M., Mazumdar, M. and Vallee, R. B. (1993). Molecular cloning of the retrograde transport motor cytoplasmic dynein (MAP 1C). *Neuron* **10**, 787-796.

Mimori, Y. and Miki-Noumura, T. (1994). ATP-induced sliding of microtubules on tracks of 22S dynein molecules aligned with the same polarity. *Cell Motil. Cytoskel.* **27**, 180-191.

Mitchell, D. R. and Brown, K. S. (1994). Sequence analysis of the *Chlamydomonas* alpha and beta dynein heavy chain genes. *J. Cell Sci.* **107**, 635-644.

Mitchell, D. R. and Rosenbaum, J. L. (1985). A motile *Chlamydomonas* mutant that lacks outer dynein arms. *J. Cell Biol.* **100**, 1228-1234.

Mitchell, D. R. and Rosenbaum, J. L. (1986). Protein-protein interactions in the 18S ATPase of *Chlamydomonas* outer dynein arms. *Cell Motil. Cytoskel.* **6**, 510-520.

Mitchell, D. R. and Warner, D. R. (1980). Interactions of dynein arms with B subfibers of *Tetrahymena* cilia: quantitation of the effects of magnesium and adenosine triphosphate. *J. Cell Biol.* **87**, 84-97.

Mitchell, D. R. and Warner, D. R. (1981). Binding of dynein 21S ATPase to microtubules. *J. Biol. Chem.* **256**, 12535-12544.

Mocz, G. (1989). Vanadate-mediated photocleavage of rabbit skeletal myosin. *Eur. J. Biochem.* **179**, 373-378.

Mocz, G., and Gibbons, I. R. (1990). Iron (III)-mediated photolysis of outer arm dynein ATPase from sea urchin sperm flagella. *J. Biol. Chem.* **265**, 2917-2922.

Moss, A. G., Gatti, J. and Witman, G. B. (1992a). The motile β/IC1 subunit of sea urchin sperm outer arm dynein does not form a rigor bond. *J. Cell Biol.* **118**, 1177-1188.

Moss, A. G., Sale, W. S., Fox, L. A. and Witman, G. B. (1992b). The α subunit of sea urchin sperm outer arm dynein mediates structural and rigor binding to microtubules. *J. Cell Biol.* **118**, 1189-1200.

Murray, J. M. (1994). Eukaryotic flagella. *Curr. Opin. Struct. Biol.* **42**, 180-186.

Muto, E., Edamatsu, M., Hirono, M. and Kamiya, R. (1994). Immunological detection of actin in the 14S ciliary dynein of *Tetrahymena. FEBS* **343**, 173-176.

Muto, E., Kamiya, R. and Tsukita, S. (1991). Double-rowed organisation of inner dynein arms in *Chlamydomonas* flagella revealed by tilt-series thin-section electron microscopy. *J. Cell Sci.* **99**, 57-66.

Niino, Y. and Miki-Noumura, T. (1992). ATPase sites in two-headed fragment of *Tetrahymena* 22S ciliary dynein. *Biochim. Biophys.Acta,* **1100**, 146-154.

Ogawa, K. (1991). Four ATP-binding sites in the midregion of the β heavy chain of dynein. *Nature* **352**, 643-645.

Omoto, C. K. and Johnson, K. A. (1986). Activation of the dynein adenosinetriphosphatase by microtubules. *Biochem.* **25**, 419-427.

Omoto, C. K. and Kung, C. (1980). Rotation and twist of the central-pair microtubules in the cilia of *Paramecium. J. Cell Biol.* **87**, 33-46.

Papahadjopoulos, D. (1972). Studies on the mechanism of action of local anaesthetics with phospholipid model membranes. *Biochim. Biophys. Acta* **265**, 169-186.

Paschal, B. M., Holzbaur, E. L. F., Pfister, K. K., Clark, S., Meyer, D. I. and Vallee, R. B. (1993). Characterisation of a 50-kDa polypeptide in cytoplasmic dynein preparations reveals a complex with p150[GLUED] and a novel actin. *J. Biol. Chem.* **268**, 15318-15323.

Paschal, B., King, S. M., Moss, A. G., Collins, C. A., Vallee, R. B. and Witman, G. B.
(1987). Isolated flagella outer arm dynein translocates brain microtubules *in vitro*. *Nature*
330, 672-674.

Paschal, B. M., Mikami, A., Pfister, K. K. and Vallee, R. B. (1992). Homology of the
74-kD cytoplasmic dynein subunit with a flagellar dynein polypeptide suggests an
intracellular targeting function. *J. Cell Biol.* **118**, 1133-1143.

Paschal, B. M., Shpetner, H. S. and Vallee, R. B. (1987). MAP 1C is a microtubule-
activated ATPase which translocates microtubules *in vitro* and has dynein-like properties.
J. Cell Biol. **105**, 1273-1282.

Paschal, B. M. and Vallee, R. B. (1987). Retrograde transport by the microtubule-
associated protein MAP 1C. *Nature* **330**, 181-183.

Pereira, A. and Goldstein, L. S. B. The kinesin superfamily. In *Microtubules* (ed. J. S.
Hyams and C. W. Lloyd), pp. 269-284.Wiley-Liss, Inc.

Pierre, P., Scheel, J., Rickard, J. E. and Kreis, T. E. (1992). CLIP-170 links endocytic
vesicles to microtubules. *Cell* **70**, 887-900.

Piperno, G. (1988). Isolation of a sixth dynein subunit adenosine triphosphatase of
Chlamydomonas axonemes. *J. Cell Biol.* **106**, 133-140.

Piperno, G., Huang, B., Ramanis, Z. and Luck, D. J. L. (1981). Radial spokes of
Chlamydomonas flagella: polypeptide composition and phosphorylation of stalk
components. *J. Cell Biol.* **88**, 73-79.

Piperno, G. and Luck, J. L. (1979a). Axonemal adenosine triphosphatases from flagella
of *Chlamydomonas reinhardtii* -purification of two dyneins. *J. Biol. Chem.* **254**, 3084-
3090.

Piperno, G. and Luck, J. L. (1979b). An actin-like protein is a component of axonemes
from *Chlamydomonas* flagella. *J. Biol. Chem.* **254**, 2187-2190.

Piperno, G. and Luck, J. L. (1981). Inner arm dyneins from flagella of *Chlamydomonas
reinhardtii*. *Cell* **27**, 331-340.

Piperno, G., Mead, K., LeDizet, M and Moscatelli, A. (1994). Mutations in the "dynein regulatory complex" alter the ATP-insensitive binding sites for inner arm dyneins in *Chlamydomonas* axonemes. *J. Cell Biol.* **125**, 1109-1117.

Piperno, G., Mead, K. and Shestak, W. (1992). The inner dynein arms I2 interact with a "dynein regulatory complex" in *Chlamydomonas* flagella. *J. Cell Biol.* **118**, 1455-1463.

Piperno, G. and Ramanis, Z. (1991). The proximal portion of *Chlamydomonas* flagella contains a distinct set of inner dynein arms. *J. Cell Biol.* **112**, 701-709.

Piperno, G., Ramanis, Z., Smith, E. F. and Sale, W. S. (1990). Three distinct inner dynein arms in *Chlamydomonas* flagella: molecular composition and location in the axoneme. *J. Cell Biol.* **110**, 379-389.

Pfarr, C. M., Coue, M., Grissom, P. M., Hays, T. S., Porter, M. E. and McIntosh, J. R. (1990). Cytoplasmic dynein is localised to kinetochores during mitosis. *Nature* **345**, 263-265.

Pfister, K. K., Haley, B. E. and Witman, G. B. (1984). The photoaffinity probe 8-azidoadenosine 5'-triphosphate selectively labels the heavy chain of *Chlamydomonas* 12S dynein. *J. Biol. Chem.* **259**, 8499-8504.

Pfister, K. K. and Witman, G. B. (1984). Subfractionation of *Chlamydomonas* 18S dynein into two unique subunits containing ATPase activity. *J. Biol. Chem.* **259**, 12072-12080.

Pollard, T. D., Doberstein, S. K. and Zot, H. G. (1991). Myosin-1. *Ann. Rev. Physiol.* **53**, 653-681.

Porter, M. E. and Johnson, K. A. (1983). Characterisation of the ATP-sensitive binding of *Tetrahymena* 30S dynein to bovine brain microtubules. *J. Biol. Chem.* **258**, 6575-6581.

Porter, M. E. and Johnson, K. A. (1989). Dynein structure and function. *Annu. Rev. Cell Biol.* **5**, 119-151.

Porter, M. E., Knott, J. A., Gardner, L. C., Mitchell, D. R. and Dutcher, S. K. (1994). Mutations in the *SUP-PF-1* locus of *Chlamydomonas reinhardtii* identify a regulatory domain in the β heavy chain. *J. Cell Biol.* **126**, 1495-1507.

Pratt, M. M. (1986). Homology of egg and flagella dynein. *J. Biol. Chem.* **261**, 956-964.

Ralston, G. (1993). Introduction to Analytical Ultracentrifugation. Beckman Instruments, Inc.

Roark, D. E., and Yphantis, D. A. (1969). Studies of self-associating systems by equilibrium ultracentrifugation. *Ann. N.Y Acad. Sci.* **164**, 245-278.

Rowe, A. J. (1984). Techniques for determining molecular weight. *Prot. Enzy. Biochem.* **BS106**, 1-37.

Sakakibara, H. and Kamiya, R. (1989). Functional recombination of outer dynein arms with outer arm-missing flagellar axonemes of a *Chlamydomonas* mutant. *J. Cell Sci.* **92**, 77-83.

Sakakibara, H., Mitchell, D. R. and Kamiya, R. (1991). A *Chlamydomonas* outer arm dynein mutant missing the α heavy chain. *J. Cell Biol.* **113**, 615-622.

Sakakibara, H., Takada, S., King, S. M., Witman, G. B. and Kamiya, R. (1993). A *Chlamydomonas* outer arm dynein mutant with a truncated β heavy chain. *J. Cell Biol.* **122**, 653-661.

Sale, W. S. and Fox, L. A. (1988). Isolated β–heavy chain subunit of dynein translocates microtubules *in vitro*. *J. Cell Biol.* **107**, 1793-1797.

Sale, W. S., Goodenough, U. W. and Heuser, J. E. (1985). The substructure of isolated and *in situ* outer dynein arms of sea urchin sperm flagella. *J. Cell Biol.* **101**, 1400-1412.

Sale, W. S. and Satir, P. (1977). Direction of active sliding of microtubules in *Tetrahymena* cilia. *Proc. Nat. Acad. Sci. USA* **74**, 2045-2049.

Satir, B., Sale, W. S. and Satir, P. (1976). Membrane renewal after dibucaine deciliation of *Tetrahymena*. *Exp. Cell Res.* **97**, 83-91.

Satir, P. (1976). Introductory remarks: cilia, eukaryotic flagella and an introduction to microtubules. In *Cell Motility book C* (ed. R. Goldman, T. Pollard, and J. Rosenbaum), pp. 841-846. Cold Spring Harbor Laboratory.

Satir, P., Barkalow, K. and Hamasaki, T. (1993). The control of ciliary beat frequency. *Trends Cell Biol.* **3**, 409-412.

Schachman, H. K. (1992). Is there a future for the ultracentrifuge? In *Analytical Ultracentrifugation in Biochemistry and Polymer Science* (ed. S. E. Harding, A. J. Rowe, and J. C. Horton), pp. 3-13. Royal Society of Chemistry.

Schiff, P. B., Fant, J. and Horwitz, S. B. (1979). Promotion of microtubule assembly *in vitro* by taxol. *Nature* **277**, 665-667.

Schnapp, B. J. and Reese, T. S. (1989). Dynein is the motor for retrograde axonal transport of organelles. *Proc. Nat. Acad. Sci. USA* **86**, 1548-1552.

Scholey, J. M., Porter, M. E., Grissom, P. M. and McIntosh, J. R. (1985). Identification of kinesin in sea urchin eggs, and evidence for its localisation in the mitotic spindle. *Nature* **318**, 483-486.

Schroer, T. A. (1994). Structure, function and regulation of cytoplasmic dynein. *Curr. Opin. Cell Biol.* **6**, 69-73.

Schroer, T. A., Steuer, E. R. and Sheetz, M. P. (1989). Cytoplasmic dynein is a minus end-directed motor for membranous organelles. *Cell* **56**, 937-946.

Shimizu, T. and Furusawa, K. (1986). Phosphorothioate analogues of adenosine 5'-triphosphate as substrates of dynein from *Tetrahymena* cilia. *Biochem.* **25**, 5787-5792.

Shimizu, T., Hosoya, N., Hisanaga, S., Marchese-Ragona, S. P. and Prat, M. M. (1992). Activation of ATPase activity of 14S dynein from *Tetrahymena* cilia by microtubules. *FEBS*, **206**, 911-917.

Shimizu, T. and Johnson, K. A. (1983a). Kinetic evidence for multiple dynein ATPase sites. *J. Biol. Chem.* **258**, 13841-13846.

Shimizu, T. and Johnson, K. A. (1983b). Presteady state kinetic analysis of vanadate-induced inhibition of the dynein ATPase. *J. Biol. Chem.* **258**, 13833-13840.

Shimizu, T. and Kimura, I. (1974). Effects of N-ethylmaleimide on dynein adenosinetriphosphatase activity and its recombining ability with outer fibers. *J. Biochem.* **76**, 1001-1008.

Shpetner, H. S., Paschal, B. M. and Vallee, R. B. (1988). Characterisation of the microtubule-activated ATPase of brain cytoplasmic dynein (MAP 1C). *J. Cell Biol.* **107**, 1001-1009.

Smith, E. F. and Sale, W. S. (1991). Microtubule binding and translocation by inner dynein arm subtype I1. *Cell Motil. Cytoskel.* **18**, 258-268.

Smith, E. F. and Sale, W. S. (1992). Regulation of dynein-driven microtubule sliding by the radial spokes in flagella. *Science* **257**, 1557-1559.

Smith, K. (1992). Nonlinear regression: cut errors by making the curve fit the data. In *Laboratory Equipment Digest*.

Spudich, J. A. and Warrick, H. M. (1991). A tale of two motors. *Curr. Opin. Struct. Biol.* **1**, 264-269.

Squire, P. G. and Himmel, M. E. (1979). Hydrodynamics and protein hydration. *Arch. Biochem. Biophy.* **196**, 165-177.

Steuer, E. R., Wordman, L., Schroer, T. A. and Sheetz, M. P. (1990). Localisation of cytoplasmic dynein to mitotic spindles and kinetochores. *Nature* **345**, 266-268.

Summers, K. E. and Gibbons, I. R. (1971). Adenosine triphosphate-induced sliding of tubules in trypsin-treated flagella of sea urchin sperm. *Proc. Nat. Acad. Sci. USA* **68**, 3092-3096.

Summers, K. E. and Gibbons, I. R. (1973). Effects of trypsin digestion on flagellar structures and their relationship to motility. *J. Cell Biol.* **58**, 618-629.

Takahashi, M. and Tonomura, Y. (1978). Binding of 30S dynein with the B-tubule of the outer doublet of axonemes from *Tetrahymena pyriformis* and adenosine triphosphate-induced dissociation of the complex. *J. Biochem.* **84**, 1339-1355.

Tanford, C. (1961). Physical Chemistry of Macromolecules. New York and London. John Wiley & Sons Inc.

Tang, W, Y., Bell, C. W., Sale, W. S. and Gibbons, I. R. (1982). Structure of the dynein-1 outer arm in sea urchin sperm flagella. I. Analysis by separation of subunits. *J. Biol. Chem.* **257**, 508-515.

Tang, W, Y. and Gibbons, I. R. (1987). Photosensitised cleavage of dynein heavy chains. *J. Biol. Chem.* **262**, 17728-17734.

Thompson, G. A., Baugh, L. C. and Walker, L. F. (1974). Nonlethal deciliation of *Tetrahymena* by a local anaesthetic and its utility as a tool for studying cilia regeneration. *J. Cell Biol.* **61**, 253-257.

Toyoshima, Y. Y. (1987a). Chymotryptic digestion of *Tetrahymena* 22S dynein. I. Decomposition of three-headed 22S dynein to one- and two-headed paritcles. *J. Cell Biol.* **105**, 887-895.

Toyoshima, Y. Y. (1987b). Chymotryptic digestion of *Tetrahymena* ciliary dynein. II. Pathway of the degradation of 22S dynein heavy chains. *J. Cell Biol.* **105**, 897-901.

Vale, R. D. (1992). Microtubule motors: many new models off the assembly line. *Trends Biochem.* **17**, 300-304.

Vale, R. D. and Goldstein, L. S. B. (1990). One motor, many tails: an expanding repertoire of force-generating enzymes. *Cell* **60**, 883-885.

Vale, R. D., Reese, T. S. and Sheetz, M. P. (1985c). Identification of a novel force-generating protein, kinesin, involved in microtublue-based motility. *Cell* **42**, 39-50.

Vale, R. D., Schnapp, B. J., Reese, T. S. and Sheetz, M. P. (1985a). Movement of organelles along filaments dissociated from the axoplasm of the squid giant axon. *Cell* **40**, 449-454.

Vale, R. D., Schnapp, B. J., Reese, T. S. and Sheetz, M. P. (1985b). Organelle, bead, and microtubule translocations promoted by soluble factors from the squid giant axon. *Cell* **40**, 559-569.

Vale, R. D., Soll, D. R. and Gibbons, I. R. (1989). One-dimensional diffusion of microtubules bound to flagellar dynein. *Cell* **59**, 915-925.

Vale, R. D. and Toyoshima, Y. Y. (1988). Rotation and translocation of microtubules *in vitro* induced by dyneins from *Tetrahymena* cilia. *Cell* **52**, 459-469.

Vale, R. D. and Toyoshima, Y. Y. (1989) Microtubule translocation properties of intact and proteolytically digested dyneins from *Tetrahymena* cilia. *J. Cell Biol.* **108**, 2327-2334.

Vallee, R. B. (1986). Purification of brain microtubules and microtubule associated protein 1 using taxol. *Meth. Enzy.* **134**, 104-109.

Vallee, R. (1991). Cytoplasmic dynein: advances in microtubule-based motility. *Trends Cell Biol.* **1**, 25-29.

Vallee, R. B., Wall, J. S., Paschal, B. M. and Shpetner, H. S. (1988). Microtubule-associated protein 1C from brain is a two-headed cytosolic dynein. *Nature* **332**, 561-563.

van Holde, K. E. (1971). Physical Biochemistry. Prentice-Hall, Inc. New Jersey.

Walczak, C. E. and Nelson, D. L. (1993). *In vitro* phosphorylation of ciliary dyneins by protein kinases from *Paramecium. J. Cell Sci.* **106**, 1369-1376.

Walker, J. E., Saraste, M., Runswick, M. J. and Gay, N. J. (1982). Distantly related sequences in the α and β-subunits of ATP synthase, myosin, kinases and other ATP-requiring enzymes and a common nucleotide binding fold. *EMBO J.* **8**, 945-951.

Warner, F. D. and McIlvain, J. H. (1986). Kinetic properties of microtubule-activated 13S and 21S dynein ATPases. *J. Cell Sci.* **83**, 251-267.

Warner, F. D., Mitchell, D. R. and Perkins, C. R. (1977). Structural conformation of the ciliary ATPase dynein. *J. Mol. Biol.* **114**, 367-384.

Warrick, H. M. and Spudich, J. A. (1987). Myosin structure and function in cell motility. *Ann. Rev. Cell Biol.* **3**, 379-421.

Weingarten, M. D., Lockwood, A. H., Hwo, S. and Kirschner, M. W. (1975). A protein factor essential for microtubule assembly. *Proc. Nat. Acad. Sci. USA* **72**, 1858-1862.

Wells, C. and Bagshaw, C. R. (1984). The characterisation of vanadate-trapped nucleotide complexes with spin-labelled myosins. *J. Mus. Res. Cell Motil.* **5**, 97-112.

Wells, C., Molina-Garcia, A., Harding, S. E. and Rowe, A. J. (1990). Self-interaction of dynein from *Tetrahymena* cilia. *J. Mus. Res. Cell Motil.* **11**, 344-350.

Wilkerson, C. G., King, S. M. and Witman, G. B. (1994). Molecular analysis of the γ heavy chain of *Chlamydomonas* flagellar outer-arm dynein. *J. Cell Sci.* **107**, 497-506.

Willison, J. H. M. and Rowe, A. J. (1980). Replica, shadowing and freeze-etching techniques. In *Practical Methods in Electron Microscopy Vol. 8.* (ed. A. M. Glauert), pp. 245-282. North-Holland Publishing Company.

Witman, G. B. (1989). Composition and molecular organisation of the dyneins. In *Cell Movement Vol. 1*. (ed. F. D. Warner, P. Satir, and I. R. Gibbons), pp. 25-35. Alan R. Liss, Inc., New York.

Witman, G. B., Johnson, K. A., Pfister, K. K. and Wall, J. S. (1983). Fine structure and molecular weight of the outer arm dyneins of *Chlamydomonas. J. Submicrosc. Cytol.* **15**, 193-197.

Witman, G. B., King, S. M., Moss, A. G. and Wilkerson, C. (1991). The intermediate chain/light chain complex: an important structural entity of outer arm dynein. *Sixth internation congress of spermatology*, **75**, 439-443.

Wright, B. D., Henson, J. H., Wedaman, K. P., Willy, P. J., Morand, J. N. and Scholey, J. M. (1991). Subcellular localization and sequence of sea urchin kinesin heavy chain: evidence for its association with membranes in the mitotic apparatus and interphase cytoplasm. *J. Cell Biol.* **113**, 817-833.

Yang, J. T., Laymon, R. A. and Goldstein, L. S. B. (1989). A three-domain structure of kinesin heavy chain revealed by DNA sequence and microtubule binding analyses. *Cell* **56**, 879-889.

Yang, J. T., Saxton, W. M., Stewart, R. J., Raff, E. C. and Goldstein, L. S. B. (1990). Evidence that the head of kinesin is sufficient for force generation and motility *in vitro*. *Science* **249**, 42-47.

Yano, Y. and Miki-Noumura, T. (1981a). Recovery of sliding ability in arm-depleted flagellar axonemes after recombination with extracted dynein 1. *J. Cell Sci.* **48**, 223-239.

Yano, Y. and Miki-Noumura, T. (1981b). Two-headed dynein arm. *Biomed. Res.* **2**, 73-78.

Yokota, E. and Mabuchi, I. (1994a). Isolation and characterisation of a novel dynein that contains C and A heavy chains from sea urchin sperm flagellar axonemes. *J. Cell Sci.* **107**, 345-351.

Yokota, E. and Mabuchi, I. (1994b). C/A dynein isolated from sea urchin sperm flagellar axonemes; enzymatic properties and interaction with microtubules. *J. Cell Sci.* **107**, 353-361.

Yokota, E., Mabuchi, I. and Sato, H. (1987). Activation of sea urchin sperm flagella dynein ATPase activity by salt-extracted axonemes. *J. Biochem.* **102**, 31-41.

Zhang, Z., Tanaka, Y., Nonaka, S., Aizawa, H., Kawasaki, H., Nakata, T. and Hirokawa, N. (1993). The primary structure of rat brain (cytoplasmic) dynein heavy chain, a cytoplasmic motor enzyme. *Proc. Nat. Acad. Sci. USA* **90**, 7928-7932.